UC Riverside

UC Riverside Electronic Theses and Dissertations

Title

Biomimetic Molecular Recognition And Oxidation Catalysis in Water

Permalink

https://escholarship.org/uc/item/4tg8w95x

Author

Mettry, Magi Adel

Publication Date

2017

Peer reviewed|Thesis/dissertation

UNIVERSITY OF CALIFORNIA
RIVERSIDE

Biomimetic Molecular Recognition and Oxidation Catalysis in Water

A Dissertation submitted in partial satisfaction
of the requirements for the degree of

Doctor of Philosophy

in

Chemistry

by

Magi Adel Mettry

June 2017

Dissertation Committee:
    Dr. Richard J. Hooley, Chairperson
    Dr. Leonard J. Mueller
    Dr. Christopher Switzer

The Dissertation of Magi Adel Mettry is approved:

_____

_____

_____
Committee Chairperson

University of California, Riverside

ACKNOWLEDGMENTS

First and foremost, I would like to thank the Lord Jesus for the blessing I have had throughout my life and my PhD. I thank Him for my life in Egypt and coming to the states, helping me learn the language, and showing me my true passion in chemistry. Thank you for your support over the last 28 years. I thank Him for every lesson through which He has walked with me. I am undeserving, yet you gave me much. Thank you for making me who I am as a scientist and as a strong woman.

Thanks to my church family in Riverside at Sandals and at Cornerstone Bible Church. Thanks to my Arabic church family for showing me that life isn't just about income or power, but that there is so much good to be done in life.

I dedicate this to my family, who gave up everything to come here and offer me a better future. I want to thank my father, Adel Mettry, for being the most gentle, polite, honest, strong, and wise man I have ever seen in my life. Thanks to my brother, Mina Mettry, for being my best friend, for helping me through all my decisions, and for protecting me from so much. I'm so glad I have two amazing gentleman in my life. Thanks to Madonna Mettry, my sister-in-law for being part of my family and suffering through the last year, hearing about my grad school experience, and loving me through the distance.

Finally, to my mother, Margerett Gabra Mettry: words could never describe how much I'm thankful for who you are as a Christian, as a strong woman, and as the most loving human being one can imagine. Your daily phone calls are what made me strive—your encouragement through the storms, your Bible verses that came in the most perfect time to lift me up. Your trust in me to be a great woman has pushed me above anything I could

iv

imagine. Words will never and could never be enough to thank you and to explain my love.

Thanks to the rest of my family starting with my uncle, Magdy Thabet, who was the reason we moved here. I wanted you to be proud of who I am and who I have become.

I want to thank my aunties, especially Ashak's family (Saad Ashak, Mervet Gabra, Angi Thabet, Sharl Thabet, Silvi Ashak, Bishoy Ashak, and baby Lillie), for their support throughout my grad school years.

I would also like to thank my astounding friend Amber Scott for being there, for proof reading my science paper without having ever taken a science class. Thanks for the hours I would practice my talks on you. You are truly my best friend for life. I can never imagine my life without your friendship and the rest of the squad. Thank you for all the adventures and random hikes. Thank you for all the game nights, Thai lunches, volleyball games, and Dodger games. Thank you for calling me your friend. Thank you for being an amazing Christian woman that God put in my life to walk with me these past seven years ever since I came to Riverside as an undergraduate. You were there not only to support me through school, but also through my personal struggles.

Thanks to my life long high school friend Nareh Sargsyan, my travel buddy, my first American friend, and my inspiration for everything creative. Thanks for all the coffee breaks, ice cream runs, and simple Skype chats. Thank you for hearing me complain for hours about school and work or for simply sitting in silence as I cried over the pain I was going through. I have always and will forever consider you family.

Grad school was hard, yet life was much harder to bare without you. Being sick my first year was just a preview of what I would face over the next five years. As I lost my godmother to a car accident, and my grandmother only a couple months later during my second year, my family was there to support and comfort me. My third year was definitely the hardest as we all faced stage three pancreatic cancer in my mother's organs. While Oxaliplatin, Leucovorin, Irinotecan, and Fluorouracil deteriorated her, God was showing us grace and mercy above and beyond. As she went into a coma, and a twelve-hour surgery, most of you were there every day and every night. Thank you for being there for her when I physically couldn't. Thank you for being there for more than two years until her recovery. Thank you for being there when I also lost my uncle in a terrible accident. As I saw him die in my hands, you were there to comfort me and lift me up during my fourth year. Without my family, I would have definitely given up a long time ago.

I especially thank Dr. Katherine Djernes for taking me as an undergraduate research assistant and showing me that research is my calling in life.

Thanks to my labmates Dr. Mike Young, Mrs. Lizeth Perez, Dr. Yoo-Jin Ghang, and the Morton lab, including Dr. Jar-Ar Bendo, Dr. Hou Ung, and Mr. Erik Romero, for making a twelve-hour work day in the lab bearable. Thank you for the fun moments and inside jokes. Thanks to Adam Gill as we started this journey together as undergraduates, taking chemistry classes and now working as PhD students on the same project.

A special thanks to Prof. Len Muller for welcoming me this past year as I work on my final project. Thanks for teaching me so much more about NMR in just one year than I

learned in my whole time at grad school. Thanks to his exceptional grad student Bethany Caulkins for being part of that project. Thanks to Dan Borchardt who help me run most of my NMR experiments. I will defiantly miss all of the coffee breaks and celebration in your lab.

Thanks to the National Science Foundation (NSF) for funding my first couple of years as a graduate student. Thanks to UC-Riverside for funding me through both a Dissertation Research Grant and a Dissertation Year Fellowship which allowed me more time to conduct and finish my research.

Finally, this thesis would have never been possible without my mentor and PI, Prof. Richard Hooley. I appreciate everything you have done for me. Starting from the day you showed me around the lab as an undergraduate, to the day you convinced me to stay and continue my PhD instead of attempting med school and every single day beyond that. You are a great advisor, and an amazing human been. Thank you for the support and mentorship in both the joyful and difficult times. Thank you for giving me the time to take care of my mother. Thank you for the support and the time off as I mourned my uncle's death. Thank you for the time as I finished my tumor treatment. Thank you for the constant mentorship intellectually, financially, and personally. I most definitely didn't make it easy with my constant questioning and the occasion stupid question. You are the main reason for my graduate school success.

The text of this dissertation, in part or in full, is a reprint of the material as they appear in the following publications:

Chapter 1: Mettry, M.; Hooley, R.J. "Receptors Based on Van der Waals' Forces" in *Comprehensive Supramolecular Chemistry II*, Atwood, J.L., Gokel, G.W., ed., Elsevier, **2016**. http://dx.doi.org/10.1016/B978-0-12-409547-2.12479-5

Chapter 2: Djernes, K.E.; Moshe, O.; Mettry, M.; Richards, D.D**.**; Hooley, R.J. "Metal-coordinated Water Soluble Cavitands act as C-H Oxidation Catalysts" *Org. Lett.* **2012**, *14*, 788-791.

Djernes, K.E.; Padilla, M.; Mettry, M.; Young, M.C.; Hooley, R.J. "Hydrocarbon Oxidation Catalyzed by Self-folded Metal-coordinated Cavitands" *Chem. Commun.* **2012**, *48,* 11576 - 11578.

Mettry, M.; Moehlig, M.P.; Gill, A.D.; Hooley, R.J. "Alkane Oxidation Catalyzed by a Self-Folded Multi-Iron Complex" *Supramol. Chem.* **2017**, *29*, 120-128

Chapter 3: Mettry, M.; Moehlig, M.P.; Hooley, R.J. "Synthesis, Guest Binding and Metal Coordination of Functionalized Self-folding Deep Cavitands" *Org. Lett.* **2015**, *17*, 1497-1500.

Chapter 4: Liu, Y.; Perez, L.; Mettry, M.; Easley, C.J.; Hooley, R.J.*; Zhong, W.* "A Self-Aggregating Deep Cavitand Acts as a Fluorescence Displacement Sensor for Lysine Methylation" *J. Am. Chem. Soc.* **2016**, *138*, 10746–10749.

Ghang, Y.-J.; Lloyd, J.J.; Moehlig, M.P.; Arguelles, J.K.; Mettry, M.; Zhang, X.; Julian, R.R.; Cheng, Q.; Hooley, R.J. "Labeled Protein Recognition at a Membrane Bilayer Interface by Embedded Synthetic Receptors" *Langmuir* **2014**, *30*, 10161-10166.

Liu, Y.; Perez, L.; Mettry, M.; Gill, A. D.; Byers, S. R.; Easley, C. J.; Bardeen, C. J.; Zhong, W.;* Hooley, R. J.* "Site Selective Reading of Epigenetic Markers by a Dual-Mode Synthetic Receptor Array" *Chem. Sci.* **2017**, *8*, 3960-3970.

Perez, L.; Mettry, M.; Hinman, S. S.; Byers, S. R.; McKeating, K. S.; Caulkins, B. G.; Chenga, Q.; Hooley, R. J. "Selective protein recognition in supported lipid bilayer arrays by tailored, dual-mode deep cavitand hosts" *Soft Matter,* **2017**, *13,* 3966-3974.

Chapter 5: Hooley, R. J.; Gavette, J.; Mettry, M.; Ajami, D.; Rebek, J., Jr. "Unusual Orientation and Reactivity of Alkyl Halides in Water-Soluble Cavitands" *Chem. Sci.,* **2014***, 5,* 4382-4387.

ABSTRACT OF THE DISSERTATION

Functionalized Self-Folding Scaffold for hydrocarbon Recognition and Oxidation

by

Magi Adel Mettry

Doctor of Philosophy, Graduate Program in Chemistry
University of California, Riverside, June 2017
Dr. Richard J. Hooley, Chairperson

A central goal of modern sustainable chemistry is to convert feedstock chemicals to more functionalized and useful products in a mild and selective manner. The most desirable transformation is the oxidation of linear unactivated hydrocarbons with regioselectivity, i.e. the ability to selectively oxidize one position on the hydrocarbon chain. This is bioinspired: enzymes are capable of selectively transforming one specific C-H bond in the presence of other equivalent bonds in the same molecule *via* proximity-based interactions. Bioinspired catalysts are known to effect C-H oxidation in mild conditions, but obtaining regioselectivity relies heavily on functional groups to direct the oxidation.

The main goal of this project is to combine the concepts of molecular recognition and oxidation catalysis to create a small molecule mimic of enzymatic CH oxidation processes that is capable of both *recognition* of a hydrocarbon substrate, and catalyze its mild, regioselective oxidation. This involves the study of both hydrocarbon recognition, and hydrocarbon oxidation catalysis. The first approach was to create an oxidation

catalyst containing a multi-metal catalytic center. The preorganized ligand scaffold is capable of coordinating multiple Fe(II) centers to form an electrophilic CH oxidation catalyst. This catalyst oxidizes unactivated hydrocarbons including simple, linear alkanes under mild conditions in good yields with selectivity for the oxidation of secondary CH bonds. To introduce molecular recognition elements to these active catalytic metal complexes, functionalized self-folding cavitands with metal coordinating groups were synthesized. The upper rim donors allow controlled noncovalent binding of suitably sized guest species via both self-complementary hydrogen bonding and space-filling interactions, and metal-mediated self-folding is possible if bidentate coordinators are incorporated. The functionalized cavitands were further explored as biological sensors for trimethylammonium species such as choline and trimethyllysine. In-depth mechanistic studies of the molecular motion of substrates inside the cavity were performed in different environments, notably in lipid micelles and magnetically ordered bicelles using 2D NMR. The in/out exchange mechanism and up/down kinetic motion of guests in cavitand scaffolds could be quantified.

TABLE OF CONTENTS

Chapter 1: Background

Chapter 2: Alkane Oxidation Catalyzed by a Self-Folded Multi-Iron Complex

Chapter 3: Metal Coordination of Functionalized Self-folding Deep Cavitands

Chapter 4: Synthesis of New Cavitands for Biosensing in Water and Complex Environments

Chapter 5: Analysis of the Molecular Motion and Exchange Kinetics of Guests in a Water Soluble Cavitand.

Chapter 6: Experimental

LIST OF FIGURES

LIST OF TABLES

Chapter 1: Background

1.1. Long Term Goal

The ability to selectively oxidize one position on a hydrocarbon chain, an oxidation of linear unfunctionalized hydrocarbons with regioselectivity, is a critical example of the central goal of the conversion of feedstock chemicals to useful products in a mild and selective manner. This is a central goal of modern sustainable chemistry, the leading edge of greener science. This bio-inspired process is demonstrated by enzymes that are capable of selectively transforming a specific and singular C-H bond in the presence of other chemically equivalent bonds in the same molecule via proximity based interactions. These types of catalysts are known to effect C-H oxidation in mild conditions in laboratory settings, but still lacks the ability to obtain regioselectivity due to the necessity of steric or functional groups to direct the oxidation. The main goal of this project is to combine the concepts of molecular recognition and oxidation catalysis to create a small molecule mimic of enzymatic CH oxidation processes that is capable of both *recognition* of a hydrocarbon substrate, and catalyze its mild, regioselective oxidation. This involves the study of both hydrocarbon oxidation catalysis and hydrocarbon recognition and motion in the scaffolds.

1.2. Enzymes And Proximity Based Oxidation

Enzymes are capable of mild and gentle regioselective C-H oxidation. The selective transformation of one CH bond in the presence of a chemically identical group in the same molecule is performed *via* proximity-based interactions. Over 10,000 enzymes are capable of hydrocarbon oxidation, and each enzyme displays a different macroscopic

structure.[1] In the biosynthesis of cholesterol, three methyl groups in the precursor lanosterol are oxidized by cytochrome P-450 in the presence of far more reactive C-H bonds. The selectivity is controlled by non-covalent molecular recognition, and the selective positioning of the substrate in the active site, which only allows those specific methyl groups access to the reactive haem group. Many enzymatic structures include one or more metal centers in the active catalytic site, such as porphyrin-derived cytochrome P450,[2] Rieske non-haem iron oxygenases,[3] galactose,[4] and methyl monooxygenases.[5]

1.2.1. Porphyrin-based enzymes: Cytochrome P450

Cytochrome P450 is a porphyrin-based enzyme family that was discovered during the 1950s with a CO binding fluorophore with an absorbance maximum of 450 nm (Figure 1.1).[2] Cytochrome P450 includes over 11,500 different proteins and enzymes that are capable of hydroxylation of aliphatic C-H bonds with different selectivity.

The active site of cytochrome P450 features an iron-centered porphyrin with a *trans* labile site: one side anchors the haem group to the protein in the axial position while the second remains open for O_2 coordination and hydrocarbon oxidation.[2,6] The resting state of the iron center is low spin Fe (III) coordinating to one water molecule. The substrate hydrocarbon interacts with the catalyst and binds close to the metal active site. This is followed by electron transport from NADPH, generating an active intermediate iron (II). Coordination of O_2 forms the superoxo OO•, and the addition of an electron from NADPH forms the peroxo iron (III) **1.4** species. Cleavage of the O-O bond generates the iron (IV) oxo species **1.5** that carries out the oxidation of the substrate and forms water as a side product. [2,6]
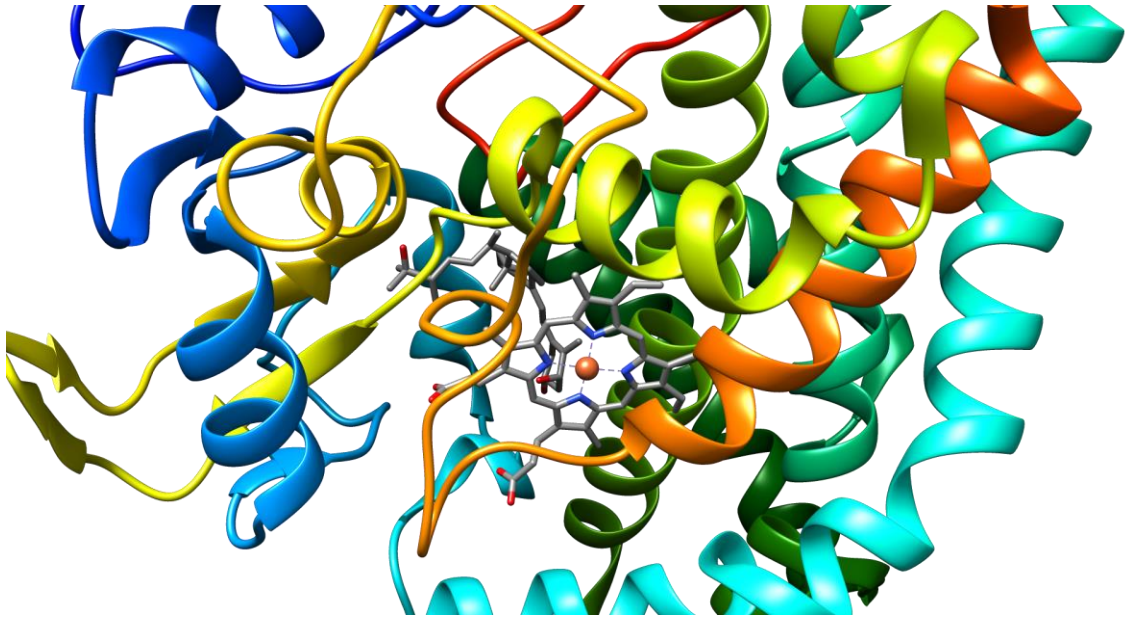
Figure 1.1. Cytochrome *P450*.
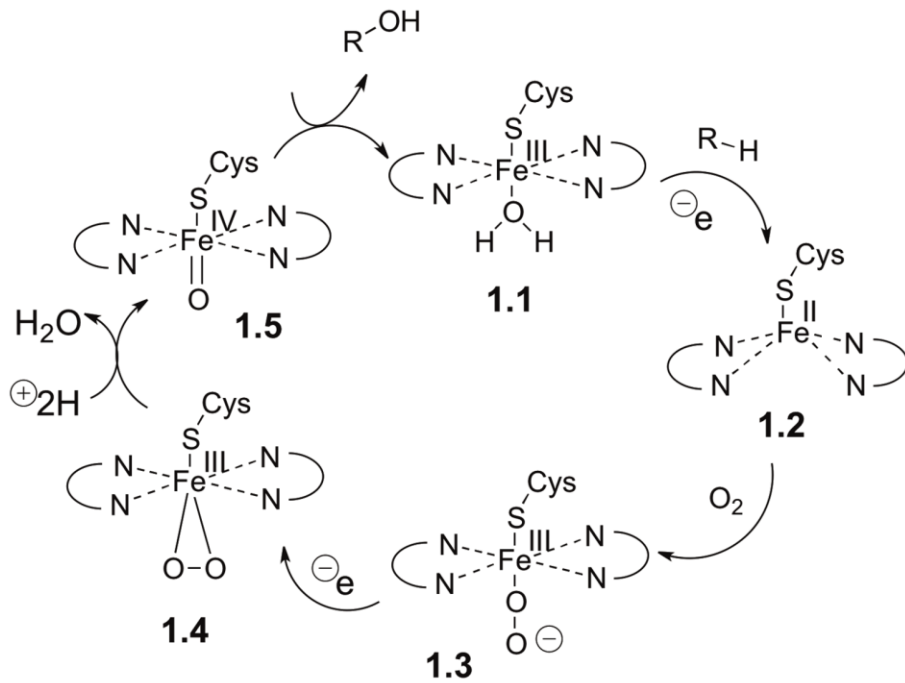
Figure 1.2. The catalytic cycle of hydrocarbon oxidation in the cytochrome P450 *trans* active site.

1.2.2. Rieske Non-Haem Iron Oxygenases

The family of Rieske non-haem iron oxygenases are not porphyrin-based enzymes, and function via a different mechanism, but the product outcomes are similar to those of cytochrome P450.[7,8] The Rieske non-haem iron oxygenases contain a [2Fe-2S] cluster, which transports electrons between three protein structures: ferredoxin, reductase, and an oxygenase that features both a Rieske [2Fe-2S] cluster domain and a mono-nuclear iron-containing catalytic domain. [3,7-10]

1.2.3. Non-Haem Methane Monooxygenases

Other similar enzymes have two-iron metal centers in close proximity, including methane monooxygenase (MMO) systems.[11-13] Methane monooxygenase produces methanol from methane in the presence of molecular oxygen. The catalytic cycle of MMO is mechanistically similar to that of the Rieske non-haem iron oxygenases.[14] The bridging coordination of the di-iron center by oxygen atoms (Fe-O-Fe) allows the selective oxidation of the C-H bond. The first metal acts as a coordinating metal to orient the substrate while the second supports the electron transfer for the oxidation. The catalytic cycle starts with the resting state of the active site having a low-spin iron (III) center. Once the substrate binds to the active site and accepts an electron from an oxidant such as NADPH,[15] forming an iron (II) intermediate, O_2 coordinates to the iron species, forming the active superoxo OO• agent to generate the active iron (IV) oxo species that transfers the oxygen to the hydrocarbon via radical mechanism (Figure 1.3).[2]
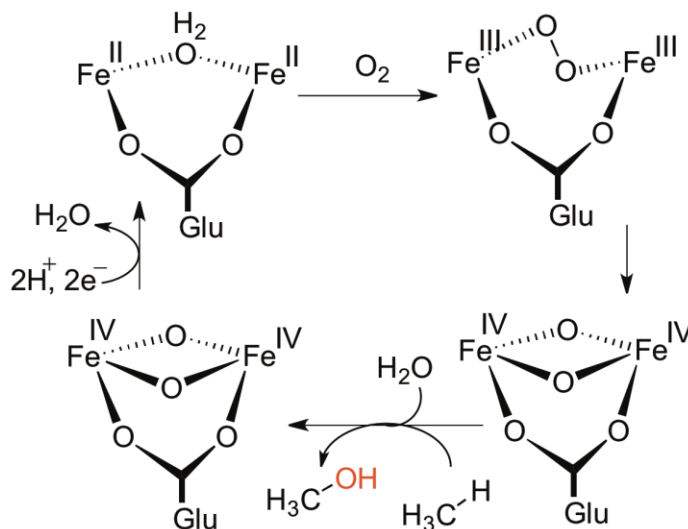
Figure 1.3. MMO catalytic cycle.[14]

1.3. Synthetic Examples of Chemoselective Oxidation

1.3.1. Chemoselective Oxidation

Enzyme catalyzed C-H oxidations are challenging to replicate in a synthetic laboratory. However, the mild pathways to activate C-H bonds are a desirable target for small molecule catalysts. Though conversion of C-H bond to functionalized species has been known for decades, many researchers have relied heavily on substrate-based steric or electronic effects to direct chemoselective oxidation.[16-19] Unactivated, linear hydrocarbon oxidation is very limited. The original approach relies on high temperature and high pressure for C-H oxidation,[20] but this lacks selectivity and causes decomposition of sensitive substrates.

In an effort to achieve selective hydrocarbon oxidation, a new generation of metal-ligand catalysts inspired by enzyme active sites have been synthesized. The most common and effective catalytic motif contains a tetradentate ligand coordinated to a

octahedral metal center, leaving two *cis*-oriented sites open to coordinate with solvent, anion, or a water molecule, which can be easily be replaced by the stoichiometric oxidant for catalysis.[21] [(TPA)Fe^{II}(CH$_3$CN)$_2$]$^{2+}$ **1.6** and the related [(BPMEN)Fe^{II}(CH$_3$CN)$_2$]$^{2+}$ **1.7** are two of the first examples of iron (V) oxo intermediates to be isolated and observed.[22] The [(TPA)Fe^{II}(CH$_3$CN)$_2$]$^{2+}$ and [(BPMEN)Fe^{II}(CH$_3$CN)$_2$]$^{2+}$ crystal structures were obtained, showing a *cis*-labile site on the metal center coordinating to the solvent.[23] [(TPA)Fe^{II}(CH$_3$CN)$_2$]$^{2+}$ stereoselectively oxidizes alkane substrates in the presence of H$_2$O$_2$ with remarkable efficiency, via similar catalytic pathways to the non-haem iron oxygenases.[24]

[(TPA)Fe^{II}(CH$_3$CN)$_2$]$^{2+}$ **1.6**   [(BPMEN)Fe^{II}(CH$_3$CN)$_2$]$^{2+}$ **1.7**
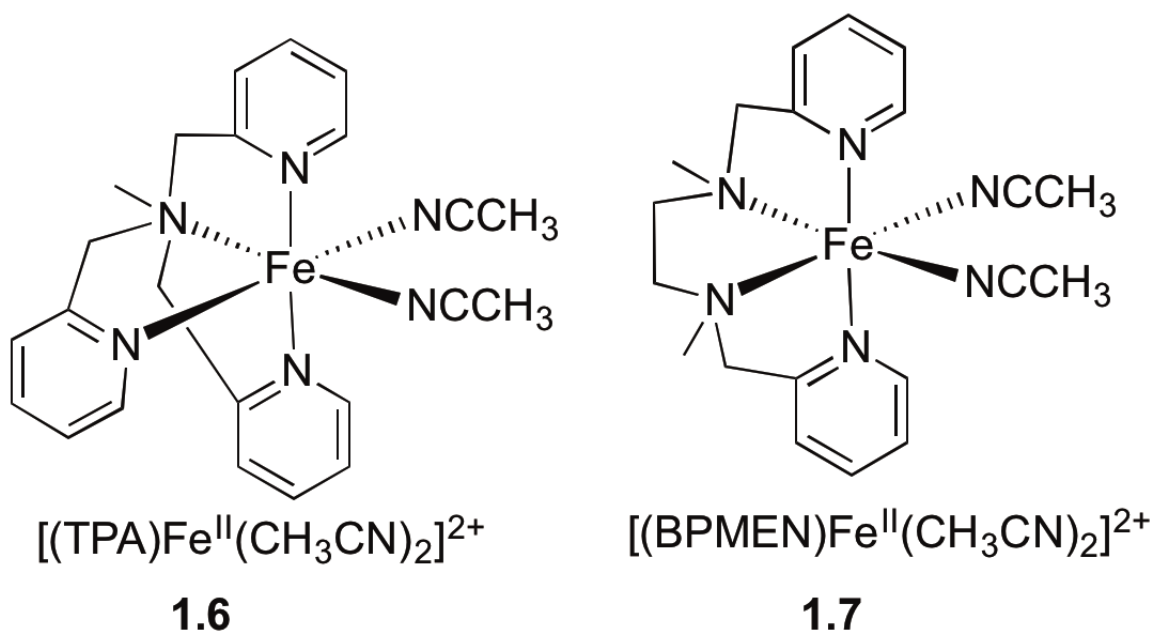
Figure 1.4. Monometal ligand catalysts **1.6** and **1.7** for chemoselective hydrocarbon oxidation.

The non-haem iron catalyst **1.6** and **1.7** features an octahedral iron center coordinating with a tetradentate ligand, leaving two *cis*-labile sites for oxidation using oxidant such as

hydrogen peroxide (H_2O_2) or tert-butyl hydroperoxide (TBHP). Other enzymes were shown to oxidize hydrocarbons *via* an iron (V) oxo **1.11** intermediate with *trans*-labile sites similar to non-haem iron catalysts (Figure 1.5).

1.8   **1.9**

1.11 Active Fe(IV) oxo species   **1.10**
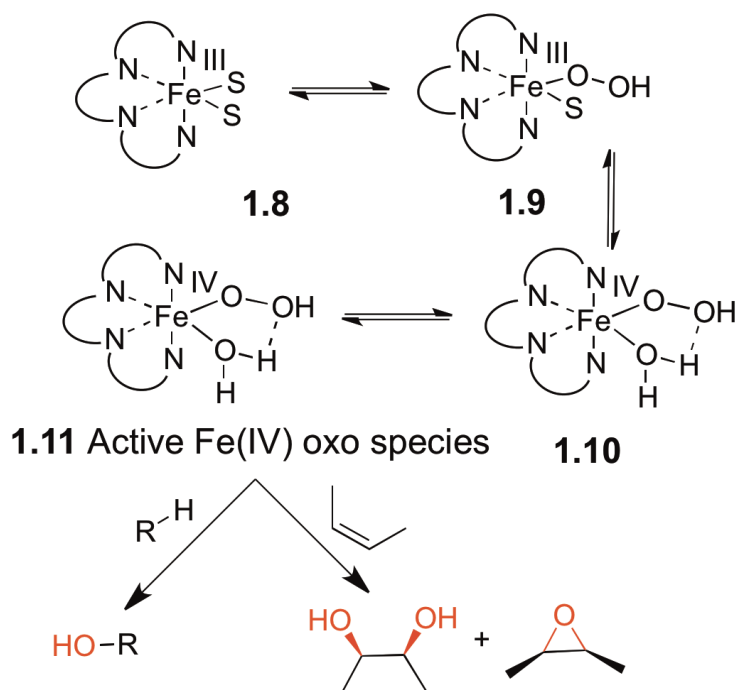
Figure 1.5. Catalytic cycle of non-haem iron oxygenases mechanism.

Both $[(TPA)Fe^{II}(CH_3CN)_2]^{2+}$ and $[(BPMEN)Fe^{II}(CH_3CN)_2]^{2+}$ can also oxidize olefins in the presence of H_2O_2 to yield epoxides and *cis*-diols. The addition of acetic acid to the oxidation reaction inhibits *cis*-dihydroxylation and enhances epoxidation. Reactions were carried out at 0 °C with 0.5 mol % catalyst for both systems in a 1:2 CH_3CN/CH_3COOH solvent mixture. High loading of the oxidant (1:1.5 olefin/H_2O_2 ratio) resulted in nearly quantitative conversions of cyclooctene to epoxide within 1 min.[16,24,25] Both $[(TPA)Fe^{II}(CH_3CN)_2]^{2+}$ and $[(BPMEN)Fe^{II}(CH_3CN)_2]^{2+}$ catalyze the hydroxylation of

alkanes to tertiary alcohols and retain the alkanes' chemical configuration. *Cis*-1,2-dimethylcyclohexane was oxidized to (1*R*,2*R* or 1*S*,2*S*)-1,2-dimethylcyclohexanol. The oxidation occurred opposite the methyl group leaving both the methyl groups *cis* to one another. Likewise, *trans*-1,2-dimethylcyclohexane was oxidized to (1*R*,2*S* or 1*S*,2*R*)-1,2-dimethylcyclohexanol, where the methyl groups once again retained their conformation (Figure 1.6). This retention of configuration was also observed in the oxidation of other cyclic *cis* and *trans*-hydrocarbons such as adamantane and *trans*-decalin. The stereoisomers observed are due to a short lived alkyl radical with shorter lived planar conformation on the alkyl substrate.[21] The theory that the mechanism goes *via* a short-lived radical was further supported by the oxidation product of methylcyclohexane.[26] The tertiary position is oxidized much faster than the secondary, with >5% methylcyclohexanone product and 86% 1-methylcyclohexanol.
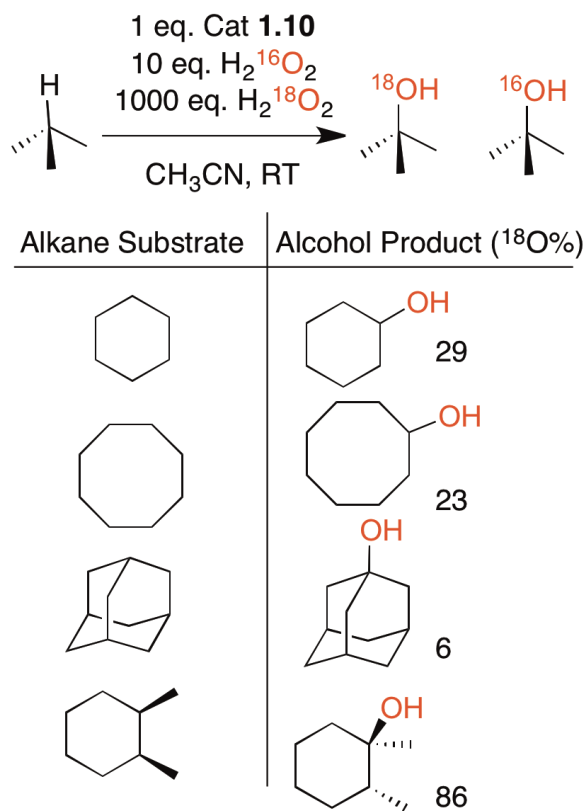
Figure 1.6. ^{18}O incorporation using catalyst **1.6** from 500 eq. of alkane substrate.

While **1.6** $[(TPA)Fe^{II}(CH_3CN)_2]^{2+}$ and **1.7** $[(BPMEN)Fe^{II}(CH_3CN)_2]^{2+}$ are mono-iron catalysts, a di-iron catalyst **1.12** was synthesized to more closely resemble an MMO catalytic active site.[6] This catalyst featured the same Fe(V)oxo core species that can be activated by water or alcohols to allow C-H bond oxidation. The substrate functionalization allowed the selective C-H oxidation over more reactive C-H bonds or even unfunctionalized substrates. With only the most reactive/steric C-H bond oxidation however, no regioselectivity was observed.
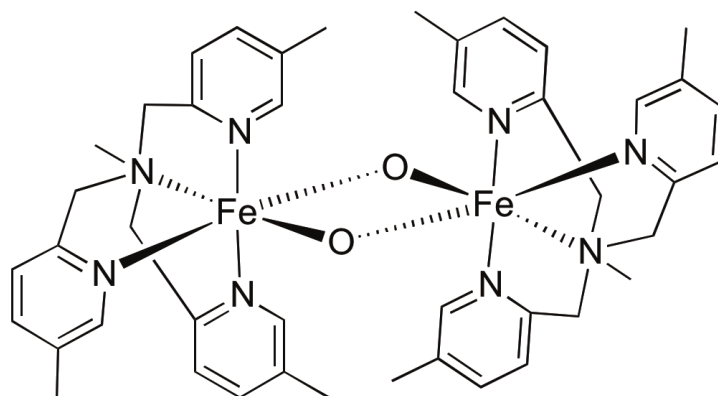
Diiron (3-Me$_3$-TPA)$_2$ Complex

1.12

Figure 1.7. Di-metal iron complex **1.12** for hydrocarbon oxidation, more accurately mimicking MMO non-haem iron oxygenases.

For a more chemoselective oxidation of unactivated sp^3 C-H bonds, a similar ligand to **1.7** was synthesized, namely (Fe(*S,S*-PDP) **1.13**. The chemoselectivity of hydrocarbon oxidation with this catalyst was dependent on the substrate structure, and the reaction occurred with stoichiometric H$_2$O$_2$ and substoichiometric acetic acid.[27] The innovative scaffold introduces small modifications to the original Fe^{II}(BPMEN), yet it shows high selectivity for the desired 3° oxidative product, as shown in Figure 1.8b.

a)

(SbF₆)₂

Fe(S,S- PDP)

1.13

b)

x Cat. 5 mol%
y% AcOH
1.2 eq H_2O_2
MeCN, rt.

Catalyst	AcOH (equiv.)	Yield (%)	Conv. (%)	Select (Yield/conv.)
Fe^{II}(BPMEN)	0	7	12	56
Fe^{II}(S,S-PDP)	0	14	15	95
Fe^{II}(BPMEN)	0.5	26	41	62
Fe^{II}(S,S-PDP)	0.5	38	42	90
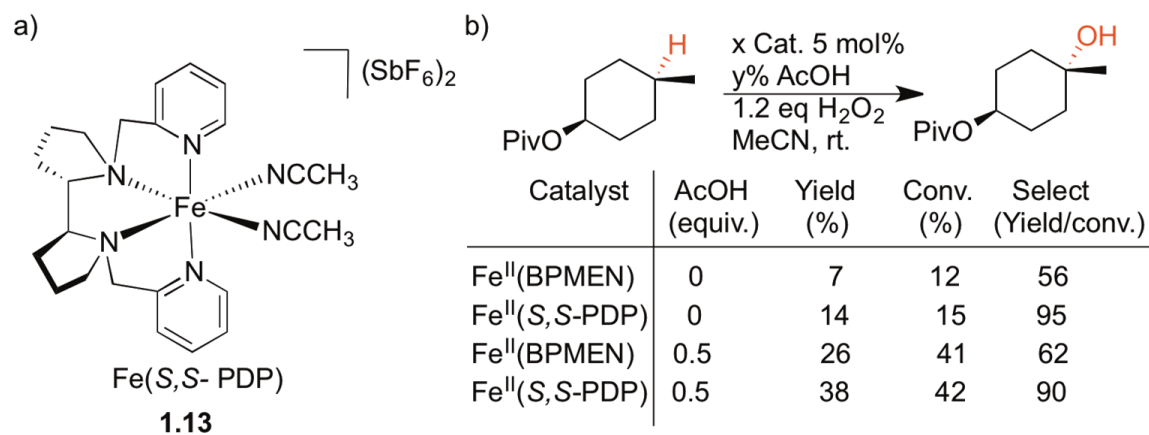
Figure 1.8. a) Chemoselective catalyst **1.13**, b) Comparison between the different catalysts **1.13** and **1.7**.

Ligand **1.13** Fe(*S,S*-PDP) also shows retention of stereochemistry in the oxidation of tertiary substrates (Figure 1.9, entry 5,6). The reaction is also tolerant to electron rich cyclic ethers, carbonates, esters, and electron deficient amides (entry 3-6). Reaction occurs mainly at the tertiary position, however the secondary CH bond can be oxidized in the absence of a tertiary CH bond with substrates such as cyclohexane.
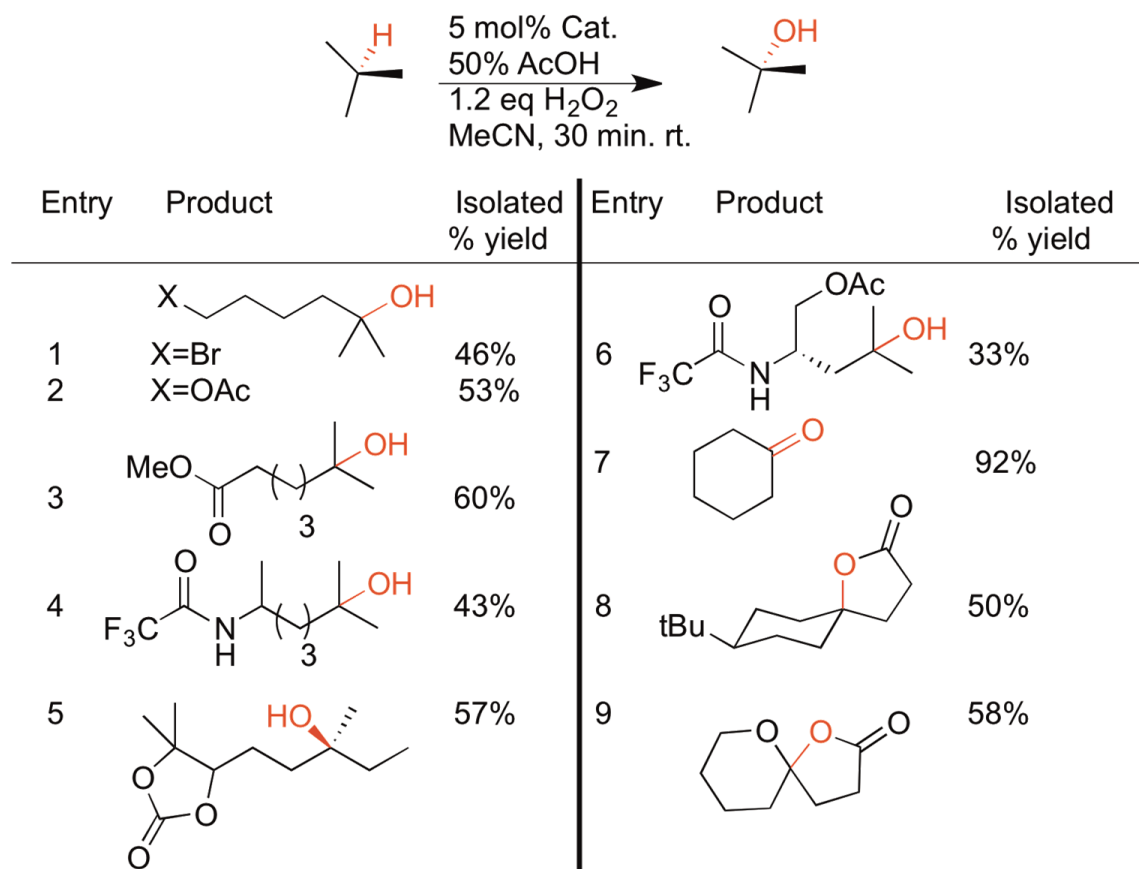
Figure 1.9. Sterically and electronically directed hydrocarbon oxidation with catalyst **1.13.**

When the electron-withdrawing group was shifted away from the tertiary position on the substrate, reaction occurs much faster, with higher isolated yields. In addition, nearby carboxylic acid groups are capable of participating in the oxidation, forming lactone products upon intramolecular oxidation of the axial tertiary C-H bond (Figure 1.9, entry 8).

These C-H oxidations are very mild, and mimic enzymatic activities, so can be used for late stage oxidation in the synthesis of complex natural products. These more advanced

applications of **1.13** were tested in the late stage oxidations of artemisinin, taxane, and gibberellic acid. These substrates undergo C-H oxidation using **1.13** as catalyst, relying on electronic and intermolecular interactions for selectivity, as shown below (Figure 1.10). [27,28]
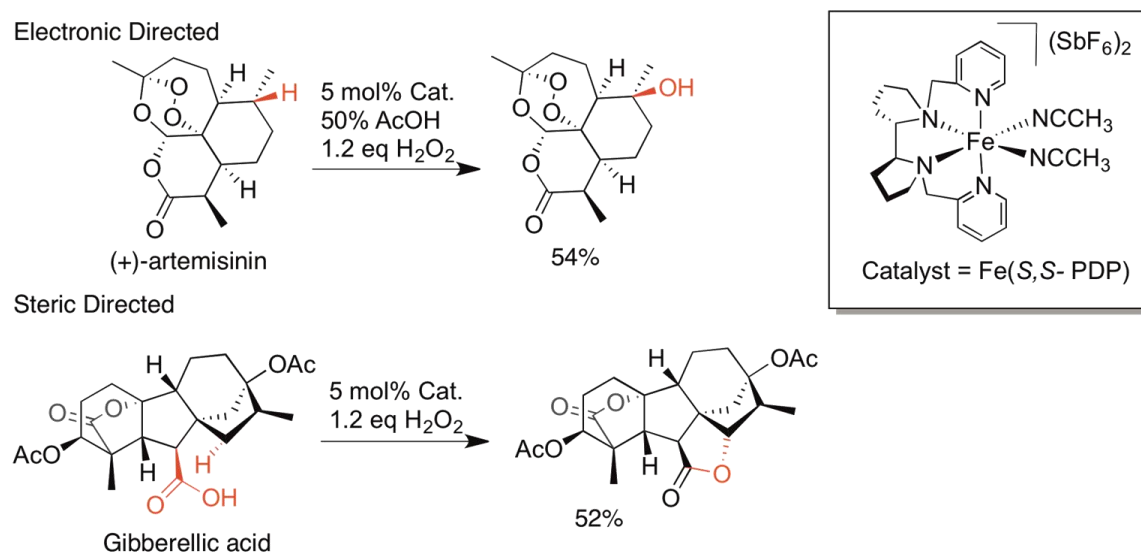
Figure 1.10. Sterically and electronically directed C-H oxidation of more complex molecules using catalyst **1.13.**

Highly successful C-H oxidation for very complex substrates was achieved with good chemoselectivity, which relies heavily on a directing group in the substrate. Chemoselective oxidation is valuable for oxidizing the most electronic rich C-H bond or at the most sterically hindered position. However, the true mimic of enzymatic activity, proximity-directed oxidation, is much harder to achieve. Synthesizing a scaffold that contains both a cavity for molecular recognition as well as a metal-containing active groups would truly mimic enzymatic structure. In that case, the oxidation will not rely as

heavily on the hydrocarbon substrate but mainly the orientation and position of the substrate near the catalytic site.

1.3.3. Synthetic Examples of Proximity-Directed Regioselective Oxidation

There is some precedent for the combination of molecular recognition and site-selective C-H oxidation. By using water-soluble recognition motifs for the binding of derivatized steroids, the target can be oriented in close proximity to a manganese-centered porphyrin, inspired by haem active sites. β-Cyclodextrin is a well-known water-soluble recognition motif, and so a scaffold that mimics cytochrome p450 was created by appending four units of β-cyclodextrins to a manganese-porphyrin core to introduce directing motifs near the active site.[29,30] Catalyst **1.14** uses the host:guest interaction of the β-cyclodextrin to correctly align large derivatized steroids, such as substrate **1.16,** towards the manganese porphyrin active site to undergo proximity-based CH oxidation. Upon binding and orienting the substrate **1.16**, only one C-H bond is close enough to the active metal to be oxidized. Although the oxidized C-H bond is not the most reactive C-H bond in the molecule, the proximity effect directs the selectivity. A slight change in the β-cyclodextrin position in relation to the active site shows much higher selectivity for oxidizing a different C-H bonds in steroid substrate **1.18**, to yield 100% formation of **1.20** rather than a 50:50 ratio of **1.19**:**1.20** oxidation products.

To enhance turnover, and the stability of the catalyst, fluorinated phenyl rings were added to the porphyrin core, forming **1.14b** and **1.15b**. The more stable fluorinated

porphyrin **1.15b** enhances the number of turnovers from 2.5 (with **1.15a**) to >90, mainly due an increase in the scaffold solubility.[31]

1.14a: R = H
1.14b: R = F

1.15a: R = H, x = H
1.15b: R = F, x = F
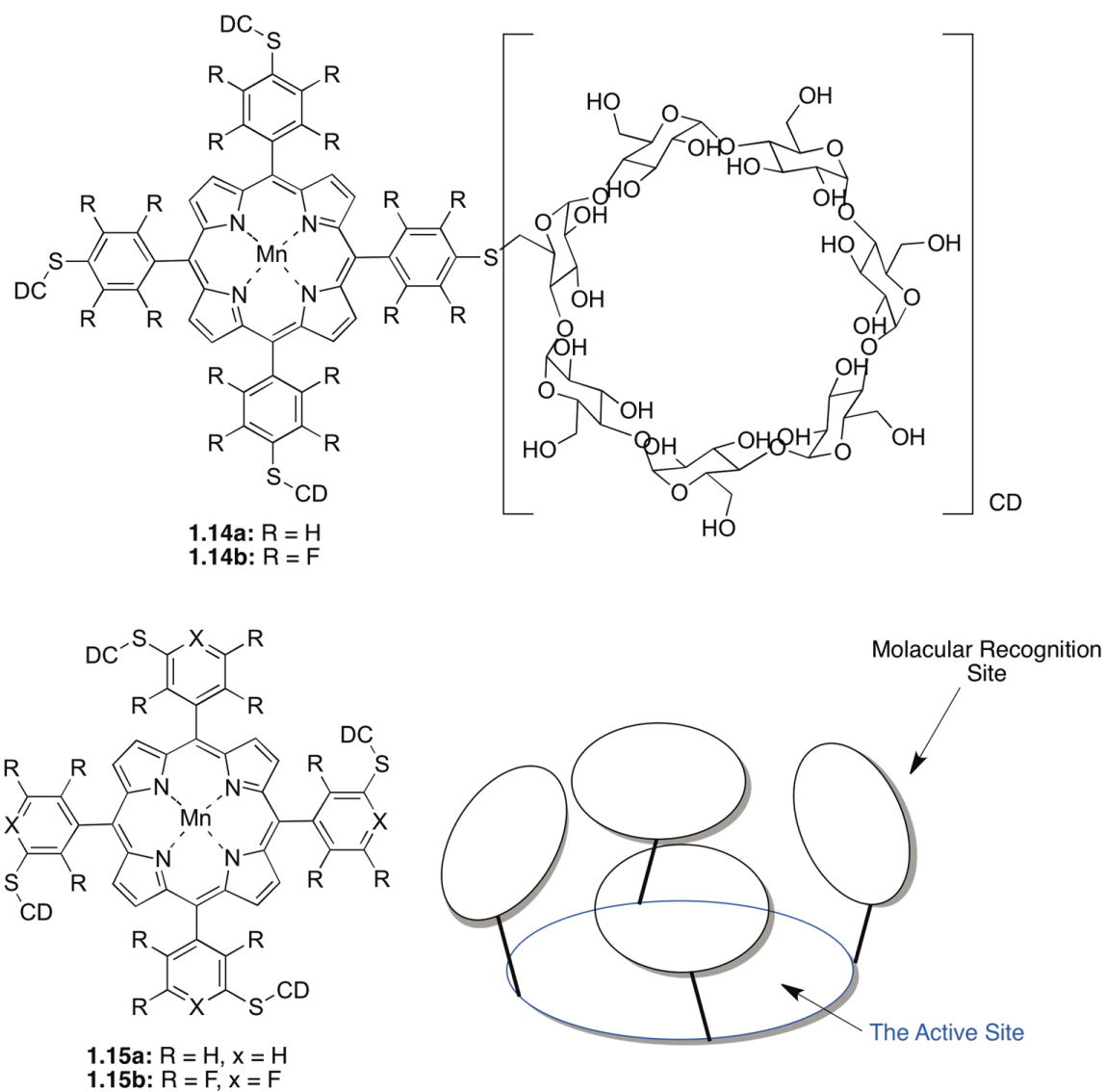
Figure 1.11. Structure of catalysts **1.14a-b** and **1.15 a-b**, and a cartoon stimulation of the catalyst structure.
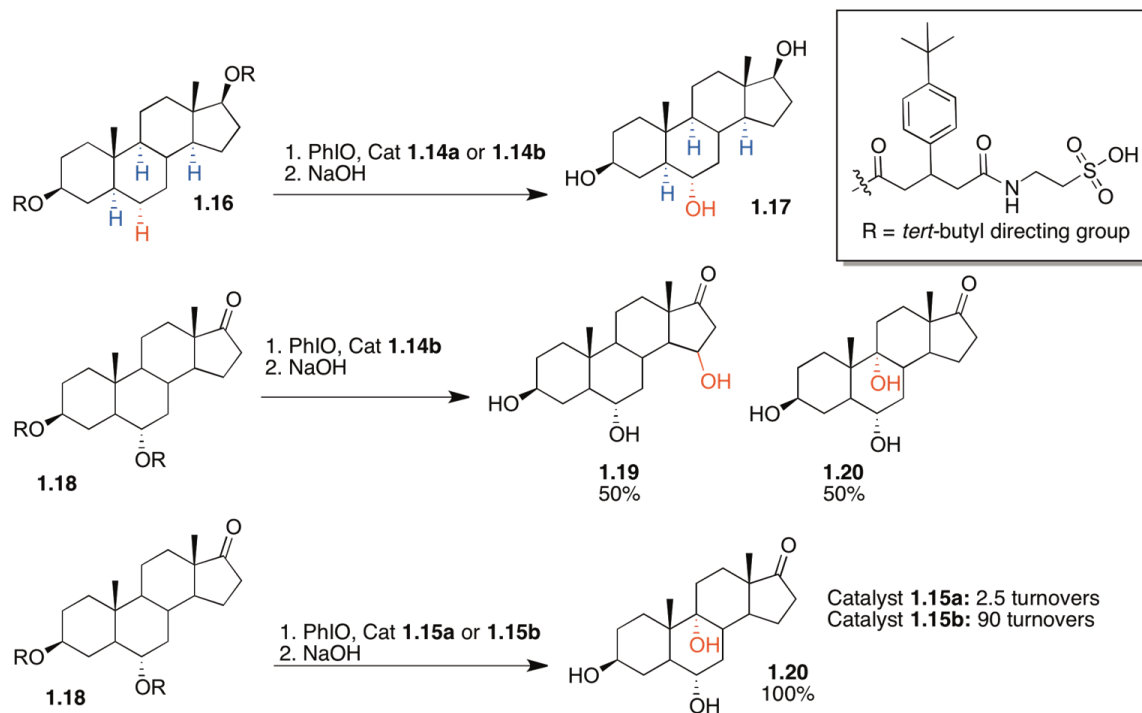
Figure 1.12: the selective oxidation of steroids **1.16** and **1.18.**

1.4. Limitations of C-H Oxidation Catalysts

1.4.1. Performing C-H oxidation in a Mild Manner

Another challenge of hydrocarbon oxidation is to not overoxidize the substrate.[32] Due to the harsh conditions of most oxidations, using strong acids such as acetic acid and strong oxidants such as H_2O_2 under high temperatures and pressure, hydrocarbons tend to fully oxidize without selectivity, which causes multiple products.

1.4.2. Non-Covalent Recognition of Hydrocarbons In Water

These P450 mimics require the presence of the *tert*-butylphenyl binding handles in the steroid derivative to allow binding to occur, and cannot oxidize unfunctionalized targets.

In addition, classical chemical catalysts are incapable of recognition and proximity-directed regioselective oxidation. Many challenges must be overcome when attempting truly biomimetic hydrocarbon oxidation. While chemoselectivity can be achieved in mild conditions, it relies heavily on steric and electronic factors present in the substrate. The selectivity is only controlled by the substrates and not the catalyst. To achieve proximity-based oxidation, the only successful example is to alter the natural state of the substrate with directing groups, such as the *tert*-butylphenyl group shown above. Those catalysts are limited to a very narrow substrate scope as they require precise alignment of the substrate with the catalyst active site, which also relies heavily on the substrate directing group rather than the intrinsic reactivity of the catalyst. A catalyst that can differentiate between C-H positions that are electronically and sterically similar for a wide scope of substrates simply does not exist. Furthermore, the use of directing groups in the substrate tends to limit the scope of oxidation. Only substrates with "directing groups" would be bound and oxidized. The catalyst would only bind to one substrate, which means for every desired substrate, a new catalysis must be synthesized.

A recognition motif utilizing hydrophobically-driven guest binding could control hydrocarbon interactions with the catalyst to align the substrate in one orientation. Water-soluble scaffolds with electron rich cavities can exploit to the hydrophobic effect to favor target binding. Upon non-covalently binding the hydrophobic hydrocarbon in the catalyst's active site, regioselective oxidation could be possible. Additionally, water is a beneficial solvent for C-H oxidation reactions because it is not prone to oxidation. To combine aspects of both successful hydrocarbon chemoselective oxidation and proximity

based oxidation of unfunctionalized substrates in mild conditions, one must utilize the hydrophobic effect. The hydrophobic effect eliminates multiple oxidations to the same molecule, as oxidized hydrocarbons tend to have higher solubility in water than their precursors. Once an unfunctionalized hydrocarbon is oxidized, the product is released into the water layer, which increases the turnover to the catalyst.

1.5. Water Soluble Scaffolds for Aqueous Hydrocarbon Recognition

Water-soluble synthetic receptors are extremely valuable because water can act as the driving force for guest binding close to the active site. Meanwhile, the hydrophobic effect controls the guest:host chemistry mainly due to the hydrophobic nature of unfunctionalized hydrocarbons. The desired hydrocarbon oxidation catalysts can be synthesized by incorporating a hydrophobic pocket in close proximity to the oxidation active site in water-soluble scaffolds. The entropic benefit of separating the hydrophobic substrate from the water molecule is complemented by the enthalpic benefit of London dispersion forces between the host and the guest. By exploiting the hydrophobic effect, a water-soluble molecular recognition scaffold with a catalytic site in close proximity would be an ideal receptor to a wide scope of close proximity C-H oxidation.

1.6. Introduction to Molecular Recognition Scaffolds

To achieve and replicate the proximity-based recognition that is seen in enzymes in a synthetic system, one must look to molecular recognition scaffolds, synthetic molecular

receptors that have found a great deal of success in supramolecular chemistry and guest recognition.

"Tweezers" and "clips" are two of the first hosts capable of hydrocarbon molecular recognition, established by Whitlock in 1978.[33,34] Clips and tweezers surround the (often aromatic) guests in order to exploit van der Waals interaction for effective molecular recognition. Most of these clips rely on functionalized U-shaped molecules that contain a flat linear spacer backbone and aromatic arms. The U-shaped recognition concept was known as a "molecular sandwich." [34] The first generation of these molecular sandwiches was **1.21,** which exploited a linear spacer with two flat, aromatic, and identical arms composed of two caffeine groups. The rigid spacer forces the arms into a *syn* conformation for desired guest binding. The initial strategy was to use an alkyne spacer of 7 Å in length, which provided sufficient space between the arms. Those first-generation scaffolds bound mostly aromatic guests such as 6-dihydroxybenzoate and 1,3-dihydroxy-2-naphthoate in buffered aqueous solution. [33] Other variations of similarly designed scaffolds were reported to bind small aromatics such as benzene and naphthalene derivatives. [35-37]

However, many of those hosts favor self-dimerization *via* π-π interactions, which competes with guest binding.[38] Host scaffolds evolved from simple tweezers to a more functionalized backbone using phenylglycoluril units by Nolte.[39] The phenylglycoluril provided a more curved backbone, which created a shallow concavity with a straightforward synthetic route *via* reacting with formaldehyde. Simple extension of the sidewalls allowed the accommodation of a variety of different guest shapes and sizes.

Most variants of **1.22a** bind aromatic substrates, varying in size from resorcinol (K_a = 200 M^{-1}) to catechol (K_a = 80 M^{-1}), in addition to more functionalized aromatics.[39] Simple changes to the aromatic substitution to **1.22b** could accommodate more electron rich aromatic molecules such as olivetol (5-pentylresorcinol), resorcinol, and dihydroxybenzene (K_a = 1500 M^{-1}, K_a = 2600 M^{-1}, and K_a = 7100 M^{-1} in $CDCl_3$, respectively).[39,40] Unfortunately, most of these scaffolds rely heavily on the functionalization of the guest, as it only binds small aromatic substrates. They are too prone to self-inclusion and often self-dimerization, at a much faster rate than binding with the desired target (Figure 1.13).[38]

1.21

1.22a: R = H,
1.22b: R = OMe

1.23a: R = $(CH_2)_3CO_2H$
1.23b: R = $(CH_2)_3SO_3Na$
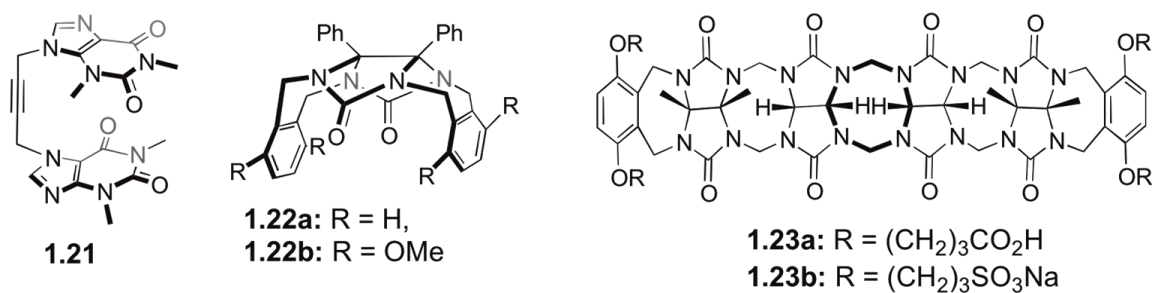
Figure 1.13. Early clips and tweezer scaffolds.

To maximize the interaction between the guest and the host walls and to minimize self-dimerization, a more evolved host of the phenylglycoluril backbone was provided by an opened macrocyclic cucurbit[*n*]uril scaffold. The open-ended macrocyclic clips are water soluble (up to 105 mM) in aqueous environments with large internal surface areas.[41] The scaffold **1.23a** shows strong binding affinities for α-ω alkanediamines, ranging from 1.4 x 10^6 M^{-1} for 1,4-butanediamine to 2.2 x 10^8 M^{-1} for the longest encapsulated alkyl chain

of 1,8-octanediamine. Large flat aromatic amines such as rhodamine 6G and *p*-xylylenediamine were also bound strongly (K_a = 2.1 x 10^5 M^{-1} and 6.8 x 10^8 M^{-1}, respectively). However, binding to more bulky polycyclic amines such as adamantanamine or *N, N'*-dipropyl-*p*-xylylenediamine was much stronger (K_a = 3.5 x 10^6 M^{-1} and 2.2 x 10^9 M^{-1}, respectively). The weaker affinity was due to the lack of ionic interaction between the guest and the open-ended host upon encapsulation, and the main driving force was only π-π or π-CH interactions between the *xylylene* walls of the host and the guest rings.[41,42] The sulfonate cucurbiturils **1.23b** were capable of drug molecule binding in challenging environments, and showed solubility enhancements of the anticancer agent albendazole.[43,44] The sulfonated scaffold bound albendazole with an affinity K_a = 5.1 x 10^4 M^{-1}, which compares very favorably with its solubilization by hydroxypropyl-β-cyclodextrin (K_a = 5.4 x 10^3 M^{-1}). More complex species such as paclitaxel, melphalan, amiodarone, clopidogrel, and cinnarizine all showed increased solubility with **1.23b** (by 2750-fold, 655-fold, 267-fold, 1220-fold, and 354-fold, respectively).[44] While these cucurbituril scaffolds are effective hosts, they are unsuitable for our purposes, as they are challenging to derivatize and lack "handles" for binding the requisite metals to allow oxidation catalysis. They also lack the preorganization to fix or orient the guest into the cavity due to their only having two available arms.

1.7. Shallow Bowls: Resorcinarenes

Toroidal and clip-shaped cucurbiturils only cover half of the surface area of the guest. Scaffolds with greater curvature are much more promising hosts for greater control and

desirable coverage of the guest. Bowl-shaped scaffolds can provide a starting point for the creation of hosts fully surround the guest. Many early systems had linear all-carbon backbones,[45-48] but synthesis of all-carbon half capsules is extremely challenging. Many of those guests tend to be cyclic or aromatic, relying heavily on π-π interactions.[49] Unfunctionalized linear hydrocarbon alkanes, however, are much more challenging to recognize due to their flexibility. To completely surround the guest in a functionalized host, a simpler strategy was to introduce an oxygen-containing carbon skeleton rather than an all-carbon skeleton. Condensation of resorcinol derivatives via electrophilic aromatic substitution reaction with aldehydes with various lengths leads to small shallow bowl scaffolds called resorcin[4]arenes **1.24**.[50] The alkyl "R" groups from the aldehyde are oriented in the same direction, and confer structural stability on the system, acting as the "feet" (Figure 1.14). The functionalization of these feet changes the system's solubility and properties without affecting the upper rim binding site.
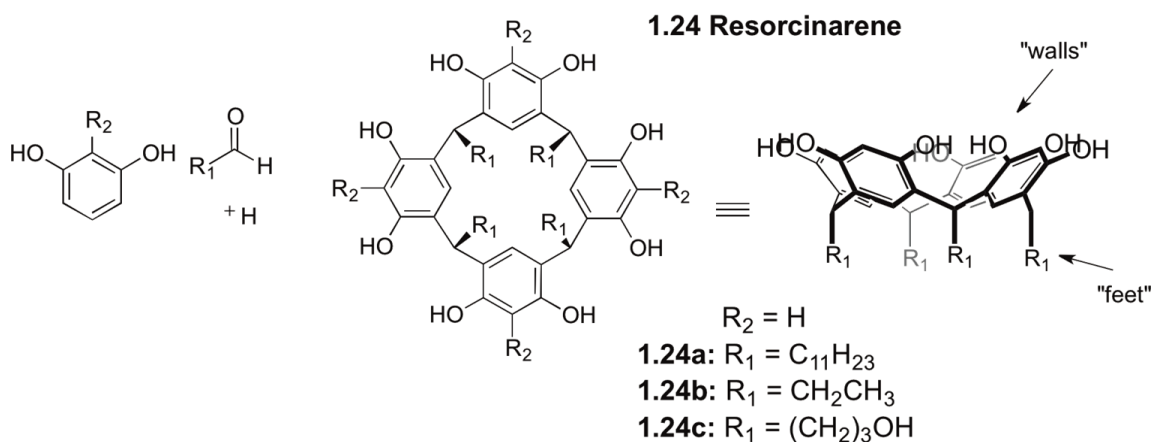
Figure 1.14. Synthesis of the shallow resorcinarene base.

This provides shallow curvature and a reactive phenolic position for derivations. The eight hydroxyl groups on the top of the bowl helps form the cavity by H-bonding with four molecules of water providing a stable shallow bowl-like structure with C_{4v} symmetry.[51-53] The parent resorcinarene forms a capsular aggregate in non-polar solvents and the solid state, forming a hexameric "snub-cube" assembly. The crystallographic properties have been extensively investigated.[54] The resorcin[4]arene hexamer cavity of 1400 Å is capable of binding multiple guests such as tetraethylammonium ($K_a = 5 \times 10^2$ M^{-1}) and tetramethylammonium cations ($K_a = 3 \times 10^5 \ M^{-1}$)[55] *via* space filling and cation-π interactions. Despite the large cavity, neutral guests are poorly bound.

1.8. Shallow and Deep Cavitands

To further functionalize the resorcin[4]arenes, Cram rigidified the skeleton by bridging the phenols with methylene units to create "cavitands" **1.25**. The cavities of those cavitands range from 3.3-4.2 Å, which provides limited and weak binding affinity to small organic molecules such as CH_2Cl_2, CH_3CN, CS_2, CD_3NO, and $C_6H_5CH_3$.[56] While cavitands **1.25** are shallow with weak binding abilities, they are amenable to further derivatization and the possibilities of creating much deeper cavities. While the first generation of cavitands binds small molecules, the cavity must be extended with "walls" in order to bind larger guests.

The two most common derivatizations exploiting the weakly nucleophilic phenols on the resorcinarene are via S_NAr reaction with either 2,3-dichloropyrazine or 1,2-difluoro-4,5-dinitrobenzene, yielding **1.26** and **1.27** respectively.[57] Cram originally synthesized

1.26a by reacting **1.25a** with 2,3 dichloroquinoxaline. The quinoxaline cavitand **1.26a** was deeper than the resorcinarene, yet the walls were flexible and interconvert (11 kcal mol^{-1}) between two conformations, called the "kite" and "vase" conformations. The energy required to interconvert between conformations is determined by the ring flip required to rotate about the C-O bonds on the resorcinarene (Figure 1.15). The quinoxaline cavitand is observed in the kite-like conformation at below 5 °C.[58-60] The main method to monitor the different conformations is ^{1}H NMR. In the case of the vase-like conformation, the methane CH proton at the bridging carbon resonates above 5 ppm. In the kite conformation, this proton resonance shifts dramatically upfield due to it being present in the induced magnetic field of the aromatic rings of the resorcinarene base, causing it to be more shielded and shifting to almost 3 ppm.
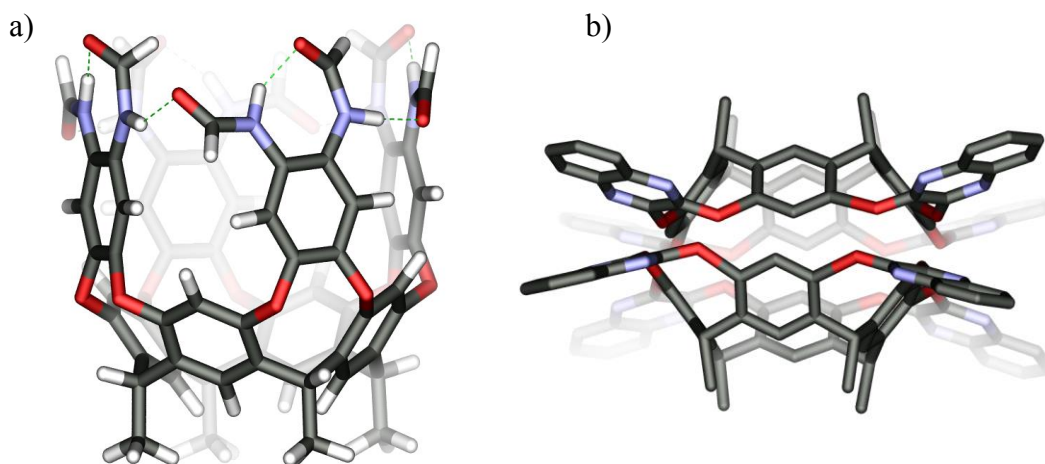
Figure 1.15. a) H-bonding interaction of octamide cavitand **1.28** forming the vase conformation, b) Quinoxaline cavitand **1.26** in velcrand conformation.

The kite conformation, which has a small cavity, often forms a dimeric aggregate (called a "velcrands") as is seen with clips and tweezers. The vase conformation is the desired conformation, as it has a deep bowl that can bind neutral guests such as disubstituted arenes with affinities of 20-200 M^{-1}.

The quinoxaline cavitands showed promising results. However, their flexibility and the dominance of the velcrand conformation caused by intermolecular π-π interactions limited the host properties. Rebek provided the solution, whereby self-folding principles are applied to the structure to introduce self-complementary hydrogen-bonds, aided by water or methanol, to stabilize the vase conformation. The scaffold competes to favor the intermolecular interaction (hydrogen bonding) rather than intramolecular interaction of the π-π stacking, which forms the velcrand.[61,62] Both self-folding scaffolds are prepared via reaction of the resorcinarene **1.24** and 1,2-difluoro-4,5-dinitrobenzene, yielding octanitro cavitand **1.27.** Cavitand **1.27** is then reduced to the parent octamine cavitand **1.28** *via* harsh reduction conditions such as hydrazine and Raney Nickel or $SnCl_2$/HCl.

1.24 Resorcinarene
  a: R = $C_{11}H_{23}$
  b: R = CH_2CH_3
  c: R = $(CH_2)_3OH$

1.25 Cavitand

1.26 Quinoxaline Cavitand

1.27 Octanitro Cavitands

$SnCl_2 \cdot 2H_2O$
HCl, EtOH, 65 °C

1.28 Octaamine Cavitands

H_3C R

1.29 Octamide Cabitand
  1.29a: R' = Et
  1.29b: R' = Ph
  1.29c: R' = CF_3
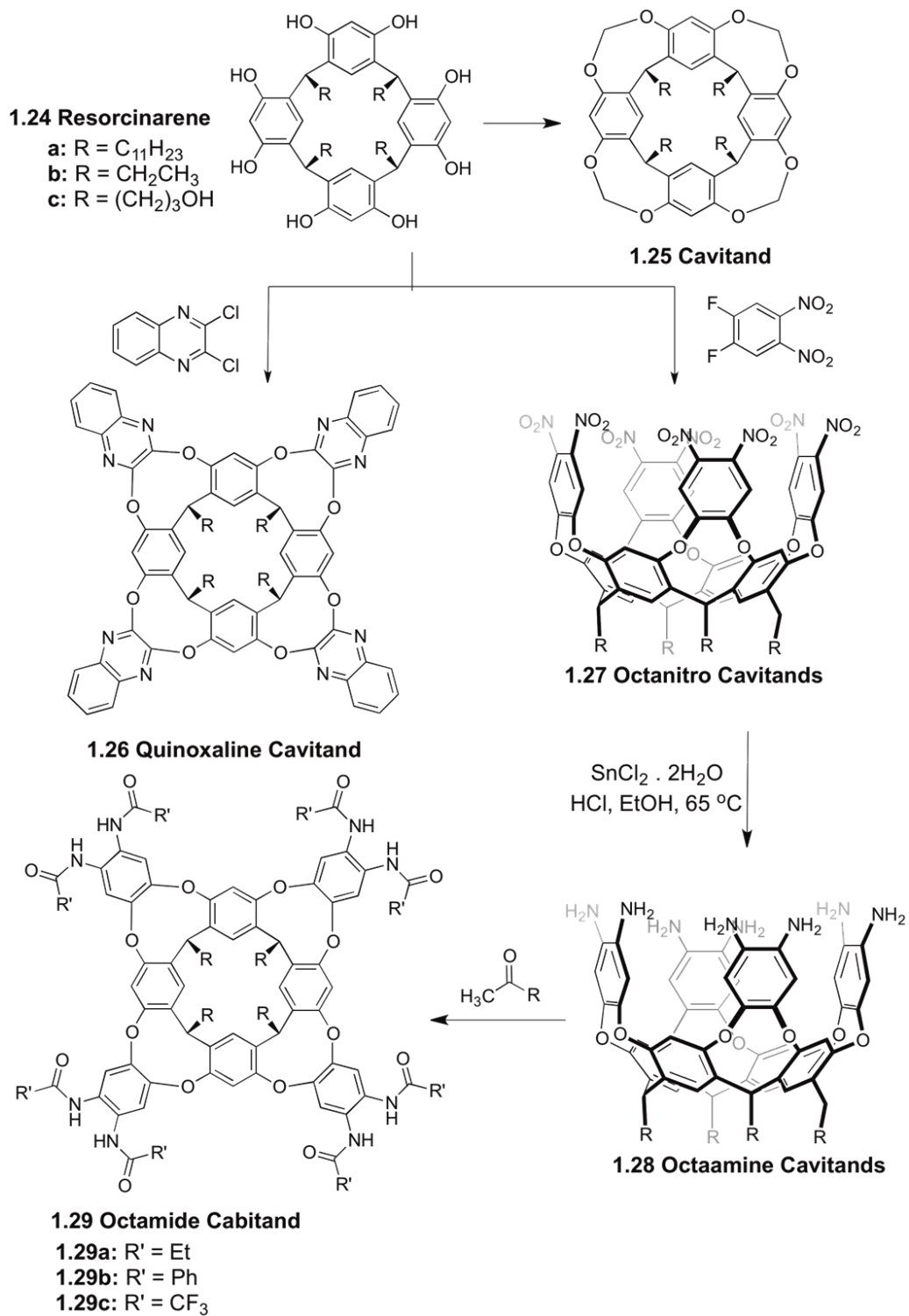
Figure 1.16. The synthesis of deep cavitand scaffolds.

26

The octamide cavitand scaffold **1.29** can be synthesized *via* acylation of the octamine cavitand **1.28**, resulting in directional hydrogen bonding at the upper rim. Both the oxygen and the N-H groups in the amides are involved in the H-bonding interaction at the rim. The ostensive chiral system favors recognition of suitably sized guests with soft charges such as trimethylammonium or alkyl quinuclidinium ions that can exploit cation-π interactions with electron-rich walls. Neutral guests with a thin coating of partial positive charge at the surface species such as hydrocarbons are also encapsulated by the octamide cavitand in solution. The strongest substrate binding typically occurs when the guest shows 55% occupancy of the cavity.[63] *N*-alkyl groups are weakly bound in organic solvents such as CDCl$_3$ due to solvent competition. Cycloalkanes and substituted cycloalkyl groups (C$_5$-C$_{12}$), cyclic amides (pyridine and caprolactam), quinuclidine, and a wide range of adamantane derivatives bind strongly even in organic solvents due to the preorganized cyclic nature which fills the internal cavity (affinities on the order of the 100-10,000 M^{-1}).[64-67] Guest in/out exchange in these scaffolds is slowed due to a high kinetic barrier ($\Delta G^{\ddagger}$ = 5-8 kcal mol^{-1}). The high kinetic barrier was due to two components: the rotation about the C-O-C bond to open the aromatic walls (similar to **1.26** quinoxaline cavitand) and the breaking of the H-bonding seam. While guest exchange was limited, guest motions such as tumbling and coiling inside the cavity were observed and well-studied with dissymmetric guests such as vinyladamantane. [68-70]

1.9. Benzimidazole Cavitands

To further deepen the octamine scaffold and study guest binding and exchange, a condensation reaction-using hydrocarbon with the precursor octamine or the octanitro cavitands **1.28** or **1.27** to yield **1.30** was utilized for introduction of various benzimidazole groups at the rim **1.30a-e**.[71] The self-folding benzimidazole cavitand **1.30a** favored the vase conformation, aided by hydrogen bonding with four water molecules, which intercalated between the benzimidazoles.[72] Guest binding ability in organic solvents was limited due to solvent competition, similar to that seen with **1.28**. Additionally, the requirement for a protic cosolvent to effect H-bonding and self-folding limited the range of solvents in which the cavitand was soluble. Substituted trimethylammonium ions were the most strongly bound guests for two reasons: these molecules' perfect size matching to fill the cavity and their cation-π interactions with the cavity walls. While the general guest-binding properties of benzimidazole seemed similar to the octamide cavitand, the benzimidazole showed a lower binding constant for neutral guests in organic solvents, due to increased solvent competition.
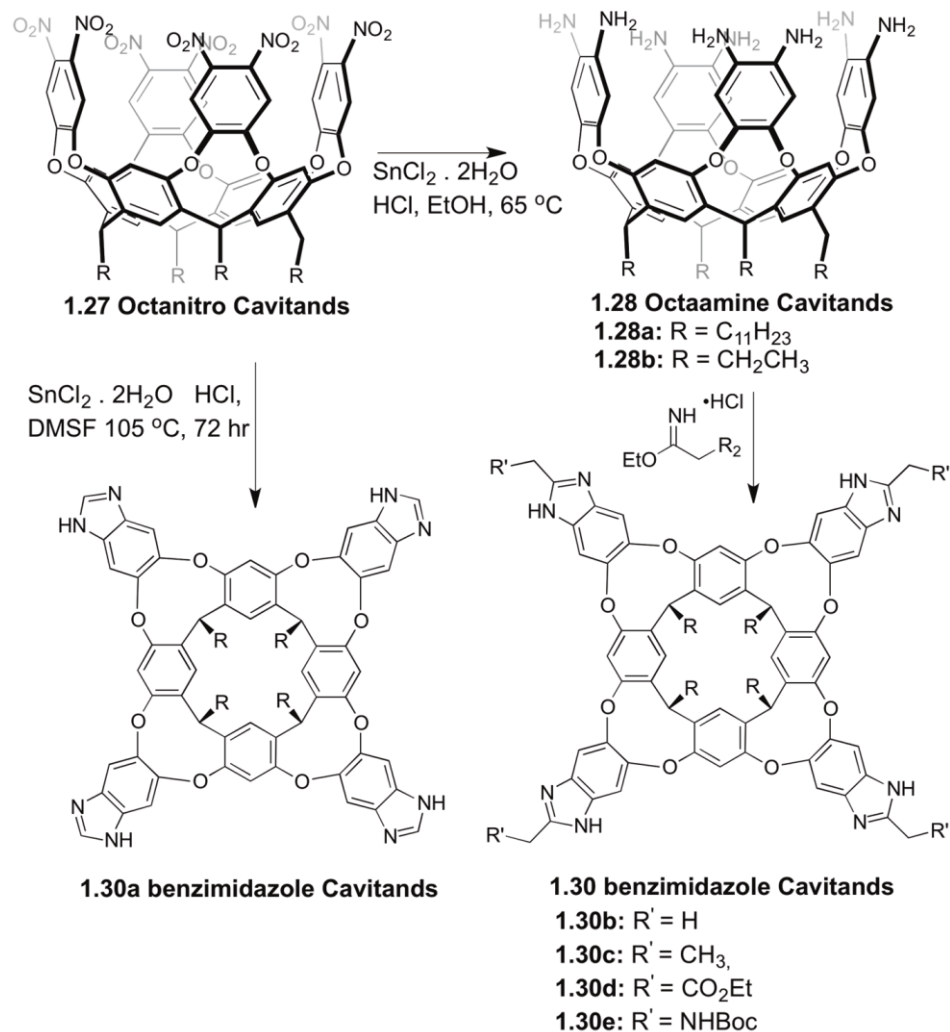
Figure 1.17. The synthesis of benzimidazole deep cavitand scaffolds **1.30a-e**.

Despite the overwhelming amount of exposed π surface, many of the short chain feet (C_2H_5) cavitands were at least somewhat water-soluble. The deepened hydrophobic interior facilitated sequestration of both neutral[73] and charged[71] small molecules *via* hydrophobic effects.

The benzimidazole cavitand scaffold is susceptible to unfolding into the kite conformation, exhibiting either C_{2v} or D_{2d} symmetry. The vase conformation results are

29

supported by the ^{1}H NMR. Base titration of NaOH to the benzimidazole scaffold interrupted the H-bonding seam on the top of the ring and causes a large upfield shifts for the cavitand wall protons. With the addition of 4 eq. NaOH, only the wall proton shifts dramatically while the methine peak at the base of the resorcinarene ring remains relatively unchanged. The addition of the base has a remarkable effect on the electronic environment of the receptor hydrogen bonding interaction between the benzimidazole amine and the water molecules. The hydrogen-bonding network is strengthened upon the deprotonation of the amine with NaOH base. Upon deprotonation, the walls are more tightly held together and minimize "breathing" or flexing of the cavity. Upon a tightly held wall increases the electron density allows greater London dispersion forces between the electron dense cavity and the partially positive charged hydrocarbon guests. This breathing effect also enhances the kinetic stability of the guest binding as a result of the electronic nature of the H-bonding seam. The breathing motion gives more flexibility to the size of the cavity complementary to the guest motion and interaction with the cavity.
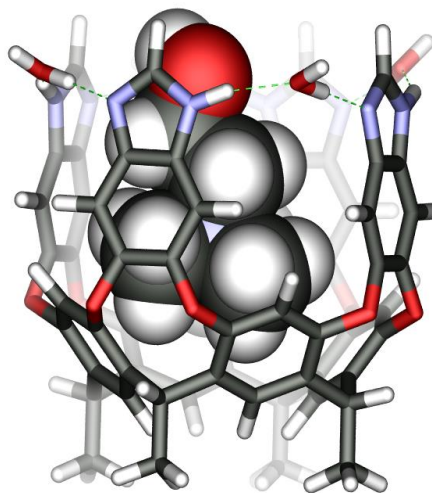
Figure 1.18. The benzimidazole cavitand scaffold with choline guest (hydrogen bonding seam highlighted in green).

1.10. Rigid Deep Cavitands Scaffolds

To introduce deep, rigid cavitand walls, Gibb steered away from bridging the phenol via aromatic substitution and returned to methylene bridging methods. The resulting deep cavitand involved bridging the resorcinarene phenol groups with α,α-dibromobenzyl groups. The scaffold oriented the aromatic rings vertically above the cavity, deepening the binding cavity to 380 Å. The scaffold could be synthesized on a large scale due to its simplicity and stability under harsh reaction conditions. This allowed for a variety of functional groups to the exterior. For water solubility, eight carboxylate species were introduced on the system **1.31a**.[74] The acidic cavitand **1.31a** has been extensively studied in sodium borate buffer as it is soluble in water due to the incorporation of eight carboxylate species at the upper rim and the lower feet. Neutral, anionic, and cationic scaffolds are also well known for their small molecule binding ability.[75-77] Binding

constants range from 10^3-10^6 M^{-1}, depending heavily on the guest's ability to efficiently pack the cavity. The **1.31a** scaffold selectively binds to hydrophilic groups containing guests such as hexanoate or adamantanecarboxylate ions (highest affinity).

1.31a: R_1 = $(CH_2)_2COOH$, R_2 = H, R_3 = COOH
Neutral
1.31b: R_1 = $(CH_2)_2Ph$, R_2 = H, R_3 = H
1.31c: R_1 = $(CH_2)_2Ph$, R_2 = Me, R_3 = H
1.31d: R_1 = OCH_2OEt, R_2 = H, R_3 = OH
Anionic
1.31e: R_1 = $(CH_2)_2COOH$, R_2 = H, R_3 = Me
Cationic
1.31f: R_1 = $(CH_2)_3NEt_2$, R_2 = CH_2NEt_2, R_3 = H
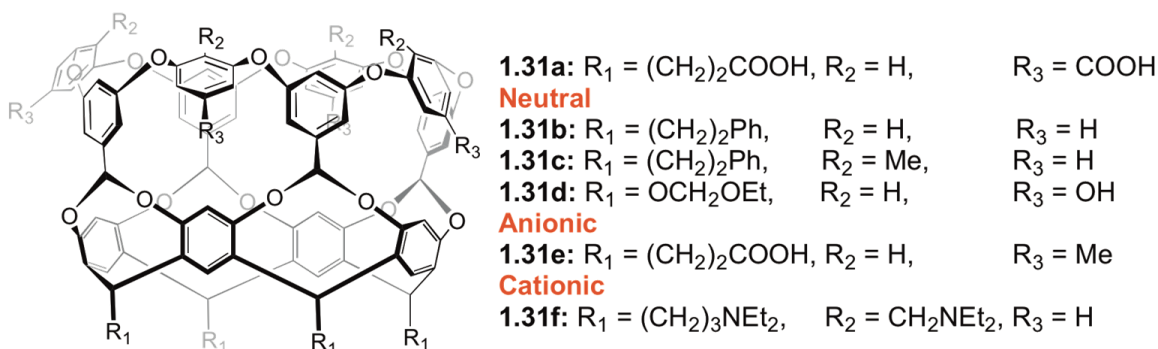
Figure 1.19. Neutral, anionic, and cationic resorcinarene based scaffolds.

Dramatic changes to the binding constant are caused not only by the guest nature but by the solvent nature as well. The neutral cavitand scaffold (**1.31b-d**) faces the same challenges as the quinoxaline cavitand **1.26** due to its limited solvent competition. Conspicuous differences in binding affinity to small guests appear in the large cavity due to solvent competition, especially in chloroform.[78-81] Evidently, **1.31b** shows a tenfold higher affinity to iodoadamantane in toluene than in chloroform (K_a = 4393 M^{-1} in toluene and 670 in $CDCl_3$ and 30 fold higher in DMSO than toluene).[82] As shown by 2D NMR studies, haloadamantanes point vertically upward in the cavity.[82]

As the electron rich cavity displays significant magnetic anisotropy, the main method of analysis for many of those host:guest interactions is ^{1}H NMR. The anisotropy effects cause upfield changes in the chemical shift, as the guest is positioned deeper into the cavity. As the chemical shifts are the resonant frequencies of the proton relative to the

magnetic field, the position of the proton chemical shifts of the bound guest are heavily affected by the electron cloud of the base of the cavity. The bound guest protons are shielded by the cavitand base, causing a diamagnetic shift to the resonant frequency. The maximum change observed in the chemical shift ($\Delta\delta$) is ~5.00 ppm, allowing for discrimination between different resonance NMR peaks of CH_2 groups of the bound guest in the cavity and the free guest in solution.

The removal of solvent competition, as well as the highly hydrophobic ionic cavity of **1.31e**, allow the encapsulation of species that were previously inaccessible in organic solution. Flexible alkanes ranging from propane to hexacosane can be encapsulated, and the large internal cavity allows a wide range of species to be coencapsulated, leading to applications in reactivity.

The self-assembly process of octaacid anionic **1.31e** is highly dependent on the nature of the guest. 1:1 binding selectivity is seen for guests that properly fill the cavity and contain a hydrophilic group such as hexanoate or adamantanecarboxylate ions.[83] The binding affinities of these guests are related to the packing efficiency and size of the hydrophobic guest portion, and range from 103 to 106 M^{-1} (adamantanecarboxylate showing the highest affinity). The self assembly of **1.31e** into a dimeric aggregate is favored in solution, however, and 1:1 cavitand:guest binding must be forced by the presence of hydrophilic groups at the rim.159 Other species that form 1:1 complexes with **1.31e** include "hydrophobic" anions such as perchlorate. [84,85]

1.11. Conclusion

To achieve regioselective hydrocarbon oxidation, a number of factors are required, but two are paramount. A scaffold is required that can non-covalently bind the hydrocarbon target, while also containing reactive functionalities that allow transformation of the C-H bonds. This work aims to use the molecular recognition properties of multi-metal host scaffolds to perform regioselective C-H oxidations. In order for guest binding to occur, the scaffolds must possess a cavity deep enough to encapsulate a guest. In addition to containing N-donor sites for metal coordination, the rigidity of the rims helps force metal labile sites toward the cavity for proximity based oxidation.

1.12. References

(1)   Dawson, J. H.; Sono, M. Cytochrome.P-450 and Chloroperoxidase - Thiolate-Ligated Heme Enzymes - Spectroscopic Determination of Their Active-Site Structures and Mechanistic Implications of Thiolate Ligation. *Chem. Rev.* **1987**, *87*, 1255-1276.

(2)   Dawson, J. H. Probing structure-function relations in heme-containing oxygenases and peroxidases. *Science* **1988**, *240*, 433-439.

(3)   Ferraro, D. J.; Gakhar, L.; Ramaswamy, S. Rieske business: structure-function of Rieske non-heme oxygenases. *Biochem. Biophys. Res. Commun.* **2005**, *338*, 175-190.

(4)   Merkx, M.; Kopp, D. A.; Sazinsky, M. H.; Blazyk, J. L.; Muller, J.; Lippard, S. J. Dioxygen Activation and Methane Hydroxylation by Soluble Methane Monooxygenase: A Tale of Two Irons and Three Proteins. *Angew. Chem. Int. Ed.* **2001**, *40*, 2782-2807.

(5)   Solomon, E. I.; Chen, P.; Metz, M.; Lee, S. K.; Palmer, A. E. Oxygen Binding, Activation, and Reduction to Water by Copper Proteins. *Angew. Chem. Int. Ed.* **2001**, *40*, 4570-4590.

(6)   Que, L., Jr.; Tolman, W. B. Biologically inspired oxidation catalysis. *Nature* **2008**, *455*, 333-340.

(7)   Coleman, R.; Wharton, D.; Rieske, J. S. Effects of P-Chloromercuriphenyl Sulfonate on Isolated Nonheme Iron-Protein from Beef Heart Mitochondria. *Biochem. Biophys. Res. Commun.* **1964**, *15*, 345-350.

(8)   Rieske, J. S.; Maclennan, D. H.; Coleman, R. Isolation + Properties of Iron-Protein from (Reduced Coenzyme Q) -Cytochrome C Reductase Complex of Respiratory Chain. *Biochem. Biophys. Res. Commun.* **1964**, *15*, 338-342.

(9)   Brown, E. N.; Friemann, R.; Karlsson, A.; Parales, J. V.; Couture, M. M. J.; Eltis, L. D.; Ramaswamy, S. Determining Rieske cluster reduction potentials. *J. Biol. Inorg. Chem.* **2008**, *13*, 1301-1313.

(10)   Harnisch, U.; Weiss, H.; Sebald, W. The Primary Structure of the Iron-Sulfur Subunit of Ubiquinol Cytochrome-C Reductase from Neurospora, Determined by Cdna and Gene Sequencing. *Eur. J. Biochem.* **1985**, *149*, 95-99.

(11)   Merkx, M.; Kopp, D. A.; Sazinsky, M. H.; Blazyk, J. L.; Muller, J.; Lippard, S. J. Dioxygen Activation and Methane Hydroxylation by Soluble Methane Monooxygenase: A Tale of Two Irons and Three Proteins A list of abbreviations can be found in Section 7. *Angew. Chem. Int. Ed.* **2001**, *40*, 2782-2807.

(12)   McEvoy, J. P.; Brudvig, G. W. Water-splitting chemistry of photosystem II. *Chem. Rev.* **2006**, *106*, 4455-4483.

(13)   Chan, S. I.; Yu, S. S. Controlled oxidation of hydrocarbons by the membrane-bound methane monooxygenase: the case for a tricopper cluster. *Acc. Chem. Res.* **2008**, *41*, 969-979.

(14)   Basch, H.; Mogi, K.; Musaev, D. G.; Morokuma, K. Mechanism of the methane -> methanol conversion reaction catalyzed by methane monooxygenase: A density functional study. *J. Am. Chem. Soc.* **1999**, *121*, 7249-7256.

(15)   Axelrod, J. The enzymatic N-demethylation of narcotic drugs. *J. Pharmacol. Exp. Ther.* **1956**, *117*, 322-330.

(16)   Gomez, L.; Garcia-Bosch, I.; Company, A.; Benet-Buchholz, J.; Polo, A.; Sala, X.; Ribas, X.; Costas, M. Stereospecific C-H oxidation with H2O2 catalyzed by a chemically robust site-isolated iron catalyst. *Angew. Chem. Int. Ed.* **2009**, *48*, 5720-5723.

(17)   Morimoto, Y.; Bunno, S.; Fujieda, N.; Sugimoto, H.; Itoh, S. Direct hydroxylation of benzene to phenol using hydrogen peroxide catalyzed by nickel complexes supported by pyridylalkylamine ligands. *J. Am. Chem. Soc.* **2015**, *137*, 5867-5870.

(18)   Borovik, A. S. Role of metal-oxo complexes in the cleavage of C-H bonds. *Chem. Soc. Rev.* **2011**, *40*, 1870-1874.

(19)   Janardanan, D.; Wang, Y.; Schyman, P.; Que, L., Jr.; Shaik, S. The fundamental role of exchange-enhanced reactivity in C-H activation by S=2 oxo iron(IV) complexes. *Angew. Chem. Int. Ed.* **2010**, *49*, 3342-3345.

(20)   Shilov, A. E.; Shul'pin, G. B. Activation of Cminus signH Bonds by Metal Complexes. *Chem. Rev.* **1997**, *97*, 2879-2932.

(21)   Costas, M.; Mehn, M. P.; Jensen, M. P.; Que, L., Jr. Dioxygen activation at mononuclear nonheme iron active sites: enzymes, models, and intermediates. *Chem. Rev.* **2004**, *104*, 939-986.

(22)   Mekmouche, Y.; Hummel, H.; Ho, R. Y.; Que, L., Jr.; Schunemann, V.; Thomas, F.; Trautwein, A. X.; Lebrun, C.; Gorgy, K.; Lepretre, J. C.; Collomb, M. N.; Deronzier, A.; Fontecave, M.; Menage, S. Sulfide oxidation by hydrogen peroxide

catalyzed by iron complexes: two metal centers are better than one. *Chem. Eur. J.* **2002**, *8*, 1196-1204.

(23)   Zheng, H.; Zang, Y.; Dong, Y. H.; Young, V. G.; Que, L. Complexes with $Fe^{III}_2(\mu\text{-O})(\mu\text{-OH})$, $Fe^{III}_2(\mu\text{-O})_2$, and $[Fe^{III}_3(\mu_2\text{-O})_3]$ cores: Structures, spectroscopy, and core interconversions. *J. Am. Chem. Soc.* **1999**, *121*, 2226-2235.

(24)   Company, A.; Gomez, L.; Guell, M.; Ribas, X.; Luis, J. M.; Que, L.; Costas, M. Alkane hydroxylation by a nonheme iron catalyst that challenges the heme paradigm for oxygenase action. *J. Am. Chem. Soc.* **2007**, *129*, 15766-15767.

(25)   Company, A.; Prat, I.; Frisch, J. R.; Mas-Balleste, R.; Guell, M.; Juhasz, G.; Ribas, X.; Munck, E.; Luis, J. M.; Que, L.; Costas, M. Modeling the cis-Oxo-Labile Binding Site Motif of Non-Heme Iron Oxygenases: Water Exchange and Oxidation Reactivity of a Non-Heme Iron(IV)-Oxo Compound Bearing a Tripodal Tetradentate Ligand. *Chem. Eur. J.* **2011**, *17*, 1622-1634.

(26)   Abu-Omar, M. M.; Loaiza, A.; Hontzeas, N. Reaction mechanisms of mononuclear non-heme iron oxygenases. *Chem. Rev.* **2005**, *105*, 2227-2252.

(27)   Chen, M. S.; White, M. C. A predictably selective aliphatic C-H oxidation reaction for complex molecule synthesis. *Science* **2007**, *318*, 783-787.

(28)   Bigi, M. A.; Reed, S. A.; White, M. C. Directed metal (oxo) aliphatic C-H hydroxylations: overriding substrate bias. *J. Am. Chem. Soc.* **2012**, *134*, 9721-9726.

(29)   Yang, J.; Gabriele, B.; Belvedere, S.; Huang, Y.; Breslow, R. Catalytic oxidations of steroid substrates by artificial cytochrome p-450 enzymes. *J. Org. Chem.* **2002**, *67*, 5057-5067.

(30)   Belvedere, S.; Breslow, R. Regioselective oxidation of steroids by a manganese porphyrin carrying metal coordinating groups. *Bioorg. Chem.* **2001**, *29*, 321-331.

(31)   Breslow, R.; Yan, J. M.; Belvedere, S. Catalytic hydroxylation of steroids by cytochrome P-450 mimics. Hydroxylation at C-9 with novel catalysts and steroid substrates. *Tetrahedron Lett.* **2002**, *43*, 363-365.

(32)   Delamare, H. E.; Rust, F. F. Intramolecular Radical Reactions - Decomposition of Pure Bis-(2-Methyl-2-Hexyl) Peroxide in the Liquid Phase. *J. Am. Chem. Soc.* **1959**, *81*, 2691-2694.

(33)   Jarvi, E. T.; Whitlock, H. W. 1,8,17,24-Tetraoxa[8.8](2,6)Naphthalenophane-3,5,19,21-Tetrayne-10,30-Dicarboxylic Acid-Derivatives, Novel Complexors of Aromatic Guests. *J. Am. Chem. Soc.* **1982**, *104*, 7196-7204.

(34)   Chen, C. W.; Whitlock, H. W. Molecular Tweezers - Simple-Model of Bifunctional Intercalation. *J. Am. Chem. Soc.* **1978**, *100*, 4921-4922.

(35)   Nemoto, H.; Kawano, T.; Ueji, N.; Bando, M.; Kido, M.; Suzuki, I. I.; Shibuya, M. A conformationally reliable spacer for molecular tweezers. *Org. Lett.* **2000**, *2*, 1015-1017.

(36)   Whitlock, B. J.; Whitlock, H. W. Effect of Cavity Size on Supramolecular Stability. *J. Am. Chem. Soc.* **1994**, *116*, 2301-2311.

(37)   Kennan, A. J.; Whitlock, H. W. Host-catalyzed isoxazole ring opening: A rationally designed artificial enzyme. *J. Am. Chem. Soc.* **1996**, *118*, 3027-3028.

(38) Ghosh, S.; Wu, A.; Fettinger, J. C.; Zavalij, P. Y.; Isaacs, L. Self-sorting molecular clips. *J. Org. Chem.* **2008**, *73*, 5915-5925.

(39) R. P. Sijbesma, A. P. M. K., E. T. G. Lutz, J. H. van der Maas, R. J. M. Nolte. Binding features of molecular clips derived from diphenylglycoluril. *J. Am. Chem. Soc.* **1993**, *115*, 8999-9005.

(40) Polavarapu, P.; Melander, H.; Langer, V.; Gogoll, A.; Grennberg, H. Modulation and binding properties of extended glycoluril molecular clips. *New J. Chem.* **2008**, *32*, 643-651.

(41) Ma, D.; Zavalij, P. Y.; Isaacs, L. Acyclic cucurbit[n]uril congeners are high affinity hosts. *J. Org. Chem.* **2010**, *75*, 4786-4795.

(42) Lucas, D.; Minami, T.; Iannuzzi, G.; Cao, L.; Wittenberg, J. B.; Anzenbacher, P., Jr.; Isaacs, L. Templated synthesis of glycoluril hexamer and monofunctionalized cucurbit[6]uril derivatives. *J. Am. Chem. Soc.* **2011**, *133*, 17966-17976.

(43) Ma, D.; Hettiarachchi, G.; Nguyen, D.; Zhang, B.; Wittenberg, J. B.; Zavalij, P. Y.; Briken, V.; Isaacs, L. Acyclic cucurbit[n]uril molecular containers enhance the solubility and bioactivity of poorly soluble pharmaceuticals. *Nat. Chem.* **2012**, *4*, 503-510.

(44) Zhang, B.; Isaacs, L. Acyclic Cucurbit[n]uril-type Molecular Containers: Influence of Aromatic Walls on their Function as Solubilizing Excipients for Insoluble Drugs. *J. Med. Chem.* **2014**, *57*, 9554-9563.

(45)   Hardouin-Lerouge, M.; Hudhomme, P.; Salle, M. Molecular clips and tweezers hosting neutral guests. *Chem. Soc. Rev.* **2011**, *40*, 30-43.

(46)   Klarner, F. G.; Lobert, M.; Naatz, U.; Bandmann, H.; Boese, R. Synthesis and supramolecular properties of trimethylene-bridged clips. *Chem. Eur. J.* **2003**, *9*, 5036-5047.

(47)   Klarner, F. G.; Kahlert, B.; Boese, R.; Blaser, D.; Juris, A.; Marchioni, F. Synthesis and supramolecular properties of molecular clips with anthracene sidewalls. *Chem. Eur. J.* **2005**, *11*, 3363-3374.

(48)   Klarner, F. G.; Kahlert, B.; Nellesen, A.; Zienau, J.; Ochsenfeld, C.; Schrader, T. Molecular tweezer and clip in aqueous solution: unexpected self-assembly, powerful host-guest complex formation, quantum chemical ^{1}H NMR shift calculation. *J. Am. Chem. Soc.* **2006**, *128*, 4831-4841.

(49)   Marchioni, F.; Juris, A.; Lobert, M.; Seelbach, U. P.; Kahlert, B.; Klarner, F. G. Luminescent host-guest complexes involving molecular clips and tweezers and tetracyanobenzene. *New J. Chem.* **2005**, *29*, 780-784.

(50)   Hoegberg, A. G. S. Two stereoisomeric macrocyclic resorcinol-acetaldehyde condensation products. *J. Org. Chem.* **1980**, *45*, 4498-4500.

(51)   Evan-Salem, T.; Baruch, I.; Avram, L.; Cohen, Y.; Palmer, L. C.; Rebek, J. Resorcinarenes are hexameric capsules in solution. *Proc. Natl. Acad. Sci. U.S.A.* **2006**, *103*, 12296-12300.

(52)   Shivanyuk, A.; Rebek, J. Reversible encapsulation by self-assembling resorcinarene subunits. *Proc. Natl. Acad. Sci. U.S.A.* **2001**, *98*, 7662-7665.

(53)   Avram, L.; Cohen, Y. Spontaneous formation of hexameric resorcinarene capsule in chloroform solution as detected by diffusion NMR. *J. Am. Chem. Soc.* **2002**, *124*, 15148-15149.

(54)   Castellano, R. K.; Rudkevich, D. M.; Rebek, J. Tetramethoxy calix[4]arenes revisited: Conformational control through self-assembly. *J. Am. Chem. Soc.* **1996**, *118*, 10002-10003.

(55)   Biros, S. M.; Rebek, J., Jr. Structure and binding properties of water-soluble cavitands and capsules. *Chem Soc Rev* **2007**, *36*, 93-104.

(56)   Cram, D. J.; Cram, J. M.: *Container Molecules and their Guests*; R. Soc. Chem., Cambridge, 1994.

(57)   Moran, J. R.; Karbach, S.; Cram, D. J. Cavitands - Synthetic Molecular Vessels. *J. Am. Chem. Soc.* **1982**, *104*, 5826-5828.

(58)   Moran, J. R.; Ericson, J. L.; Dalcanale, E.; Bryant, J. A.; Knobler, C. B.; Cram, D. J. Vases and Kites as Cavitands. *J. Am. Chem. Soc.* **1991**, *113*, 5707-5714.

(59)   Cram, D. J.; Choi, H. J.; Bryant, J. A.; Knobler, C. B. Host-Guest Complexation .62. Solvophobic and Entropic Driving Forces for Forming Velcraplexes, Which Are 4-Fold, Lock-Key Dimers in Organic Media. *J. Am. Chem. Soc.* **1992**, *114*, 7748-7765.

(60)   Soncini, P.; Bonsignore, S.; Dalcanale, E.; Ugozzoli, F. Cavitands as Versatile Molecular Receptors. *J. Org. Chem.* **1992**, *57*, 4608-4612.

(61)   Haino, T.; Kobayashi, M.; Fukazawa, Y. Guest encapsulation and self-assembly of a cavitand-based coordination capsule. *Chem. Eur. J.* **2006**, *12*, 3310-3319.

(62)   Haino, T.; Rudkevich, D. M.; Shivanyuk, A.; Rissanen, K.; Rebek, J., Jr. Induced-fit molecular recognition with water-soluble cavitands. *Chem. Eur. J.* **2000**, *6*, 3797-3805.

(63)   Mecozzi, S.; Rebek, J. The 55% solution: A formula for molecular recognition in the liquid state. *Chem. Eur. J.* **1998**, *4*, 1016-1022.

(64)   Pochorovski, I.; Knehans, T.; Nettels, D.; Muller, A. M.; Schweizer, W. B.; Caflisch, A.; Schuler, B.; Diederich, F. Experimental and computational study of BODIPY dye-labeled cavitand dynamics. *J. Am. Chem. Soc.* **2014**, *136*, 2441-2449.

(65)   Ampurdanes, J.; Crespo, G. A.; Maroto, A.; Sarmentero, M. A.; Ballester, P.; Rius, F. X. Determination of choline and derivatives with a solid-contact ion-selective electrode based on octaamide cavitand and carbon nanotubes. *Biosens. Bioelectron.* **2009**, *25*, 344-349.

(66)   Korom, S.; Martin, E.; Serapian, S. A.; Bo, C.; Ballester, P. Molecular Motion and Conformational Interconversion of Ir(I)**.**COD Included in Rebek's Self-Folding Octaamide Cavitand. *J. Am. Chem. Soc.* **2016**, *138*, 2273-2279.

(67)   Zuidema, E.; Sarmentero, M. A.; Bo, C.; Ballester, P. A combined experimental and theoretical study of the molecular inclusion of organometallic sandwich complexes in a cavitand receptor. *Chem. Eur. J.* **2008**, *14*, 7285-7295.

(68)   Trembleau, L.; Rebek, J., Jr. Helical conformation of alkanes in a hydrophobic cavitand. *Science* **2003**, *301*, 1219-1220.

(69)   Scarso, A.; Trembleau, L.; Rebek, J. Helical folding of alkanes in a self-assembled, cylindrical capsule. *J. Am. Chem. Soc.* **2004**, *126*, 13512-13518.

(70)   Trembleau, L.; Rebek, J., Jr. Interactions between a surfactant and cavitand in water blur distinctions between host and guest. *Chem. Commun.* **2004**, 58-59.

(71)   Menozzi, E.; Onagi, H.; Rheingold, A. L.; Rebek, J. Extended cavitands of nanoscale dimensions. *Eur. J. Org. Chem.* **2005**, 3633-3636.

(72)   Schramm, M. P.; Hooley, R. J.; Rebek, J., Jr. Guest recognition with micelle-bound cavitands. *J. Am. Chem. Soc.* **2007**, *129*, 9773-9779.

(73)   Hooley, R. J.; Biros, S. M.; Rebek, J., Jr. Normal hydrocarbons tumble rapidly in a deep, water-soluble cavitand. *Chem. Commun.* **2006**, 509-510.

(74)   Gibb, C. L.; Gibb, B. C. Well-defined, organic nanoenvironments in water: the hydrophobic effect drives a capsular assembly. *J. Am. Chem. Soc.* **2004**, *126*, 11408-11409.

(75)   Jordan, J. H.; Gibb, B. C. Molecular containers assembled through the hydrophobic effect. *Chem. Soc. Rev.* **2015**, *44*, 547-585.

(76)   Laughrey, Z. R.; Gibb, B. C. Macrocycle synthesis through templation. *Templates in Chemistry* **2005**, *249*, 67-125.

(77)   Laughrey, Z.; Gibb, B. C. Water-soluble, self-assembling container molecules: an update. *Chem. Soc. Rev.* **2011**, *40*, 363-386.

(78)   Gibb, C. L. D.; Stevens, E. D.; Gibb, B. C. C-H center dot center dot center dot X-R (X = Cl, Br, and I) hydrogen bonds drive the complexation properties of a nanoscale molecular basket. *J. Am. Chem. Soc.* **2001**, *123*, 5849-5850.

(79)   Green, J. O.; Baird, J. H.; Gibb, B. C. Reduced-symmetry deep-cavity cavitands. *Org. Lett.* **2000**, *2*, 3845-3848.

(80)   Xi, H. P.; Gibb, C. L. D.; Gibb, B. C. Functionalized deep-cavity cavitands. *J. Org. Chem.* **1999**, *64*, 9286-9288.

(81)   Xi, H. P.; Gibb, C. L. D.; Stevens, E. D.; Gibb, B. C. Deep-cavity cavitands: synthesis and solid state structure of host molecules possessing large bowl-shaped cavities. *Chem. Commun.* **1998**, 1743-1744.

(82)   Laughrey, Z. R.; Gibb, C. L. D.; Senechal, T.; Gibb, B. C. Guest binding and orientation within open nanoscale hosts. *Chem. Eur. J.* **2003**, *9*, 130-139.

(83)   Sun, H.; Gibb, C. L. D.; Gibb, B. C. Calorimetric analysis of the 1 : 1 complexes formed between a water-soluble deep-cavity cavitand, and cyclic and acyclic carboxylic acids. *Supramol. Chem.* **2008**, *20*, 141-147.

(84)   Gibb, C. L.; Gibb, B. C. Anion binding to hydrophobic concavity is central to the salting-in effects of Hofmeister chaotropes. *J. Am. Chem. Soc.* **2011**, *133*, 7344-7347.

(85)   Gibb, B. C. Supramolecular Assembly and Binding in Aqueous Solution: Useful Tips Regarding the Hofmeister and Hydrophobic Effects. *Isr. J. Chem.* **2011**, *51*, 798-806.

Chapter 2: Alkane Oxidation Catalyzed by a Self-Folded Multi-Iron Complex

2.1. Approach

We sought to create a flexible, self-folding ligand system that could coordinate multiple iron centers for hydrocarbon oxidation catalysis inspired by non-haem oxygenase catalysts.[1] A number of biomimetic oxidation catalysts are known that provide a tetradentate ligand coordinated to a single Fe(II) center.[1,2] However, non-haem oxygenase catalytically active sites commonly contain multiple metal centers each coordinating to a tetradentate ligand in close proximity.[3,4] Though multi-metal catalysts are much more challenging to synthesize, they are often more catalytically active than their monometal counterparts.[5,6]

In order to properly fold the hosts into the correct form, one must seek a multi-metal scaffold with preorganized self-folding properties to constrain the guest, orient the reactive metal site, and then proceed with the oxidation. The metal helps in two main ways: acting as a catalyst for the hydrocarbon oxidation, but also structural support of the cavity, which was previously only accomplished by H-bonding. This allows one to design scaffolds with deeper binding pockets and more rigid rims, as well as to introduce the N-donor sites for oxidation. In this thesis, we will aim to create a scaffold to achieve hydrocarbon selective oxidation, utilizing a preorganized scaffold containing N-donor sites, the self-folding of which can be aided by metal ions. The metal ions are positioned directly on top of the cavity, theoretically allowing for regioselectivity in oxidation.

As well as catalysis, molecular recognition must be considered. A host with a large

cavity is required to fully surround the hydrocarbon guest. The main idea is to utilize the hydrophobicity of the hydrocarbon guests to control host-guest binding. Utilizing hydrophobicity would control hydrocarbon interaction with the scaffold to encapsulate and align the substrate in one orientation. A water-soluble scaffold with an electron rich cavity could surround the hydrophobic target in its active site. The affinity is driven by the hydrophobic effect. Using water as a solvent is beneficial in two ways - as water oxidation is a high energy process, there will be minimal oxidation of solvent to consume the catalyst, and water will allow strong guest binding via the hydrophobic effect.
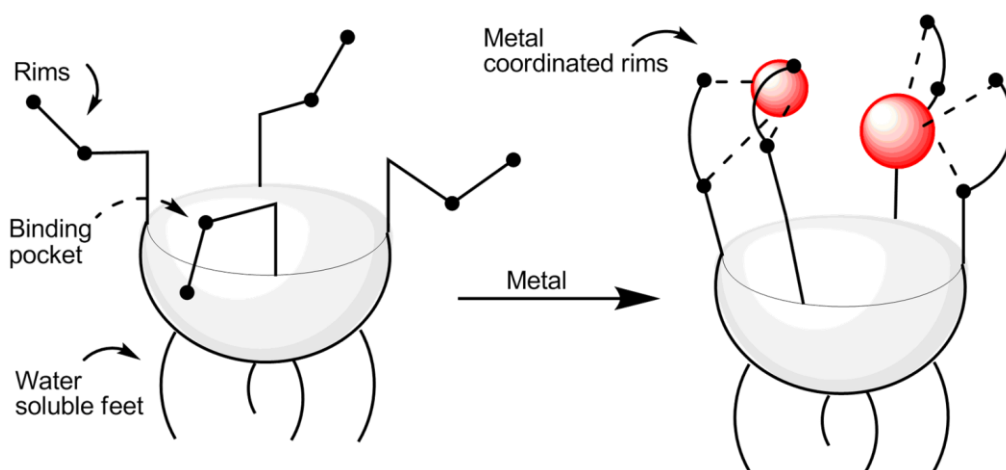
Figure 2.1. Preorganized self-assembly and catalyst incorporation via metal-ligand coordination.

2.2. Shallow Cavitands

The main challenge of creating a multiple centered metal-coordination motif so far has been the introduction of multiple ligating groups. Self-folding motifs have been exploited, as described in Chapter 1 in a variety of different fields as sensors and

supramolecular assembly with in-depth study of their stability,[7] solubility,[8-14] and reactivity.[15-18] Many of the previously discussed self-folding systems are heavily reliant on hydrogen bonding or/and metal ligand coordination for assembly. The organization of the ligand is generally post-synthetic rather than exploiting a preorganized scaffold.

The initial attempts to make functionalized cavitands started with the rigid, shallow benzylic resorcinarene cavitand. This approach used a radical benzylic bromination reaction with *N*-bromosuccinimide in DMF to introduce a reactive group at the upper rim, followed by introducing N-donor sites to the system. 2-Methylresorcinol was utilized to synthesize the octahydroxyl resorcinarene scaffold **1.14c** with functionalizable methyl groups at the rim. Following a radical bromination with NBS at the benzylic positions, S_N2 substitution with sodium azide gave the corresponding tetra-azide cavitand **2.3** in 98% yield. The insolubility of the hydroxyl-footed cavitand required the use of a protecting group. The "feet" hydroxyls were protected as acetates for the bromination and substitution. Deprotection of the acetate feet *via* refluxing in MeOH/K_2CO_3 in THF gave **2.3b**.[19]

Functionalization of tetra-azide cavitand **2.3** *via* CuAAC click chemistry using $CuSO_4$ •$6H_2O$ in DMSO and Blm$_3$ (co-catalyst) allowed for the incorporation of a variety of different substituents at the rim of the cavitands, including a variety of more complicated amine-containing rims **2.4a-d**. The most promising scaffolds for metal binding came from the reactions of 3-pyridylamide ligand **2.4c$_2$** or commercially available 2-ethynylpyridine **2.4b$_2$** with the tetra-azide cavitand **2.3**.
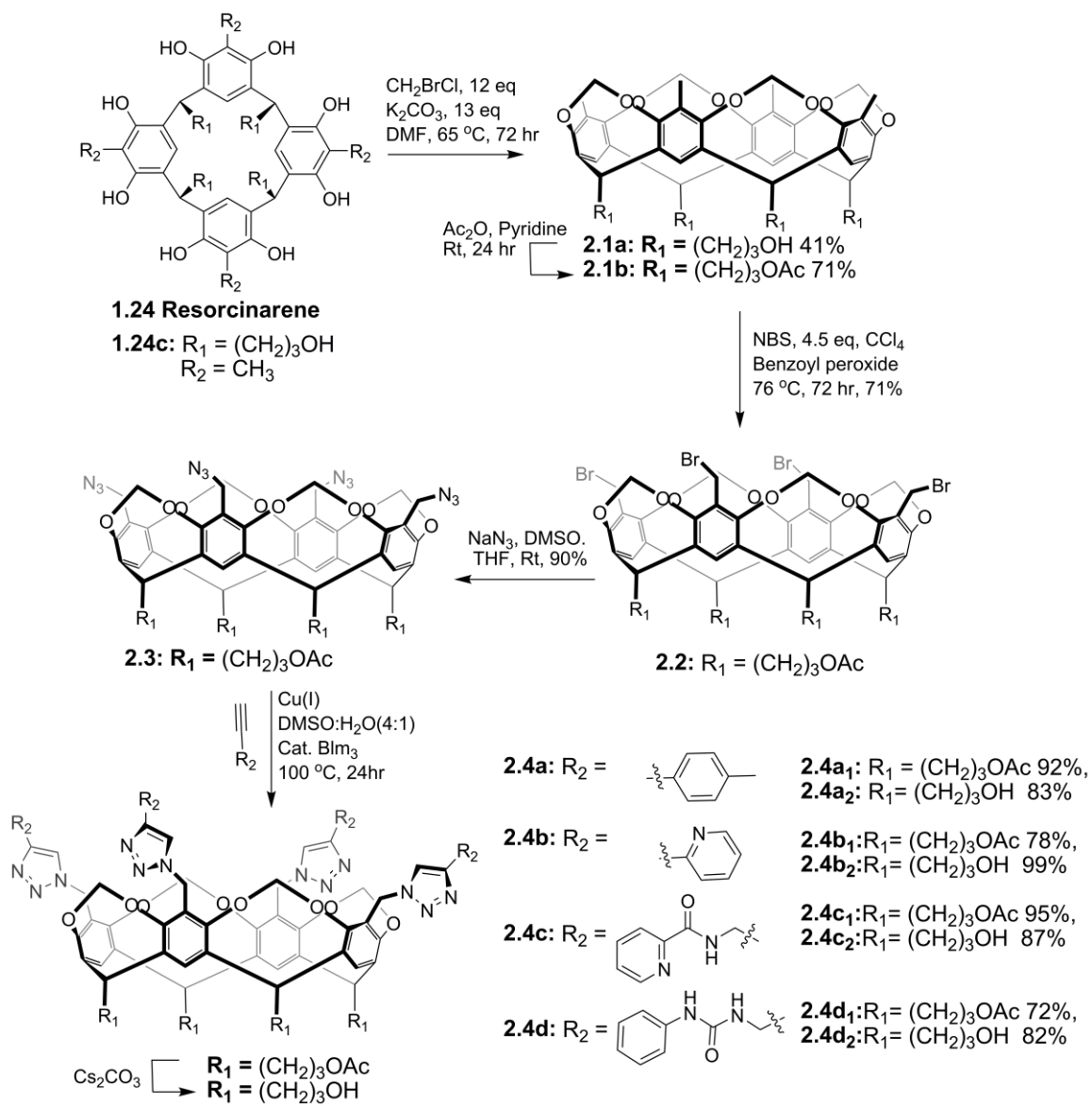
Figure 2.2. The synthesis of metal containing shallow cavitand scaffolds.

2.3. Metal Ion Complexation To Shallow Cavitands

Both cavitand scaffold **2.4b$_2$** and **2.4c$_2$** showed metal coordination to multiple metal ions. The metal complex showed different physical properties from the reactant, as they precipitated from solution upon addition of metal. They were then isolated and filtered for more detailed study. A slight shift in the ^{1}H NMR suggested that cavitand **2.4c$_2$** showed binding affinity to $AgBF_4$, $Al(NO_3)_3$, $Cr(NO_3)_3$, $Ga(NO_3)_3$, $CuBF_4$ and $FeSO_4$ in CD_3CN solution. The addition of the metal ions caused broadness and slight shifts to the aromatic peaks, and it was hard to quantitatively confirm the present of one or two metal ions. Those results were also confirmed and verified by MALDI mass spectrometry. Cavitand **2.4b$_2$** showed similar results with $CuBF_4$ and $FeSO_4$. The literature precedent that hydrocarbon oxidation occurs with Fe and Cu complexes focused our studies on those reactive metal. Although we were unable to grow X-ray quality crystals of the cavitand and metal complexes, the MALDI and the molecular modeling using Hartree-Fock calculation suggested two states: either one metal ion coordinating to all four triazole nitrogens, or two metals, with one metal coordinating to two arms (Figure 2.3).
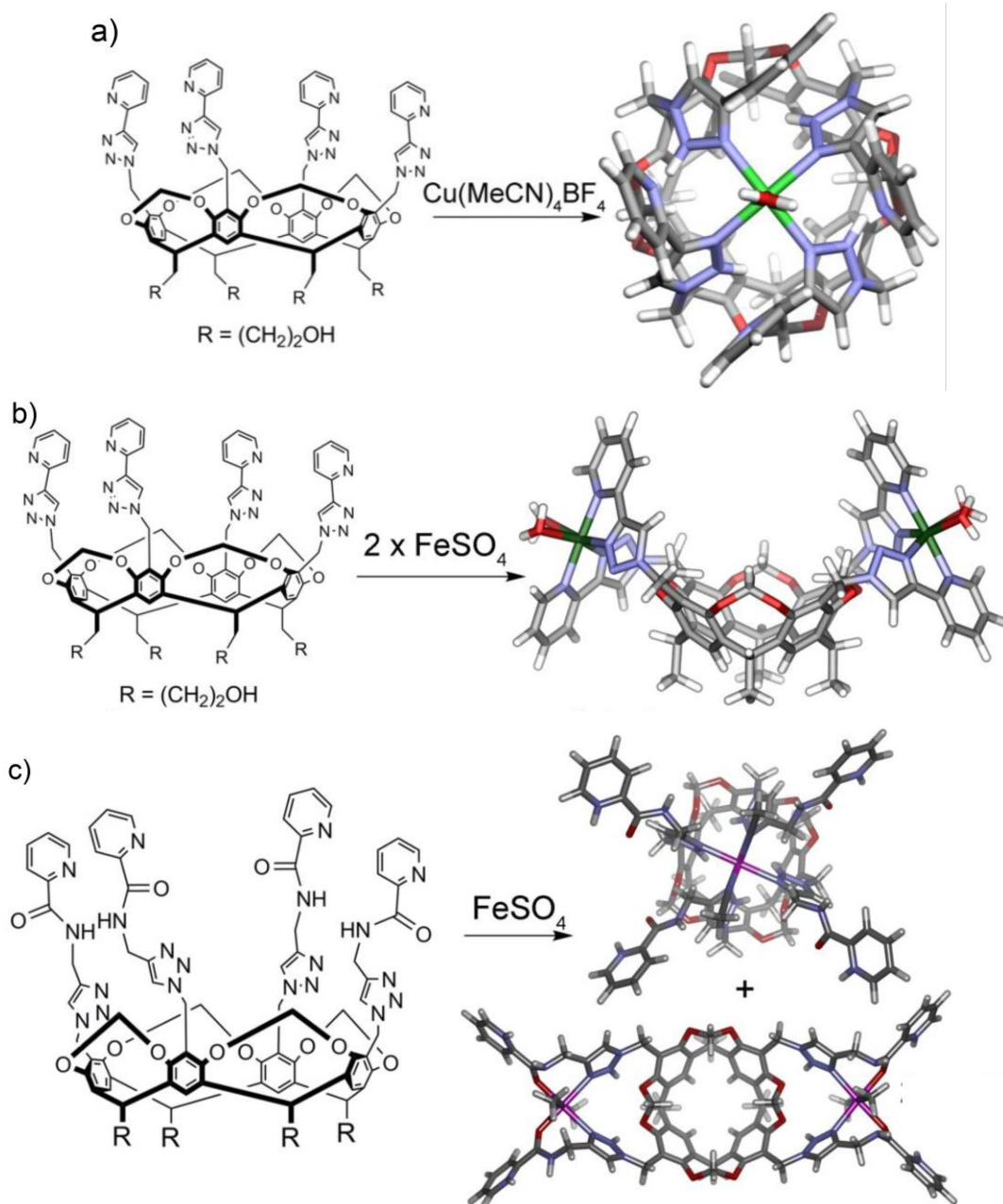
Figure 2.3. The formation of a) Cavitand **2.4b₂•Cu**, b) **2.4b₂•Fe₂**, c) **2.4c₂•Fe** + **2.4c₂•Fe₂**
2.4c₂•Fe and the minimized models of the catalyst complex structures (SPARTAN, Hartree-Fock forcefield, counter ions omitted for clarity).

51

2.4. Hydrocarbon Oxidation With Shallow Cavitands

After complexation to $FeSO_4$, cavitand $Fe_2 \bullet \textbf{2.4b}_2$ was able to successfully catalyze the oxidation of unactivated cyclic hydrocarbons such as cyclooctane, *cis*-decalin*, trans*-decalin, adamantane and cyclododecane to their corresponding ketones, or in the case of species containing 3º CHs, alcohols. When compared to the activity of uncomplexed $FeSO_4$, cavitand $\textbf{2.4b}_2$ showed higher reactivity. More than a threefold increase of oxidation product using synthesized catalyst cavitand $\textbf{2.4b}_2$ was observed, compared to $FeSO_4$ alone. In the case of *cis*-decalin*,* a 2:1 selectivity of 3º:2º oxidation products was observed. Similar results for adamantane oxidation shows the high selectivity for the 3º product, rather than oxidation of the 2º C-H bond. However, in the case of *trans*-decalin, no 3º C-H oxidation was detected, only 2º C-H bond oxidation (Table 2.1).
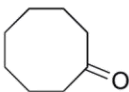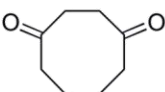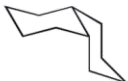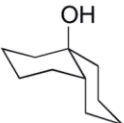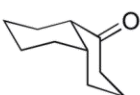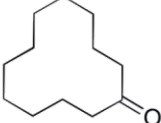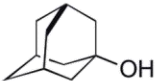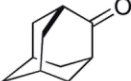
Substrate	Product Yields (%)				Total Yield (%)
		a) 56% b) 19%		a) 5% b) 0%	a) 61% b) 19%
		a) 38% b) 9%		a) 15% b) 5%	a) 53% b) 14%
		a) 50% b) 24%		a) 24% b) 0%	a) 74% b) 24%
		a) 50% b) 17%			a) 50% b) 17%
		a) 44% b) 3%		a) 25% b) 4%	a) 69% b) 7%

Table 2.1. The oxidation of hydrocarbon substrates as catalyzed by a) **2.4b$_2$•Fe$_2$** and b) FeSO$_4$.

Some reactivity occurred for more strained cyclic and polycyclic hydrocarbons. Less strained rings such as cyclododecane were less reactive but did undergo single oxidation. Cavitand **2.4c$_2$** showed a slight increase in total conversion to the oxidation product, but only in the more strained cyclic hydrocarbons such as cyclododecane and *trans*-decalin. Cavitand **2.4c$_2$•Cu$_2$** was capable of catalyzing the same hydrocarbon oxidations, but showed lower reactivity than the **2.4c$_2$•Fe$_2$** complex and similar reactivity to copper sulfate as control.
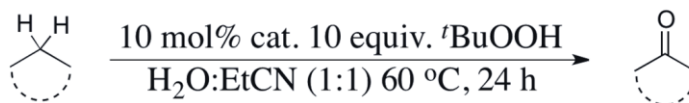
Substrate	Product Yields (%)			Total Yield (%)
		a) 70% b) 75%	a) 16% b) 14%	a) 86% b) 89%
		a) 42% b) 20%	a) 17% b) 7%	a) 69% b) 27%
	OH a) 54% b) 36%		a) 17% b) 10%	a) 71% b) 46%
		a) 45% b) 30%		a) 45% b) 30%
		a) 39% b) 13%	a) 18% b) 7%	a) 57% b) 20%

Table 2.2. The oxidation of hydrocarbon substrates as catalyzed by a) **2.4c$_2$•Fe$_2$** and b) **2.4c$_2$•Cu$_2$**.

While the cavitands were catalytically active and water-soluble, proximity-directed regioselective oxidation was not observed. The major issues were that no effective molecular recognition was possible. The flexible ligand arms were capable of metal coordination, but not in the correct orientation for guest recognition. For example, **Cu•2.4.b$_2$** has the coordinated metal sitting over the cavity of the host, completely blocking access to the binding site (Figure 2.3a). Alternatively, the Fe$_2$•**2.4b$_2$** cavitand

positions the labile sites at which the oxidation occurs away from the cavity (Figure 2.3b). In the case of **2.4c₂,** molecular modeling shows the *cis*-labile site point completely away from the cavity due to the flexibility of the arms. As the C-H oxidation happened outside the cavity, any selectivity was dominated by substrate-based steric and electronic effects, and proximity-based selective oxidation was not observed.

2.5. Other Catalysts from the Shallow Cavitand Scaffold

The first scaffold shows that water-soluble cavitands can be synthesized with N-donor sites for metal coordination and that these cavitands show some catalytic activity in C-H oxidation. The limitation in the current design of the scaffolds lies in the recognition element of the catalyst and on the ability of the hydrocarbon to be oriented towards the center of the cavity where proximity-directed oxidation is possible. To form a more suitable host:guest complex, we exploited a stronger metal coordinating ligand, 2-dipicolylamine **2.5,** which was used in previous chemoselective catalysts.[20] A simple S_N2 reaction of the tetrabromo cavitand **2.2** with 2-dipicolylamine yielded the octapicolyamine cavitand **2.6** in good yields (61%).
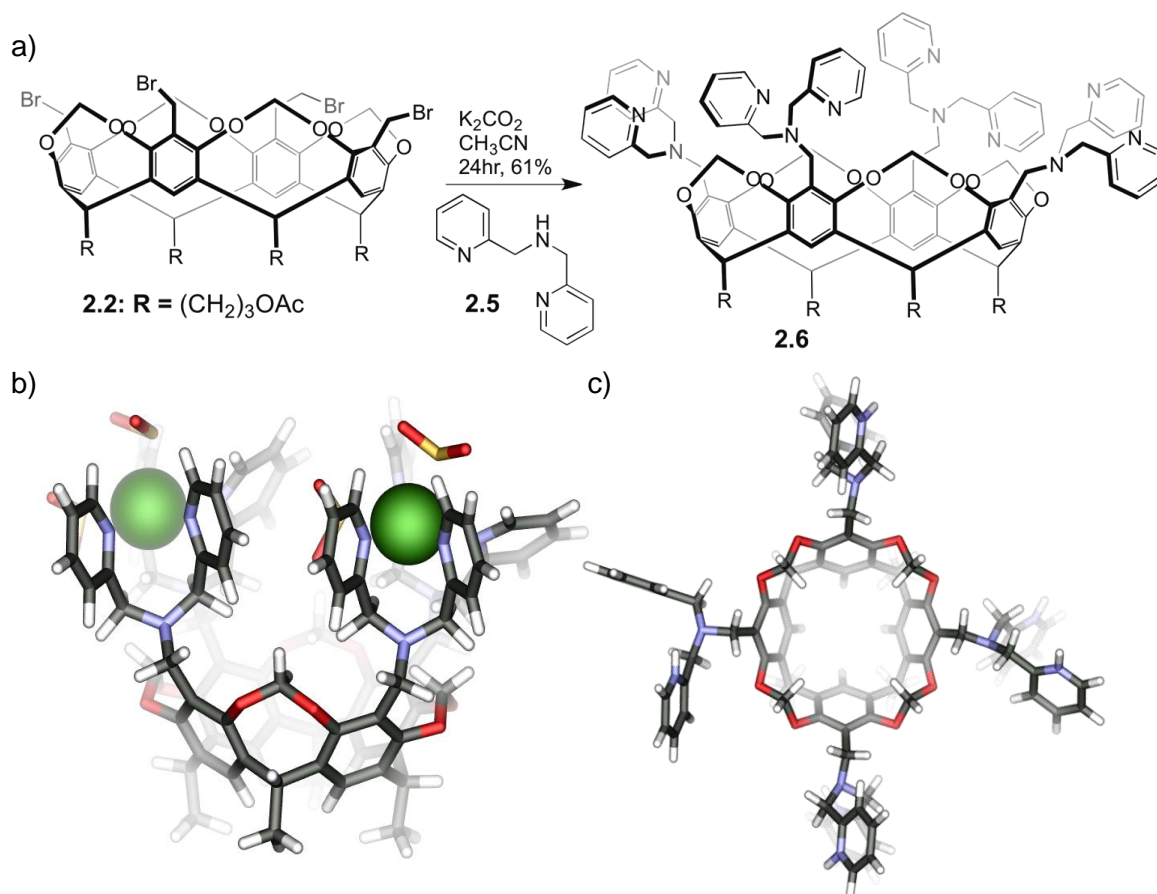
Figure 2.4. a) The synthesis of metal containing shallow cavitand scaffolds b) side view of minimized models of the $Fe_2 \cdot \textbf{2.6}$ catalyst complex structures, (SPARTAN, Hartree-Fock forcefield, SO_4^{2-} as counterion), c) Top view of the minimized model of the ligand **2.6** structure, (SPARTAN, Hartree-Fock forcefield).

Cavitand **2.6** contains tridentate coordinating groups at the rim that allow for metal binding. Isolation of the metal complexes was based on the change in the physical properties between the ligand and the metal complex. Addition of two molar equivalents of $FeSO_4$ to **2.6** in MeOH formed an insoluble $\textbf{2.6} \cdot Fe_2(SO_4)_2$ complex, which precipitated out of methanol. A similar isolation method was conducted to produce $\textbf{2.6} \cdot Ni_2(OAc)_2$ for

benzylic oxidation. Unfortunately, metal coordinating cavitand **2.6**•Fe$_2$(SO$_4$)$_2$ showed no hydrocarbon oxidation activity (Table 2.3). Minimal benzylic oxidation was observed with **2.6**•Ni$_2$(OAc)$_2$ with no selectivity.

Table 2.3. The oxidation of a) hydrocarbon substrates as catalyzed by **2.6**•Fe$_2$SO$_4$ and b) aromatic substrates as catalyzed by **2.6**•Ni$_2$(OAc)$_2$.

The hydrophobic binding site of these hosts does not significantly help pre-organize or orient the guest for regioselective C-H oxidation. These shallow cavitands were incapable of binding hydrocarbons. In addition, limited reactivity was also observed, due to the fully saturated state of the metal binding site. The presence of 6 nitrogens surrounding each metal ion formed an inactive metal complex. Therefore, we focused on alternate smaller scaffolds that would be more reactive and provide better molecular recognition.

2.6. Porphyrin-based Scaffold

Following Cram's preorganization motif, we steered away from complicated synthetic cavitands and navigated toward a simpler approach to regioselective oxidation: small multi-metal ligands. A porphyrin-based scaffold was our second approach to position multiple metals in close proximity to a large aromatic surface for recognition. Initially, we sought to synthesize the unsymmetrical porphyrin scaffold **2.11.** Molecular modeling of scaffold **2.11** showed a promising route to accomplish binding and C-H activation of aromatic substrates via π-π stacking. To synthesize the porphyrin scaffold, we formed 2,2'-(phenylmethylene)bis(1*H*-pyrrole), followed by an aldehyde condensation to form **2.7**. This reaction was unsuccessful, and gave multiple products (mono, di, and tri addition products, Figure 2.5). The coupling reaction gave only 1% yield of target as well as requiring extensive purification. The product was also air sensitive, decomposing from dark purple to tar-like black within one day of isolating.
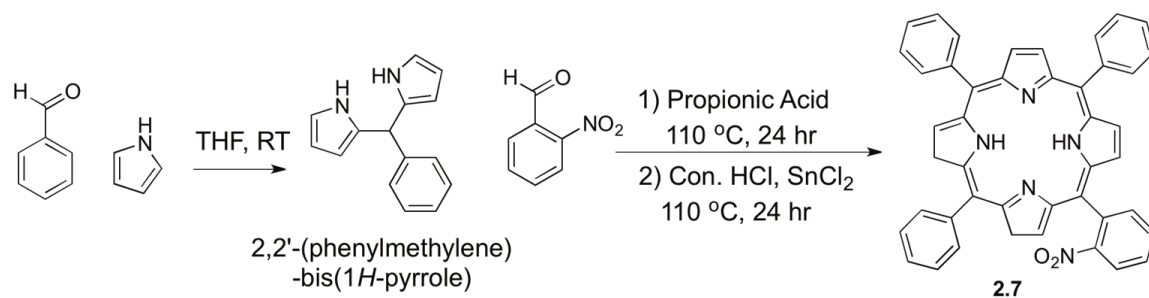
Figure 2.5. First rough for unsymmetrical porphyrin scaffold.

We pursued a one pot reaction to synthesize 5-(*ortho*-aminophenyl)-10, 15, 20-triphenyl porphyrin **2.8** by formation of 5-(*o*-nitrophenyl)-10, 15, 20-triphenyl porphyrin **2.7** under N_2 atmosphere to eliminate decomposition followed by the immediate reduction to the amine without isolation of **2.7**. The single step reaction used 2.0 mol-eq. benzaldehyde, 1.0 mol-eq. *o*-nitrobenzaldehyde and 3.0 mol-eq. pyrrole in the presence of propionic acid without purification. This reaction was followed by reducing the nitro group to the subsequence amine *via* $SnCl_2$.HCl and yielded multiple impurities of the mono/di amine substrate **2.8**. There were multiple failed attempts to isolate the mono-amine product using recrystallization methods in CH_2Cl_2:heptane. However, extraction followed by silica column chromatography eluted with EtOAc:Toluene yielded clean product, albeit in only 3% yield. Attempts to increase the yield of the mono product **2.8**, such as distilling 1*H*-pyrrole in a closed system immediately followed by injections of the nitrobenzaldehyde and benzaldehyde only increased the yield to 15% (Figure 5.2). The formation of 5-(O-azidophenyl)-10, 15, 20-triphenyl porphyrin **2.9** after Zn ion complexation on a small scale showed multiple challenges due to presence of Zn metal in the complex as well as the low yield, and so we focused on an alternate scaffold for oxidation reactions that was more simple to synthesize.
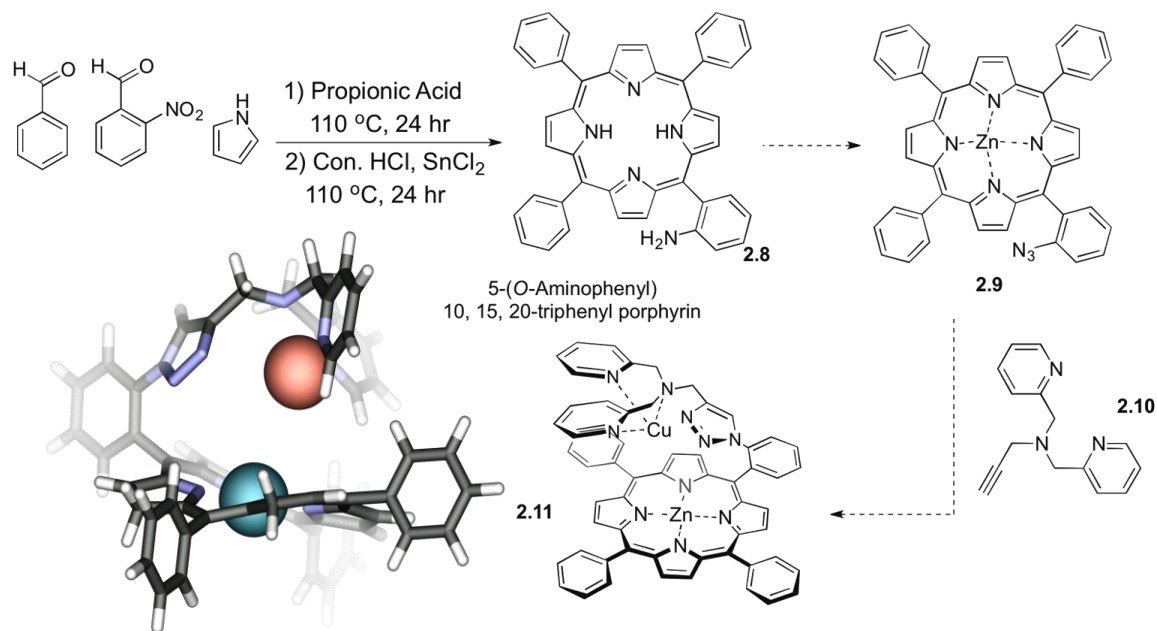
Figure 2.6. Proposed second route to form an unsymmetrical porphyrin scaffold, with minimized models of the proposed metal-ligand **2.11** catalyst-complex structures (Zn ion blue, Cu ion red) (SPARTAN, Hartree-Fock forcefield, counter ions omitted for clarity).

2.7. Benzenetrimethylamine Scaffolds

We sought to create a simple, flexible, self-folding ligand with a preorganized motif that was capable of multiple metal coordination.[21] The 2,4,6,-trisubstituted-1,3,5-triethylbenzene scaffold is an inviting precursor to a preorganized motif. The three ethyl groups are oriented to the same face of the aromatic ring, allowing the three substituted arms to occupy the opposite site of the benzene ring, as shown in **2.12**. Previously, this scaffold has been applied to the creation of species that can bind cations[22,23], anions[24] or saccharides. The azide precursor **2.13** is often reduced to the primary amine for further derivatization, but as we had experience with CuAAC couplings using azide cavitands, this became an interesting and unexplored scaffold for metal complexation.

Utilizing copper(I) catalyzed alkyne-azide cycloaddition (CuAAC) chemistry, we reacted the precursor triazide **2.13** with oligopyridyl-containing alkyne groups to extend the scaffold and provide multiple coordinators. We hoped that this scaffold would also provide a small cavity for guest binding and selectivity.
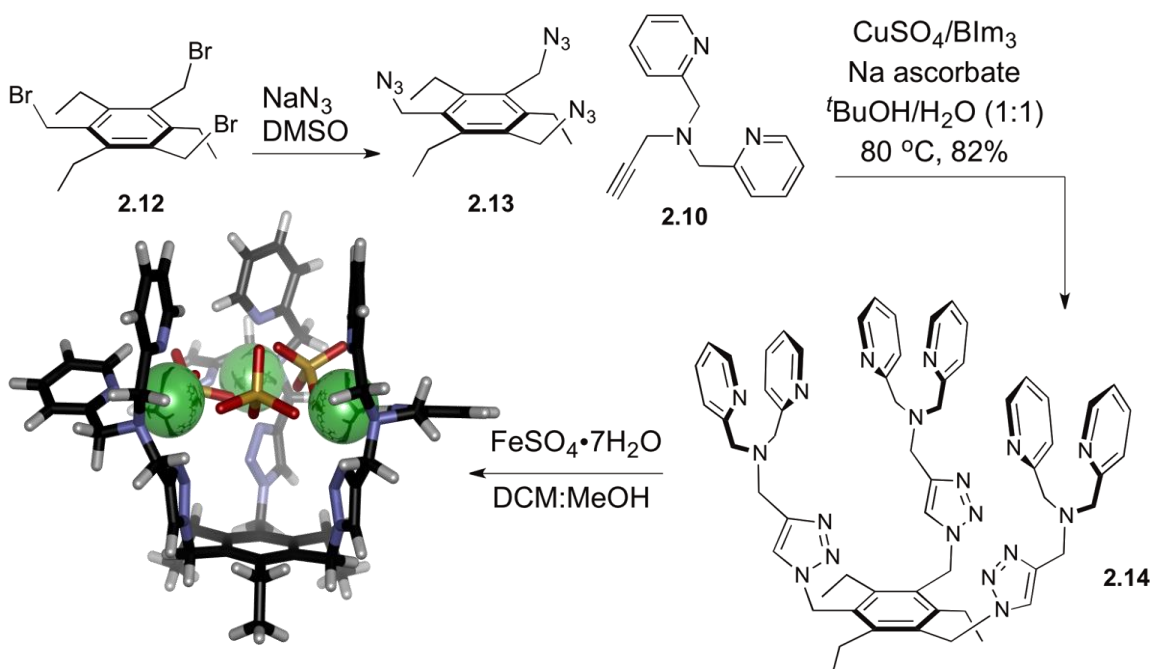
Figure 2.7. Synthesis of the self-folding Fe-binding ligand **2.14** with minimized models of the Fe$_3$•**2.14** catalyst complex structure, (SPARTAN, Hartree-Fock forcefield, SO$_4^{2-}$ as counterions).

A simple S$_N$2 reaction of 2,4,6,-trisbromomethyl-1,3,5-triethylbenzene **2.12** with sodium azide at room temperature gave the trisubstituted azide **2.13** (80%), which could be derivatized with a variety of pyridyl groups. Precursor **2.13** was initially reacted with bis-pyridyl alkyne ligand **2.10** (Figure 2.7). The product **2.14** displayed three tetradentate coordinating groups around the center of the triethylbenzene scaffold. While the CuAAC

reaction proceeded smoothly, isolation of pure ligand **2.14** faced multiple challenges. Bis-pyridyl alkyne **2.10** itself was unstable and very sensitive to oxygen.[20] The synthesis of **2.10** was performed in completely air free conditions, followed by chromatographic purification with basic alumina. The product **2.10** was then rapidly reacted with **2.13** before it could decompose. The most difficult challenge in the click reaction step, which used a Cu^+ catalyst, was that the product **2.14** and the reactant **2.10** are both strong metal coordinators, and can preferentially complex the Cu^+ salts. To minimize loss of Cu^+ catalyst, we introduced the tetradentate coordinator BIm_3 as a co-ligand (Figure 2.8). Even in the presence of the strongly coordinating BIm_3 ligand:$CuSO_4$ system, the reaction required elevated temperatures and long reaction times in a ^tBuO:H_2O mixture to achieve good yields. To ensure the complete removal of the Cu^+ salt from the scaffold, the organic mixture was washed four separate times with an aqueous solution of NaEDTA. Additionally, the product was purified *via* column chromatography in neutral alumina, followed by recrystallization from CH_2Cl_2.
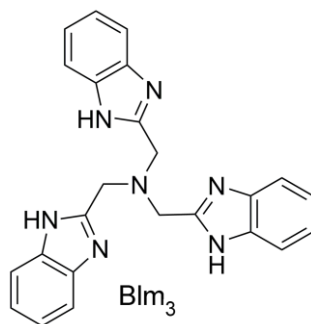
Figure 2.8. Co-ligand BIm_3 used for CuAAC reaction.

2.8. Metal Coordination Properties of the Tri-substituted Scaffold

The extremely strong binding ability of **2.14** to Cu salts suggested that it would be capable of coordinating other metal ions that would confer catalytic activity on the system. To test this, the ligand was combined with three equivalents of FeSO$_4$ in a mixture of CH$_2$Cl$_2$:MeOH, and the metal complex was isolated upon precipitation, after 30 mins of stirring via simple filtration. Unfortunately, it was challenging to produce X-ray quality crystals to unambiguously assign of the complex structure, so we sought other methods of studying the metal complex. In addition, as the **2.14•Fe$_x$** metal complex was weakly paramagnetic and gave rise to broad NMR signals, we determined the coordination stoichiometry using Zn(OTf)$_2$ as a diamagnetic surrogate.

While the coordination modes of Zn^{II} and Fe^{II} can vary, Zn^{II} can act as a suitable diamagnetic surrogate to the Fe^{II} complex due to the similar coordinative properties. **2.14•Zn$_3$** complex was synthesized in similar manner as the **2.14•Fe$_3$** complex. ^{1}H NMR analysis of the **2.14•Zn** complex showed the formation of a stable complex after the addition of three equivalents of Zn^{2+}. Multiple broad and undefined peaks appeared upon the addition of one equivalent of Zn(OTf)$_2$ to **2.14** in DMSO-d_6, and after the addition of one equivalent of Zn(OTf)$_2$, peaks for ligand **2.14** were still present in the sample. After three equivalents of Zn(OTf)$_2$ were added, only one set of aromatic peaks were present, and were shifted down field. The methylene peaks shifted from 3.6 ppm to multiple peaks between 4.0-4.5 ppm, indicating the reduced symmetry and diastereotopic nature of the complex, suggesting that all six pyridyl groups are coordinated to the Zn^{II} ions. The addition of 5 equivalents of Zn(OTf)$_2$ conferred no changes to the spectrum (Figure 2.9).
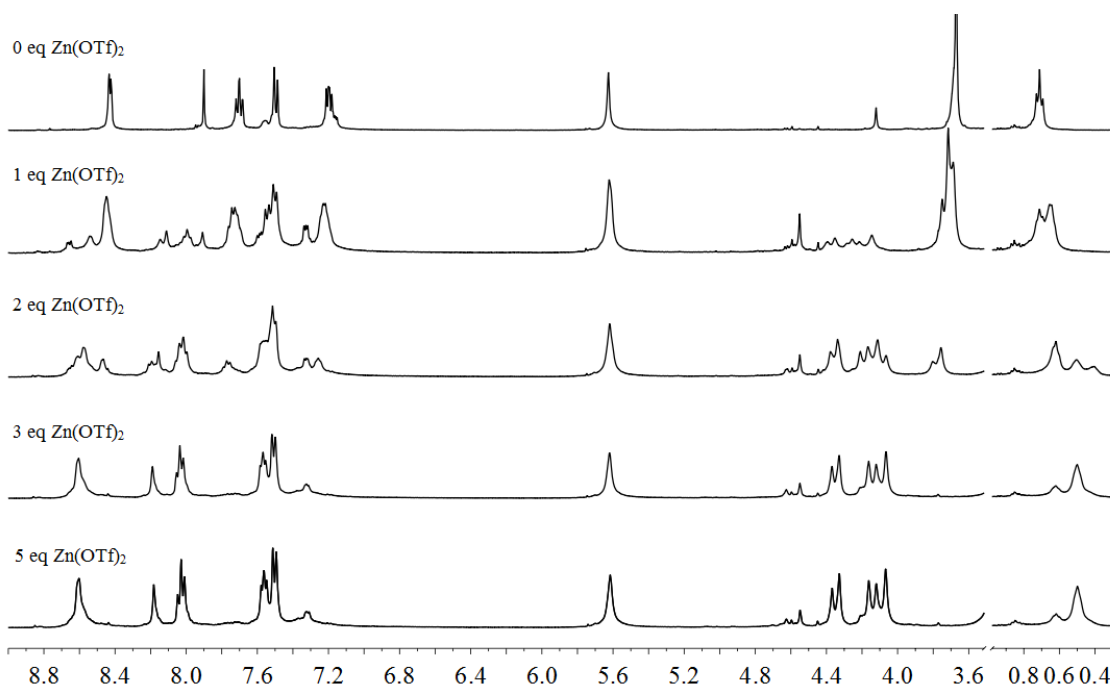
Figure 2.9. Downfield regions of the ^{1}H NMR spectra (400 MHz, 298 K, CDCl$_3$, 2.5 mM **4**) of the addition of Zn(OTf)$_2$ to Hexapicolyl ligand **2.14.**

Analysis of the **2.14•Zn$_3$** complex using MALDI-MS shows only the present of the parent [**2.14•**Zn$_3$(OTf)$_5$]$^+$ ion, as well as a peak corresponding to the loss of one zinc ion (Figure 2.9). MS analysis was also used to determine the stoichiometry of the Fe^{2+} coordination. ESI-MS analysis of **2.14•**Fe$_3$(SO$_4$)$_3$ shows the parent ion [**2.14•**Fe$_3$(SO$_4$)$_3$ H$_2$O•OH]$^+$ as the largest *m/z* species. The major losses were the SO$_4$ groups and the formation of the iron-oxo species under the ionization/injection conditions as evidenced by matching the isotope pattern to the three Fe-containing system.
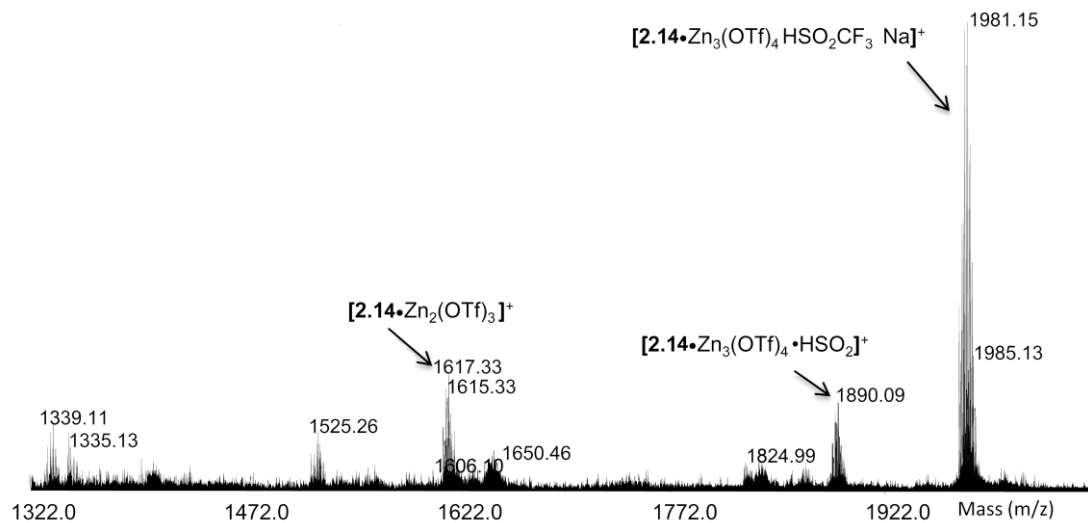
Figure 2.10. ESI-MS full spectrum of Hexapicolyl complex **2.14**•Zn$_3$(OTf)$_6$.
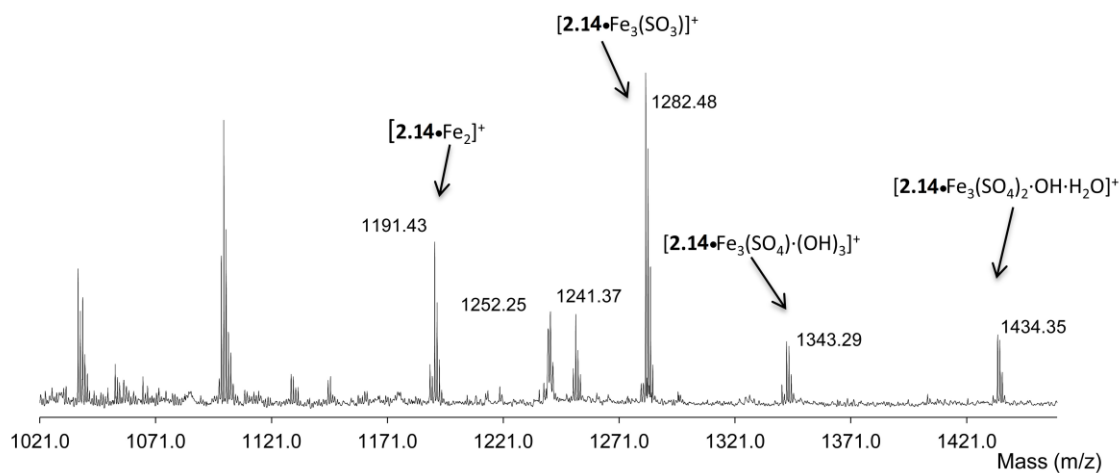
Figure 2.11. ESI-MS full spectrum of Hexapicolyl complex **2.14**•Fe$_3$(SO$_4$)$_3$.

65

In effort to grow a grow X-ray quality crystals of the **2.14•**metal complexes we used a variety of metal ions and different counterion such as **2.14•**Zn$_3$(OTf)$_6$, **2.14•**Fe$_3$(SO$_4$)$_3$, **2.14•**Co$_3$(SO$_4$)$_3$, and **2.14•**Fe$_3$(ClO$_4$)$_6$. As we were unable to grow X-ray quality crystals of the **2.14•**Metal complex, the microcrystals of **2.14•**Fe$_3$(SO$_4$)$_3$ were characterized by elemental analysis, which showed the proposed stoichiometry as well as traces of an additional species with four Fe metals on the complex. No evidence of a four-Fe species was observed in the MS analysis or NMR titration. Nevertheless, ICP analysis of a microcrystalline sample of **2.14•**Fe$_3$(SO$_4$)$_3$ consisted of this mixture with three and four-Fe centers (Table 2.4). The C-H-N combustion analysis showed similar results, which explains the challenges in forming quality X-ray crystals. The weak coordination of the fourth Fe center in the solid state is possible, but the most stable structure in the solution is **2.14•**Fe$_3$(SO$_4$)$_3$. Evidently, weak coordination of an additional Fe^{2+} ion occurs to the **2.14•**Fe$_3$ complex and fast on/off exchange occurs in solution.

Trial	Mass Fraction of Fe in **2.14** (mmol)	(ppm)(vol (l)) / mg total*100
1	0.038	3.806
2	0.0368	3.685
3	0.0378	3.787
Average	0.0376	3.76

Table 2.4. ICP analysis of Hexapicolyl complex **2.14•**Fe$_3$(SO$_4$)$_3$ in 1% nitric acid solution.

Molecular modeling showed the minimized structure of **2.14•**Fe$_3$(SO$_4$)$_3$ with sulfate templation of the structure (Figure 2.12). The close proximity of the metal ions blocks the cavity of the scaffold as shown in the top view of the minimized structure.
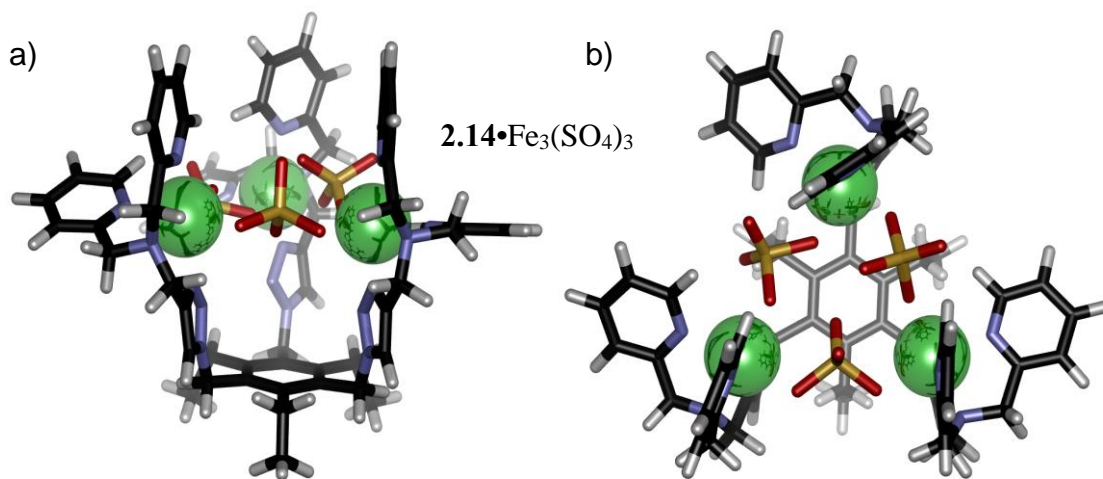
Figure 2.12. a) Side view, b) top view of minimized models of the **2.14•**Fe$_3$(SO$_4$)$_3$ catalyst complex structure (SPARTAN, Hartree-Fock forcefield, SO$_4^{2-}$ as counter ions).

2.9. Optimizing the Oxidation Reaction

Despite the lack of an obvious cavity in the scaffold, we analyzed its capabilities as a hydrocarbon oxidation catalyst. The close proximity of the metals to each other active sites provides a desirable scaffold for hydrocarbon oxidation. The reaction conditions were optimized using cyclooctane, as that is a relatively reactive hydrocarbon due to the torsional strain release upon oxidation. Literature examples of hydrocarbon oxidation generally use hydrogen peroxide (H$_2$O$_2$) as stoichiometric oxidant in a mixture of CH$_3$CN:H$_2$O in the presence of strong acid.[25,26] Maximal conversion from cyclooctane to cyclooctanone in our system was achieved with 10% catalytic loading of the

2.14•Fe$_3$(SO$_4$)$_3$ complex with *tert*-butylhydroperoxide (TBHP) as oxidant. The addition of acid didn't show any increase to either the total conversion or selectivity (entry 4,5). TBHP was the most effective oxidant, and only small or no conversion was observed using NMO and H$_2$O$_2$ respectively (entry 8,9, Table 2.5).
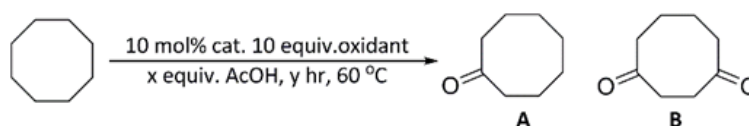
Entry[a]	Oxidant	Time (hr)	Eq. AcOH	Yield (%)	% **A**	% **B**
1	^{t}BuOOH	2	0	29	29	0
2	^{t}BuOOH	6	0	50	50	0
3	^{t}BuOOH	18	0	56	56	0
4	^{t}BuOOH	24	0	84	74	10
5	^{t}BuOOH	24	2	86	73	13
6	^{t}BuOOH	24	5	80	74	6
7	^{t}BuOOH	24	10	80	74	6
8	H$_2$O$_2$	24	0	0	0	0
9	NMO	24	0	53	53	0

Table 2.5. Optimization of oxidation conditions with **2.14**•Fe$_3$(SO$_4$)$_3$.

2.10. Hydrocarbon Oxidation Scope

The optimal reaction conditions employed 10% **2.14•**$Fe_3(SO_4)_3$ with 10 mol.-eq. TBHP and heating to 60 ^{o}C for 24 h. We then determined the scope of the reaction using more challenging substrates. The **2.14•**$Fe_3(SO_4)_3$ complex was an effective catalyst for the oxidation of a variety of unstrained, unactivated cyclic hydrocarbons such as *cis-* and *trans*-decalin, adamantane, methylcyclohexane and linear hydrocarbon *n*-octane (Table 2.5).

The catalyst also provided some interesting regioselectivity. Whereas most C-H activations show strong selectivity for 3° substrates,[26-32] the **2.14•**$Fe_3(SO_4)_3$ complex showed selectivity for 2° C-H bonds. Oxidation of methylcyclohexane (entry 4) gives a 5:1 selectivity for the various ketone isomers over 3° oxidation. *Cis*-decalin (entry 5) displays a 2:1 selectivity towards 2° oxidations, with the terminal ketone product most favored. In the case of *trans*-decalin (entry 6), the overall conversion was higher than *cis*-decalin, with a greater proportion of secondary oxidation occurring, with a 4.4:1 ratio of 2°:3° oxidation. No selectivity between the 2° oxidation products was observed, but good selectivity between 2° and 3° oxidation was possible. The only case where 3° rather than 2° oxidation was favored was in the case of adamantane-carboxylic acid (entry 9), which occurred due to the increase in ring strain upon incorporation of a ketone into the tricyclic system. The carboxylic acid functional group showed no directing effect on the oxidation outcome, as unfunctionalized adamantane showed similar oxidation tendencies (entry 2). Activated C-H bonds were much easier to oxidize, as expected: 4-ethyltoluene was

rapidly oxidized in excellent yields with complete selectivity for ketone formation. Reaction of dibutyl ether provided the corresponding ester with small amount of hydrolysis product. Critically, the usually non-reactive linear n-octane was susceptible to oxidation by multi-metal complex. Also the reaction was not highly selective between 2° oxidation, but did show some unusual regiochemical outcomes.

10 mol% cat. 10 equiv. ^{t}BuOOH
60 °C, 24h

Entry	Substrate	Total (%)	Product yields (%)

1[a] — 84 — 74 — 10

2[b] — 5 — HO 4 — O 1

3[a] n-Octane — 55 — 20 — 17 — 18

4[a] — 47 / 79 — OH 8 — 8 — 21 — 10

5[a] — 88 — OH 27 — OH 11 (2 isomers) — 15 — 26

6[a] — 72 — OH 12 — HO 24 (2 isomers) — O 35 — 17

7[a] nBu$_2$O — 98 — 43 — 29 (OH)

8[a] — 32 — 98

9[b] — CO$_2$H — OH CO$_2$H 26 — O CO$_2$H 6

Table 2.6. Scope of unactivated hydrocarbon oxidation with **2.14**•Fe$_3$(SO$_4$)$_3$. a) reaction performed in 1:1 MeCN: H$_2$O. b) reaction performed in 1:1 EtCN: H$_2$O.

71

2.11. Control Scaffold Synthesis

In an effort to demonstrate the requirement for multiple metal ions in close proximity for the catalytic activity, four other ligand systems were synthesized as controls, as shown in Figures 2.13 and 2.15. The analogue of the same core scaffold with fewer N-donor sites was accessed using tri(bromomethyl) triethyl-benzene **2.13** and 2-ethynylpyridine **2.15** *via* click reaction with Blm₃ as co-catalyst yielding tris-pyridyl triazine **2.16**. Ligand **2.18** provides the same tetracoordinating metal complexing group, but contains only one of them. Bis-pyridyl alkyne **2.10** was reacted with with 9-(azidomethyl)anthracene **2.17** under similar conditions as before, yielding **2.18** (Figure 2.13a,b). To offer a larger aromatic group for target recognition, 1-azidopyrene **2.19** was synthesized from 1-aminopyrene followed by CuAAC reaction with the bis-pyridyl alkyne **2.10,** yielding **2.20** in very low yields due to challenges in purification. Lastly, the analogue **2.22** is capable of complexing two metals, without the possibility of preorganization. **2.21** was synthesized from its precursor 9, 10-bromomethyl anthracene, followed by S_N2 reaction to yield 9, 10-dipicolyl-anthracene **2.22** in 92% yield (Figure 2.15a,b). Molecular modeling showed the minimized structures of **2.16**•FeSO₄ and **2.18**•Fe₃SO₄, including sulfate temptation of the structures (Figure 2.14).
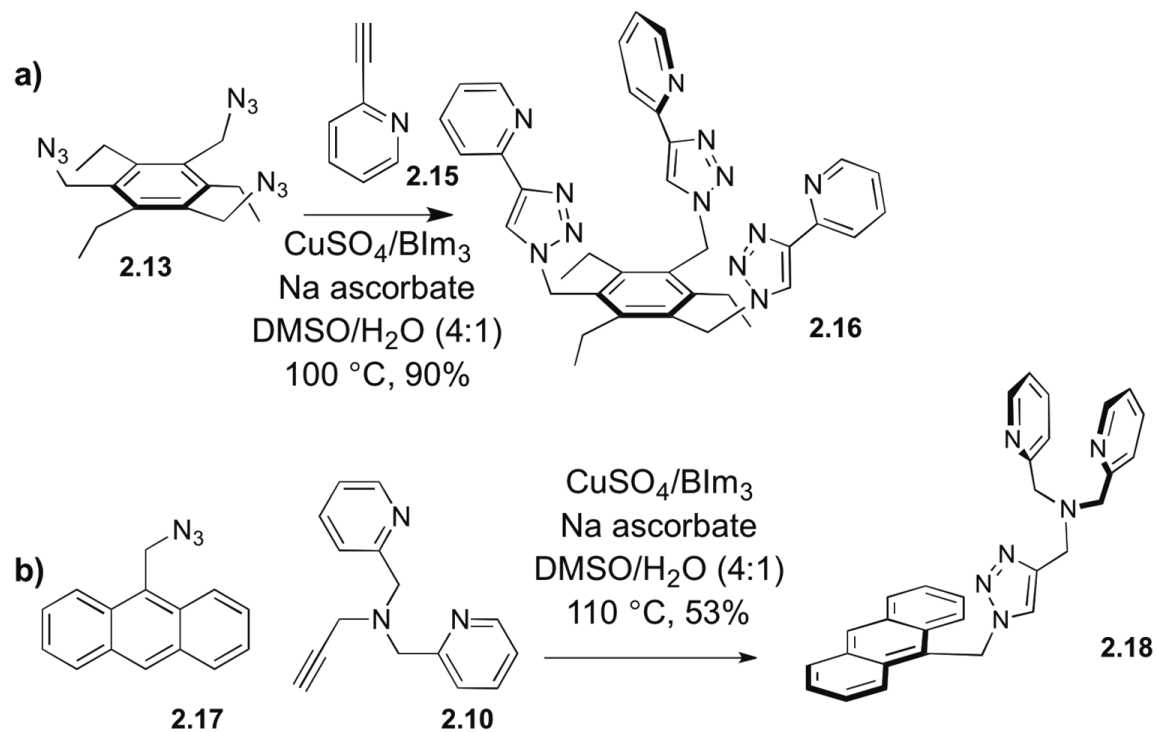
Figure 2.13. a) Synthesis of the control Fe-binding ligands **2.16**, b) and **2.18.**
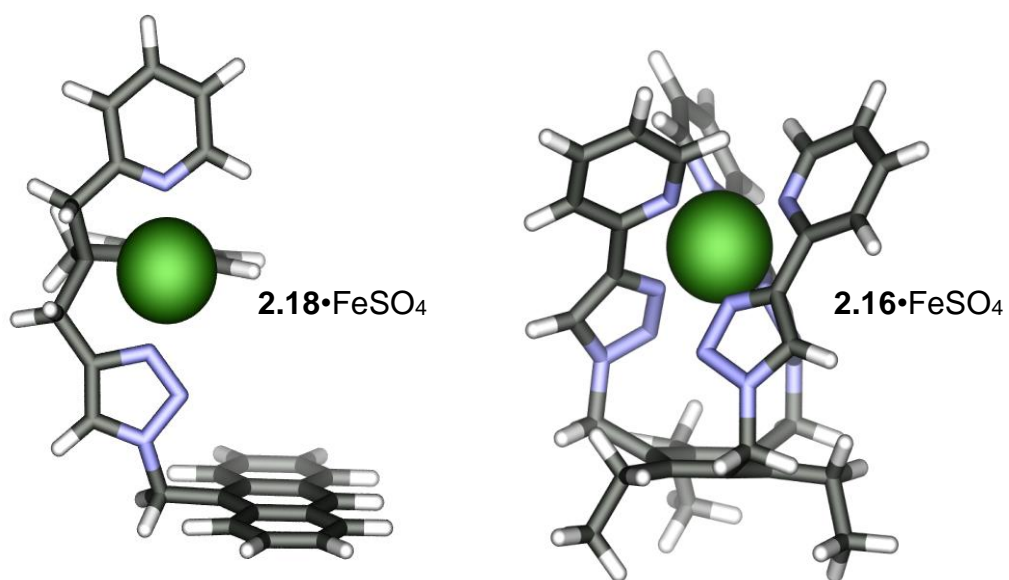
Figure 2.14. Minimized models of the control Fe-ligand **2.16**, and **2.18** catalyst complex structures, (SPARTAN, Hartree-Fock forcefield, counter ions omitted for clarity).
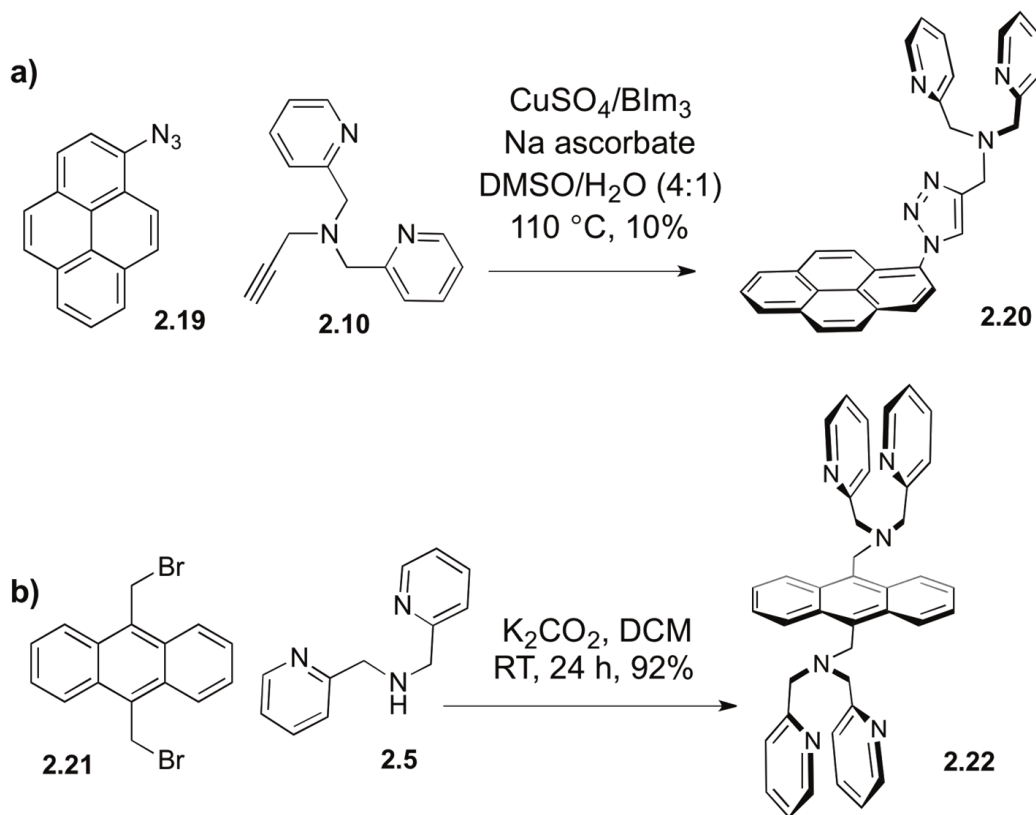
Figure 2.15. a) Synthesis of control Fe-binding ligand **2.20**, b) and **2.22.**
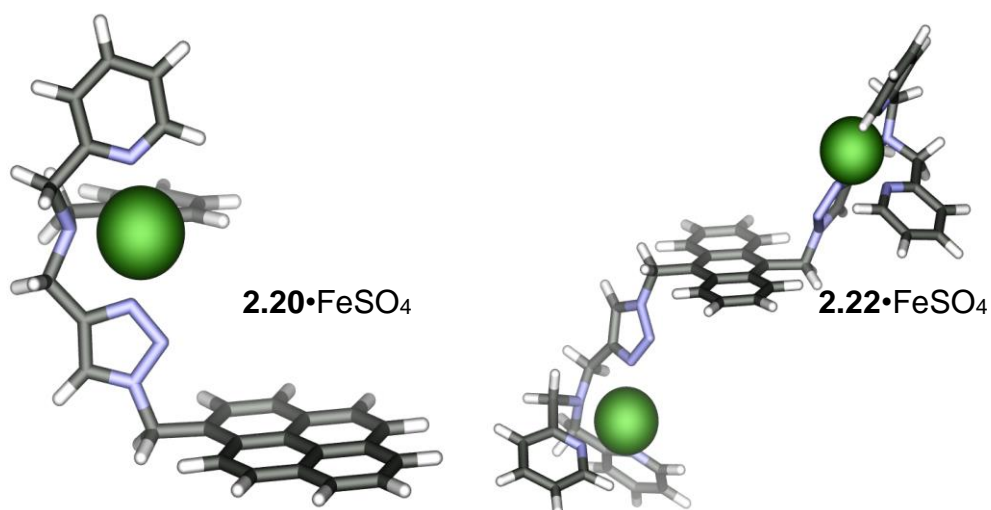
Figure 2.16. Minimized models of the control Fe-ligand **2.20**, and **2.22** catalyst complex structures, (SPARTAN, Hartree-Fock forcefield, counter ions omitted for clarity).

2.12. Metal Coordination of the Mono-substituted Scaffolds

As expected, ^{1}H NMR analysis of the Zn complex of the control ligands showed the formation of a stable complex in the presence of a single equivalent of metal ion. Broad and undefined peaks appeared upon the addition of one equivalent of Zn(OTf)$_2$ to the ligand in CDCl$_3$. With the addition of one equivalent of Zn(OTf)$_2$ to ligand **2.16**, the aromatic peak have shifted slightly and broadened out with limitate changes to the CH$_2$ peaks. NMR titration of Zn(OTf)$_2$ with **2.16** showed no change in the chemical shift after the addition of more than one equivalent of Zn ion (Figure 2.17). Similar behavior was observed with the **2.18** and **2.20** scaffolds.
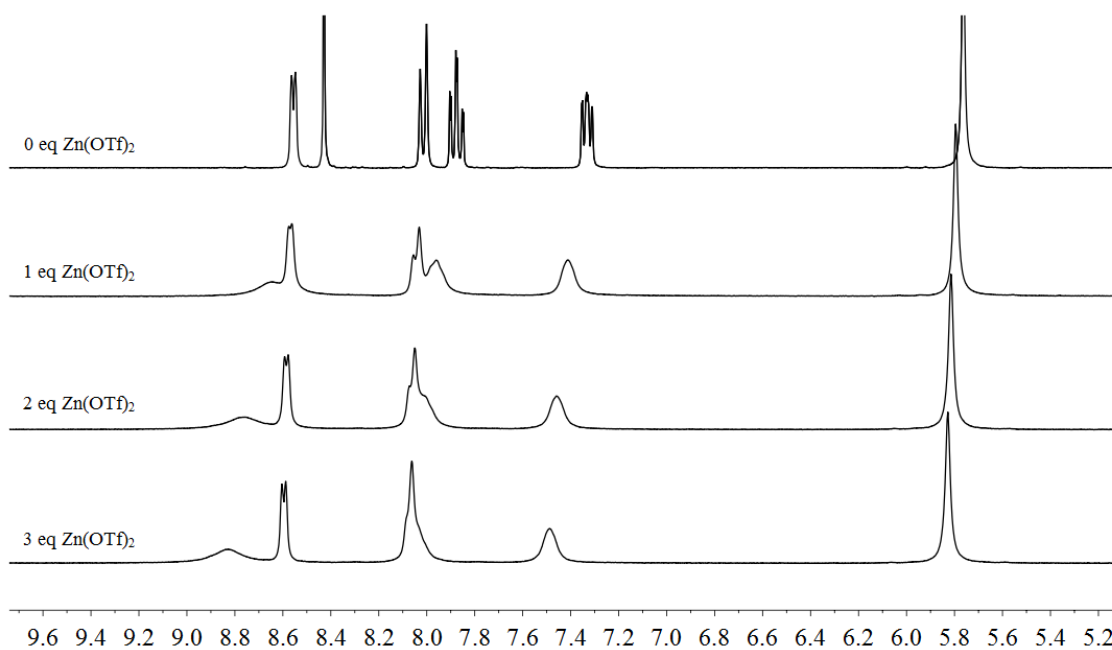
Figure 2.17. Downfield regions of the ^{1}H NMR spectra (400 MHz, 298 K, CDCl$_3$, 2.5 mM **2.16**) of the addition of Zn(OTf)$_2$ to Tris-pyridyl ligand **2.16**.

The control ligands **2.16** and **2.18** were simpler in their purification and coordination properties than the multi-metal binding **2.14**. ESI-MS analysis showed the presence of only one Fe^{II} ion when **2.16** or **2.18** were complexed with $FeSO_4$, as expected (Figure 2.18). Interestingly, the Fe-N coordination was stronger than the N-C bond, as a fragment in the mass spectrum shows the binding site with the metal ion as it fragmented from the aromatic region at 447.3 *m/z*. ESI-MS showed the loss of the anthracenyl group via C-C cleavage rather than the loss of the Fe ion (Figure 2.18). ICP analysis was consistent with a monomeric coordination of $FeSO_4$ to **2.18** scaffold, as shown in Table 2.7.
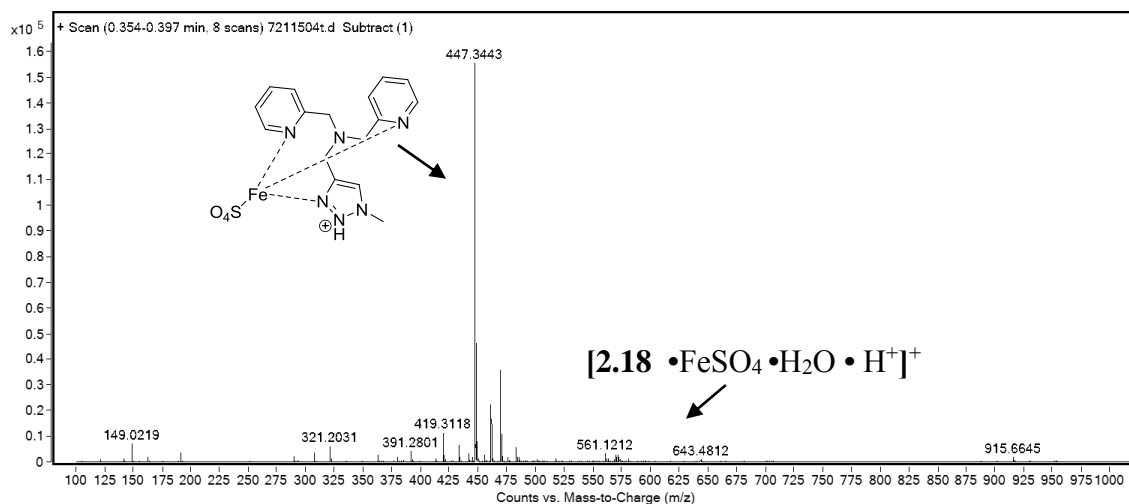
Figure 2.18. ESI-MS full spectrum of Dipicolyl complex **2.18** •$FeSO_4$.

Trial	Mass Fraction Ligand **2.18** (mmol)	(ppm)(vol (l)) / mg total*100
1	0.01598	1.6
2	0.0164	1.6
3	0.017	1.7
Average	0.0164	1.64

Table 2.7. ICP analysis of Dipicolyl complex **2.18**•FeSO$_4$ in 1% nitric acid solution.

2.13. Hydrocarbon Oxidation with Control Complexes

In contrast to the effective oxidation performance of **2.14**•Fe$_3$(SO$_4$)$_3$ complex, the control complexes **2.16**•FeSO$_4$ and **2.18**•FeSO$_4$ a much narrower scope of hydrocarbon oxidation reactions. The obtained yields for cyclooctane and *trans*-decalin oxidation in similar oxidation conditions were similar for catalysts **2.16**•FeSO$_4$ and **2.18**•FeSO$_4$, and showed lower oxidation yields as compared to the **2.14**•Fe$_3$(SO$_4$)$_3$ complex. The most noticeable difference between the control catalysts and **2.14**•Fe$_3$(SO$_4$)$_3$ was in the challenging substrate *n*-octane. Both control complexes **2.16**•FeSO$_4$ and **2.18**•FeSO$_4$ showed no product at all in the oxidation of *n*-octane. Even when the catalyst loading was increased to 30%, neither catalyst **2.16**•FeSO$_4$ and **2.18**•FeSO$_4$ showed activity to *n*-octane oxidation (Table 2.8). While the more reactive substrates can be oxidized by single Fe center, only the self-folded, multi-metal catalyst **2.14**•Fe$_3$(SO$_4$)$_3$ is capable of oxidizing the more challenging linear, unactivated hydrocarbons. Minimal to no

oxidation of *trans*-decalin was observed with **2.22**•Fe$_2$(SO$_4$)$_2$, due to instability of the scaffold as evidenced by the presence of 9,10-anthracenedione.

Substrate	Cat. loading	Total (%)	Product yields (%)			
	10% **2.16**•FeSO$_4$	74	69	5		
	30% **2.16**•FeSO$_4$	72	72	0		
	10% **2.18**•FeSO$_4$	53	53	0		
	30% **2.18**•FeSO$_4$	47	47	0		
	10% **2.16**•FeSO$_4$	28	1	8	11	8
	30% **2.16**•FeSO$_4$	19	2	2	8	7
	10% **2.18**•FeSO$_4$	38	5	3	13	17
	30% **2.18**•FeSO$_4$	27	4	2	10	11
	10% **2.16**•FeSO$_4$	0	0	0	0	
	30% **2.16**•FeSO$_4$	0	0	0	0	
	10% **2.18**•FeSO$_4$	0	0	0	0	
	30% **2.18**•FeSO$_4$	0	0	0	0	

Table 2.8. Scope of unactivated hydrocarbon oxidation with monometal complexes.

2.14. Conclusion

The initial synthesis of molecular recognition scaffolds for hydrocarbon oxidation were shallow cavitands, but these showed limited proximity direction in hydrocarbon oxidation, although they were effective catalysts. Therefore, we decided to on focus on improving the hydrocarbon oxidation catalytic activity. Multimetal hydrocarbon oxidation catalyst **2.14** showed great success in oxidizing linear unfunctionalized

hydrocarbons. Unfortunately, while scaffold **2.14** shows extremely promising results as a catalyst for hydrocarbon oxidation, its lack of a cavity removes any possibility of a recognition element. To provide proximity-directed regioselective hydrocarbon oxidation, scaffolds must recognize, encapsulate, and then orient the hydrocarbon prior to the oxidation step. As we were successful in oxidizing those difficult substrates, we moved to solve the recognition element to our scaffolds. To achieve such a complicated goal, we moved away from the benzene-based scaffold to a larger template capable of molecular recognition. Returning back to cavitand scaffolds requires the incorporation of an active site on the upper rims. The challenge there was to incorporate the successful catalytic motifs from **2.14** into a more complex structure that contains a molecular recognition element.

2.15. References

(1)   Abu-Omar, M. M.; Loaiza, A.; Hontzeas, N. Reaction mechanisms of mononuclear non-heme iron oxygenases. *Chem. Rev.* **2005**, *105*, 2227-2252.

(2)   Costas, M.; Mehn, M. P.; Jensen, M. P.; Que, L., Jr. Dioxygen activation at mononuclear nonheme iron active sites: enzymes, models, and intermediates. *Chem. Rev.* **2004**, *104*, 939-986.

(3)   Solomon, E. I.; Chen, P.; Metz, M.; Lee, S. K.; Palmer, A. E. Oxygen Binding, Activation, and Reduction to Water by Copper Proteins. *Angew. Chem. Int. Ed.* **2001**, *40*, 4570-4590.

(4)   Chan, S. I.; Yu, S. S. Controlled oxidation of hydrocarbons by the membrane-bound methane monooxygenase: the case for a tricopper cluster. *Acc. Chem. Res.* **2008**, *41*, 969-979.

(5)   Mekmouche, Y.; Hummel, H.; Ho, R. Y.; Que, L., Jr.; Schunemann, V.; Thomas, F.; Trautwein, A. X.; Lebrun, C.; Gorgy, K.; Lepretre, J. C.; Collomb, M. N.; Deronzier, A.; Fontecave, M.; Menage, S. Sulfide oxidation by hydrogen peroxide catalyzed by iron complexes: two metal centers are better than one. *Chem. Eur. J.* **2002**, *8*, 1196-1204.

(6)   Duboc-Toia, C.; Menage, S.; Ho, R. Y.; Que, L., Jr.; Lambeaux, C.; Fontecave, M. Enantioselective Sulfoxidation as a Probe for a Metal-Based Mechanism in H_2O_2-Dependent Oxidations Catalyzed by a Diiron Complex. *Inorg. Chem.* **1999**, *38*, 1261-1268.

(7)   Ampurdanes, J.; Crespo, G. A.; Maroto, A.; Sarmentero, M. A.; Ballester, P.; Rius, F. X. Determination of choline and derivatives with a solid-contact ion-selective electrode based on octaamide cavitand and carbon nanotubes. *Biosens. Bioelectron.* **2009**, *25*, 344-349.

(8)   Zhang, K. D.; Ajami, D.; Gavette, J. V.; Rebek, J., Jr. Alkyl groups fold to fit within a water-soluble cavitand. *J. Am. Chem. Soc.* **2014**, *136*, 5264-5266.

(9)   Zhang, K. D.; Ajami, D.; Gavette, J. V.; Rebek, J., Jr. Complexation of alkyl groups and ghrelin in a deep, water-soluble cavitand. *Chem. Commun.* **2014**, *50*, 4895-4897.

(10)   Zhang, B.; Isaacs, L. Acyclic Cucurbit[n]uril-type Molecular Containers: Influence of Aromatic Walls on their Function as Solubilizing Excipients for Insoluble Drugs. *J. Med. Chem.* **2014**, *57*, 9554-9563.

(11)   Lledo, A.; Rebek, J., Jr. Deep cavitand receptors with pH-independent water solubility. *Chem. Commun.* **2010**, *46*, 8630-8632.

(12)   Hooley, R. J.; Van Anda, H. J.; Rebek, J., Jr. Extraction of hydrophobic species into a water-soluble synthetic receptor. *J. Am. Chem. Soc.* **2007**, *129*, 13464-13473.

(13)   Haino, T.; Rudkevich, D. M.; Shivanyuk, A.; Rissanen, K.; Rebek, J., Jr. Induced-fit molecular recognition with water-soluble cavitands. *Chem. Eur. J.* **2000**, *6*, 3797-3805.

(14)   Gibb, C. L.; Gibb, B. C. Anion binding to hydrophobic concavity is central to the salting-in effects of Hofmeister chaotropes. *J. Am. Chem. Soc.* **2011**, *133*, 7344-7347.

(15)   Suman, M.; Freddi, M.; Massera, C.; Ugozzoli, F.; Dalcanale, E. Rational design of cavitand receptors for mass sensors. *J. Am. Chem. Soc.* **2003**, *125*, 12068-12069.

(16)   Strutt, N. L.; Forgan, R. S.; Spruell, J. M.; Botros, Y. Y.; Stoddart, J. F. Monofunctionalized pillar[5]arene as a host for alkanediamines. *J. Am. Chem. Soc.* **2011**, *133*, 5668-5671.

(17)   Paolesse, R.; Di Natale, C.; Nardis, S.; Macagnano, A.; D'Amico, A.; Pinalli, R.; Dalcanale, E. Investigation of the origin of selectivity in cavitand-based supramolecular sensors. *Chem. Eur. J.* **2003**, *9*, 5388-5395.

(18)   Mokhtari, B.; Pourabdollah, K. Application of Calixarenes in Development of Sensors. *Asian J. Chem.* **2013**, *25*, 1-12.

(19)   Djernes, K. E.; Moshe, O.; Mettry, M.; Richards, D. D.; Hooley, R. J. Metal-coordinated water-soluble cavitands act as C-H oxidation catalysts. *Org. Lett.* **2012**, *14*, 788-791.

(20)   Rosenthal, J.; Lippard, S. J. Direct detection of nitroxyl in aqueous solution using a tripodal copper(II) BODIPY complex. *J. Am. Chem. Soc.* **2010**, *132*, 5536-5537.

(21)   Mettry, M.; Moehlig, M. P.; Gill, A. D.; Hooley, R. J. Alkane oxidation catalysed by a self-folded multi-iron complex. *Supramol. Chem.* **2017**, *29*, 120-128.

(22)   Hughes, A. D.; Anslyn, E. V. A cationic host displaying positive cooperativity in water. *Proc. Natl. Acad. Sci. U.S.A.* **2007**, *104*, 6538-6543.

(23)   Sather, A. C.; Berryman, O. B.; Rebek, J., Jr. Selective recognition and extraction of the uranyl ion. *J. Am. Chem. Soc.* **2010**, *132*, 13572-13574.

(24)   Perreault, D. M.; Cabell, L. A.; Anslyn, E. V. Using guanidinium groups for the recognition of RNA and as catalysts for the hydrolysis of RNA. *Bioorg. Med. Chem.* **1997**, *5*, 1209-1220.

(25)   Bigi, M. A.; Reed, S. A.; White, M. C. Directed metal (oxo) aliphatic C-H hydroxylations: overriding substrate bias. *J. Am. Chem. Soc.* **2012**, *134*, 9721-9726.

(26)   Chen, M. S.; White, M. C. A predictably selective aliphatic C-H oxidation reaction for complex molecule synthesis. *Science* **2007**, *318*, 783-787.

(27)   Que, L., Jr.; Tolman, W. B. Biologically inspired oxidation catalysis. *Nature* **2008**, *455*, 333-340.

(28)   Litvinas, N. D.; Brodsky, B. H.; Du Bois, J. C-H hydroxylation using a heterocyclic catalyst and aqueous H_2O_2. *Angew. Chem. Int. Ed.* **2009**, *48*, 4513-4516.

(29)   Gomez, L.; Garcia-Bosch, I.; Company, A.; Benet-Buchholz, J.; Polo, A.; Sala, X.; Ribas, X.; Costas, M. Stereospecific C-H oxidation with H2O2 catalyzed by a chemically robust site-isolated iron catalyst. *Angew. Chem. Int. Ed.* **2009**, *48*, 5720-5723.

(30)   Morimoto, Y.; Bunno, S.; Fujieda, N.; Sugimoto, H.; Itoh, S. Direct hydroxylation of benzene to phenol using hydrogen peroxide catalyzed by nickel complexes supported by pyridylalkylamine ligands. *J. Am. Chem. Soc.* **2015**, *137*, 5867-5870.

(31) Borovik, A. S. Role of metal-oxo complexes in the cleavage of C-H bonds. *Chem. Soc. Rev.* **2011**, *40*, 1870-1874.

(32) Janardanan, D.; Wang, Y.; Schyman, P.; Que, L., Jr.; Shaik, S. The fundamental role of exchange-enhanced reactivity in C-H activation by S=2 oxo iron(IV) complexes. *Angew. Chem. Int. Ed.* **2010**, *49*, 3342-3345.

Chapter 3: Metal Coordination of Functionalized Self-folding Deep Cavitands

3.1. Introduction

The metal-coordinating complex **2.4b, 2.4c** was an effective hydrocarbon oxidation catalyst, but did not have a large enough cavity for hydrocarbon recognition and preorganization. To combine the effective catalytic activity of **2.4** in a host system, we sought a more complex deep cavitand-based scaffold. The initial strategy was to deepen the shallow benzyl cavitand scaffold **1.24** to create deep, rigid walls while including an acetylene group for CuAAC derivatization. This would allow us to introduce the N-donor sites needed for metal complexation.

3.2. Rigid Acetylene Cavitand

Our first promising pathway to deepen the cavity as well as fix the triazole sites further from the cavity is to access functionalized deep cavitands with more rigid rims forcing the labile site to point inward toward the cavity. This route used resorcinarene-based cavitand **1.24b** as the starting point. Tetra-acetylene **3.2** was synthesized by bridging the hydroxyl group of the resorcinarene **1.24b** with 4-iodo-α,α-dibromotoluene, yielding cavitand **3.1**. This route eliminates the CH_2 linker from cavitands **2.4a-d**, which caused flexibility in the walls and poor folding outcomes. The reaction yielded only 10% desired product due to the high number of stereochemical possibilities. To introduce the acetylene group, a Sonogashira coupling reaction was performed between trimethylsilylacetylene and **2.1.** Removal of the TMS group yields tetraacetylene **3.2**,

which could be identified by the presence of a new sharp resonance at δ 3.07 ppm for the acetylene proton ^{1}H NMR. Further functionalization of this deep cavitand was challenging, however, and CuAAC reactions with a variety of substituted azides containing *N*-donor sites for metal coordination only gave incomplete reaction. The presence of an electron rich N-donor site for metal ion complexation resulted in deleterious Cu binding, and it was challenging to remove the Cu ion out of the scaffold after the click reaction, even in the presence of BIm$_3$ co-ligand.
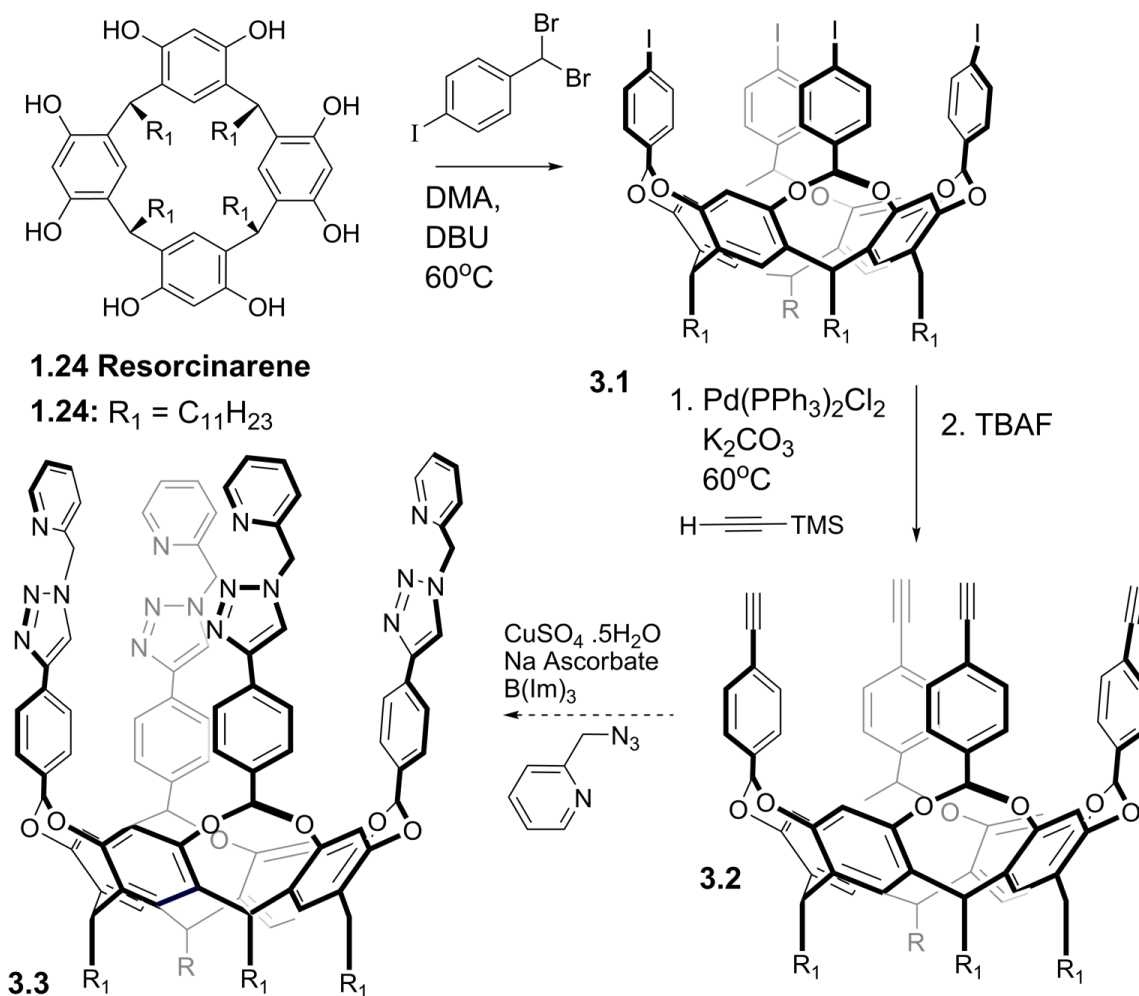
Figure 3.1. Proposed synthesis of the rigid self folded cavitand catalyst.

Molecular modeling suggests that cavitand **3.3** should be capable of coordinating two iron centers at the rim of the cavitand through the pyridyl nitrogens as well as one triazole nitrogen, leaving two remaining valences on the metal centers pointing toward the cavity (Figure 3.2). However, isolation and characterization of the cavitand was difficult, and due to the low reaction yield and challenging purification, we decided to avoid rigid scaffolds and move to investigating the introduction of functional groups to the well-known self-folding benzimidazole cavitand scaffold.[1-7]
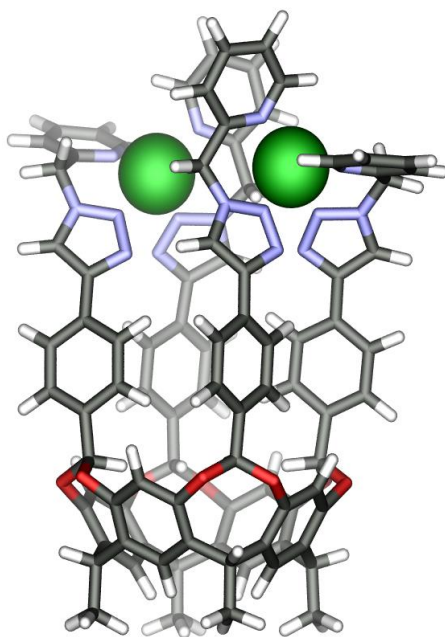
Figure 3.2. Minimized model of the proposed host structures **3.3**•Fe$_2$ (SPARTAN, Hartree-Fock forcefield).

3.3. Challenges of Functionalizing Benzimidazole Cavitands

The water-soluble self-folding benzimidazole cavitands **1.26-1.30** were very encouraging scaffolds, as they showed excellent binding affinity for hydrocarbon guests.

However, to use this scaffold as a catalyst, the bound guests must be exposed to an incorporated metal species, and this requires introducing metal binding arms to the deep cavitand scaffold, which is rare.[8-10] The attachment of N-donor functional groups to the scaffold has been limited due to the challenges in benzamidazole formation and the product solubility. The main challenge was the formation of the insoluble velcrands as previously discussed.[11] The successful folding of benzimidazole cavitands requires additives that contain both hydrogen bond donors and acceptors, such as water and methanol to form the intramolecular hydrogen-bonding seam around the top rim of the cavitands.[12] The addition of alkyl groups or esters can be achieved by treating the precursor octaamine with corresponding orthoester,[13] alkoxyimidate, [14,15] or aldehyde in the presence of oxidizing agents (Figure 3.3).[16] The introduction of amines, heterocycles, or other functions is poorly tolerated *via* this route, however, yielding a limited scope of functionalized benzamidazole deep cavitands. There are three methods for the formation of the benzimidazole cavitand: condensation of an orthoester,[13] oxidative coupling of an aldehyde[6] and condensation of a nitrile derived imidate.[17] There are many drawbacks to all three methods which make it nearly impossible to introduce an N-donor metal binding groups. The use of orthoesters requires dehydration or deamination of esters or nitriles, which involves harsh conditions. The oxidative coupling of an aldehyde relies on harsh coupling conditions and extensive purification steps. However, the condensation of an imidate HCl salt occurs in mild conditions and limited to no purification steps are needed. Although the imidate condensation reaction was promising, imidate formation from nitriles with nitrogen-containing substrates such as pyridine groups failed upon the

addition of HCl due to protonation of the substrate. To functionalize the scaffold with our metal-coordinators, we required alternative synthetic methods in order to introduce the N-donor metal binding groups. Two different methods for introducing heteroatoms to the cavitand backbone were investigated. To utilize the deep cavitand scaffold in the presence of the N-donor sites, one must form the benzimidazole first, and then subsequently introduce the nitrogen-containing substrates in the final step.
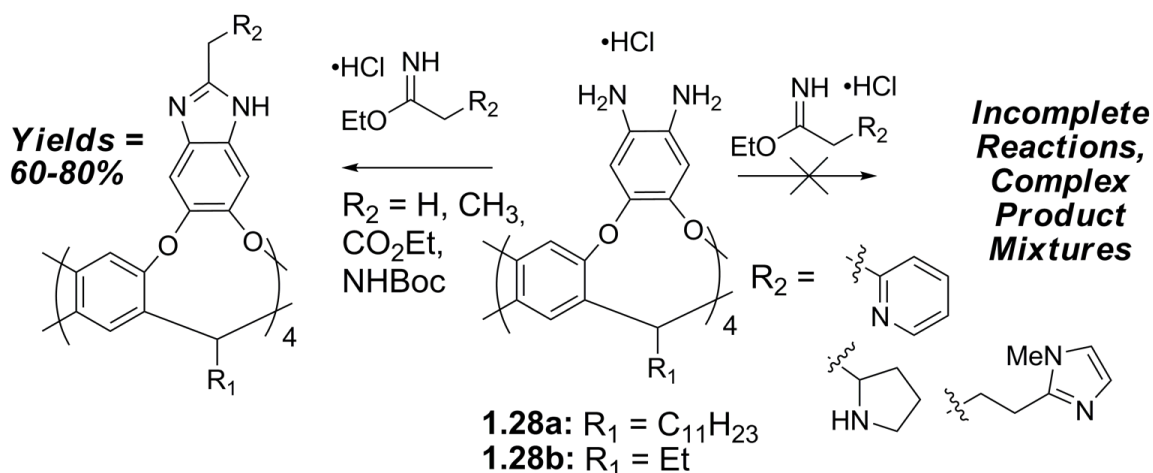
Figure 3.3. Imidate condensation reaction scope for benzimidazole formation.

3.4. Thiobenzimidazole Cavitands

Our first approach was to incorporate thiol-containing walls to the scaffold, as they can be easily derivatized by simple substitution.[18,19] The formation of the thiobenzimidazole unit followed similar synthetic routes to the original benzamidazole cavitand scaffold.[19] Resorcinarenes **1.24a-c** were reacted with 4,5-difluoro-1,2-dinitrobenzene to form octanitro cavitands **1.27a-c** (Figure 3.4). Reduction with SnCl$_2$ in EtOH yielded octaamine cavitands **1.28** as previously discussed. Treatment of octaamine cavitand **1.28a**

with carbon disulfide under basic conditions provides the thiol-containing benzimidazole cavitand **3.4a** with long $C_{11}H_{23}$ feet. Cavitand **1.28** synthesized with the different lower rims such as C_2H_5 and $C_{11}H_{23}$, however the $C_{11}H_{23}$ foot was much easier to hander for purification and isolation. Cavitands with ethyl and alcoholic feet were synthesized for their water solubility (see Chapter 4), however the intermediate cavitands are poorly soluble and much harder to handle. Cavitand **3.4a** gave a broad ^{1}H NMR spectrum at 298 K, but showed a sharp proton peak at 11.87 ppm corresponding to the symmetric SH protons at 350 K. High temperature NMR is required to average out the peaks for the two different tautomers of the SH-NH thiobenzimidazole group. The NMR also shows the present of sharp CH methine peak at δ 5.32 corresponding to the self-folded conformation of the cavitand aided by the water molecules present in the wet chloroform solution. The proposed synthesis can also be carried out with ethyl-footed resorcinarene **1.24b**.

To introduce the metal coordinating sites above the cavity, derivatizations *via* nucleophilic substitution reactions with suitable reactive alkyl halides were tested. Reaction of **3.4a** with bromide precursor **3.6** produced functionalized C_{11}-cavitands **3.5a-b** in good yield. Cavitand **3.5a** contains bidentate coordinating groups at the rim that allow for metal binding, and cavitand **3.5b** is a non-coordinating control that allows for simple analysis of the folding and conformation of the hosts.
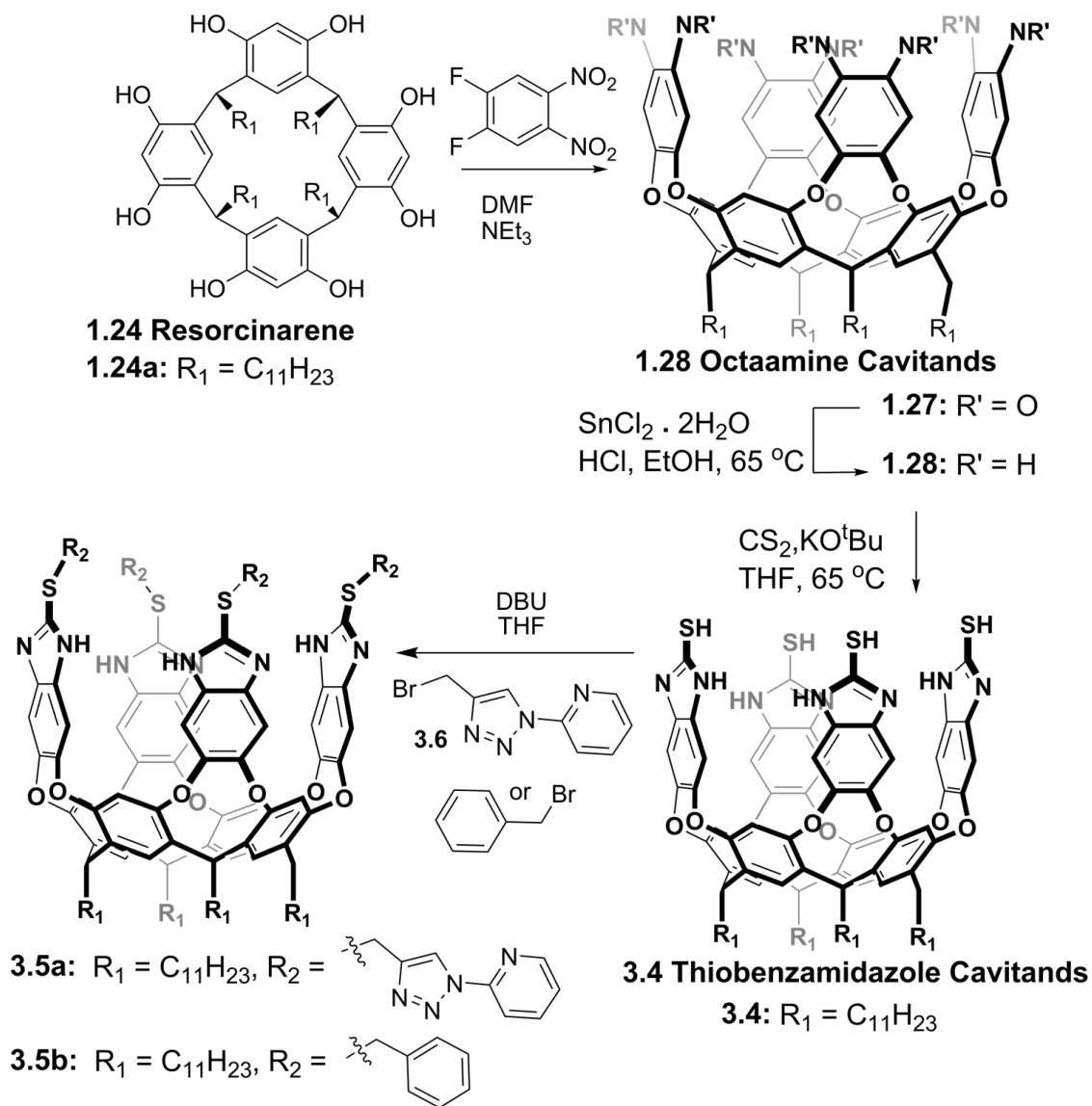
Figure 3.4. Synthesis of thiobenzimidazole cavitand catalyst scaffolds.

In the presence of appropriately sized guests such as chloroform, as well as protic solvents to supply the H-bonding seam, **3.5a** self-folds into the desired vase-like conformation. ^{1}H NMR shows downfield changes in the chemical resonance of the methine proton on the base of the cavitand. The methine proton resonance of **3.5a** shifts

downfield from δ 5.3 ppm to > δ 5.8 ppm due to different anisotropic shielding effects in the vase conformation (Figure 3.5). Also, the scaffold is promising for metal coordination: the four rim functionalized groups form a self-folding motif that allows the binding of a neutral guest without a coordinated metal at the triazole groups. Guest binding studies show very weak binding of choline derivatives driven by cation-π interactions.
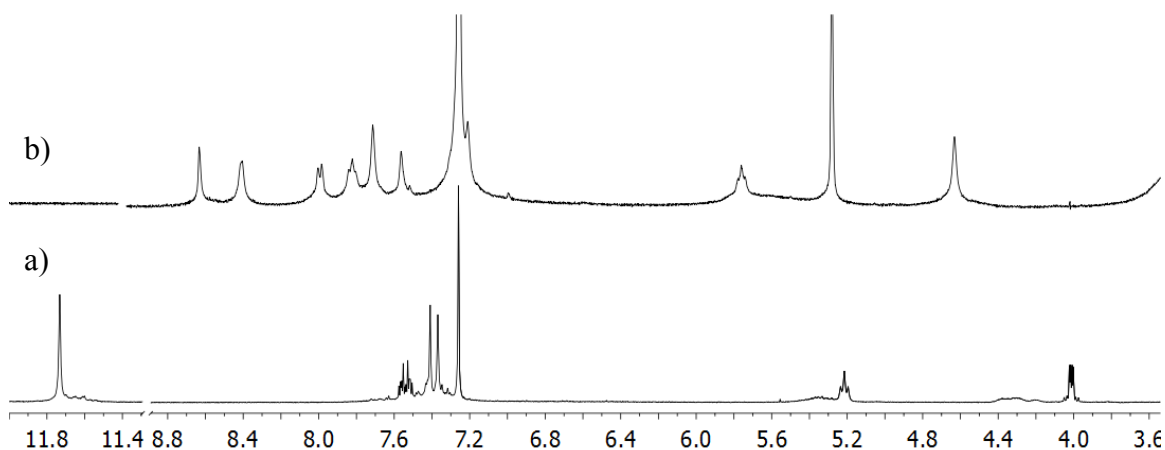
Figure 3.5. ^{1}H NMR of a) thiobenzimidazole cavitands a) **3.4a** and b) **3.5a** (anhydrous CDCl$_3$ at 350K, 400MHz).

3.5. Metal Coordination with Thiobenzimidazole Cavitands

Metal binding studies between **3.5a** and Fe(II) proved challenging to characterize by ^{1}H NMR due to the paramagnetic nature of the **3.5a•**Fe(II) complex. When Zn(OTf)$_2$ was used as a diamagnetic surrogate, titration experiments showed the binding of two metal atoms to **3.5a**, as shown by the shifted and sharp CH methine peaks. However, the aromatic region revealed broadened peaks, indicating a kinetically unstable conformation of the host, and perhaps weak Zn^{II} binding. Molecular modeling shed a light on the

conformation of those complexes. The CH_2 units introduced in the S_N2 step cause a large number of degrees of freedom in the upper rim groups, which caused the weak affinity for metals and broadness in the ^{1}H NMR spectrum.

The thiobenzimidazole **3.5a** is a somewhat competent host, even if it is a poor metal coordinator. Guest binding studies with **3.5a** show the encapsulation of small guests occurs in the absence of metal. Acetylcholine and choline were the only guests that were bound in the cavity, although this occurred with low binding affinity. The guest binding was determined to occur inside the cavity by the presence of proton resonances in the negative ppm region of the ^{1}H NMR spectrum.
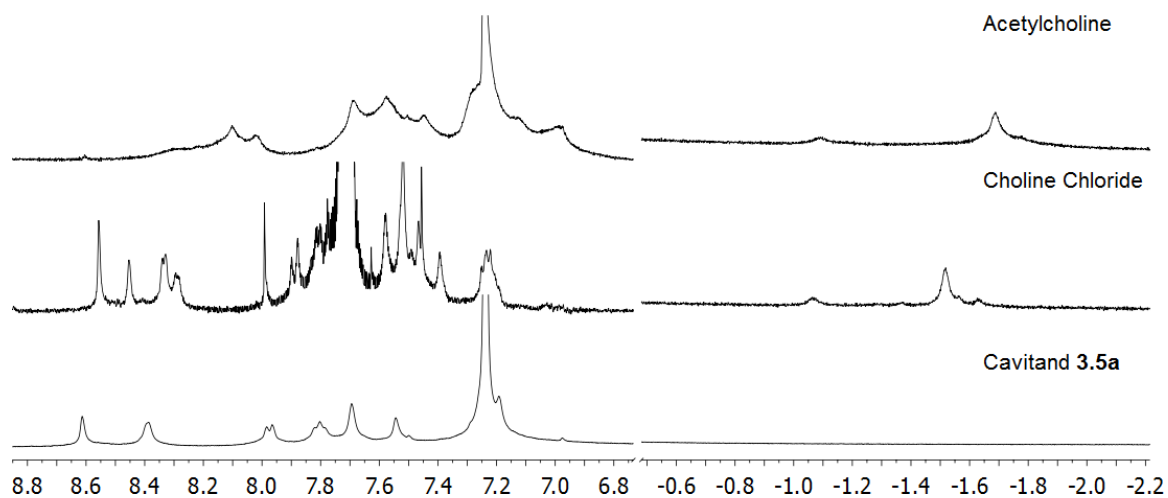
Figure 3.6. ^{1}H NMR of thiobenzimidazole **3.4a** and hydrocarbon guest (anhydrous CDCl$_3$ at 350K, 400MHz).

Due to the paramagnetic nature of FeSO$_4$, Zn(OTf)$_2$ was used as a surrogate to monitor metal complexation with ^{1}H NMR. The Zinc titration showed broad and undefined peaks in the aromatic region and the presence of two different methine peaks at 5.5 ppm and 5.7

ppm, one of which is sharp at 5.5 ppm. The broad beaks of the cavitand were caused due to the weak coordination and the flexible C-S-C bonds on the upper rims. The sigma bond between the C-S-C bonds provides the cavitand to unfold as predicted with the molecular modeling.
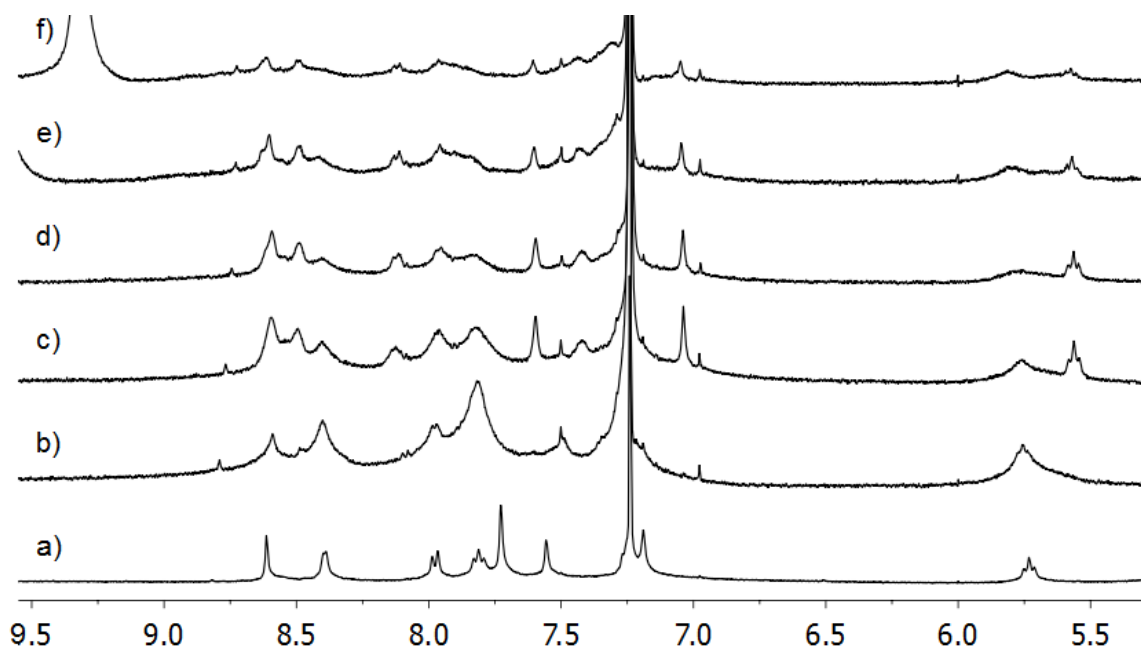
Figure 3.7. Downfield regions of the ^{1}H NMR spectra of the titration of 0-3 mol. eq. Zn(OTf)$_2$ to **3.5a**. (anhydrous CDCl$_3$, 298 K, 400MHz, 6 mg **3.5a**) a) **3.5a**; b) **3.5a** + 1 eq. Zn(OTf)$_2$ c) 1.5 eq. Zn(OTf)$_2$, d) 2.0 eq. Zn(OTf)$_2$, e) 2.5 eq. Zn(OTf)$_2$, f) 3.0 eq. Zn(OTf)$_2$.
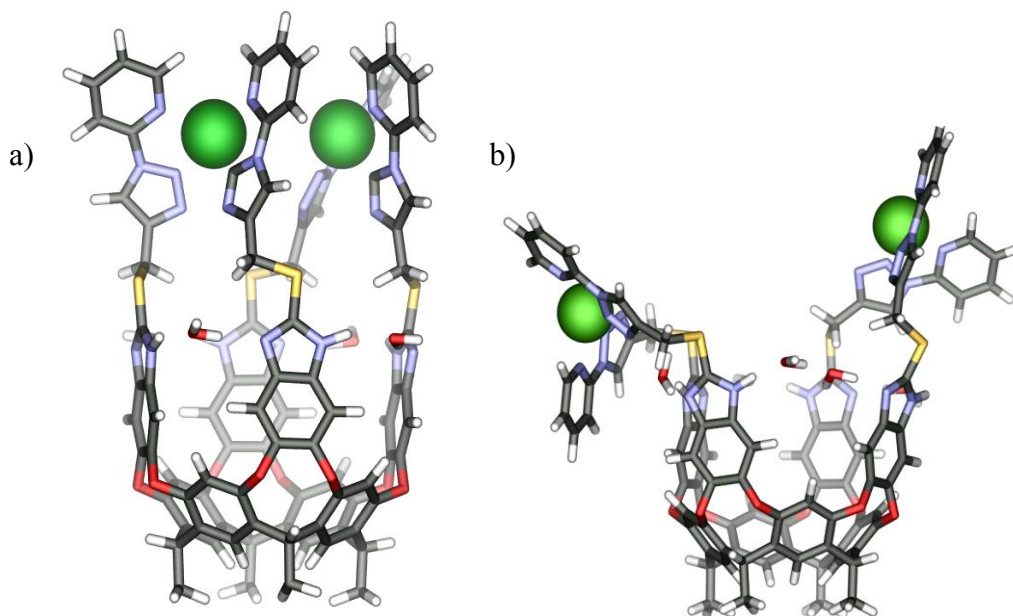
Figure 3.8. Proposed iron complex of a) **3.5a** cavitand scaffolds expected, b) **3.5a** cavitand scaffolds observed (SPARTAN, semi-empirical calculation, AM1 forcefield).

The difference in physical properties of the iron metal complex allowed easy access to the **3.5a**•Fe$_2$(SO$_4$)$_2$ complex by filtration. Similar methods were used to isolate **2.5a**•Cu$_2$(CH$_3$CN)$_2$(BF$_4$)$_2$. After isolating the **3.5a**•**Fe** complex we tested the oxidation of some typical hydrocarbons such as cyclooctane *cis*-decalin, *trans*-decalin, fluorene, and methylcyclohexane. However, oxidation was limited to fluorene, which was converted to fluorenone in 98% conversion, as the cavitand backbone sulfur underwent oxidation to sulfone. The scaffold lost its self-folding ability as well as its catalytically active group. The limitation of cavitand **2.5a** was due to the flexible thioether group in the backbone, which caused similar rotation as previous shallow cavitands. We therefore investigated other methods to functionalize the benzimidazole scaffold.

3.6. Arylimine Cavitands

To eliminate rim flexibility in previous thiobenzimidazole scaffold, we returned to the carbon backbone of the benzimidazole scaffold.[20] The major roadblock in benzimidazole cavitand synthesis is the requirement for acid-catalyzed heterocycle formation. While simple hydrocarbon or ester group can be easily added to the octaamine *via* condensation with the corresponding imidate HCl salt in anhydrous ethanol, introducing N-donor groups is far more challenging. To resolve the challenge, we decided to attempt the introduction of the N-donor group in a secondary step following the benzimidazole ring formation.

The alternative synthetic route exploited tetraethylacetal cavitands **3.7** (Figure 3.9).[21] The acetal imidate precursor was synthesized in good yield and the HCl salt of imidate is stable for about a week at -5 °C. Condensation of the imidate with octamine cavitand **1.8a** gave the tetraethylacetal cavitand **3.7** in 77% yield. This tetraacetal is a protected aldehyde, and so we attempted an acid-catalyzed deprotection and imine-forming condensation in one step. Treatment of **3.7** with amine containing substrates and trifluoroacetic acid under previously published conditions[21] gave poor conversions to the desired imine-containing cavitands. Using alternative methods to convert dialkyl acetals to substituted imines using anhydrous strong Lewis Acids such as $Ti(O^iPr)_4$ and $AlCl_3$ *via* condensation reactions was also unsuccessful. Fortunately, reaction with softer Lewis acids such as $La(OTf)_3$ proved effective. To test the scope of the rim functionalization process we introduced a variety of different amine nucleophiles in the presence of catalytic $La(OTf)_3$.[22] The more basic amines such as primary alkylamines (*n*-butylamine,

unsym-dimethylethylenediamine and 2-picolylamine) showed unsuccessful, incomplete reaction. Less basic nucleophiles such as aniline derivatives were excellent substrates for the reaction, and formed tetraimine products **3.8-3.10**, which were easy to purify. The reaction was highly tolerant to functionalized substrates such as carboxylic acids as well as donor nitrogen groups such as pyridines.
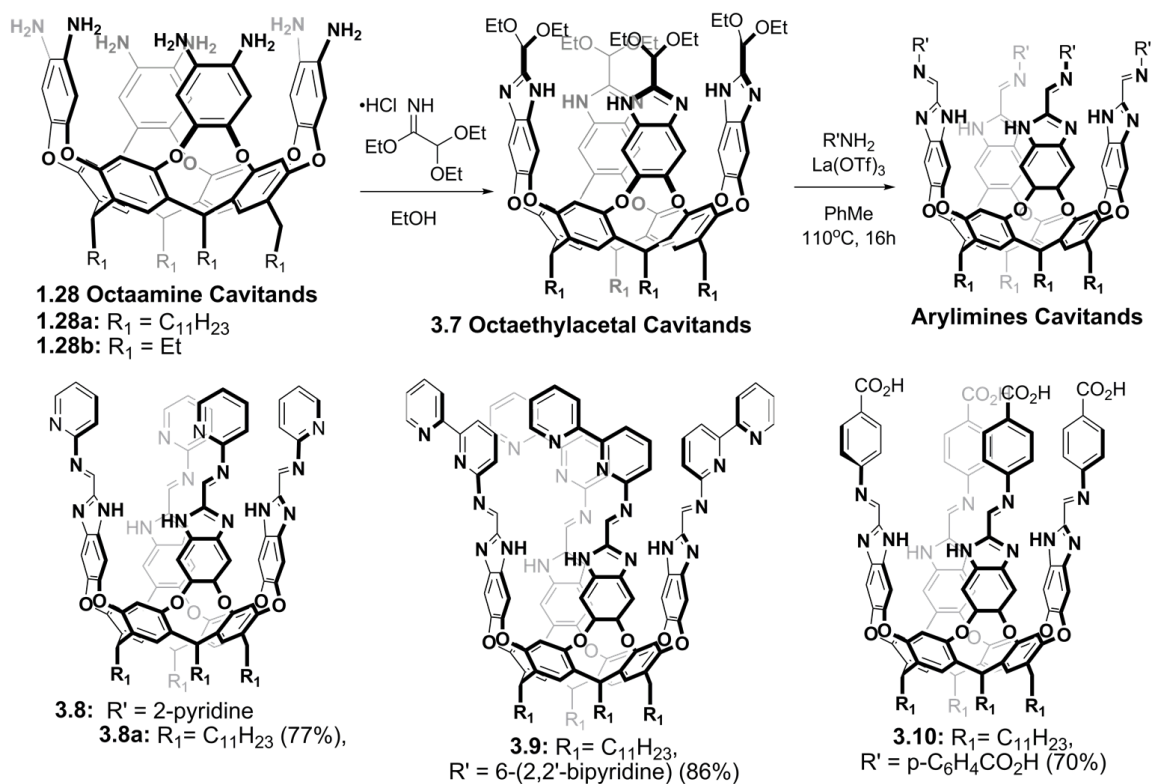
Figure 3.9. Synthesis of arylimine deep cavitand scaffolds.

97

3.7. Unusual H-bonding Interactions

The derivatized tetraimine cavitands **3.8-3.10** displayed unusual folding properties. In anhydrous $CDCl_3$, the ^{1}H NMR spectrum showed a kinetically unstable conformation. The broad NMR peaks of the resorcinarene protons were attributed to fast flexing between the vase and kite conformation, which is to be expected. However, even in the presence of hydrogen bonding additives such as water or methanol, effective self-folding did not occur. Most benzimidazole cavitands fold into kinetically stable vase conformations in the presence of four molecules of water or methanol[12] due to hydrogen bonding seams formed around the rim, but this was not the case for our tetraimine cavitands **3.8-3.10**. None of the protic solvents help stabilize the self-folding of the cavitand rims. Unexpectedly, with the addition of 1-5% DMSO-d_6 to the NMR solution, a well-defined sharp ^{1}H NMR spectrum appeared immediately, which suggested the cavitand is folded and exists only as the vase-like conformation (Figure 3.10). Evidently, the strongly donating imine nitrogen atoms in **3.8-3.10** that are introduced at the rim outcompete the benzimidazoles for H-bonding donors such as water, preventing seam formation. If solely hydrogen bond acceptors such as DMSO are introduced, they can only interact with the benzimidazole N-H group to form a stable seam on the rim, unaffected by strongly donating nitrogen atoms on the top of the rims. The DMSO does not provide both an H-bond donor and acceptor group, therefore only two DMSO molecules are incorporated between two benzimidazole NH groups at the rim rather than the usual four water molecules (Figure 3.11). The ^{1}H NMR spectrum appears C_4-symmetric at room temperature for $C_{11}H_{23}$ scaffolds, indicating rapid exchange between

the NH groups and DMSO. At lower temperatures, significant broadening of the cavitand

peaks occurs which indicates an intermediate exchange rate of the DMSO molecules.
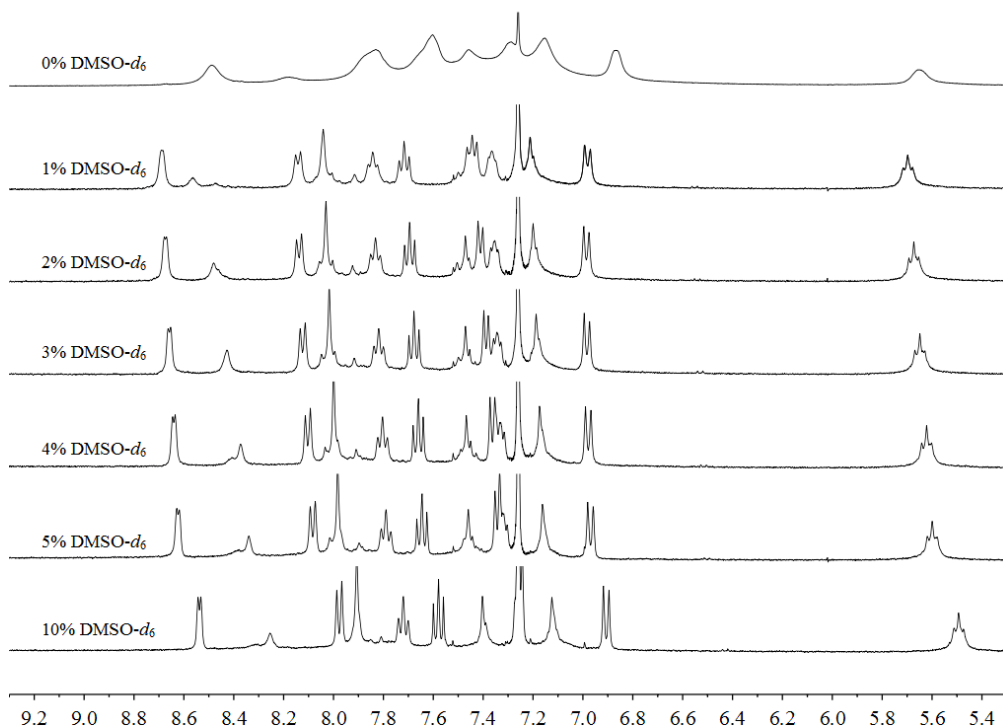
Figure 3.10. ^{1}H NMR titration of DMSO with **3.9** (dry CDCl$_3$, 400 MHz).
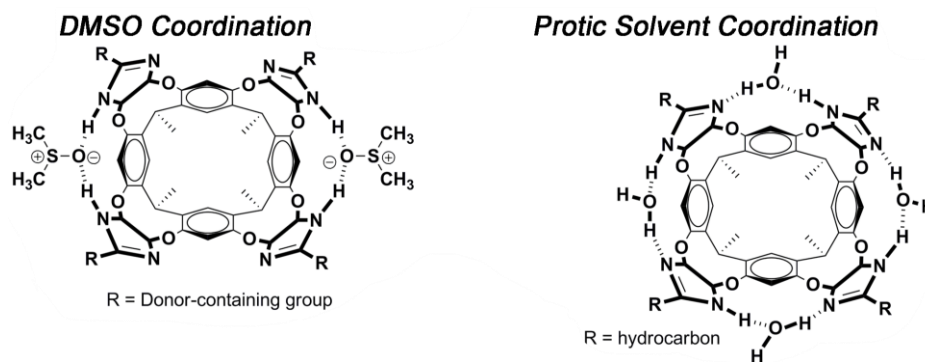
Figure 3.11. Hydrogen bonding interaction of benzimidazole rims with DMSO (H-bonding acceptor) and H$_2$O (H-bonding acceptor and donor).

3.8. Alkylimine Cavitands

While the direct functionalization of acetal cavitand **3.7** by this method failed to introduce alkyl amine groups, these more basic nucleophiles can be simply introduced by transimination. The arylimine cavitands **3.8-3.10** are susceptible to reaction with strong nucleophiles including alkyl amine-containing substrates. Simple sonication of any of the arylimine cavitands with primary alkylamines such as 2-picolylamine or *unsym-N,N-*dimethylethylenediamine in a mixture of CH_2Cl_2/MeOH for 5 min - 1 hr smoothly yielded the corresponding alkylimines **3.11-3.14** as a precipitate due to their lower solubility in polar solvents. This combination of synthetic strategies allows access to a great range of functionalized cavitands, with either direct reactivity from acetal cavitand **3.7** or via subsequent transamination of arylimine cavitands **3.8-3.10**.

3.8: R' = 2-pyridine
3.8a: $R_1 = C_{11}H_{23}$ (77%),
3.8b: R_1 = Et (80%)

Alkylimines Cavitands

3.11: R_2 = -CH_2-(2-pyridyl) (73%)

3.12: R' = -$(CH_2)_2NMe_2$ (81%)

3.14: R_2 =

3.14: $R_1 = C_{11}H_{23}$ (70%),

3.13: R_2 = n-C_4H_9 (89%)
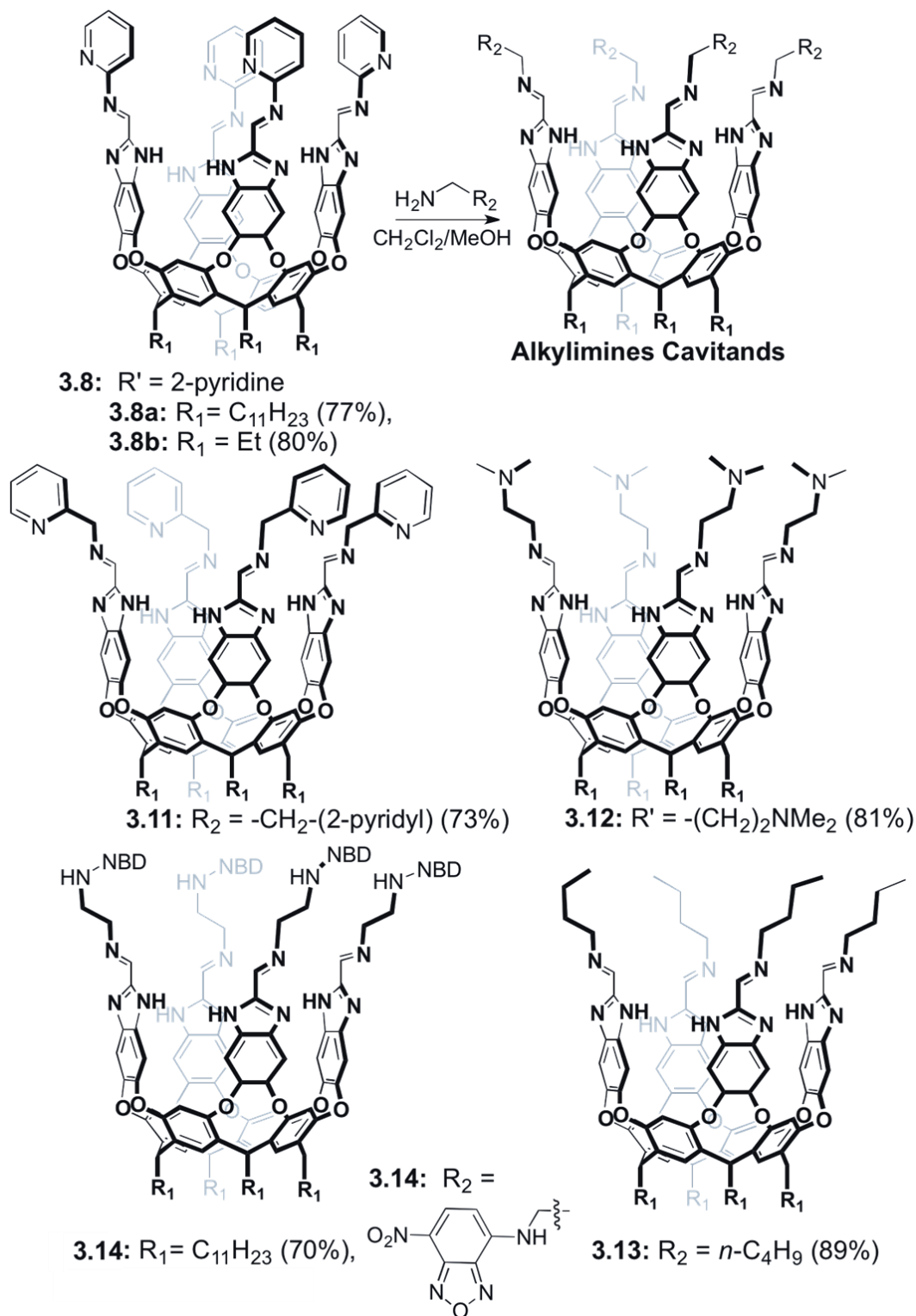
Figure 3.12. Synthesis of deep alkylimine cavitands **3.11-3.14.**

101

3.9. Metal Coordination

Cavitands **3.8, 3.9, 3.11,** and **3.12** provide the opportunity to coordinate metal ions at the cavitand rim. The synthetic route allows for the simple introduction of a variable number of *N*-donors at each wall, including the imine nitrogen that is present in all cases. The cavitands can be separated into three distinct types: 4x2, 4x2/1 and 4x1 donors, referring to the number of accessible N donors on each wall. Bipyridyl cavitand **3.9** displays two donor nitrogens from each of the four bipyridyl groups, and the imine nitrogen is unlikely to participate due to angle strain, hence the 4x2 designation. Cavitands **3.8, 3.11** and **3.12** provide one donor nitrogen from each wall, but in these cases participation of the imine nitrogen is more likely, leading to two possible coordination types 4x1/2. Cavitand **3.10,** and **3.11** can only use its pyridyl nitrogen for coordination, and is described as 4x1. **3.9** showed physical changes when a metal ion was added, however, with both Fe^{2+} and Cu^+, the paramagnetic nature of the complexes between these metals and **3.9** led to broadened ^1H NMR spectra and limited the possible structural analysis, so $Zn(OTf)_2$ was used to study metal-coordination with cavitand **3.9** by ^1H NMR (Figure 3.13).
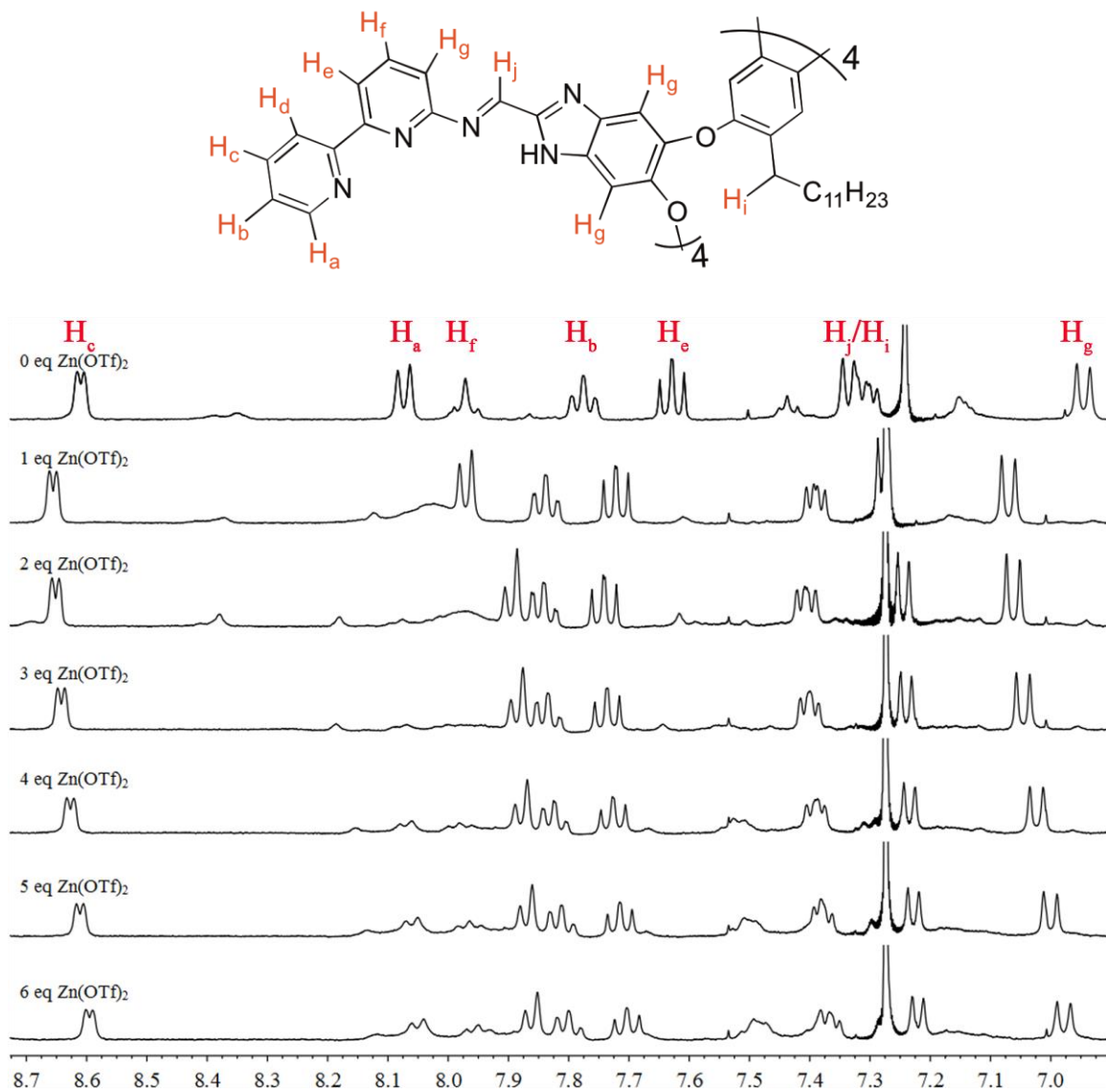
Figure 3.13. Downfield regions of the ^1H NMR spectra (400 MHz, 298 K, 5 % DMSO-d_6 in CDCl$_3$, 2.5 mM 2.9) of the addition of Zn(OTf)$_2$ to Bipyridyl Imine Cavitand **3.9**.

The ^1H NMR spectra indicate the reversible binding ability of the cavitand to Zn^{2+}. Upon the addition of one equivalent Zn^{2+}, many resonances shifted. The *ortho* proton H$_a$ resonances shifted the most, displaying a higher upfield chemical shift due to the rotation

of the pyridine that surrounds the metal. The *para* proton H_b, H_e showed similar dramatic shifts down-field. The imine CH proton H_f remained relatively unchanged, suggesting that Zn^{2+} ions only bind symmetrical to the pyridine groups. Upon addition of two equivalents of metal ions, a single complex was formed with no further changes to the ^{1}H NMR spectrum. The addition of five or more equivalents shows hardly any changes in the metal complex peaks. The proton NMR shows the presence of uncoordinating ligand peaks due to metal slow exchange. The affinity of the metal ion to the ligand is relatively strong as evidenced by the low concentration of NMR sample. The presence of metal ion alone is not sufficient for self-folding the cavitand in the absence of DMSO-d_6. The addition of Zn^{2+} in the absence of coordinating DMSO-d_6 showed discrete folding structure. Minimized molecular modeling using SPARTAN AM1 forcefield also supported the favorable coordination mode, whereby each Zn^{2+} ion is coordinated by two bipyridyl units, as shown in Figure 3.14. Cavitand **3.9** is also capable of coordinating with other metal ions such as $La(NO_3)_3$ similar to Zn^{2+}, however with much weaker binding ability due to the size difference of the lanthanide ions (Figure 3.15).
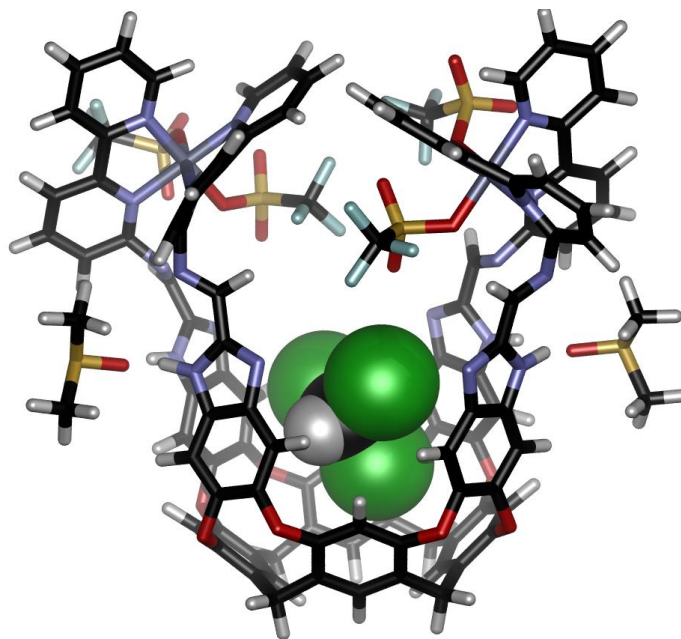
Figure 3.14. Functionalized deep cavitand **3.9** with Zn(OTf)$_2$ complex (SPARTAN, semi-empirical calculation, AM1 forcefield).
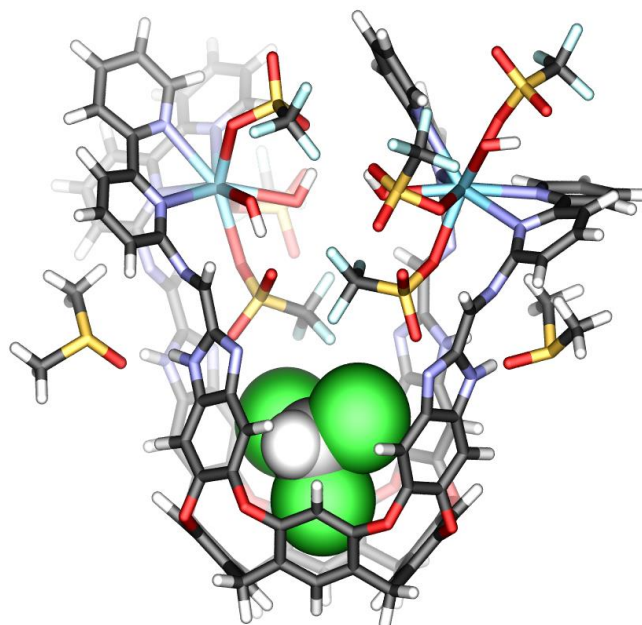
Figure 3.15. Functionalized deep cavitand **3.9** with La(OTf)$_3$ complex (SPARTAN, semi-empirical calculation, AM1 forcefield).
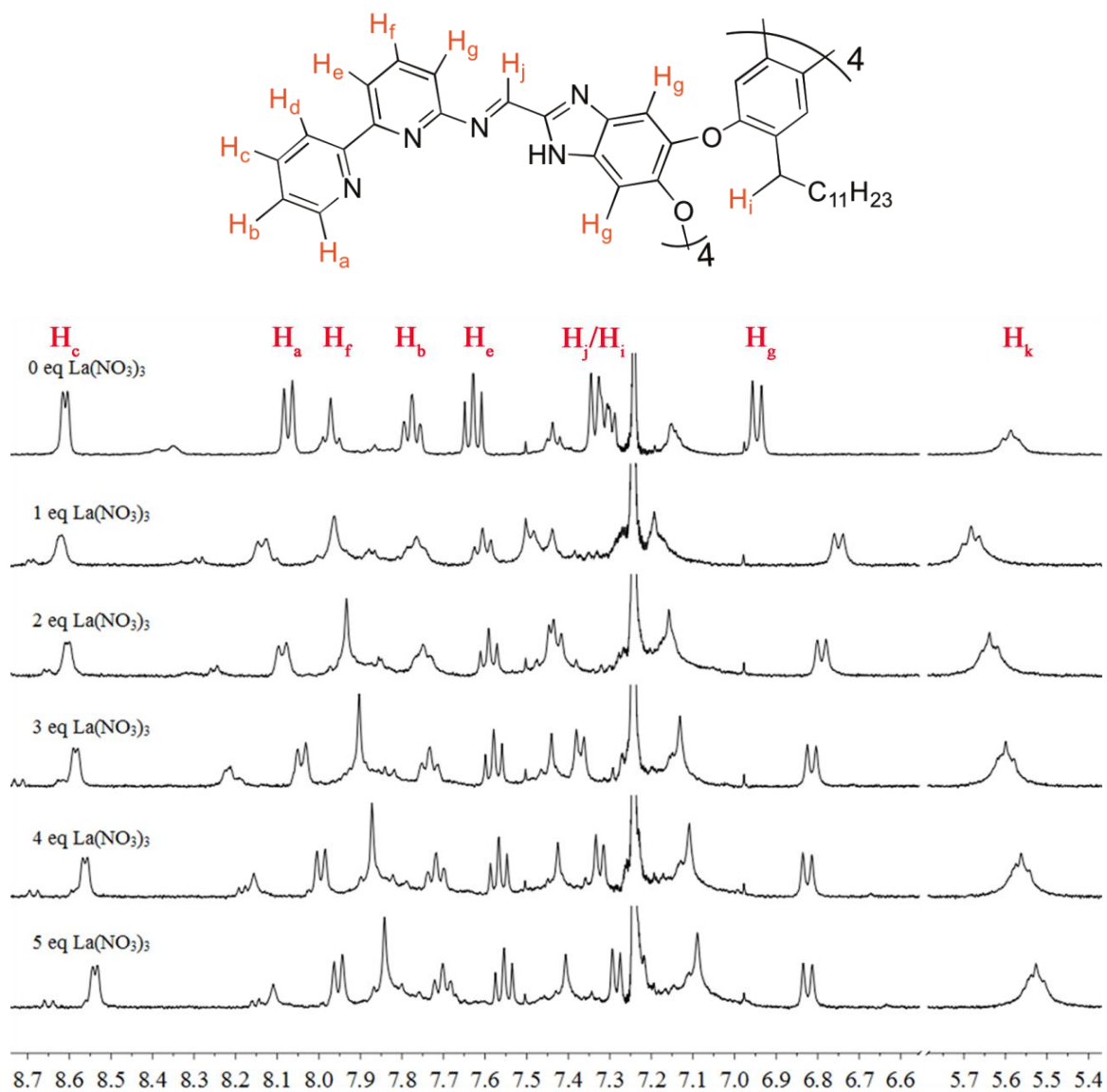
Figure 3.16. Downfield regions of the ^{1}H NMR spectra (400 MHz, 298 K, 5 % DMSO-d_6 in CDCl$_3$, 2.5 mM **3.9**) of the addition of La(NO$_3$)$_3$ to Bipyridyl Imine Cavitand **3.9**.

3.10. Guest Binding

Cavitand **3.9** was a very poor host in the presence of organic solvents such as $CDCl_3$ due to solvent competition. A variety of small guests were tested such as cyclohexane and choline (both of which showed a strong binding with previous benzamidazole cavitands),[1-7,23] all of which showed with minimal affinity for **3.9**, with $K_a < 10$ M^{-1}. The addition of the large bipyridyl group at the rim that blocked the cavity, as well as the solvent competition from $CDCl_3$ minimized the binding ability of the scaffold. Binding studies were not tested in non-organic solvents due to the lack of solubility of the lipophilic **3.9**. Even when guests were added in great excess, larger guests such as cyclooctane and adamantane showed no affinity. The metal complex **3.9**•Zn^{2+} was even less effective due to the rigidified arms which caused a great barrier to the guest incorporation. The more strongly donating cavitands such as **3.11** and **3.12** did show some affinity for Zn^{2+}, as evidenced by ^{1}H NMR analysis that showed minor shifts to the proton peaks. The donor groups displayed weak coordination with the metal ions, and no discrete complex formed due to the lack of full coordination to the metal sites.
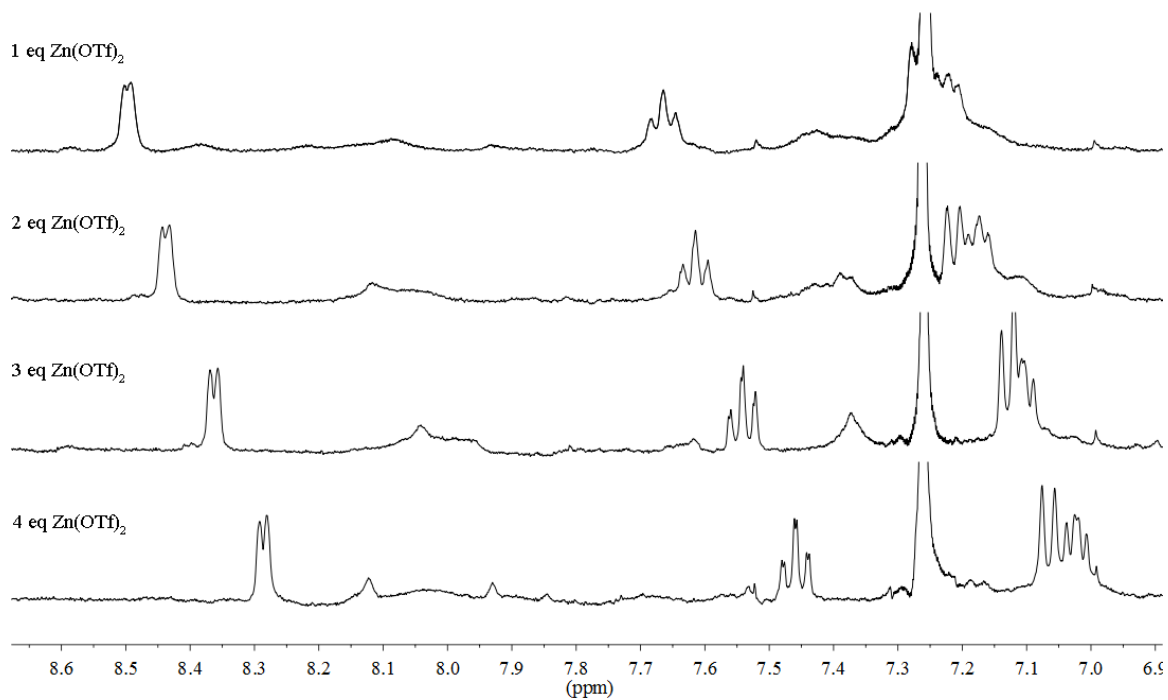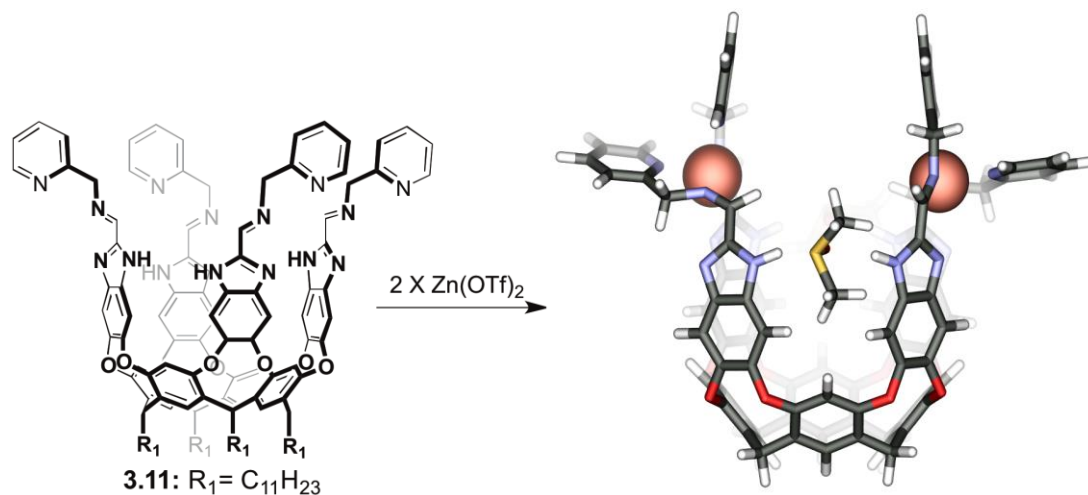
Figure 3.17. Downfield regions of the ^{1}H NMR spectra (400 MHz, 298 K, 5 % DMSO-d_6 in CDCl$_3$, 2.3 mM **3.11**) of the addition of Zn(OTf)$_2$ to Picolyl Imine Cavitand **3.11**.

Cavitand **3.11** showed no affinity for unfunctionalized hydrocarbon guests such as cyclohexane, sodium cyclohexane-carboxylate and NMe$_4$Br. Surprisingly, cavitand **3.11** did show affinity for functionalized hydrocarbon guests such as adamantanamine, cyclohexylamine, cyclooctylamine, hexylamine, and cyclohexanecarboxylic acid in CDCl$_3$:5% DMSO-d_6, all of which overcome solvent competition. Guest binding required both a protic group and a size suitable to fill the cavity, similar to previously studied amine-binding cavitands.[24] The amine points upwards as shown in the minimized structures, which plays a role in the binding of these guests. While cyclooctane and adamantane showed no affinity for the host, their amine counterparts do: the orientation provides an extra variable in the binding event, and the nitrogen atom in the rim groups provides a favorable H-bonding with the guest NH$_2$ group, as shown in Figure 3.19. The more flexible **3.12** cavitand showed similar binding ability to suitable sized protic guests such as adamantanamine, cyclohexylamine, cyclooctylamine, and cyclohexane-carboxylic acid (Figure 3.18). Short amines such as *iso*-butylamine, *tert*-butylamine and *n*-butylamine were not encapsulated due to their mismatched size with the cavity.
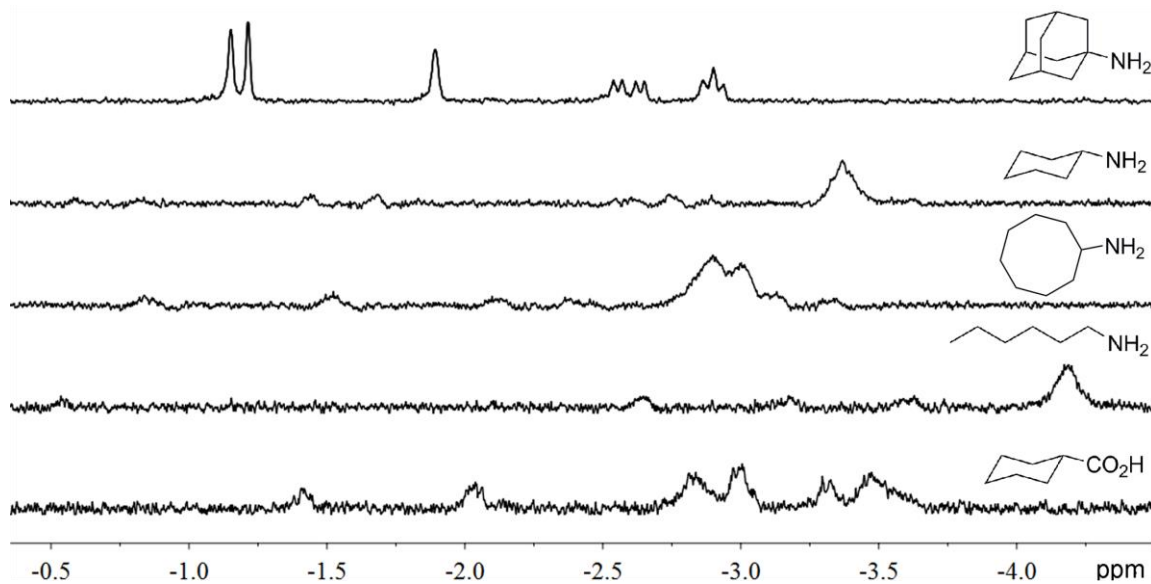
Figure 3.18. Upfield regions of the ^{1}H NMR spectra (400 MHz, 5% DMSO-d_6 in CDCl$_3$).
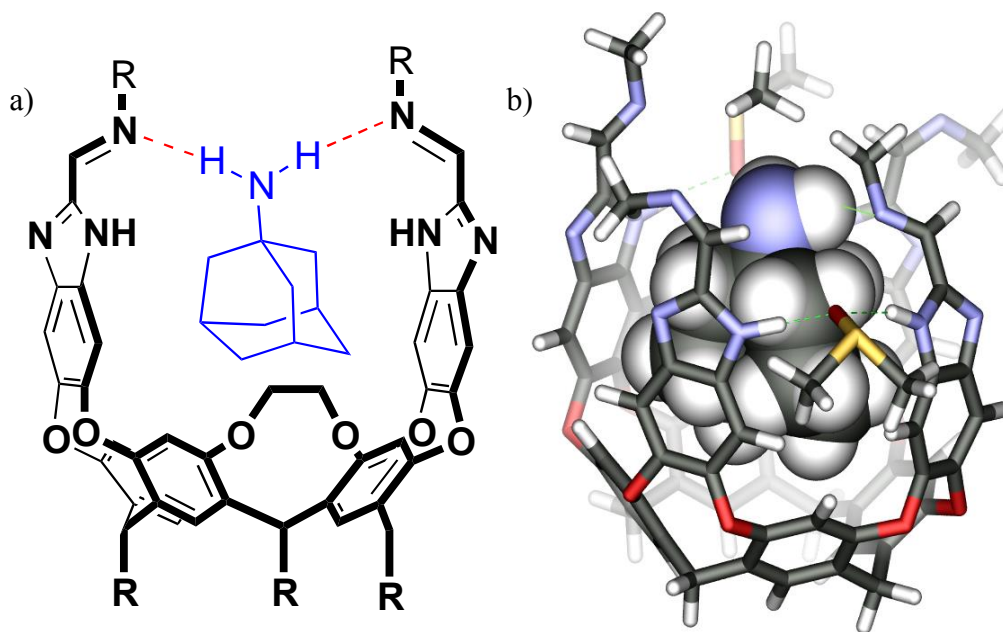
Figure 3.19. Proposed H-bonding interaction of imidate cavitand and adamantanamine guests of a) Representation of proposed H-bonding with removal of front and back cavitand wall for clarity, b) Minimized model of H-bond interaction observed (SPARTAN, semi-empirical calculation, AM1 forcefield).

A new cavitand **3.13** was synthesized which lacked the nitrogen atoms at the rim (other than the imine nitrogen), to test the binding effects on the amine-functionalized hydrocarbon. Cavitand **3.13** showed similar affinity towards functionalized hydrocarbons that contained both a protic group and were of a size suitable to fill the cavity.
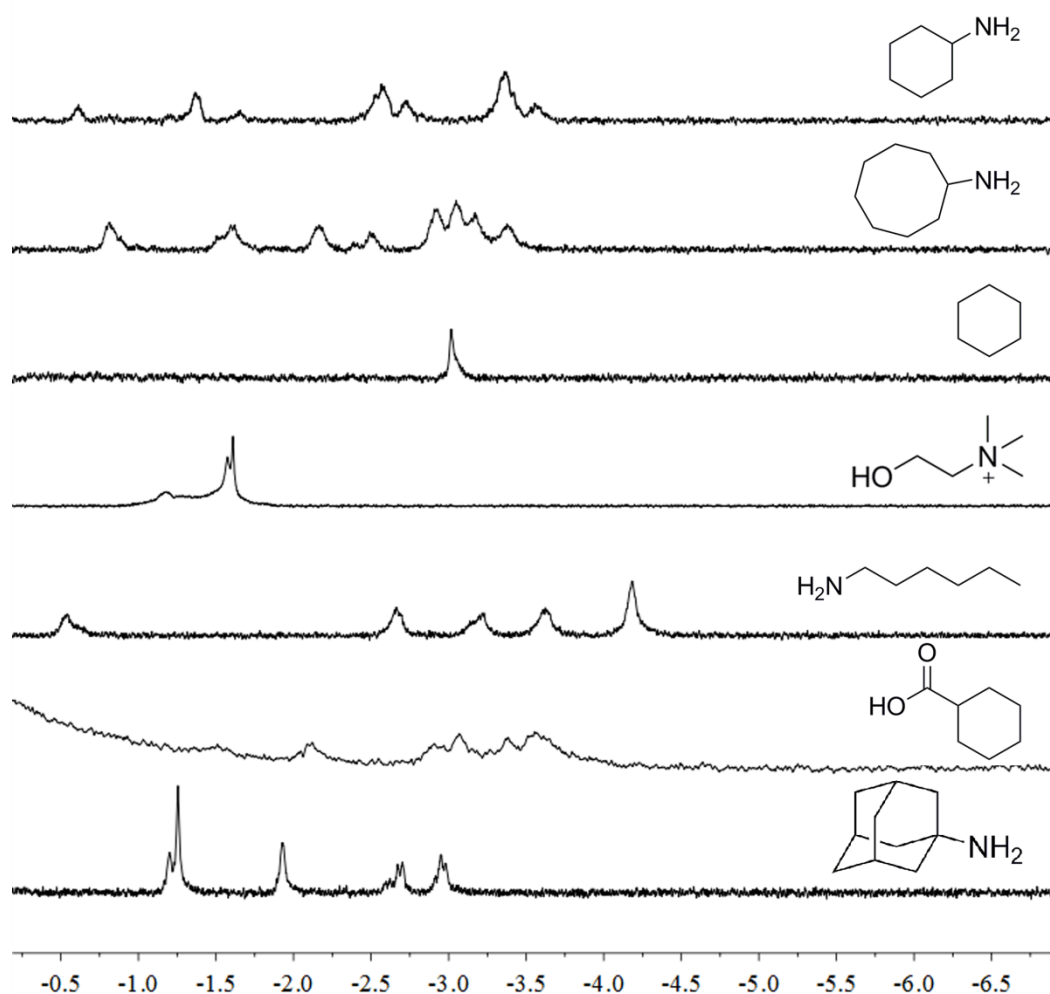
Figure 3.20. Upfield regions of the ^{1}H NMR spectra (400 MHz, 5 % DMSO-d_6 in CDCl$_3$, 298 K, 4 mM **3.13**) obtained upon addition of excess guests to butyl imine cavitand **3.13**.

3.11. Guest binding in the Deep Cavitand-Metal Complexes

Unfortunately, 2-pyridyl cavitands **3.8** showed a lack of guest binding in the presence of metal ions. Also, cavitand **3.9** should high affinity for metal ions, however guest binding was very weak due to guest competition with chloroform and rigidity of the rims upon complexation.
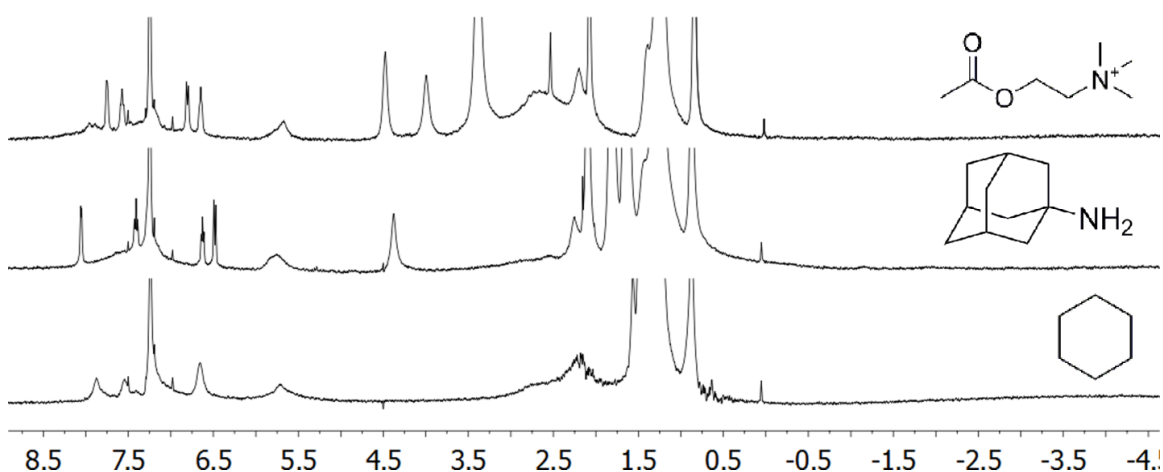
Figure 3.21. ^{1}H NMR spectra (400 MHz, 5 % DMSO-d_6 in CDCl$_3$, 298 K, 4 mM **3.8**) obtained upon addition of excess guests to pyridyl imine cavitand **3.8**.
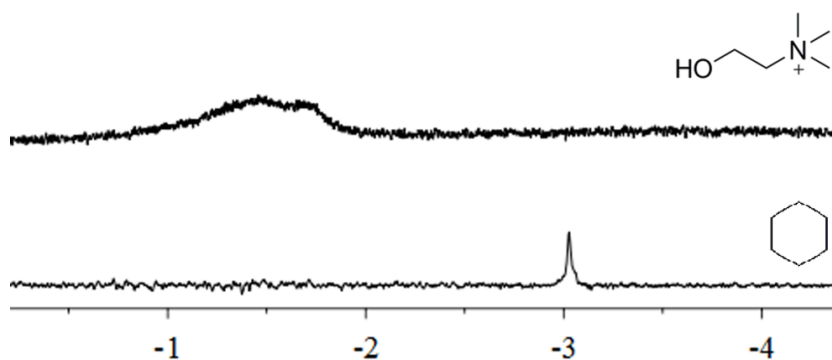
Figure 3.22. Upfield regions of the ^{1}H NMR spectra (400 MHz, 5 % DMSO-d_6 in CDCl$_3$, 298 K, 4 mM **3.9**) obtained upon addition of excess protic guest to bipyridyl imine cavitand **3.9**.

3.12. Conclusion

In this chapter, we have achieved both metal coordination as well as strong amine functionalized hydrocarbon binding in a series of host cavitands. Although several cavitands (**3.8, 3.9,** and **3.11)** were capable of metal coordination, and others (**3.8, 3.12,** and **3.13**) were capable of amine substrate recognition, none maintained their recognition element in the presence of metal ions. The strong molecular recognition ability directed our research to a deeper investigation into the scaffold's recognition ability, rather than reactivity as catalysts.
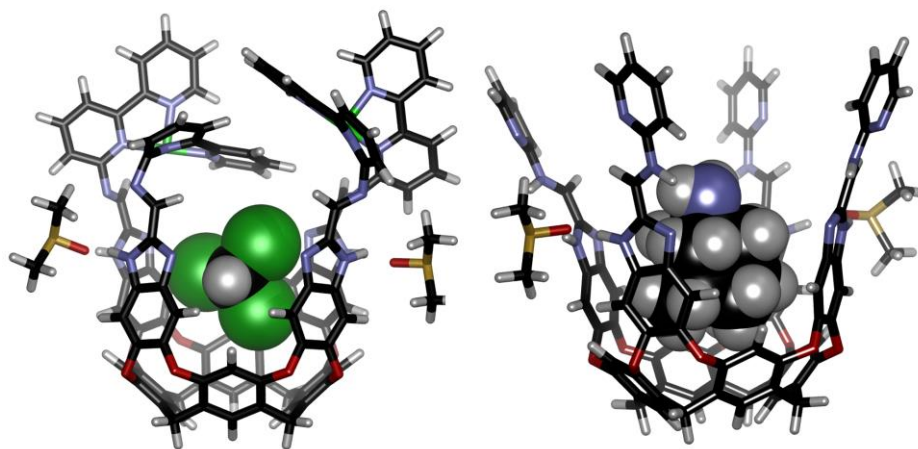
Figure 3.23. Functionalized deep cavitand **3.9** with Zn(OTf)$_2$ complex and cavitand:host complex **3.8** with cyclooctylamine (SPARTAN, semi-empirical calculation, AM1 forcefield).

3.13. References

(1)   Schramm, M. P.; Hooley, R. J.; Rebek, J., Jr. Guest recognition with micelle-bound cavitands. *J. Am. Chem. Soc.* **2007**, *129*, 9773-9779.

(2)   Hooley, R. J.; Rebek, J., Jr. Self-complexed deep cavitands: alkyl chains coil into a nearby cavity. *Org. Lett.* **2007**, *9*, 1179-1182.

(3)   Choi, H. J.; Park, Y. S.; Song, J.; Youn, S. J.; Kim, H. S.; Kim, S. H.; Koh, K.; Paek, K. Structural properties of benzimidazole cavitand and its selective recognition toward 4-methylbenzamide over 4-methylanilide. *J. Org. Chem.* **2005**, *70*, 5974-5981.

(4)   Ruiz-Botella, S.; Vidossich, P.; Ujaque, G.; Vicent, C.; Peris, E. A Tetraferrocenyl-Resorcinarene Cavitand as a Redox-Switchable Host of Ammonium Salts. *Chem. Eur. J.* **2015**, *21*, 10558-10565.

(5)   Soberats, B.; Sanna, E.; Martorell, G.; Rotger, C.; Costa, A. Programmed enzyme-mimic hydrolysis of a choline carbonate by a metal-free 2-aminobenzimidazole-based cavitand. *Org. Lett.* **2014**, *16*, 840-843.

(6)   Menozzi, E.; Onagi, H.; Rheingold, A. L.; Rebek, J. Extended cavitands of nanoscale dimensions. *Eur. J. Org. Chem.* **2005**, 3633-3636.

(7)   Trembleau, L.; Rebek, J., Jr. Helical conformation of alkanes in a hydrophobic cavitand. *Science* **2003**, *301*, 1219-1220.

(8)   Gibson, C.; Rebek, J., Jr. Recognition and catalysis in allylic alkylations. *Org. Lett.* **2002**, *4*, 1887-1890.

(9)   Lucking, U.; Chen, J.; Rudkevich, D. M.; Rebek, J., Jr. A self-folding metallocavitand. *J. Am. Chem. Soc.* **2001**, *123*, 9929-9934.

(10)   Durola, F.; Rebek, J., Jr. The ouroborand: a cavitand with a coordination-driven switching device. *Angew. Chem. Int. Ed.* **2010**, *49*, 3189-3191.

(11)   Moran, J. R.; Ericson, J. L.; Dalcanale, E.; Bryant, J. A.; Knobler, C. B.; Cram, D. J. Vases and Kites as Cavitands. *J. Am. Chem. Soc.* **1991**, *113*, 5707-5714.

(12)   Ballester, P.; Shivanyuk, A.; Far, A. R.; Rebek, J., Jr. A synthetic receptor for choline and carnitine. *J. Am. Chem. Soc.* **2002**, *124*, 14014-14016.

(13)   Far, A. R.; Shivanyuk, A.; Rebek, J. Water-stabilized cavitands. *J. Am. Chem. Soc.* **2002**, *124*, 2854-2855.

(14)   Hof, F.; Trembleau, L.; Ullrich, E. C.; Rebek, J., Jr. Acetylcholine recognition by a deep, biomimetic pocket. *Angew. Chem. Int. Ed.* **2003**, *42*, 3150-3153.

(15)   Haas, C. H.; Biros, S. M.; Rebek, J. Binding properties of cavitands in aqueous solution - the influence of charge on guest selectivity. *Chem. Commun.* **2005**, 6044-6045.

(16)   Menozzi, E.; Busi, M.; Ramingo, R.; Campagnolo, M.; Geremia, S.; Dalcanale, E. Design and self-assembly of ditopic and tetratopic cavitand complexes. *Chem. Eur. J.* **2005**, *11*, 3136-3148.

(17)   Biros, S. M.; Ullrich, E. C.; Hof, F.; Trembleau, L.; Rebek, J. Kinetically stable complexes in water: The role of hydration and hydrophobicity. *J. Am. Chem. Soc.* **2004**, *126*, 2870-2876.

(18)   Elokhina, V. N.; Yaroshenko, T. I.; Nakhmanovich, A. S.; Amosova, S. V. Reaction of Thiourea and Substituted Thioureas with 1,3-Dibromopropyne. *Russ. J. Gen. Chem.* **2008**, *78*, 1949-1951.

(19)   Asadi, A.; Ajami, D.; Rebek, J. Bent Alkanes in a New Thiourea-Containing Capsule. *J. Am. Chem. Soc.* **2011**, *133*, 10682-10684.

(20)   Mettry, M.; Moehlig, M. P.; Hooley, R. J. Synthesis, guest binding, and metal coordination of functionalized self-folding deep cavitands. *Org. Lett.* **2015**, *17*, 1497-1500.

(21)   Asadi, A.; Ajami, D.; Rebek, J., Jr. Covalent capsules: reversible binding in a chiral space. *Chem. Sci.* **2013**, *4*, 1212-1215.

(22)   Heaney, H.; Simcox, M. T.; Slawin, A. M. Z.; Giles, R. G. Lanthanide Triflate Catalysed Reactions of Acetals with Primary Amines and Cascade Cyclisation Reactions. *Synlett* **1998**, *6*, 640-642.

(23)   Ebbing, M. H.; Villa, M. J.; Valpuesta, J. M.; Prados, P.; de Mendoza, J. Resorcinarenes with 2-benzimidazolone bridges: self-aggregation, self-assembled dimeric capsules, and guest encapsulation. *Proc. Natl. Acad. Sci. U.S.A.* **2002**, *99*, 4962-4966.

(24)   Hooley, R. J.; Shenoy, S. R.; Rebek, J., Jr. Electronic and steric effects in binding of deep cavitands. *Org. Lett.* **2008**, *10*, 5397-5400.

Chapter 4: Synthesis of New Cavitands for Biosensing in Water and Complex Environments

4.1. Introduction

Noncovalent molecular recognition in cell membranes and selective recognition of biomacromolecules is an area of active research.[1,2] Several synthetic receptors have been created that exploit selective, noncovalent recognition of guests into the cavity such as cyclodextrins,[3-5] cyclophanes,[6,7] calixarenes,[8,9] and cucurbituril[10-12] derivatives. They also have been utilized as molecular receptors for drug candidates and drug delivery scaffolds.

The most effective and well-studied cavitand host is **4.2,** which was first synthesized by condensation of the octaamine cavitand **1.28b** with ethyl 3-ethoxy-3-iminopropionate, yielding tetraester benzimidazole cavitand **4.1**. Subsequently, saponification resulted in the negatively charged tetracarboxylate cavitand **4.2**.[13,14] Tetracarboxylate cavitand **4.2** is a far more effective host than quinoxaline deep cavitands, due to intramolecular H-bonding interactions at the rim. This leads to a host of 10 x 8 Å dimensions that is capable of extracting neutral hydrocarbons into the binding pocket in aqueous solution.[14,15] Cavitand **4.2** has two important characteristics for aqueous molecular recognition: an electron rich aromatic surface that surrounds the cavity, allowing cation-π interactions with guests, and the upper rim carboxylates and the short ethyl feet that allow dissolution in water.
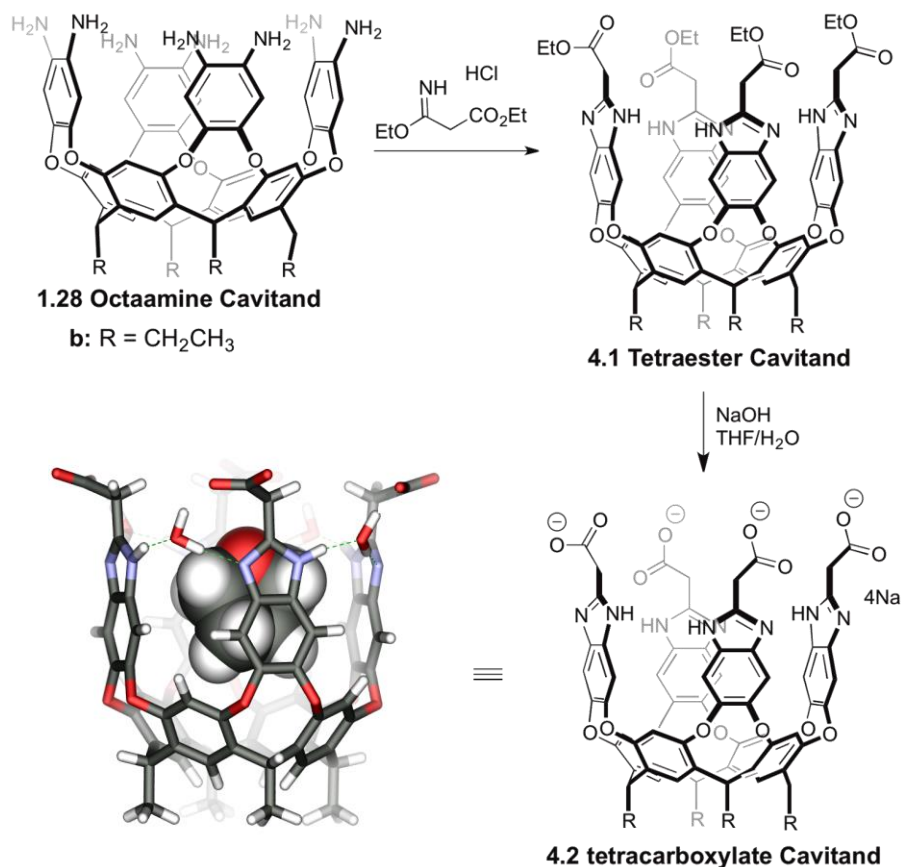
Figure 4.1. The synthesis of deep cavitand scaffold **4.2** and the minimized models representation of the cavitand **4.2** complex structures with THF (SPARTAN, Hartree-Fock forcefield, included H-bonding.)

Cavitand **4.2** shows high binding affinity ($K_a > 10^4$ M^{-1}) to trimethylammonium salts (R-NMe_3^+), such as choline **4.3** and acetylcholine **4.4** via cation-π interactions with the electron rich walls. In pure aqueous solution, the association constants of R-NMe_3^+ guests, such as choline **4.3** ($K_a = 2.6 \times 10^4$ M^{-1}) and acetylcholine **4.4** ($K_a = 1.2 \times 10^5$ M^{-1}), are relatively consistent. The "upper limit" for guest association in free solution is on the order of 2×10^5 M^{-1}. Favorable cation-π interactions with the electron rich aromatic

surface provide the optimal conditions for guest binding.[14] While cavitand **4.2** is selective in its affinity for substituted trimethylammonium (R-NMe$_3$)$^+$ groups due to these cation-π interactions, its open-ended nature allows the remainder of the molecule to protrude above the host into the external solvent. Larger guests with the R-NMe$_3^+$ anchor such as **4.5** show similar binding affinities as choline, affinities that are somewhat dependent on the favorability of H-bonding interactions between the upper rim carboxylate groups and the guest NH group with the proper spacing (CH$_2$CH$_2$) from the trimethylammonium bottom.
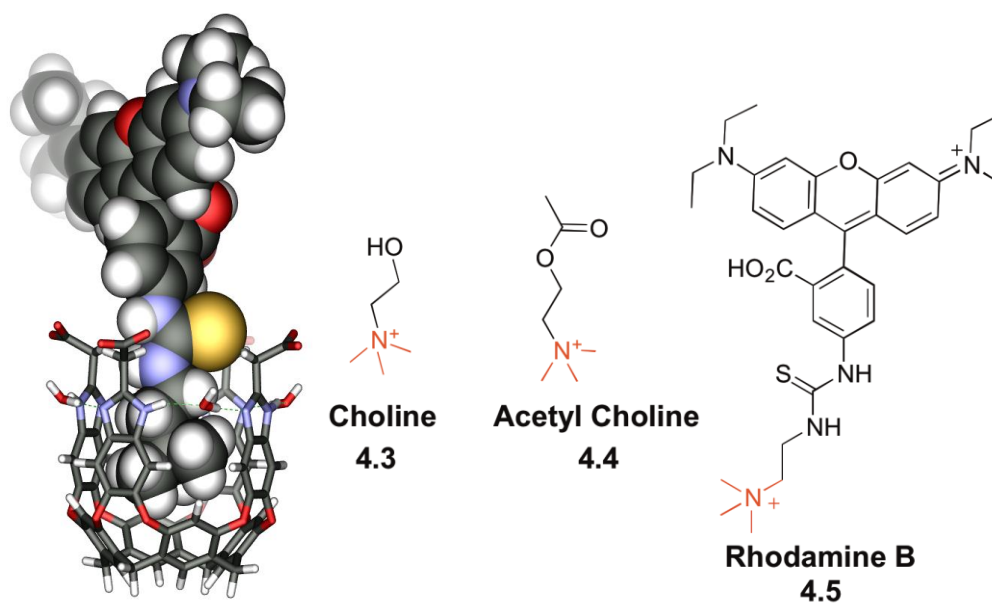
Figure 4.2. The molecular minimized representation of the cavitand **4.2** complex with trimethylated-rhodamine B **4.5** (SPARTAN, Hartree-Fock forcefield, with monitoring H-bonding), and (R-NMe$_3^+$) guests.

4.1.1. Molecular Recognition in Living Cells

Cavitand **4.2** binds a variety of molecules with R-NMe$_3^+$ binding handles. The recognition properties are extensive, and are functional in cellular environments.[16] To investigate the binding and transport ability of cavitand **4.2**, different fluorescent guests were synthesized with variable binding groups (**4.6a-c**) and compared to underivatized fluorescein **4.7** (Figure 4.3). As observed by confocal fluorescence and differential interference contrast (DIC) microscopy, the fluorescently labeled choline derivative **4.6a** (50 µM) could be transported into HeLa cells in the presence of 50 µM cavitand **4.2**, after only one hour incubation. In the absence of the cavitand, confocal fluorescence microscopy images showed minimal transport of the fluorescent guest, even after 24 h incubation. Guest **4.6a** showed strong binding to cavitand **4.2** followed by controlled endocytosis of the complex into the interior of HeLa cells (Figure 4.5).

In the absence of the trimethylammonium binding handle, fluorescein **4.7** was not transported (Figure 4.6), indicating that the presence of choline-derived binding handles in **4.6a** was essential for molecular recognition.[16] Mono- and di-methylated fluorescein guests **4.6c** and **4.6b** were also synthesized: NHMe$_2^+$ dye **4.6b**, NH$_2$Me$^+$ dye **4.6c**, and fluorescein **4.7** would be expected to have increasingly smaller affinities for cavitand **4.2** due to mismatches in shape and charge-fitting with the internal cavity.
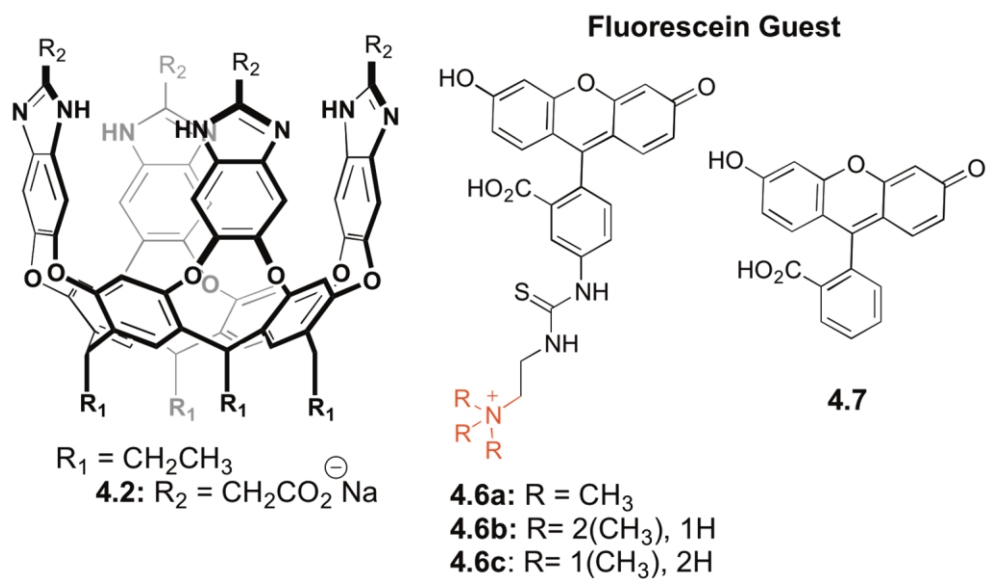
Figure 4.3. Suitable fluorescein guest **4.6a-c,** and derivatives **4.7**.
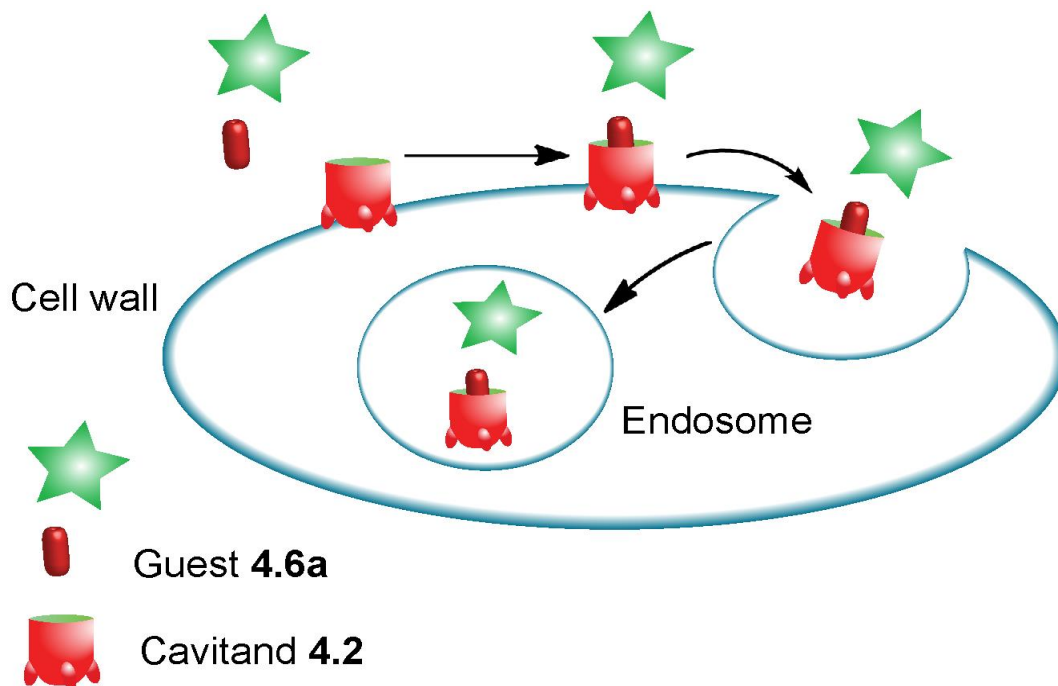
Figure 4.4. A cartoon representation of the transport process (endocytosis) of fluorescein guest **4.6a** mediated by cavitand **4.2**.
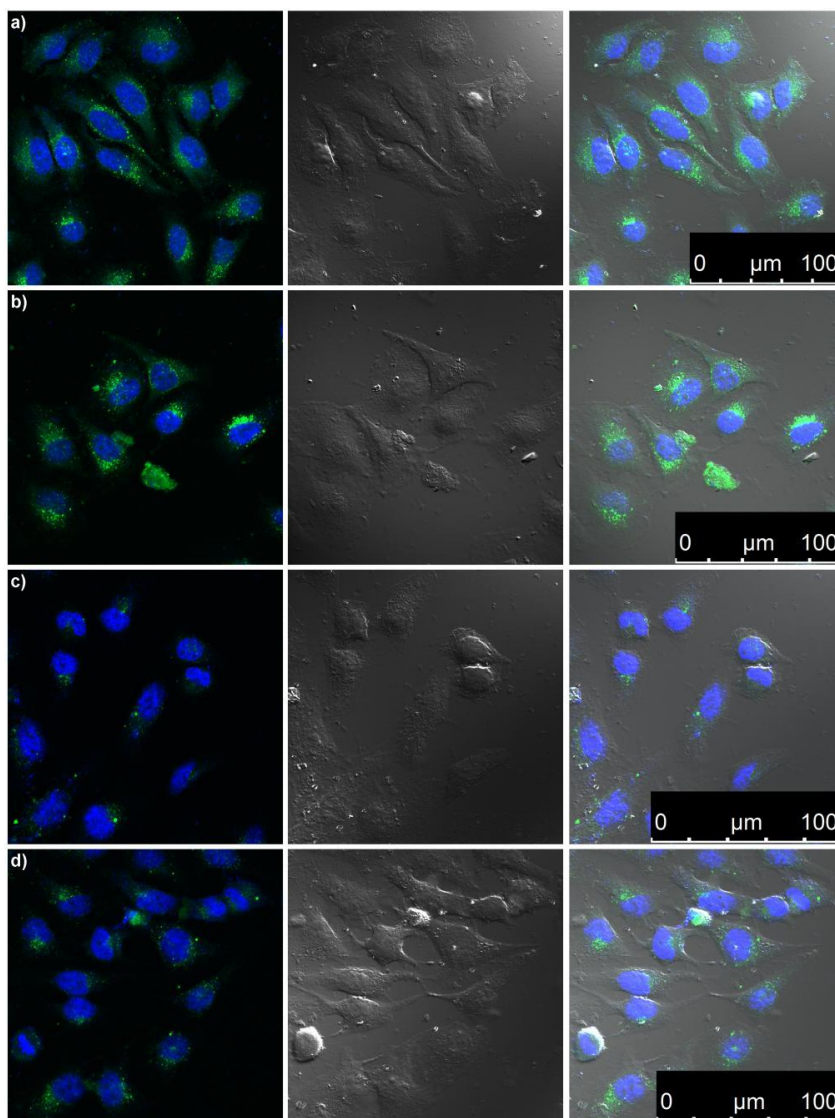
Figure 4.5. Confocal fluorescence microscopy, DIC, and combined images of the addition of fluorescently labeled choline derivative **4.6a** to HeLa cells (nuclei stained with DAPI): (a) 50 µM fluorescently labeled choline derivative **4.6a**, 50 µM cavitand **4.2**, 1 h incubation; (b) 50 µM fluorescently labeled choline derivative **4.6a**, 50 µM cavitand **4.2**, 24 h incubation; (c) 50 µM fluorescently labeled choline derivative **4.6a** only, 1 h incubation; (d) 50 µM fluorescently labeled choline derivative **4.6a** only, 24 h incubation.[16]
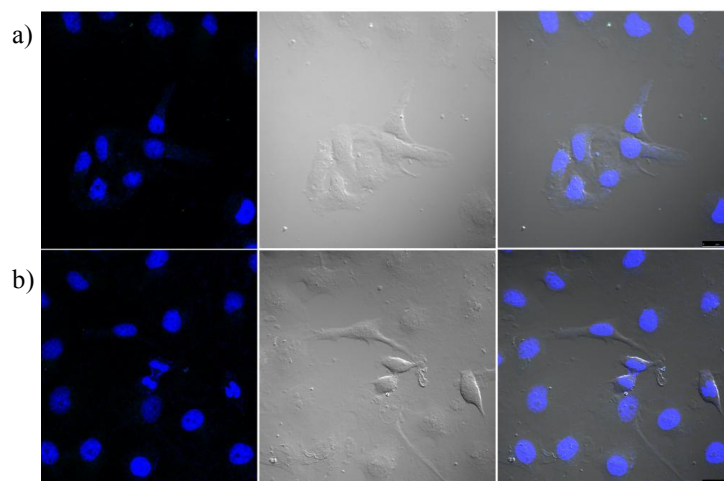
Figure 4.6. Confocal fluorescence microscopy, DIC, and combined images of the addition of fluorescently labeled choline derivative **4.6a** to HeLa cells (nuclei stained with DAPI): (a) 50 µM fluorescein **4.7**, 50 µM cavitand **4.2**, 1 h incubation; (b) 50 µM fluorescein **4.7**, 50 µM cavitand **4.2**, 24 h incubation.

4.1.2. Molecular Recognition in Solution and Aggregation-based Quenching

The effectiveness recognition of **4.6a** in complex environments was exciting, but we required a more detailed explanation of the behavior in controlled systems. Initially, we used ^{1}H NMR to study the binding affinity of fluorophore guests to the negative cavitand **4.2**. The resulting spectra showed unexpected behavior.

4.8
trans-4-4 dimethylamino
styryl-1-methylpyridinium
iodide
(**DMSI**)

When guest fluorophores (either **4.6a** or trans-4-4 dimethylamino styryl-1-methylpyridinium iodide **4.8**) were titrated into a D$_2$O solution of cavitand **4.2** (2 mM), proton signals for both the trimethylated fluorescent guest and cavitand disappeared (Figure 4.7).[17] Meanwhile, peaks corresponding to expunged THF, which is present in the

cavity from the final isolation step, appeared (Figure 4.7e). The disappearance of the peaks for both host and guest is caused by the formation of large, slowly tumbling aggregates in solution. The newly presented THF peaks indicate the binding of the guest with **4.6a**. The aggregation process is controlled by both the highly selective host behavior and the self-aggregative properties of **4.2**. Only guests with mildly lipophilic NMe_3^+ guests such as **4.6a** have been shown to cause this aggregation: hydrocarbon guests do not, and the phenomenon only occurs for small charged species such as choline at higher concentrations.[18] The aggregation interaction only occurs in solution: the cavitand preferentially incorporates in other lipid environments and no assembly is seen.[17]
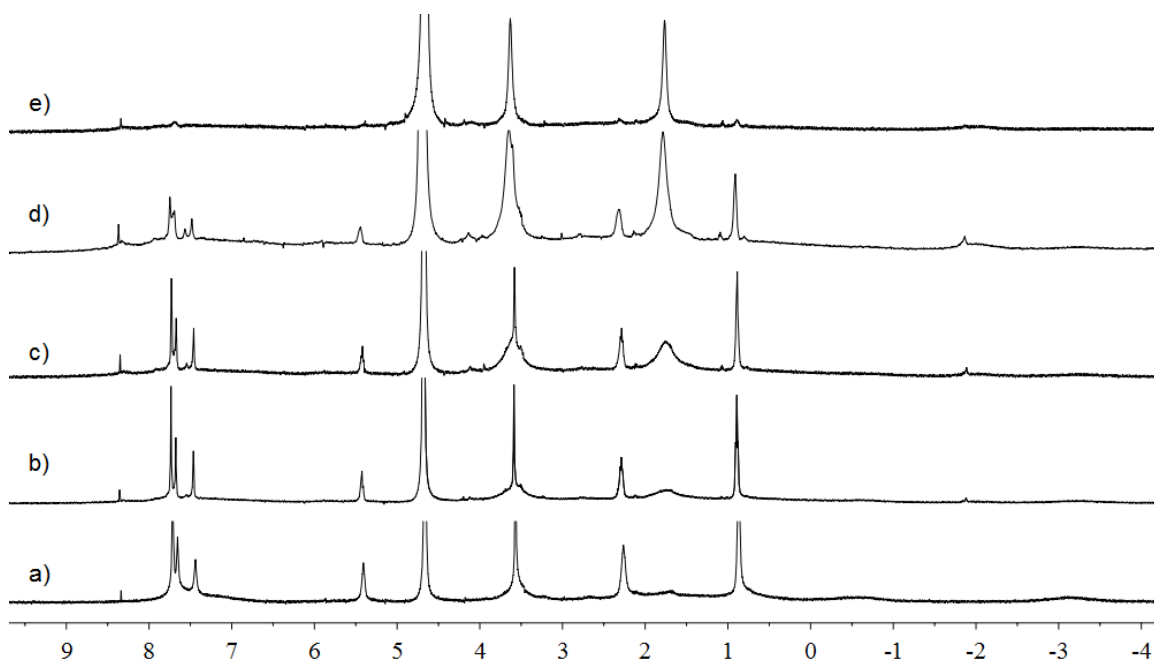
Figure 4.7. ^{1}H NMR titration of DMSI guest in 5 µM solution of cavitand **4.2** (400 MHz, D_2O) a) 0 eq. DMSI, b) 0.4 eq. DMSI, c) 0.8 eq. DMSI, d) 1.4 eq. DMSI, e) 1.8 eq. DMSI.

4.1.3. Binding Affinity Studies Using UV/Vis Spectroscopy

While the aggregation limited ^{1}H NMR studies, UV/Vis absorption and fluorescence spectroscopy was much more useful. The aggregation of the **4.2•4.6a** complex positions the fluorescein groups in close proximity to one another in the self-assembled aggregate, forming micellar environments. Self-quenching of the fluorescence signal is then observed. Minimal changes in fluorescence were observed upon addition of **4.2** to fluorescein and NH_2Me^+ guest **4.6c**, and only a slight decrease in fluorescence was observed for NMe_2H^+ guest **4.6b**. However, when NMe_3^+ guest **4.6a** was added, a strong loss in fluorescence was observed, reaching maximal quenching in the presence of 20 μM **4.2**, when only 30% of the original fluorescence was retained. The dissociation constant (K_d) of the **4.2•4.6a** complex was estimated to be 17 μM. The K_d values for NMe_2H^+ fluorescein **4.3c**, NH_2Me^+ fluorescein **4.6b**, and fluorescein **4.7** were at least 10 times larger than that of **4.3a**, indicating weak or non-specific binding.[17] The binding affinity for cavitands **4.2** and **4.16** is much stronger than with fluorescein guest **4.5** and **4.6**, and the quenching is more efficient, occurring upon simple 1:1 complex formation.[19]

4.1.4. Fluorescence Displacement Sensor for Trimethylated Lysine Peptides.

Biorelevant recognition was illustrated by the binding of trimethylated histone peptides, including H3K9 and its modified equivalent H3K9Me$_3$, which is a 21 amino acid histone fragment containing a trimethylated lysine (KMe$_3$) residue.[17] The fluorescence H3K9Me$_3$ displaced the trimethylated fluorescein **4.6a** in the cavitand **4.2**. Although the dissociation constant (K_d) of the **4.2•4.6a** complex was 17 μM, the addition of only 2 μM

trimethylated peptide such as H3K9Me3 caused a significant recovery of the fluorescence

signal of **4.6a.** The parent unmethylated peptide H3K9 showed no displacement of the

fluorescent guest **4.6a**.[20]
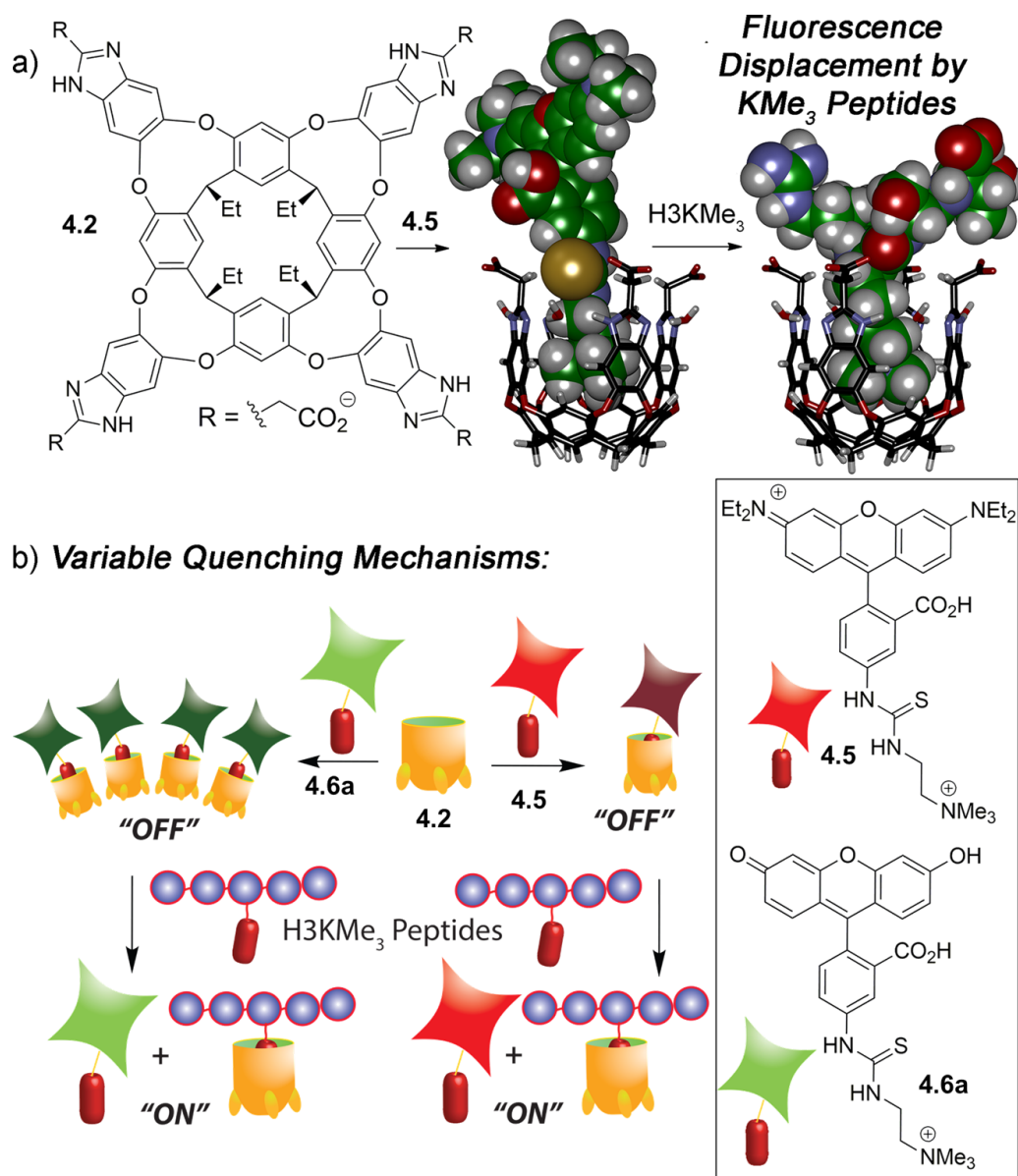
Figure 4.8. a) Structure of cavitand **4.2** and minimized models of the **4.2•2.5** and the replacement **4.2•**(AR(KMe3)ST) host:guest complexes (SPARTAN); b) the aggregation-based quenching displacement sensor.

4.2. Variation of Cavitand Upper Rim

Cavitand **4.2** is a synthetic receptor that is capable of selective KMe_3 binding. However, as previously mentioned, cavitands such as **3.8, 3.12,** and **3.13** required both suitable size and H-bonding interactions with the rim for stronger binding. The binding affinity increased dramatically upon the addition of an H-bonding interaction component to the guest:host complex. Therefore, varying the upper rim functions could allow selectivity in target binding beyond a simple cavity-based effect. We investigated the synthesis of differently functionalized cavitand scaffolds with the same cavity and ethyl feet with variation of the upper rim functions.

4.3. Neutral cavitand

Utilizing the short-footed ethyl cavitand scaffold, we set out to functionalize the upper rim, which can be tailored to bind not only suitable sized guests, but utilize complimentary charge interactions. To measure the importance of the charged species on the top of cavitand **4.2**,[21,22] CH benzimidazole cavitand **1.30a** was used, as mentioned in chapter 1. The binding ability of benzimidazole scaffolds in organic solvents was limited due to the solvent competition, and substituted $R-NMe_3^+$ ions were the only strongly bound guests. The neutral cavitand **1.30a** provides a simple scaffold to study only the cavity binding affinity without the negatively charged tetracarboxylate group present in cavitand **4.2**.
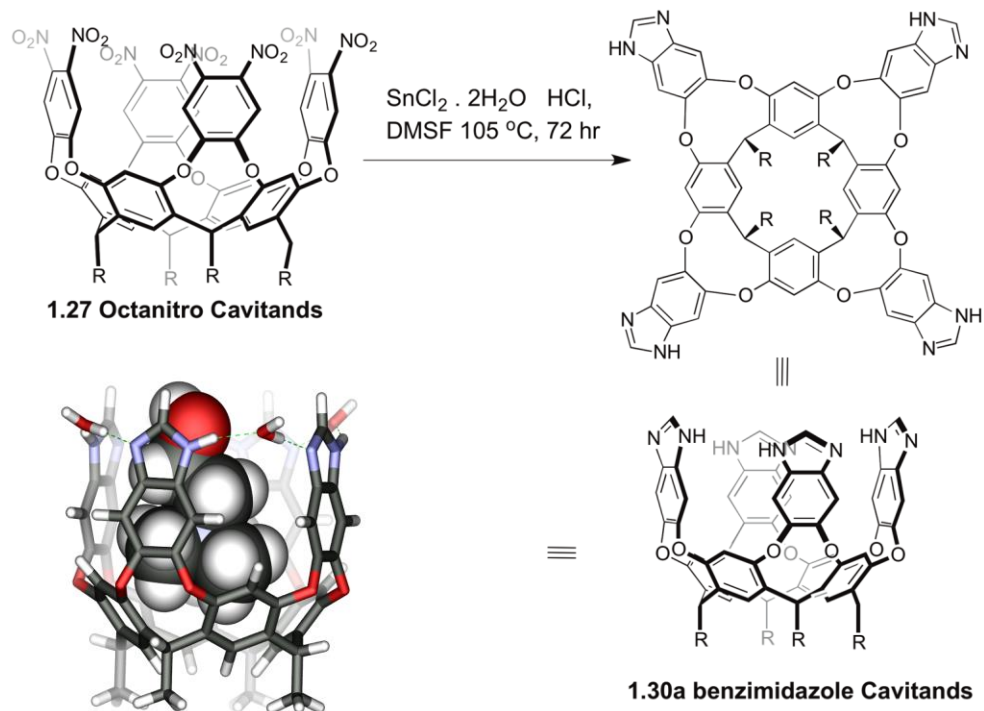
Figure 4.9. The synthesis of deep cavitand scaffold **1.30a,** and the minimized representation of the cavitand complex structure with choline (SPARTAN, Hartree-Fock forcefield, with monitoring H-bonding.)

4.3. Positive cavitand

To provide cationic rims, positively charged cavitands were also synthesized following previously published procedure with minimal modification.[23] Reacting octamine cavitand **1.28** with cyanogen bromide allowed the formation of the 2-aminobenzimidazole cavitand **4.9** under N_2, which provides positively charged rims. The cavitand has previously been used as a catalyst for the hydrolysis of choline carbonates.[23] This biomimetic, metal free hydrolysis involves three steps: guest:host interaction, carbamoylation, and enzyme-like hydrolysis. The hydrolysis is driven by the water

molecules that aid the folding of the cavitand.[23] The binding and close proximity of the

guest to the water molecules by the rims aids the hydrolysis and drives it to completion.
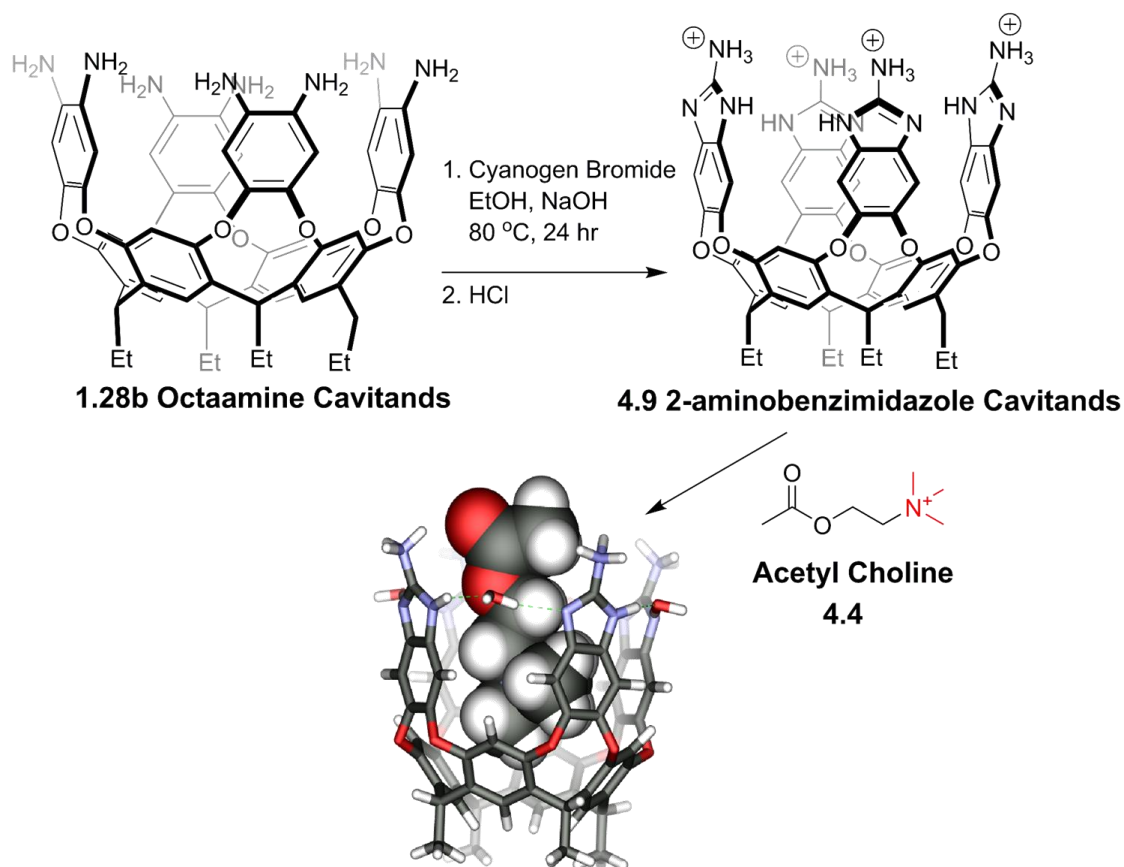
Figure 4.10. The synthesis of deep 2-aminobenzimidazole cavitand scaffold **4.9** and the minimized representation of the cavitand complex structure with acetyl choline **4.4** (SPARTAN, Hartree-Fock forcefield).

4.4. New Functionalized Scaffolds Utilizing our Newly Discovered Methods

While cavitand **1.30a**, **4.2**, and **4.9** provided neutral, negatively, and positively charged

rims to the water soluble benzimidazole scaffolds, synthesis of additional variations on

the cavitand rim would provide a far greater scope of recognition. The challenge is to introduce variable functionalization such as strong acid, strong base, zwitterions, and fluorescent groups to the benzimidazole rims. The host:guest interactions could be tailored to monitor and sense desired biological and enzymatic activities, metal sensing, and more. A fluorescent cavitand scaffold would not only allow direct monitoring of the endocytosis process, but it would provide a larger understanding of the cavitand interaction with anticancer drugs and monitor fluorescent guest binding in cells and bilayer environments.

One major challenge in creating fluorescent hosts is that many easily accessible fluorescent labels contain electrophilic functionality such as the chloroarene in 4-chloro-7-nitrobenzofurazan (NBD-Cl) or the isothiocyanate group in rhodamine B isothiocyanate and fluorescein 5(6)-isothiocyanate. To introduce such linkers, one must either form a nucleophilic cavitand or functionalize the fluorescent sensor with a more reactive nucleophilic group.

4.5. Synthesis of the Tetraethylacetal Cavitand Followed by Condensation

There are two sites where fluorophores could be added: at the feet, or at the upper rim. Forming the benzimidazole tetracarboxylate cavitand **4.2** with nucleophilic OH feet was unsuccessful, which limited the introduction of the fluorophores at the cavitand base. While the synthesis of an electrophilic fluorescent functionalized ligand was unsuccessful, many nucleophilic groups can be added to the upper rim of the cavitand *via* transamination.[24] We sought to exploit successful synthesis processes discussed in

chapter 3 with the long hydrophobic feet ($C_{11}H_{23}$), and to apply this synthetic route to the more water soluble ethyl footed scaffold.

Utilization of the condensation reaction to introduce the arylimine cavitand to the ethyl foot scaffold showed difficulties, however. Solubility played a large role in isolating the tetraethylacetal cavitand **3.7** scaffolds. The long lipophilic feet helped the scaffold to precipitate out of the ethanol solution and undergo recrystallization in cold EtOH. The shorter ethyl feet scaffold, however, was soluble in most organic solvents such as EtOH, and so isolation and purification of the tetraethylacetal cavitand scaffolds was challenging. Similarly, challenges were faced in converting the ethyl-footed tetraethylacetal cavitand to the arylimine scaffold, namely solubility and sensitivity to water in the open-air environment. Synthesis was possible by modifying the procedure for the previously synthesized arylimine cavitands with lipophilic feet **3.7**. Condensation of freshly prepared imidate with octamine cavitand **1.18b** produced the tetraethylacetal cavitand **4.10** with short ethyl feet in 57% yield. The reaction was run in N_2 atmosphere and the cavitand scaffold was isolated by precipitation from anhydrous EtOH at -5 °C. Treatment of **4.10** with amine containing aromatic substrates such as 2-aminopyridine and a soft Lewis acid such as La(OTf)$_3$ in extremely dry conditions provided the desired imine-containing cavitand **4.11** in 80% yield. The nucleophilic NBD fluorophore was synthesized by reacting commercial NBD-Cl with either hydrazine to yield **4.12** or diethylenediamine to yield **4.13.** These fluorescent nucleophiles can be simply introduced onto the cavitand scaffold by transamination with **4.11**. Simple sonication of arylimine cavitand **4.11** with primary NBDamines **4.12** and **4.13** in a mixture of CH_2Cl_2/MeOH for

five minutes smoothly yielded the corresponding alkylimines **4.14** and **4.15** respectively. The scaffolds were isolated by removing the solvent mixture then resuspending it in CH$_2$Cl$_2$, as the scaffolds have a lower solubility in polar solvents. Incomplete reaction was desirable here, as the substitution of all four pyridyl groups by the amine will provide four fluorescent groups in close proximity, which could cause self-quenching of the fluorescence signal. Complete addition of four NBD linkers may also cause blocking on the cavity, lowering the binding affinity to suitable sized guests.[25] Therefore, 0.5 equivalents of **4.12**/**4.13** were added to favor incomplete fluorescent group addition and to minimize self-quenching. The increase of the absorbance spectrum using UV/Vis indicates a successful transamination reaction with space between the NBD units.
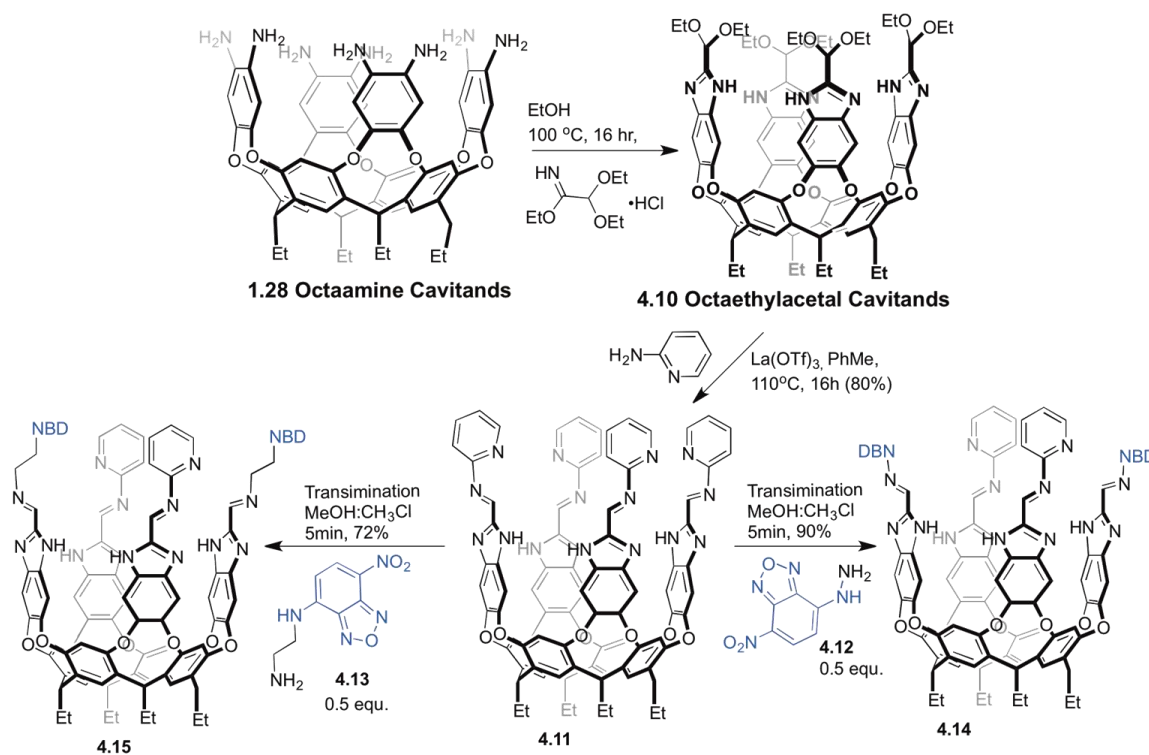
Figure 4.11. The synthesis of fluorescent cavitand scaffolds **4.14** and **4.15.**

The characterization of the fluorescent cavitands was challenging. Due to the sub-millimolar solubility in either D_2O or anhydrous $CDCl_3$ of cavitand **4.14,** sharp ^{1}H NMR spectra were only obtained in $CDCl_3$ and 5% DMSO-d_6. ^{1}H NMR in $CDCl_3$ showed a broad and unfolded cavitand scaffold. Addition of cetyltrimethylammonium bromide as templating guest broadens the proton peaks. Guest binding with adamantanamine and choline in $CDCl_3$ and 5% DMSO-d_6 was not observed due to solvent competition. UV-Vis spectroscopy of the fluorescence cavitand **4.14** was inconclusive, as the absorption spectrum in MeCN:1%DMSO showed peaks at 466 and 360 nm, which correspond to the NBD group, but are unchanged from the NBD amine **4.12**. The intensity of the signals was somewhat enhanced. The addition of a choline guest conferred no changes on the absorption spectrum.
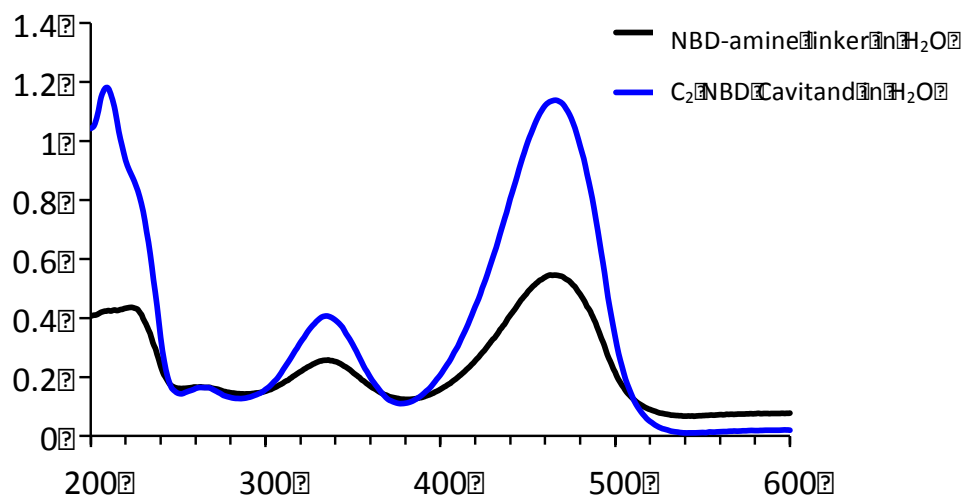
Figure 4.12: UV/Vis absorption spectra of **4.12 (black)** and **4.14 (blue)** in H_2O.

4.6. Synthesis of Thiobenzimidazole Scaffolds

An alternative route for the introduction of upper rim functional groups could involve the thiobenzimidazole scaffold **3.4**, but aqueous applications requires synthesis of the ethyl-footed equivalent. Although the synthesis of the thiobenzimidazole cavitand **3.4** ($C_{11}H_{23}$ thiobenzimidazole) was simple, functionalization of the ethyl footed equivalent was much more difficult. The short ethyl footed cavitand scaffold was water-soluble which introduced similar challenge during reaction and isolation procedures. Using dry THF under controlled N_2 atmosphere, the thiobenzimidazole **4.16** was isolated in good yields.
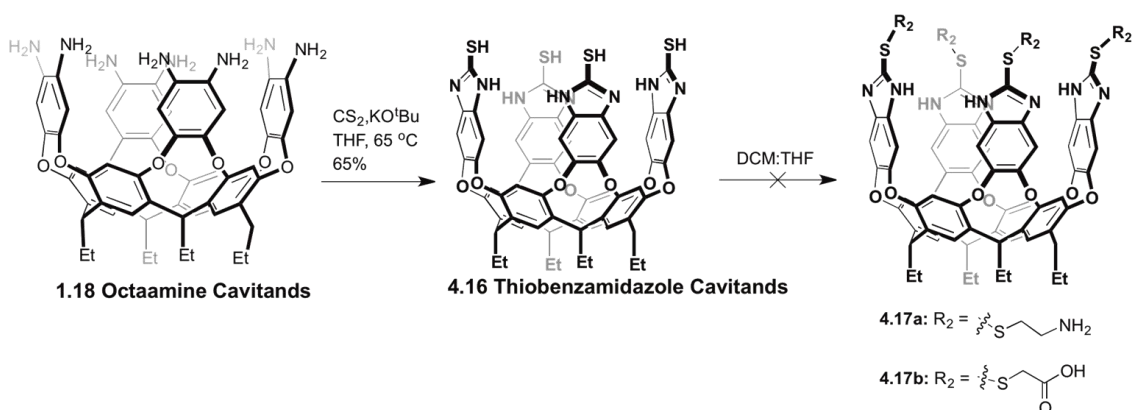
Figure 4.13. The synthesis of the thiobenzimidazole cavitand scaffold **4.16.**

Disulfide exchange reactions were tested to introduce either strongly acidic or strongly basic groups to the thiobenzimidazole cavitand. Multiple efforts to form the disulfide bond with either mercaptoacetic acid or cysteamine resulted in multiple products. The reaction never went to completion, which caused difficulty in isolating and purifying the product. The addition of NaOD and DBr to **4.17b** and **4.17a** respectively showed no

change in sample solubility, and the ionic charged species were hard to isolate. ^{1}H NMR analysis shows a very broad spectrum. Fortunately, although the disulfide reaction showed many challenges, cavitand **4.16** shows high selectivity for binding Ag$^+$ ions in aqueous solution. The thiobenzimidazole cavitand **4.16** was utilized by Yang Liu in the Zhong lab at UCR (our collaborators) for metal sensing such as $UO_2(OAc)_2$ and $Hg(OAc)_2$ at pH 7.4 and fluorescent displacement studies. This combination of synthetic strategies allows access to a great range of functionalized cavitands with short water-soluble feet.
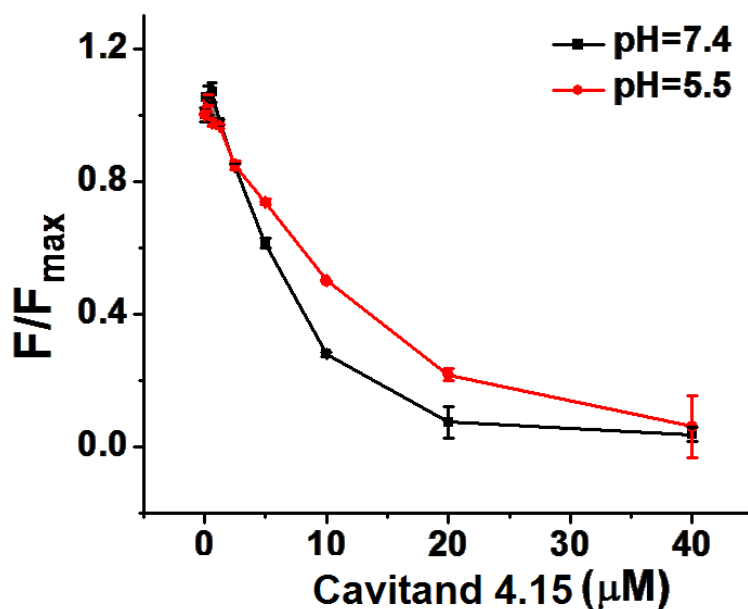
Figure 4.14. Fluorescence response of the self-quenching fluorescence guest **4.5** 3 μM with increasing concentrations of cavitand **4.16** in pH 7.5 and pH5.5
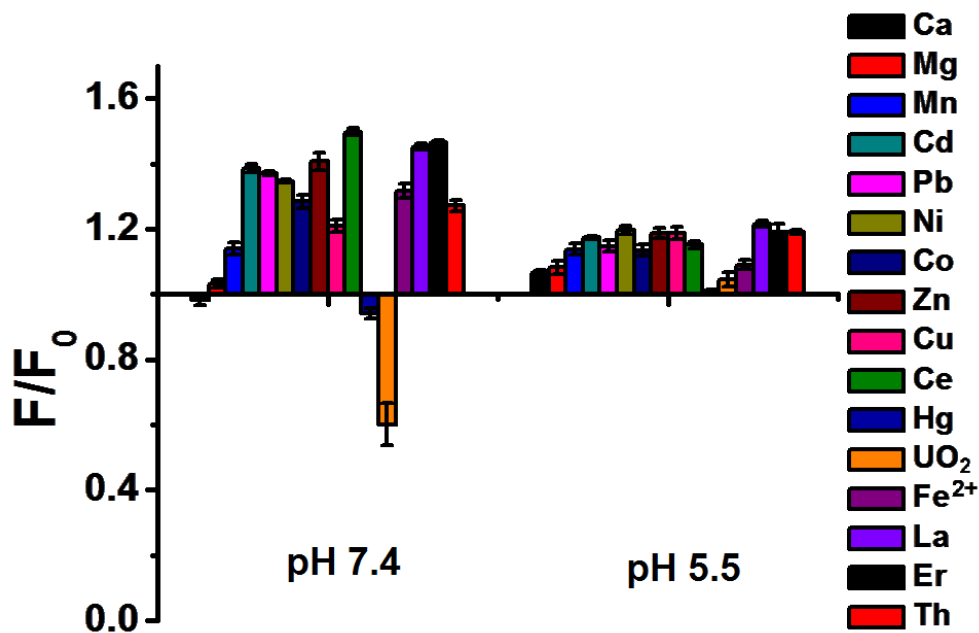
Figure 4.15. The complete screening data for the metal sensors using our fluorescent guest-cavitand **4.16•2.5**. The sensor elements were constructed by pre-incubating guest **2.5** at 3 μM with cavitand **4.16** at 5 μM in the solutions of 7.4 pH and 5.5 pH. Metal used $MgCl_2$, $CaCl_2$, $MnCl_2$, $FeSO_4$, $CoCl_2$, $NiCl_2$, $CuCl_2$, $ZnCl_2$, $CdCl_2$, $Hg(OAc)_2$, $Pb(NO_3)_2$, $LaCl_3$, $CeCl_3$, $ErCl_3$, $ThCl_3$, and $UO_2(OAc)_2$.

4.7. Utilizing Charged/uncharged Cavitands in Membranes

The successful syntheses of a variety of new functionalized cavitands **4.2, 1.30a, 4.9,** and **4.16** have opened the door to multipurpose scaffolds that are tailored to a variety of new biorelevant recognition strategies. These cavitands have been exploited for biological and physical studies by others in or lab and our collaborators.[16,17,26-29] The negatively charged **4.2**, positively charged **4.9**, and neutral **1.30b** as well as metal binding **4.16** cavitand scaffolds confer a variety of upper rim interactions to the appropriate

guest(s), and are efficiently embedded in supported lipid bilayers due to their hydrophobicity.

The scaffolds were utilized for multiple different studies for recognition of suitably labeled proteins at the bilayer interface. Short ethyl footed cavitands can be self-incorporated into a supported lipid bilayer (SLB) and monitored by Surface Plasmon Resonance Spectroscopy (SPR), which is a surface-based method of analyzing recognition at bilayer interfaces.[30] Alternatively, in solution, fluorescence displacement process can be exploited to establish homogeneous in-solution displacement assays for the detection of suitable substrates, if the substrate is a sufficiently good guest to displace the fluorescent **4.5** or **4.6a**. The array of cavitands and guest interactions can be tested in SLB or solution.

4.7.1. Incorporation of Water-soluble Functionalized Cavitands in Supported Lipid Bilayers

SPR/CE analysis of large guest binding in membrane-embedded **4.2** showed an unusual result: large protein targets were bound with far higher affinities in the membrane-bound cavity of **4.2**.[29] Even though the binding event was monovalent, and the R-NMe$_3^+$ binding handle was identical, labeled hemoglobin bound stronger than choline-tagged cytochrome c in a POPC SLB, which bound stronger than choline itself with an order of magnitude in **4.2**.[16,29,31] The addition of a substituted choline derived binding handle to different proteins demonstrated an *in situ* labeling/recognition method for large biomacromolecules on supported lipid bilayers. The binding interactions show a

137

micromolar dissociation constant *via* monovalent binding stoichiometry between the cavitand and the injected protein using POPC.[29]

4.7.2. Matched and Mismatched Charged Guest Binding in Solution

The binding affinity for guests to the cavitands depends not only on R-NMe$_3^+$ handles and cavity size, but also on the interactions of the rim with the guest, as explained in Chapter 3. To better understand the interactions of the charged rim with different guests having varied H-bonding and charge matching and mismatching properties, we tested our differently charged scaffolds with multiple charged guests. The suite of upper rim functionalized self-folding deep cavitands can act as a "chemical nose,"[32-34] or a fluorescence displacement sensor in an array-based format.
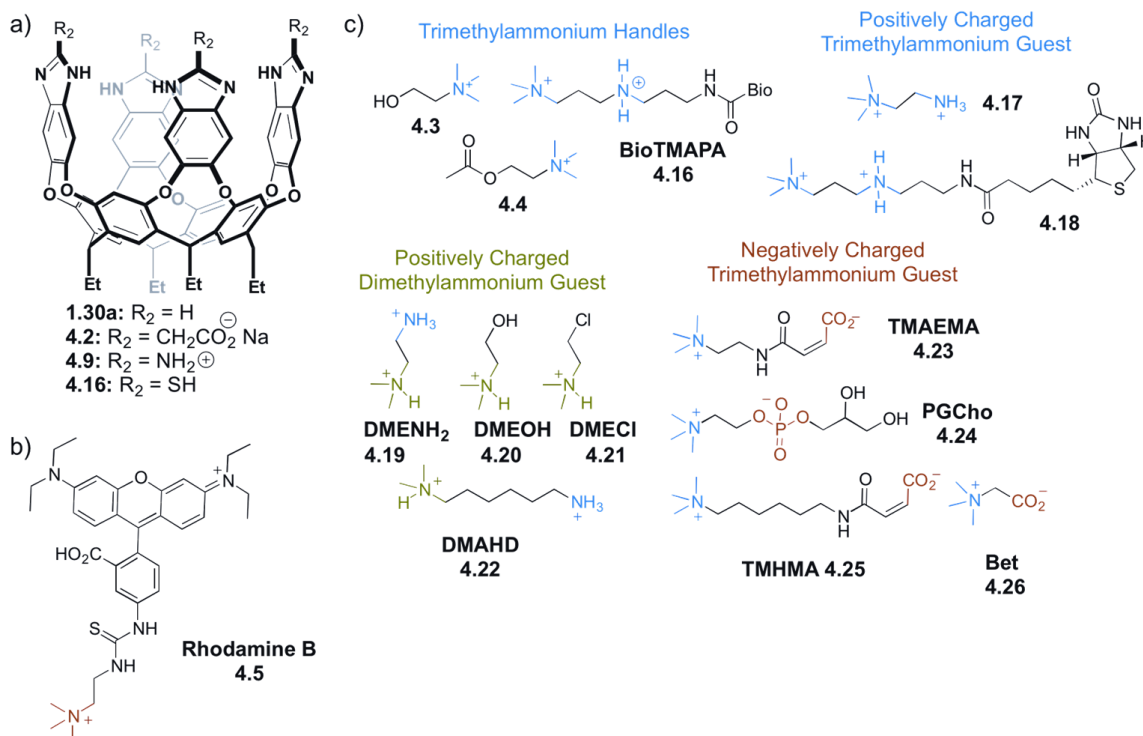
Figure 4.16. Small molecule guest scope with varying charge interaction.

Fluorescent rhodamine B guest **4.5** allows the use of multiple cavitands for the sensing, as it requires no self-aggregation upon cavitand binding. As previously discussed, the binding affinity for cavitands **4.2, 1.30a, 4.9,** and **4.16** is much stronger than with fluorescein guest **4.5** and **4.6**, and the quenching is more efficient, occurring upon simple 1:1 complex formation.[19]

Small changes in guest structure were targets for testing, including variation of the bottom (trimethylated **4.3**, **4.4**, and **4.16** vs. dimethylated **4.20**) and the top (negatively charged **4.23-4.26** vs. positively charged **4.16-4.18**) of the guest. Other variations tested were the position of the charge on the guest substrate, which includes cationic ammonium groups **4.16, 4.18,** anionic guests such as **4.23-4.26**, and neutral guests that still participate in H-bonding such as choline **4.3** and acetyl choline **4.4**.

In 98-well plates at a 100 µM concentration, the **4.2•4.5** complex fluorescence was measured before (F_{min}) and after (F) mixing of the guest. In the same concentration, only the fluorescent guest **4.5** was also measured (F_{max}) as maximum fluorescence before quenching with the cavitands. Guest displacement was measured by $(F-F_{min})/F_{max.}$

The system was extremely sensitive to small differences in the guest. Clear discrimination was observed between choline **4.3** and **4.17**, as well as the dimethylated guest **4.19** positively charged top ($^+NH_3$) and **4.20** with OH top. As expected, maximal displacement occurred with the trimethylated guest **4.3** choline and **4.4** the acetalcholine with >12% and 8% increase respectively. At neutral and basic pH, much higher percentages of fluorophore displacement occur with choline, and acetylcholine with all

139

three hosts **4.2, 1.30a,** and **4.9**. However, cavitand **4.2** showed the largest changes under the acidic conditions.

Guest **4.5** exhibited far stronger binding than the dimethylated guests, which all caused less than 5% displacement in basic pH. The reason for pH dependence in binding of neutral **1.30a** at basic pH has been previously described to be due to a breathing hydrogen bonding seam that shrinks the cavity size and increases non-covalent space-filling and CH-π interactions with the bound guest.[19] The affinity of guest binding also was affected by the variations in the protonation states of some or all of the CO_2^-/CO_2H groups in **4.2**, or the NH_2/NH_3^+ groups in **4.9** caused by the change of pH conditions, as well as the variations in the guest protonation states. The NMe_3^+ group fits snugly in the binding pocket, positioning the OH, PO_3^-, NH_3^+, and NH_2R^+ groups in close proximity with the charged upper rim receptor changed the binding affinity dramatically between the four different cavitand scaffolds.

4.7.3. Utilizing Charged/uncharged Cavitands for Site-Selective Sensing of Histone Methylation Enzyme Activity in-situ

The array of cavitands and the displacement assay in solution introduces the possibility of detecting the trimethylated KMe_3 position and enzymatic modification to lysine *in situ*. Arrayed deep cavitands are capable of site-selective recognition and discrimination of lysine post-translational methylations in complex histone mixtures. An application of this process is the discrimination between histone KMe_3 peptides and the undesired KH_3, KMe, and KMe_2, and the extension to site-selective discrimination between different

KMe$_3$ peptides. This discrimination is much more challenging and requires multiple variable receptors in an arrayed format. The recognition can be coupled to a fluorescence-based supramolecular tandem assay that allows in situ monitoring of the reaction catalyzed by the lysine methytransferase PRDM9 or the lysine demethylase JMJD2E. An arrayed sensor system containing only three cavitand components can detect the specific substrates of enzyme modification in the presence of other histone peptides in the enzyme assay. In addition, the sensor is capable of rapid recognition of decreased methylation in histones extracted from cells with one methyltransferase gene being knocked out. This expands the scope of supramolecular tandem assays, enabling investigation of critical enzyme functions such as cross-reactivity over multiple methylation sites and interference from non-substrate peptides.

As previously shown, the combination of cavitand **4.2** and a suitable R-NMe$_3^+$ fluorophore guests **4.5** and **4.6a** allows sensing of KMe$_3$ peptides via a fluorescent displacement assay process. An extension study to the post-translation modifications (PTMs) of lysines was studied in a similar fashion. The application of multiple different cavitands **4.2, 4.9,** and **1.30a** and fluorophores in an array-based format allows for a sensitive discrimination of KMe$_3$ residues at different positions on the peptide fragments.

Three different histone H3 peptides with trimethylation (KMe$_3$) modifications at different positions (H3K4Me$_3$, H3K9Me$_3$, H3K27Me$_3$) were combined and added to an array of hosts:guest complexes for displacement studies. The systematic array testing was constructed by incorporating the three cavitands **4.2, 4.9,** and **1.30a** at 4 μM and their complexes with guest **4.5** at 3 μM concentration at two different pHs (pH 7.4 and 9.0),

for a total of six variables. The peptide mixture was added to each sensor solution in a 96-well plate at a concentration of 10 μM. The relative fluorescence recovery detected for each well showed the high selectivity of the trimethylated KMe$_3$ and the differently charged interaction with the upper rims of the cavitand. The scaffolds show exquisite selectivity and discrimination between small molecule targets and are capable of detecting positional variation in histone peptides carrying lysine methylation, phosphorylation, and acetylation PTMs.
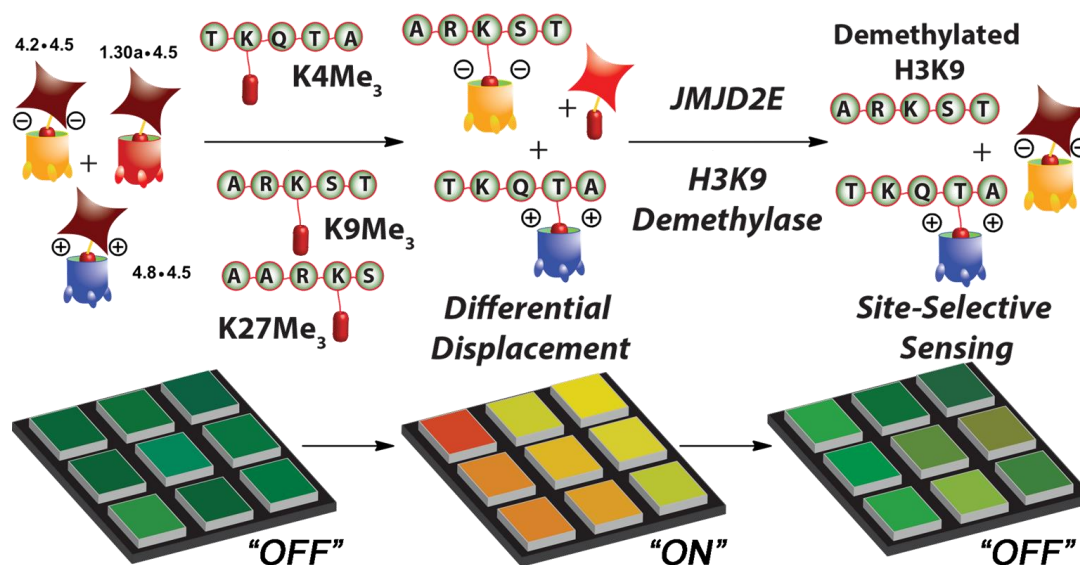
Figure 4.17. Illustration of the site selective array for sensing histone methylation enzyme activity *in situ*.

4.8. Conclusion

Cavitand scaffold **4.2** showed ability to bind their appropriate target molecules while embedded in lipid vesicles as well as supported lipid bilayers and HeLa cells, but the lack of NMR analysis leaves some understanding of the thermodynamic and kinetic properties

of the recognition unanswered, such as why did the trimethylated peptide show a higher binding constant than the very similar trimethylated fluorescent guest **4.5**, and why did the aggregation effect increase the binding constant? While many of the synthesized scaffolds showed biosensor abilities, and many were utilized as drug delivery agents and PTM sensors, more detailed study was required. To understand the effects of membrane incorporation and aggregation on the molecular recognition properties, and to investigate the orientation, conformation, and motion of the guest inside the scaffolds, we turned to NMR studies in lipid environments.

4.9. References

(1)   Conner, S. D.; Schmid, S. L. Regulated portals of entry into the cell. *Nature* **2003**, *422*, 37-44.

(2)   Chinai, J. M.; Taylor, A. B.; Ryno, L. M.; Hargreaves, N. D.; Morris, C. A.; Hart, P. J.; Urbach, A. R. Molecular recognition of insulin by a synthetic receptor. *J. Am. Chem. Soc.* **2011**, *133*, 8810-8813.

(3)   Xu, H.; Ling, X. Y.; van Bennekom, J.; Duan, X.; Ludden, M. J.; Reinhoudt, D. N.; Wessling, M.; Lammertink, R. G.; Huskens, J. Microcontact printing of dendrimers, proteins, and nanoparticles by porous stamps. *J. Am. Chem. Soc.* **2009**, *131*, 797-803.

(4)   Ludden, M. J.; Mulder, A.; Tampe, R.; Reinhoudt, D. N.; Huskens, J. Molecular printboards as a general platform for protein immobilization: a supramolecular solution to nonspecific adsorption. *Angew. Chem. Int. Ed.* **2007**, *46*, 4104-4107.

(5)   Ludden, M. J.; Reinhoudt, D. N.; Huskens, J. Molecular printboards: versatile platforms for the creation and positioning of supramolecular assemblies and materials. *Chem. Soc. Rev.* **2006**, *35*, 1122-1134.

(6)   Ingerman, L. A.; Cuellar, M. E.; Waters, M. L. A small molecule receptor that selectively recognizes trimethyl lysine in a histone peptide with native protein-like affinity. *Chem. Commun.* **2010**, *46*, 1839-1841.

(7)   James, L. I.; Beaver, J. E.; Rice, N. W.; Waters, M. L. A synthetic receptor for asymmetric dimethyl arginine. *J. Am. Chem. Soc.* **2013**, *135*, 6450-6455.

(8)   Daze, K. D.; Hof, F. The cation-pi interaction at protein-protein interaction interfaces: developing and learning from synthetic mimics of proteins that bind methylated lysines. *Acc. Chem. Res.* **2013**, *46*, 937-945.

(9)   McGovern, R. E.; Fernandes, H.; Khan, A. R.; Power, N. P.; Crowley, P. B. Protein camouflage in cytochrome c-calixarene complexes. *Nature* **2012**, *4*, 527-533.

(10)   Ma, D.; Zavalij, P. Y.; Isaacs, L. Acyclic cucurbit[n]uril congeners are high affinity hosts. *J. Org. Chem.* **2010**, *75*, 4786-4795.

(11)   Ma, D.; Hettiarachchi, G.; Nguyen, D.; Zhang, B.; Wittenberg, J. B.; Zavalij, P. Y.; Briken, V.; Isaacs, L. Acyclic cucurbit[n]uril molecular containers enhance the solubility and bioactivity of poorly soluble pharmaceuticals. *Nature* **2012**, *4*, 503-510.

(12)   Zhang, B.; Isaacs, L. Acyclic Cucurbit[n]uril-type Molecular Containers: Influence of Aromatic Walls on their Function as Solubilizing Excipients for Insoluble Drugs. *J. Med. Chem.* **2014**, *57*, 9554-9563.

(13)   Hof, F.; Trembleau, L.; Ullrich, E. C.; Rebek, J., Jr. Acetylcholine recognition by a deep, biomimetic pocket. *Angew. Chem. Int. Ed.* **2003**, *42*, 3150-3153.

(14)   Biros, S. M.; Ullrich, E. C.; Hof, F.; Trembleau, L.; Rebek, J. Kinetically stable complexes in water: The role of hydration and hydrophobicity. *J. Am. Chem. Soc.* **2004**, *126*, 2870-2876.

(15)   Biros, S. M.; Rebek, J. Structure and binding properties of water-soluble cavitands and capsules. *Chem. Soc. Rev.* **2007**, *36*, 93-104.

(16)   Ghang, Y. J.; Schramm, M. P.; Zhang, F.; Acey, R. A.; David, C. N.; Wilson, E. H.; Wang, Y.; Cheng, Q.; Hooley, R. J. Selective cavitand-mediated

endocytosis of targeted imaging agents into live cells. *J. Am. Chem. Soc.* **2013**, *135*, 7090-7093.

(17)   Liu, Y.; Perez, L.; Mettry, M.; Easley, C. J.; Hooley, R. J.; Zhong, W. Self-Aggregating Deep Cavitand Acts as a Fluorescence Displacement Sensor for Lysine Methylation. *J. Am. Chem. Soc.* **2016**, *138*, 10746-10749.

(18)   Li, V.; Ghang, Y. J.; Hooley, R. J.; Williams, T. J. Non-covalent self assembly controls the relaxivity of magnetically active guests. *Chem. Commun.* **2014**, *50*, 1375-1377.

(19)   Schramm, M. P.; Hooley, R. J.; Rebek, J., Jr. Guest recognition with micelle-bound cavitands. *J. Am. Chem. Soc.* **2007**, *129*, 9773-9779.

(20)   Ghang, Y. J.; Perez, L.; Morgan, M. A.; Si, F.; Hamdy, O. M.; Beecher, C. N.; Larive, C. K.; Julian, R. R.; Zhong, W.; Cheng, Q.; Hooley, R. J. Anionic deep cavitands enable the adhesion of unmodified proteins at a membrane bilayer. *Soft Matter* **2014**, *10*, 9651-9656.

(21)   Far, A. R.; Shivanyuk, A.; Rebek, J. Water-stabilized cavitands. *J. Am. Chem. Soc.* **2002**, *124*, 2854-2855.

(22)   Choi, H. J.; Park, Y. S.; Song, J.; Youn, S. J.; Kim, H. S.; Kim, S. H.; Koh, K.; Paek, K. Structural properties of benzimidazole cavitand and its selective recognition toward 4-methylbenzamide over 4-methylanilide. *J. Org. Chem.* **2005**, *70*, 5974-5981.

146

(23)   Soberats, B.; Sanna, E.; Martorell, G.; Rotger, C.; Costa, A. Programmed enzyme-mimic hydrolysis of a choline carbonate by a metal-free 2-aminobenzimidazole-based cavitand. *Org. Lett.* **2014**, *16*, 840-843.

(24)   Mettry, M.; Moehlig, M. P.; Hooley, R. J. Synthesis, guest binding, and metal coordination of functionalized self-folding deep cavitands. *Org. Lett.* **2015**, *17*, 1497-1500.

(25)   Hooley, R. J.; Van Anda, H. J.; Rebek, J. Cavitands with revolving doors regulate binding selectivities and rates in water. *J. Am. Chem. Soc.* **2006**, *128*, 3894-3895.

(26)   Perez, L.; Ghang, Y. J.; Williams, P. B.; Wang, Y. S.; Cheng, Q.; Hooley, R. J. Cell and Protein Recognition at a Supported Bilayer Interface via In Situ Cavitand-Mediated Functional Polymer Growth. *Langmuir* **2015**, *31*, 11152-11157.

(27)   Perez, E. M.; Martin, N. pi-pi interactions in carbon nanostructures. *Chem. Soc. Rev.* **2015**, *44*, 6425-6433.

(28)   Ghang, Y. J.; Perez, L.; Morgan, M. A.; Si, F.; Hamdy, O. M.; Beecher, C. N.; Larive, C. K.; Julian, R. R.; Zhong, W. W.; Cheng, Q.; Hooley, R. J. Anionic deep cavitands enable the adhesion of unmodified proteins at a membrane bilayer. *Soft Matter* **2014**, *10*, 9651-9656.

(29)   Ghang, Y. J.; Lloyd, J. J.; Moehlig, M. P.; Arguelles, J. K.; Mettry, M.; Zhang, X.; Julian, R. R.; Cheng, Q.; Hooley, R. J. Labeled protein recognition at a membrane bilayer interface by embedded synthetic receptors. *Langmuir* **2014**, *30*, 10161-10166.

(30)   Phillips, K. S.; Han, J. H.; Martinez, M.; Wang, Z.; Carter, D.; Cheng, Q. Nanoscale glassification of gold substrates for surface plasmon resonance analysis of protein toxins with supported lipid membranes. *Anal. Chem.* **2006**, *78*, 596-603.

(31)   Perez, L.; Ghang, Y. J.; Williams, P. B.; Wang, Y.; Cheng, Q.; Hooley, R. J. Cell and Protein Recognition at a Supported Bilayer Interface via In Situ Cavitand-Mediated Functional Polymer Growth. *Langmuir* **2015**, *31*, 11152-11157.

(32)   Diehl, K. L.; Anslyn, E. V. Array sensing using optical methods for detection of chemical and biological hazards. *Chem. Soc. Rev.* **2013**, *42*, 8596-8611.

(33)   Sun, X.; Dahlhauser, S. D.; Anslyn, E. V. New Autoinductive Cascade for the Optical Sensing of Fluoride: Application in the Detection of Phosphoryl Fluoride Nerve Agents. *J. Am. Chem. Soc.* **2017**, *139*, 4635-4638.

(34)   Sun, X.; Reuther, J. F.; Phillips, S. T.; Anslyn, E. V. Coupling Activity-Based Detection, Target Amplification, Colorimetric and Fluorometric Signal Amplification, for Quantitative Chemosensing of Fluoride Generated from Nerve Agents. *Chem. Eur. J* **2017**, *23*, 3903-3909.

Chapter 5: Analysis of the Molecular Motion and Exchange Kinetics of Guests in a Water Soluble Cavitand.

5.1. Background

The displacement of the trimethylated-fluorescent guests **4.5** and **4.6a** by different targets, and their varied recognition in bilayer environments has raised many questions, not only the difference binding ability, but the increase of the binding constant in bilayer systems. Previously, mechanistic studies on the molecular recognition process with small guests were only possible in free aqueous solution. Charged guests such as **4.5** and **4.6a** trigger the formation of cavitand aggregates as discussed in chapter 4, which limited guest binding studies *via* ^{1}H NMR. NMR binding studies have not been performed on any guests in more complicated systems such as lipid bilayers. Here, a mechanistic study of the in/out exchange mechanism and up/down kinetic motion of guests in tetracarboxylate cavitand **4.2** is undertaken, with a focus on the effect of the external environment.

5.2. In/Out Exchange Mechanism in Free Solution

Guest binding in all cavitands requires the wall opening. The cavitand must unfold into a kite conformation to allow guest exchange, and this is the rate determining step. For octamide cavitand **1.19**,[1] the barrier is determined by both the hydrogen bond seam breaking, which has a Gibbs Free Energy of $\Delta G^+ = 5\text{-}8$ kcal mol^{-1}, and a barrier for wall opening via rotation about the C-O bonds of the resorcinarene with a barrier of ~ 11 kcal mol^{-1} (Figure 5.1). The total barrier to the exchange is approximately 16.5 kcal mol^{-1}. There is one variable in water-soluble **4.2** that is not present in octamide **1.19**, however:

as the exchange process occurs in water, the exposed surface area of the guest is involved in the barrier, and the hydrophobic guest must be solvated by water upon unfolding of the host. As a result, the in/out exchange rate varies with guest size, with on/off rates ranging from 14.6 s^{-1} (cyclohexane) to 1.7 s^{-1} (cyclooctadiene).[1,2]
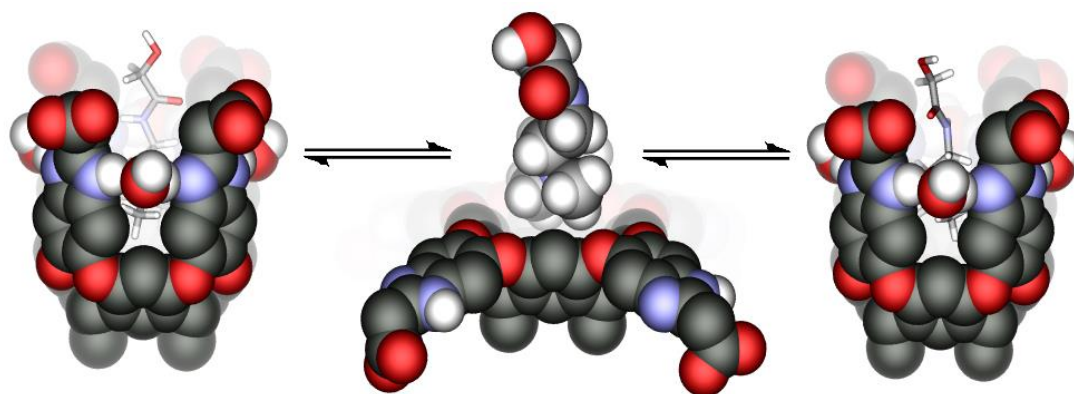

Figure 5.1. Minimized models of cavitand **4.2** "breathing" motion for in/out exchange of choline in solution (SPARTAN, Hartree-Fock forcefield).

5.2.1. Guest Motions in the Cavitand: Linear Hydrocarbons

Cavitand **4.2** binds most linear hydrocarbons strongly. Pentane is too small to adequately fit, but other alkanes (hexane – tridecane) showed much higher affinity.[3] The cavity is fully occupied by *n*-octane, and flexible alkanes longer than that must protrude from the host, leading to hydrophobic repulsion with external water and a lowering of the guest binding constant. However, extended alkane conformations are too narrow to properly fill the cavity, and the bound alkanes coil into a helical conformation to properly take advantage of van der Waals contacts with the cavitand walls. The energetic penalty for adopting the helical conformation is 0.55 kcal mol^{-1} per extra gauche interaction,[4]

which is less stable than the extended conformation—the extra CH-π contacts compensate for the energy difference. The guest binding of alkanes is driven by the hydrophobic effect and is strongly entropically favored. This confers phase-transfer properties on the system. Conversion of neutral guests to hydrophilic guests (via nucleophilic addition of solubilizing groups) removes all binding affinity, even though the binding "handle" is unchanged.[5]

Cavitand **4.2** is also capable of flexing, or "breathing" while binding its targets, and many guests undergo motion while on the interior of the cavity. Linear alkanes undergo rapid rotation in the cavity, and this is shown in the average of the chemical shifts for the different protons.[6] For example, bound *n*-octane only shows four peaks in the ^{1}H NMR spectrum, averaged between the two possible positions. The up/down exchange rate is too fast to measure by NMR techniques (especially due to the high freezing point of water). The mechanism of up/down motion was investigated by NMR techniques,[2] and two possibilities were shown: molecular motion with the longest linear chain of 5 or fewer carbons were able to rapidly rotate in the cavity, whereas longer chains had to "snake" past each other. Wider, more substituted alkanes with the longest linear chains <5 carbons (e.g. 2-methylpentane) showed rapid up/down rotation.
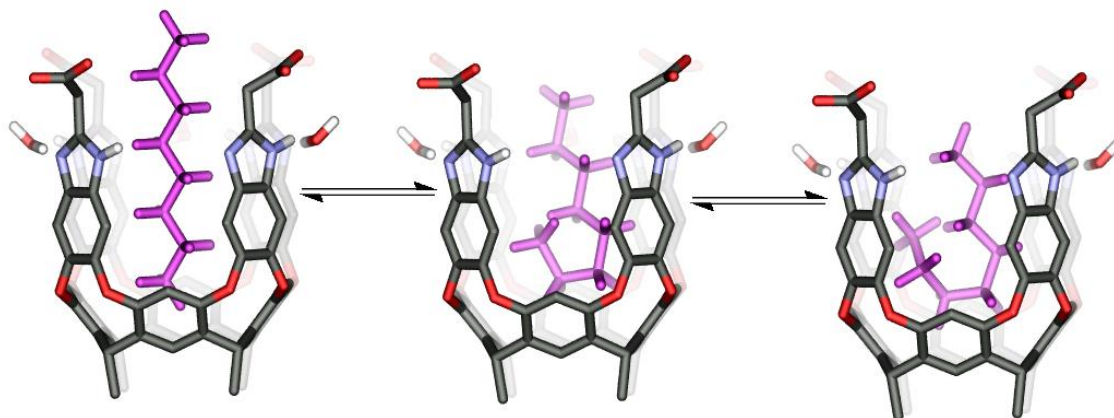
Figure 5.2. Minimized models of cavitand **4.2** "snaking" motion of linear hydrocarbon in solution (SPARTAN, Hartree-Fock forcefield).

5.2.2. Guest Motions in the Cavitand: Cyclic and Aromatic Hydrocarbons

Cyclic hydrocarbons are stronger guests for **4.2**, as they have the coiling disadvantage "prepaid" in the structure. Ring systems ranging in size from cyclopentane to trans-decalin are effectively bound.[7] Substituted longer species or cyclic systems (*trans*-decalin, *trans*-1,4-dimethylcyclohexane, 2-methylheptane) cannot efficiently "snake" past each other while in the confines of the cavity, and therefore showed intermediate up/down interconversion. Any rigid species longer than *trans*-decalin showed no internal motion on the NMR timescale: up/down exchange in those cases requires in/out exchange to occur as well.[2]

The association constants for all these hydrocarbons are on the order of 1 x 10^4 M^{-1}. Remarkably, while *n*-alkanes longer than C$_8$ are bound in **4.2** with steadily decreasing affinity, rigid guests that are 12.0 Å or longer show a sharp cutoff in binding affinity. 1,4-Di-*tert*-butylbenzene (linear van der Waals' length = 8.7 Å) and 4,4'-dimethylbiphenyl

(11.9 Å) are strongly bound ($K_a > 10^4$ M^{-1}). Surprisingly, similar sized guests to the C_8 alkenes such as 4-methyl-*trans*-stilbene (12.8 Å) show no affinity at all.[2] The compressibility of linear alkanes evidently allows them to flex into the pocket, "hiding" their hydrophobic surface, which the rigid guests cannot do.

Aromatic guests are too narrow to effectively fill the cavity, however, and small aromatics such as benzene or toluene are not strong substrates for the host. Larger aromatic molecules such as pyrene and anthracene and substituted aromatics such as di-*tert*-butylbenzene can be extracted into the host. In order to encapsulate large aromatics such as pyrene, sonication for over 6 hours is necessary. These rigid species do not tumble inside the cavitand, and the individual peaks can be seen in the ^{1}H NMR, which shows about a 3 ppm shift in the pyrene aromatic signal upfield shown in Figure 5.3 and a change of symmetry to the pyrene protons.
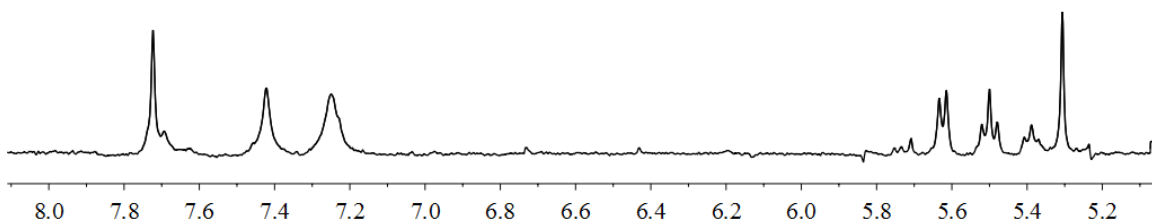

Figure 5.3. ^{1}H NMR of tetracarboxylate cavitand scaffold **4.2** and with pyrene encapsulation (400 MHz, D₂O, 298 K).

5.2.3. Guest Motions in the Cavitand: Disubstituted Haloalkanes

α,ω-Dihaloalkanes are also bound in the cavity with a rapid interconversion between the degenerate carceroisomers.[8] The resulting spectra show clean uptake by **4.2** and the

simplicity of the spectra indicates rapid tumbling of the guests in the interior space. Hydrolysis of the longer bound species occurs to the α-halo alcohols, indicating that the halide ends can reside deep in the cavity, despite their polarity.
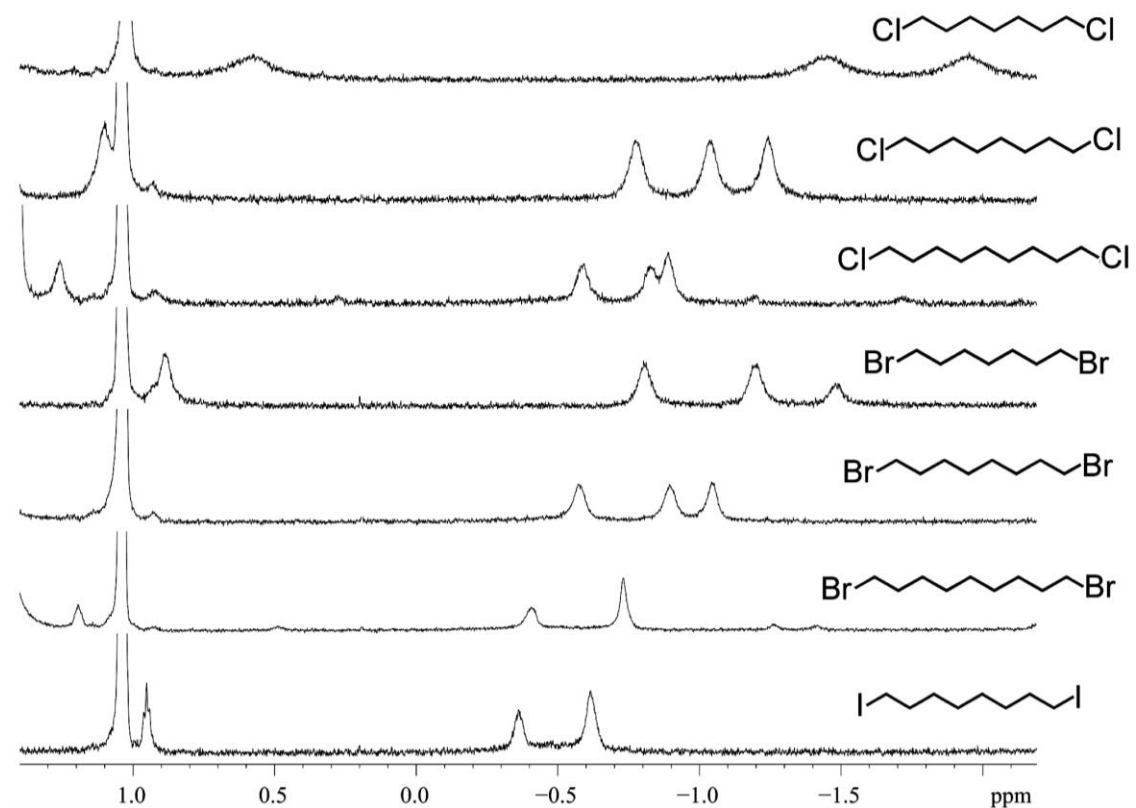

Figure 5.4. The ^{1}H NMR spectra of dihalides in cavitand **4.2**, (600 MHz, D$_2$O, 298 K). Rapid tumbling inside the cavitands leads to simplified signal patterns.

5.2.4. Guest Motions in the Cavitand: Monosubstituted Hydrocarbons

Substituted alkanes with strong hydrogen bonding groups (sulfate, carboxylate, OH, CHO) bind with the polar species oriented outside the cavity and the alkyl chain coiled into the representative helix. The hydrogen binding interaction forces the formation of a single carceroisomer of those guests.
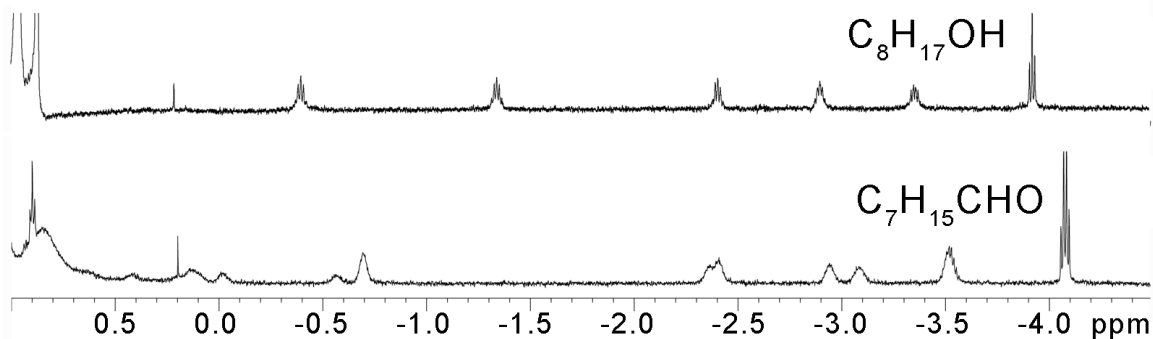
154

Figure 5.5. The ^{1}H NMR spectra of mono-substituted hydrocarbon guests in cavitand **4.2**, (600 MHz, D$_2$O, 298 K).

However, substituted haloalkanes behave differently: groups such as Cl, Br, I and SH are tolerated in the cavity interior and display "biased" rapid tumbling (Figure 5.6).[8] Whereas *n*-alkanes are symmetrical and the up/down exchange occurs between degenerate species, *n*-haloalkanes can display carceroisomers upon up/down interconversion.[9] The softer, less polar groups are more favored on the cavity interior than more polar groups: *n*-iodononane shows a 50:50 distribution between up/down carceroisomers, while *n*-bromononane, with a ratio of 73:27, favors the isomer where the Br is pointed externally. The tumbling rate is rapid on the NMR timescale, as was seen with the *n*-alkanes.
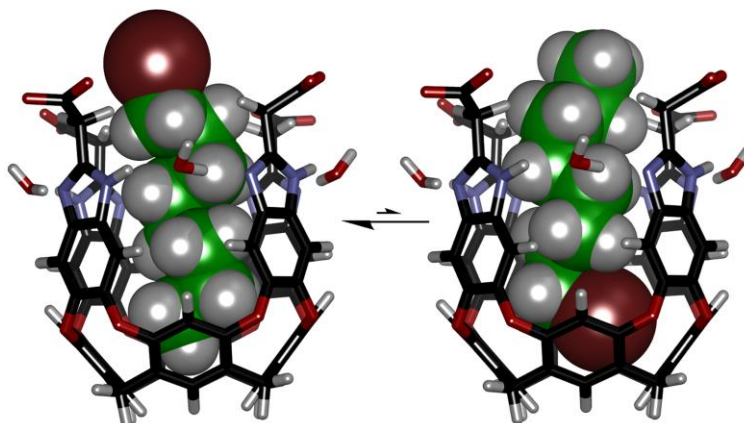
Figure 5.6. Minimized models of the two observed conformations of the **2.4**•α-bromononane host: guest complex (Macromodel, AMBER forcefield).

While oxygen is not favored on the cavity interior, sulfur is diffuse enough to occupy the resorcinarene and 1-octanethiol shows biased tumbling behavior. The bound thiol- and bromooctanes display almost identical spectra, corresponding to ~20% of their head-groups near the resorcinarene and ~80% exposed to the water solvent. While the bromooctanes are susceptible to hydrolysis, octanethiol is not, which allows for study of the aggregate properties without any chemical changes to the guest. Not only does the octanethiol act as a guest, it also aggregates to form a micellar environment. The lipophilic cavitand is well known for embedding itself micelles: in this case, it also binds the lipid as a guest.[10] The large sized aggregates result in a slow tumbling rate and spin diffusion is seen between adjacent CH_2 groups in the bound hydrocarbon.

5.3. Novel Conformations of Bound Guests

Dihaloalkanes could be bound in the cavitand, as the cavity accepts the soft halides. This led to the question of whether a long α,ω-dialkanol could bind. For octanol and 1-octanal, the methyl end was buried deep in the cavity with low in/out exchange. In an effort to force the OH group into the depth of the cavity, linear alkanediol guests were added to **4.2**. As expected, short diols such as 1,6-hexanediol showed no binding in the cavity.

In the case of 1,12-dodecanediol, the spectrum showed unexpected results, as it indicated guest binding, but with an unusual pattern, showing only half of the expected peaks. The OH groups cannot reside inside the cavity, so the guest binds in a U-shaped folded conformation, burying the hydrocarbon chain and leaves both OH groups exposed to the solvent.[8,11-14] This conformation is uniquely observed for 1, 12-dodecanediol, although similar conformations can be seen in other deep cavitands.[8] This conformation requires a wider cavity than normal, and forces an "opening" of the cavity wall. This is achieved through the addition of water molecules to the hydrogen seam at the benzimidazole rim: the weak forces holding the cavitand in the vase conformation can be extended to allow variable guest conformations.
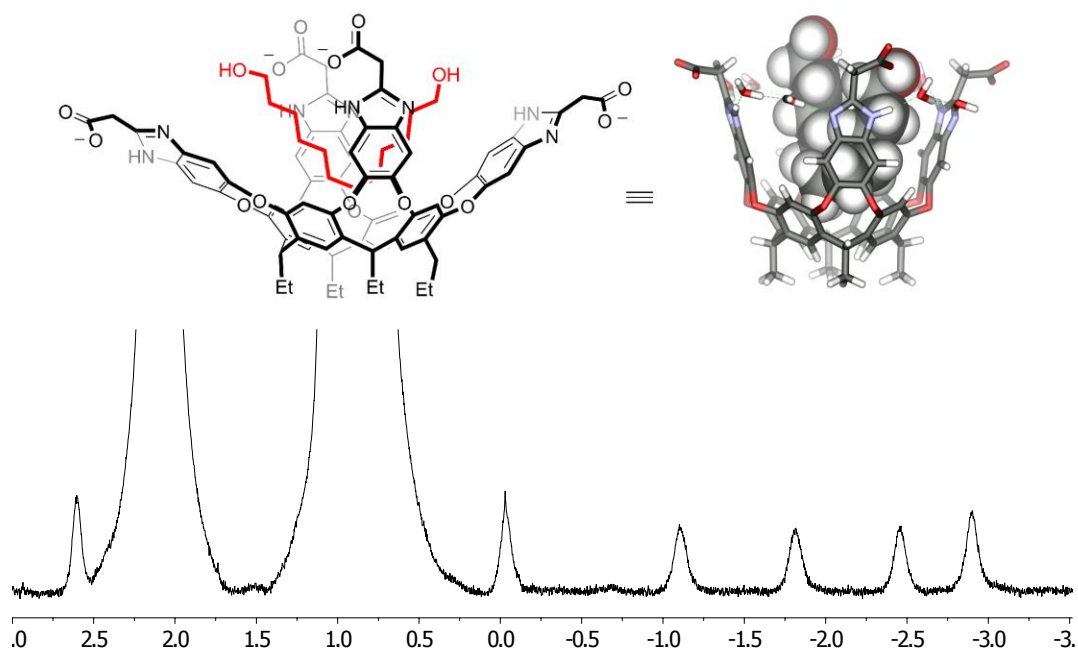
Figure 5.7. a) Representation of the 1,12 dodecanol interaction with cavitand **4.2** and minimized models of cavitand **4.2** "extended" H-bonding seam in solution (SPARTAN, Hartree-Fock forcefield). b) ^{1}H NMR spectra (500 MHz, D$_2$O, 298K) of 1,12-dodecanol in a 1 mM solution of **4.2**.

5.4. Molecular Recognition Properties in Lipid Aggregates

The in/out kinetics of bound guests in free aqueous solution have been extensively investigated using 2D NMR techniques,[7] as has the motion of these guests while inside the cavity.[8] Qualitative observation of guest binding has been tested for complexes of cavitands such as **4.2** in simple phosphocholine micelles.[10] The host properties of **4.2** dramatically changed in the different environment. The observation of unusual guest conformations and varied binding effects in lipid aggregates inspired a deeper study of the cavitand:guest interaction in bilayer environments such as micelles and ordered bicelles (Figure 5.8).
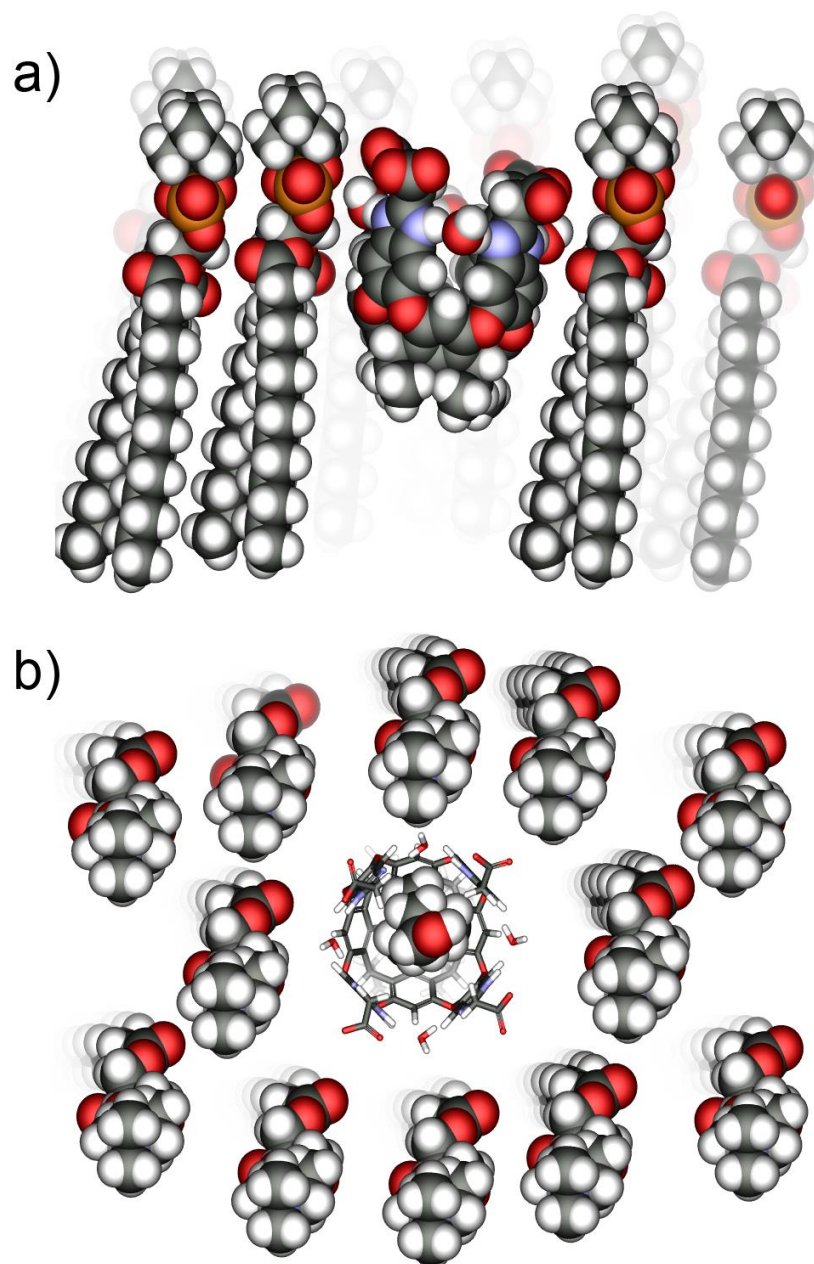
158

Figure 5.8. Representation cavitand **4.2** in lipids a) side view of minimized models of empty cavitand **4.2** in lipid aggregates, b) top view of minimized models of choline-cavitand **4.2** complex in lipid aggregates, (SPARTAN, Hartree-Fock forcefield).

Moreover, ethyl-footed cavitands incorporate into biomimetic or natural lipid aggregates such as micelles[10,15] and supported lipid bilayers.[16-18] While ^{1}H NMR is extremely helpful in studying orientation,[8,19] conformation,[9,20,21] motion[9,22] and unusual isomerism[23,24] of bound small molecule substrates in solution, ^{1}H NMR experiments in lipid aggregates are much more challenging to monitor and understand due to the slow tumbling of the large aggregates. It is sometimes possible to observe the bound guest while the cavitand is embedded in large lipid aggregates (or even human serum),[25-29] but more sensitive NMR experiments are rendered impractical, and other methods such as UV/Vis or fluorescence spectroscopy are required. These methods are poorly matched for analysis of guest motion and binding kinetics in synthetic cavity-containing hosts, as the processes tend to occur on the NMR timescale.

5.5. Different Lipid Systems: Micelles and Magnetically Ordered Bicelles

Magnetically ordered bicelles are well-known as suitable membrane mimics for NMR studies of membrane proteins and other biomacromolecules.[28,30,31] By using a combination of short and long lipids (a 3.2:1 mix of dimyristoylphosphocholine (DMPC) and dihexylphosphocholine (DHPC)) in D_2O or H_2O allows controlled formation of defined lipid aggregates. The system forms magnetically ordered bicelles at 35 ºC and disordered (isotropic) micelles at 10 ºC, which provides the ability to study both environments in the same sample. In the bicellar environment, the shorter DHPC is segregated on the curved bicelle rim, while DMPC mainly resides in the planar section of the bicelles. The order of the lipid aggregates can be monitored *via* a ^{31}P NMR

experiment, as the micelles are disordered and give one phosphate peak, while the bicelles show two peaks. The peak splitting is caused by the two different alignments of the phosphate groups: the flat surface and the curvature on the end. The bicelle planar section is interesting for the study of the cavitand guest:host system, unlike the micelles which have a strong curvatures. The bicelles' flat surface is similar to the supported lipid bilayers used in previous studies. The mixture of DHPC:DMPC allows us to study both interactions, with only a slight change in temperature as seen in Figure 5.10.
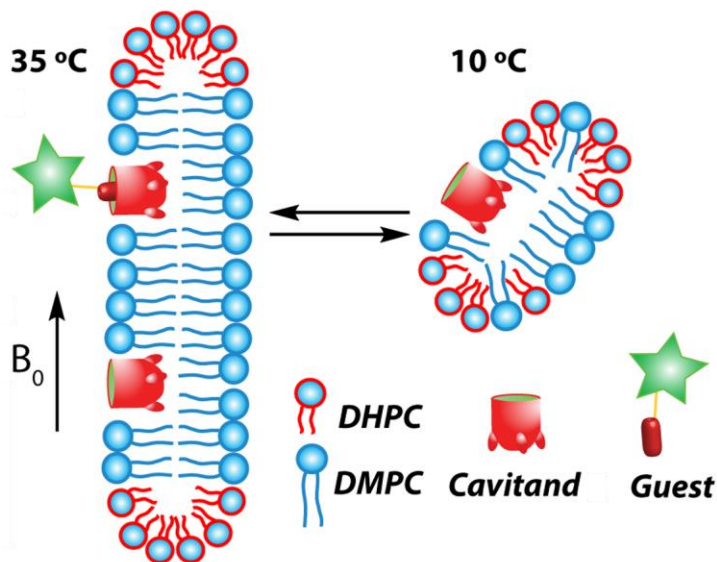
Figure 5.9. Illustration of lipid environments of DMPC/DHPC with cavitand and guest binding, micelles DMPC/DHPC at 10 °C and magnetically ordered bicelles DMPC/DHPC at 35 °C.
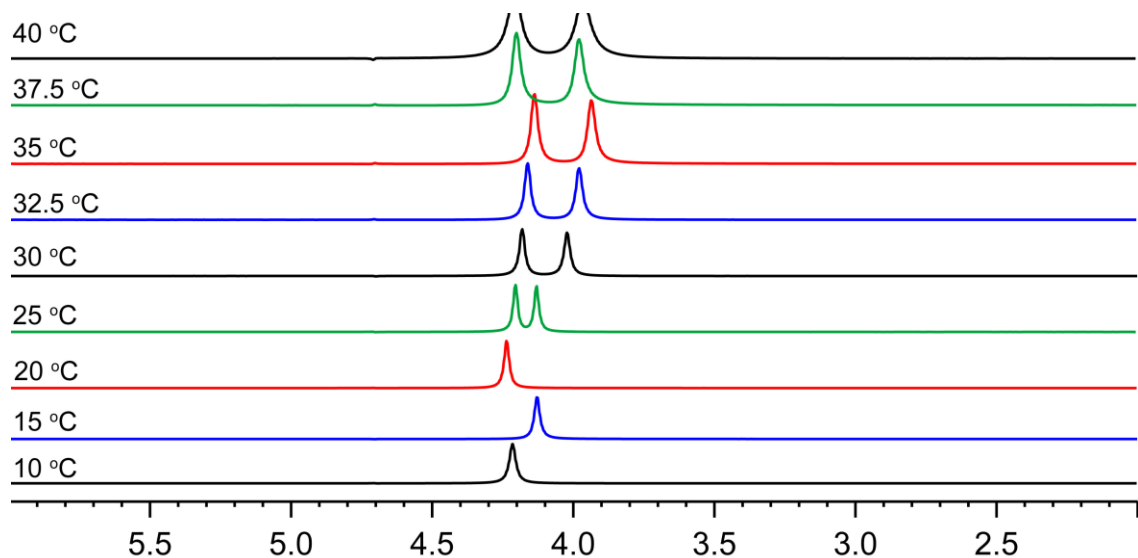
Figure 5.10. ^{2}H NMR spectra of 3.2:1 mix of DMPC/DHPC, with temperature change to form magnetically ordered bicelles.

5.6. Initial Studies in Different Lipid Systems

The addition of a 5 mM cavitand solution caused no disruption to the lipid aggregates, as seen in Figure 5.11 b/e. The addition of excess guest molecules is similarly non-disruptive to the assemblies of the lipids in either the micellar or bicellar environment (Figure 5.11 c/f). The ^{2}H NMR shows similar behavior to the ^{31}P NMR. The D$_2$O peak splitting is caused by the two different alignments of the phosphate groups: the flat surface and the curvature on the end of the ordered bicelles (Figure 5.11).
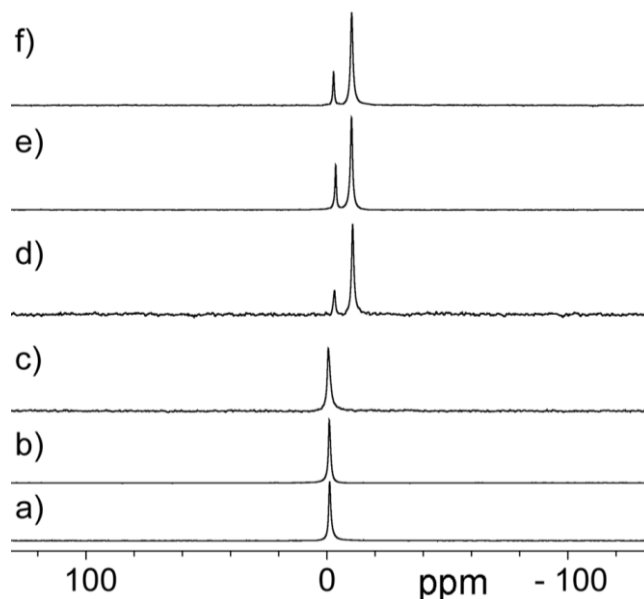
Figure 5.11. Temperature dependence of the lipid aggregation. ^{31}P NMR spectra of the DMPC/DHPC aggregates a) alone, 10 ºC; b) + 5 mM **4.2,** 10 ºC; + 5 mM **4.2** + excess xylene labeled guest, 10 ºC; d) alone, 35 ºC; b) + 5 mM **4.2,** 35 ºC; + 10 mM **4.2** + excess xylene labeled guest, 35 ºC.

5.6.1. Challenges of ^{1}H NMR Studies: Magnetically Ordered Bicelles

^{1}H NMR experiments in DMPC/DHPC lipid aggregates are still challenging to monitor and understand. In the case of the magnetically ordered bicelles, the ^{1}H NMR spectrum showed broad and undefined peaks due to the slow tumbling of the large bicelles aggregates (Figure 5.12). Therefore, monitoring the small changes of the guest peaks in the negative region was impractical.
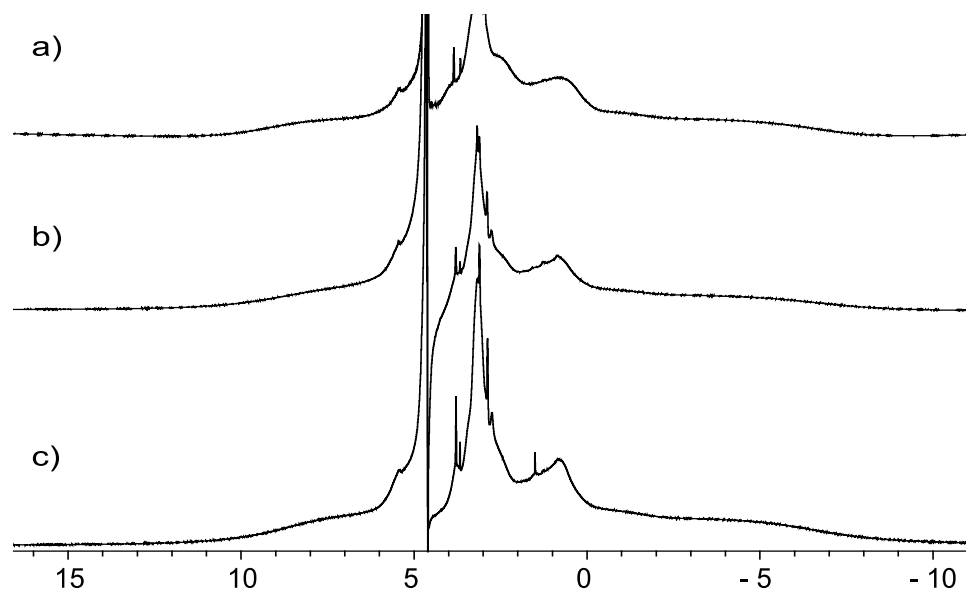
Figure 5.12. The ^{1}H NMR spectra (600MHz, D$_2$O, 35 $^\circ$C) of a) magnetically ordered bicelles DMPC/DHPC aggregates, b) addition of cavitand **4.2** to magnetically ordered bicelles, c) addition of 20 eq. cyclooctane to cavitand **4.2** and magnetically ordered bicelles complex.

5.6.2. Challenges of ^{1}H NMR Studies: Micellar Environment

In the micellar environment on the other hand, ^{1}H NMR analysis of the binding processes in lipid micellar environments faces a different challenge. ^{1}H NMR is much more complicated due to the presence of the massive hydrocarbon peaks from the lipid environment. The large ^{1}H NMR peaks cause a large broad peak in the spectrum, which tends to cover cavitand and guest peaks. ^{1}H NMR in micellar environments shows bound guest peaks such as cyclooctane in the negative region only.

Cyclooctane tumbles rapidly in the cavity of **4.2** and shows a simple averaged-out singlet in solution. While the ^{1}H NMR spectrum shows the incorporation of cavitand and

encapsulation of guest in a confined micellar environment, 2D exchange NMR using ^{1}H as target nucleus for quantitative study was much more difficult to achieve due to the lack of distinguished free guest NMR peaks.
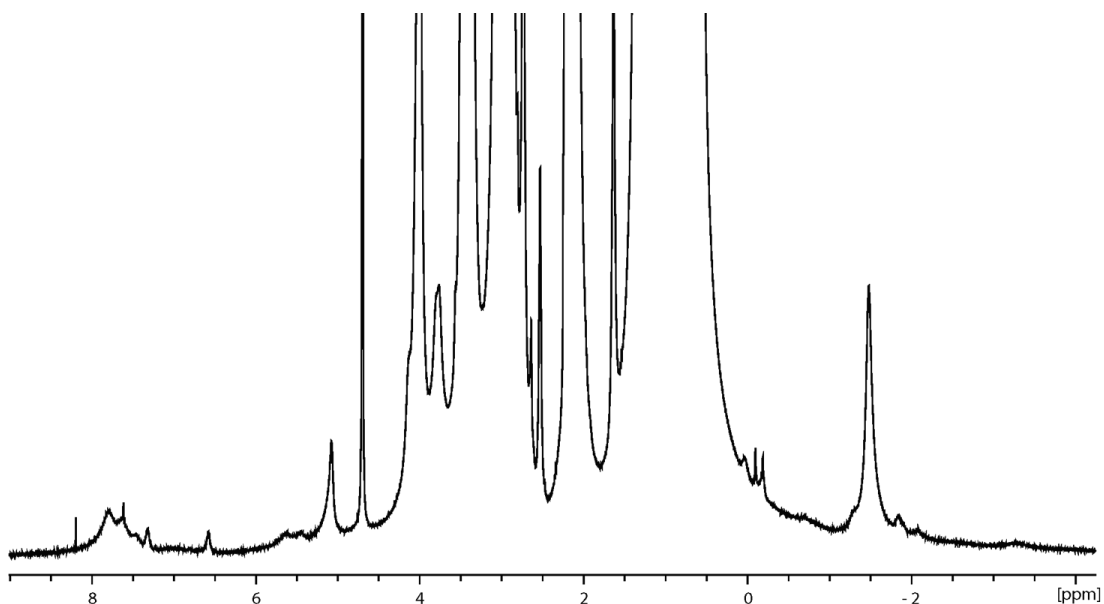

Figure 5.13. The ^{1}H NMR spectra (600MHz, D_2O, 10 ºC) of a) Micelles DMPC/DHPC aggregates, b) addition of cavitand **4.2**•cyclooctane**.**

5.7. NMR Analysis of Trimethylammonium Guest Binding in a Micellar Environment

To quantitatively study the guest binding interaction using 2D NMR, we must utilize a technique and a nucleus other than ^{1}H NMR. To study the in/out guest exchange and up/down molecular motion, we looked at isotopically enriched guests. As the exact guest properties were unknown, we sought to synthesize a library of enriched guest molecules that would allow investigation of all types of molecular motion and exchange.

The initial attempts focused on attaining a guest that could be analyzed by ^{19}F NMR. Fluorinated guest **5.2** could be accessed by reacting N,N,-dimethylethylenediamine and trifluoroacetic anhydride in pyridine at room temperature, followed by methylation with methyl iodide. Unfortunately, guest **5.2** was easily hydrolyzed and decomposed in aqueous solution.
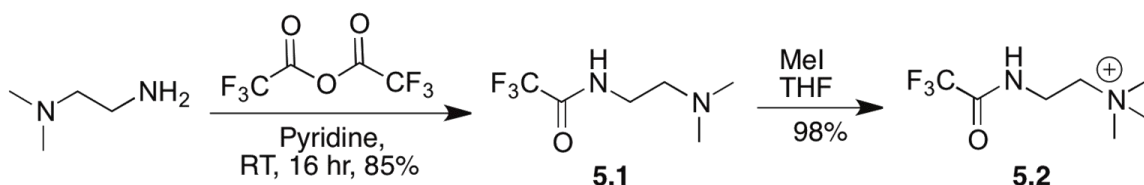

Figure 5.14. Synthesis of the fluorinated trimethylated **5.2** guest.

Deuterium-enriched guests with the desirable trimethylammonium handle and the appropriate space-filling requirement, such as **5.4,** could be accessed from *p*-xylene-d_{12}. Radical benzylic bromination of *p*-xylene-d_{12} gave 1,4-bis-α-bromoxylene-d_8 **5.3** in 94% yield as a white solid. Nucleophilic substitution of **5.3** with trimethylamine at 60 °C for 2 h yielded a pure, white precipitate of guest **5.4.** This guest showed the desired enriched ^{2}H nuclei, as well as trimethylammonium groups on both sides.
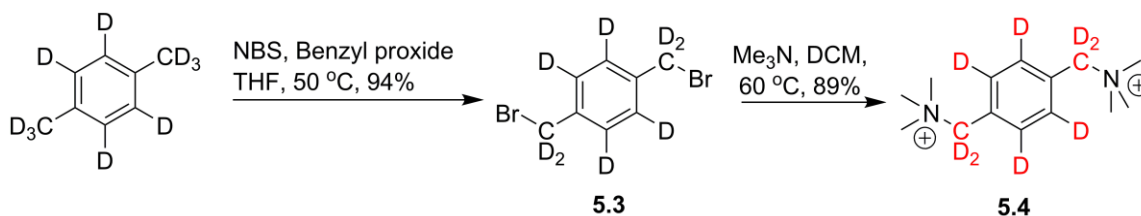

Figure 5.15. Synthesis of the deuterium enriched guest **5.4**.

For qualitative and quantitative studies, 2D dynamic NMR was used. Dynamic NMR would allow us to studies the physical changes of the guest: host complex on the NMR timescale. 2D EXSY experiments can be use qualitatively to map exchange pathways and quantitatively to determine rate constants which we can use to calculate the exchange rate of the guest, either in/out of the cavity, or up/down inside the cavity and the effect of the surrounding environment on such a process. The exchange must be slow on the NMR time scale, since the exchanging resonances must be resolved in order to observe the transfer between them. Yet, the exchange must also not be too slow otherwise relaxation processes occurring during τ_m will remove all memory of the exchange process. 2D EXSY are sensitive experiments to exchange systems with $k_{ex} \sim 10^2$-10^{-2} s^{-1}. After multiple ^2H EXSY spectra were taken of **5.4** in cavitand **4.2** in lipid micelles, with different mixing times to appropriately choose τ_m (10 ms mixing time), we observed only one set of exchange peaks, between the deuterium atom of CD_2 at 4.1 ppm and CD_2 at 4.9 ppm, where 4.9 ppm correspond to "up" CD_2 and 4.1ppm correspond to bound CD_2 "down" in the cavity (Figure 5.16). The exchange peak of the aromatic deuterium was expected, yet not observed. The difference in chemical shift between "up" and "down" was much smaller, which caused broadening in diagonal peaks. Due to the symmetrical nature of the guest, the exchange peaks didn't clearly state whether the guest is tumbling only on the inside of the cavity (snaking-up/down) or exchanging with free guest in solution (in/out motions).
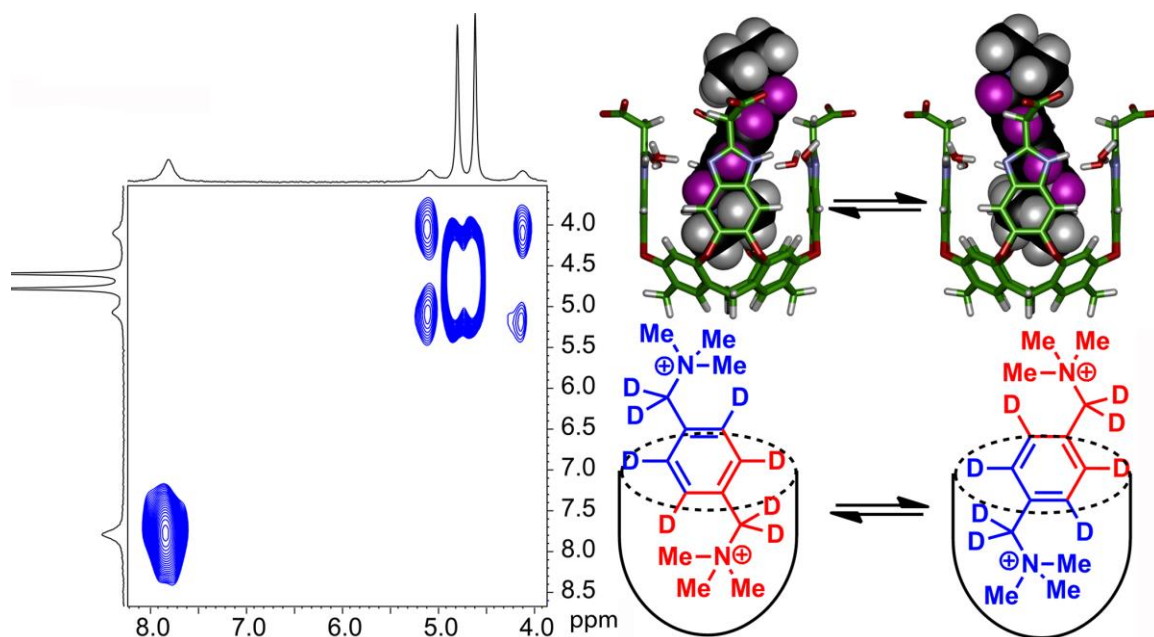
Figure 5.16. ^{2}H EXSY spectrum of micellar system with 5 mM cavitand **4.2** and 1.2 eq. Deuterated labeled xylene-d_8 **5.4** with in/out cross peaks (H$_2$O, 700 MHz, mixing time = 10 ms, 298 K).

5.8. In/out Exchange of ^{13}C-labeled Trimethylammonium Guests in Micelles

To investigate the rate of in/out exchange in the cavitand, carbon-13 enriched guests were synthesized by methylation using ^{13}CH$_3$I. Isolation of monolabeled guest **5.5** yielded a desirable binding handle with an undesirable dimethylated bulky top. Guest **5.5** contains a strong binding handle, and under physiological conditions, the dimethylamine will be protonated causing a favorable charge interaction with the negatively changed rim. Guest **5.6** was also synthesized using ^{13}CH$_3$I in acetonitrile to ensure the presence of the positive charge for an ionic interaction between the guest and the top rim. As a control guest, **5.7** was synthesized, containing a longer alkyl chain with NMe$_3^+$ ends.

168
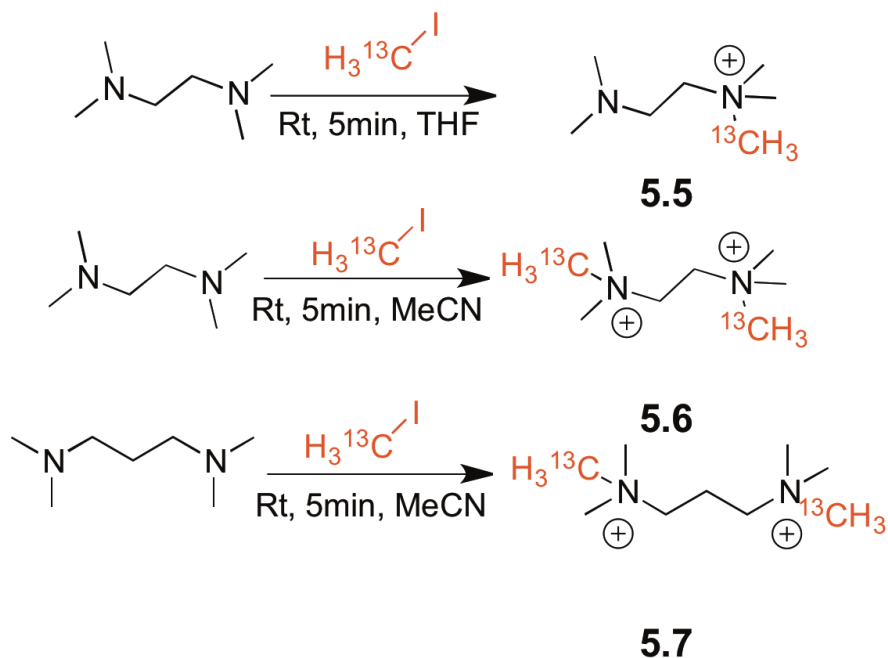
Figure 5.17. Synthesis of the ^{13}C enriched guests **5.5-5.7.**

NMR analysis of the interaction with **4.2** in solution without lipids showed no clear peaks for bound guest, and aggregation of the system was observed (as with previously discussed guest **4.5** and **4.6a**). The bound guest was only observed in micelles rather than in solution. For guest **5.5**, the repulsion interaction between the top of the rim and the dimethylated amine caused the guest to exchange quickly, with the in/out exchange rate being 12 s^{-1} with saturation at 200 ms mixing time. The micellar environment eliminated the aggregation of the guest and limited the breathing of the cavitand, aiding the guest binding. Interestingly, the more sterically hindered guest **5.6** showed no binding in either solution or lipid environment. This is despite the favorable ionic charged interaction between the positively charged trimethylammonium guest and the negatively charged cavitand rim: evidently the increased bulk and lack of hydrogen bond donor at the rim

prevented binding. Increasing the length of the guest to place the trimethylated group farther away from the rim had no effect, and **5.7** also showed no binding affinity to the cavitand. The trimethylated propyl guest **5.7** minimal encapsulation due to steric interactions with the upper rim.
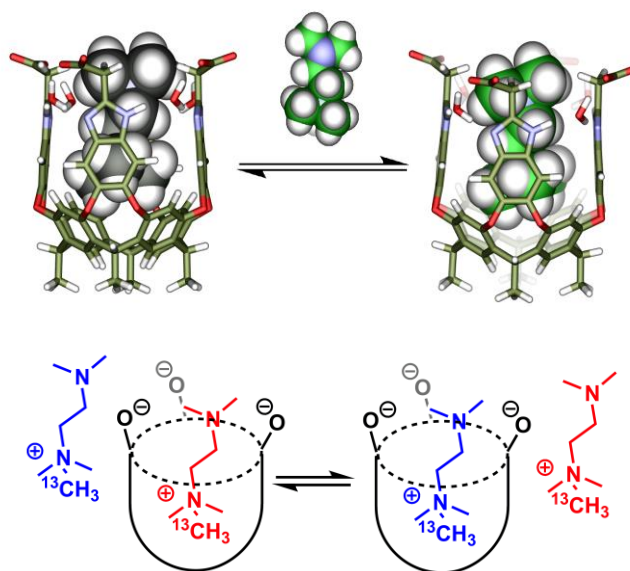

Figure 5.18. Representation of the in/out exchange process between cavitand **4.2** and the ¹³C enriched guest **5.5**.
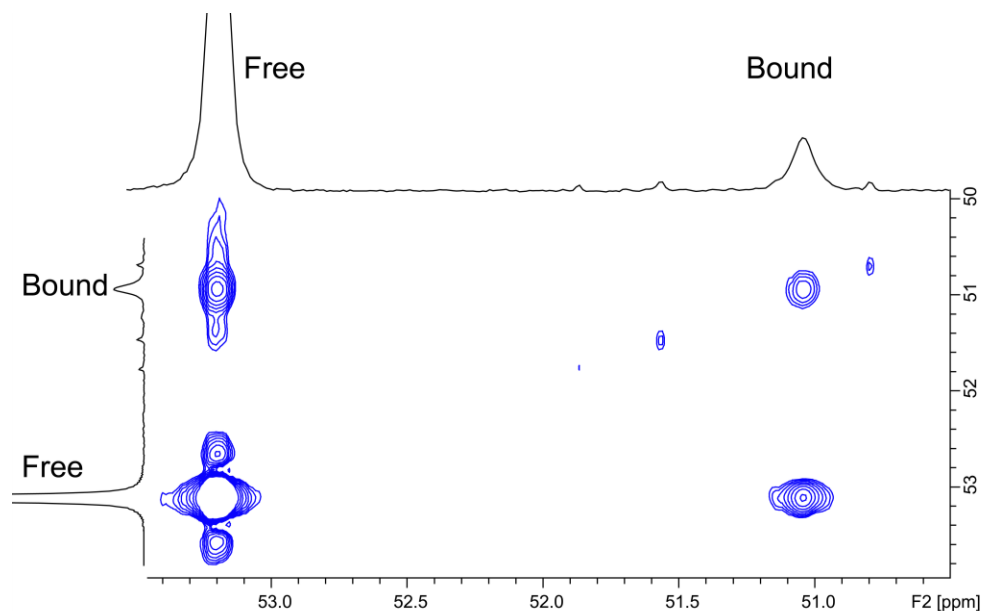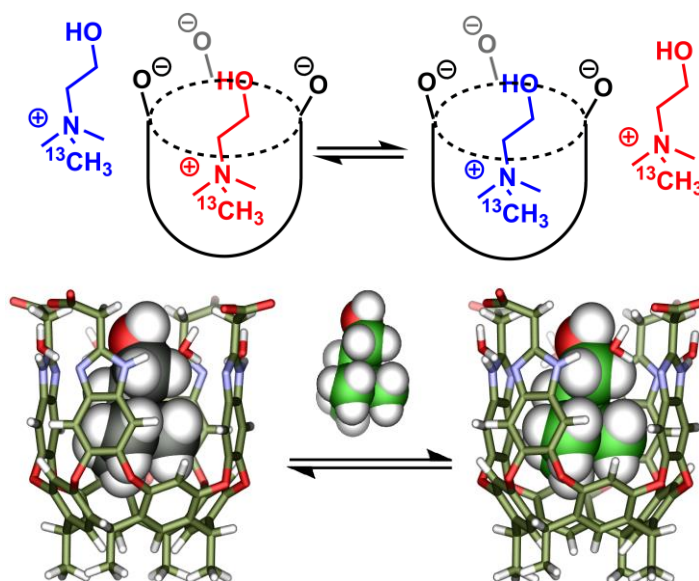
Figure 5.19. ^{13}C EXSY spectrum of micellar system with 5 mM cavitand **4.2** and 3 eq. ^{13}C- 2-(dimethylamino)-N,N,N-trimethylethanaminium **5.5** with in/out cross peaks (D$_2$O, 600 MHz, mixing time = 250 ms, 298 K).

5.9. In/out Exchange of Favored H-bonding ^{13}C Trimethylammonium Guest in Micelles

To investigate the effect of upper rim variation on guest exchange, we synthesized ^{13}C enriched choline, via the same method as for **5.5** from commercially available N, N dimethylaminoethanol, giving ^{13}C-choline **5.8** using H$_3$^{13}CI in 90% yield. The H-bonding donor of the OH top and the negatively charged carboxylates provide complementary hydrogen bonding at the cavitand rim, with **5.8** showing strong binding a much slower exchange rate of 8.3 s^{-1} and saturation at 250 ms. ^{13}C EXSY experiments showed an

exchange peak between 49.5 ppm and 59.8 ppm corresponding to bound CH_3 and free CH_3 respectively.
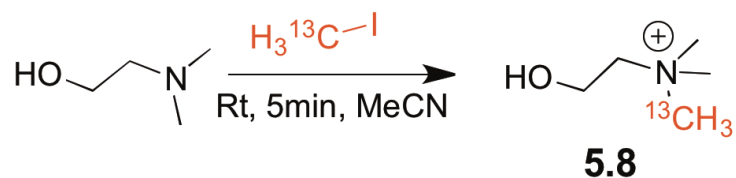
Figure 5.20. Synthesis of the ^{13}C enriched choline **5.8.**

Figure 5.21. Representation of the in/out exchange process between cavitand **4.2** and the ^{13}C enriched guest **5.8.**
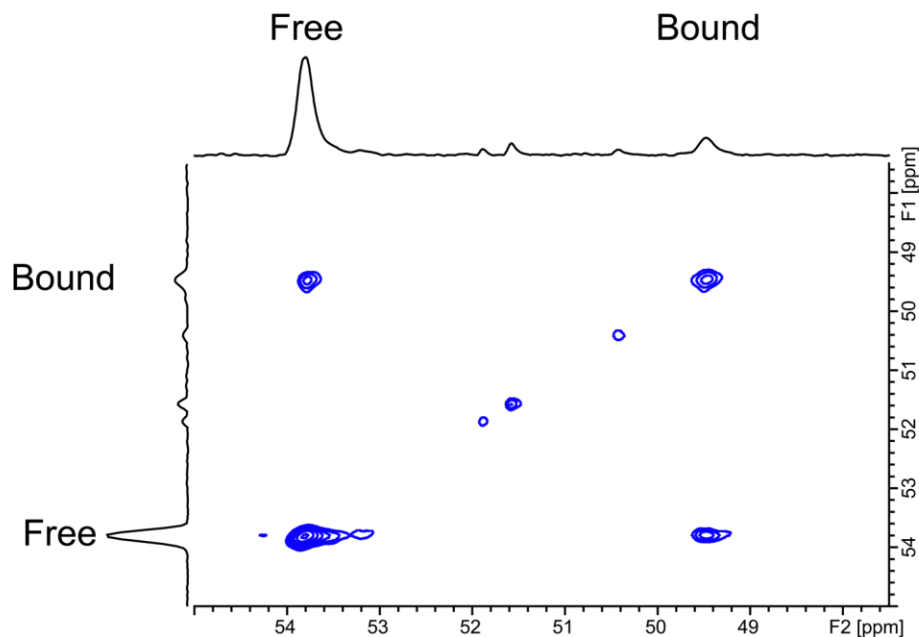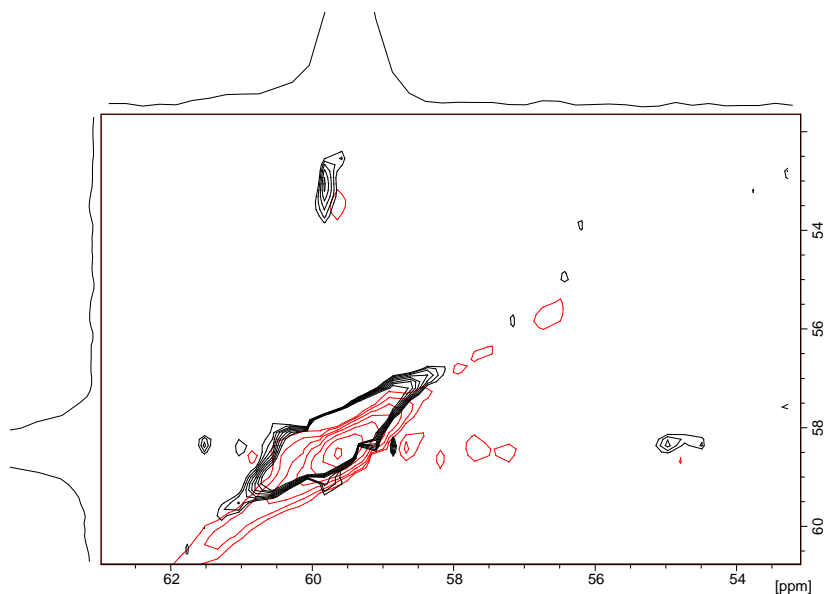
Figure 5.22. Exchange dynamics in cavitand. ^{13}C EXSY spectrum of micellar system with 5 mM cavitand **4.2** and 3 eq. ^{13}C enriched choline **5.8** with in/out cross peaks (D_2O, 600 MHz, mixing time = 250 ms, 298 K).

5.10. In/Out Motions of Bound Guest in Magnetically Ordered Bicellar Environment

As the bicellar environment is a more complicated system to study, we initially investigated the possibility of applying simple ^1H NMR spectroscopy in these systems. As expected, at 35°C, the ^1H NMR showed large, broad, and undefined peaks. The dipolar interaction were stronger, and chemical shifts started to spread out, similar to results seen in the solid state. In these circumstances, the ^1H spectra showed very broad signals that were not informative, especially in the negative chemical shift region where

guest signals inside of cavitands are normally expected, as shown in the previous scaffold.

^{13}C EXSY experiments using the ^{13}C enriched guests, such as choline **5.8** and ethylenediamine **5.5**, were possible, and showed similar trends to the micellar environment. The more sterically bulky guest, ethylenediamine **5.5**, showed a much faster exchange rate than choline. Unfortunately, due to the much lower signal-to-noise ratio in the bicelles experiment, it was not possible to quantitatively calculate the exchange rate. Qualitatively, choline **5.8** showed more than a tenfold slower exchange rate than the ethylenediamine guest **5.5** in the bicellar environment: guest **5.5** exchange was saturated at 20 ms, whereas the choline guest was saturated at 750 ms. While the overall exchange was faster at ethe elevated temperatures, the relative exchange trend was consistent with the micelle experiments. The peak for the free guest at 60 ppm appeared much larger than the cross peak of the bound at 54.5 ppm, which was due to the overlap with the trimethylammonium peaks from the lipid aggregates. Similar results were observed in the ^{13}C EXSY experiments with the larger ethylenediamine guest **5.5**, where a larger diagonal peak than the exchanged peaks occurred.

Figure 5.24. ^{13}C EXSY spectrum of bicellar system with 5 mM cavitand **4.2** and 3 eq. ^{13}C-choline **5.8** with in/out cross peaks (D$_2$O, 100 MHz, 350 K): a) red, mixing time = 250 ms, b) black, mixing time = 1000 ms.
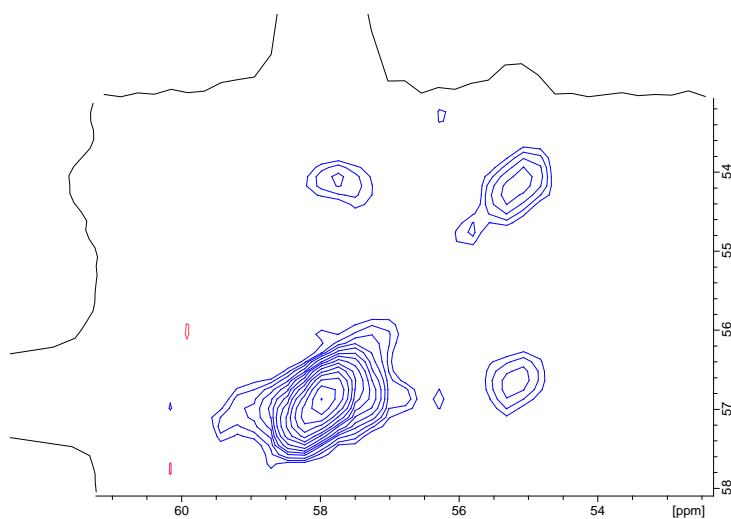

Figure 5.25. ^{13}C EXSY spectrum of bicellar system with 5 mM cavitand **4.2** and 3 eq. ^{13}C-2-(dimethylamino)-N,N,N-trimethylethanaminium **5.5** with in/out cross peaks (D$_2$O, 100 MHz, mixing time = 20 ms, 350 K).

5.11. Future Work: Up/down Tumbling Motions of Bound Guest in Micellar and Bicellar Environments

As most of the previously synthesized guests showed in/out exchange due to the hydrophilic nature of the guests, a more hydrophobic guest is needed to study up/down motion. We seek to study the snaking/tumbling motions of linear hydrocarbons in more complicated environments, such as micelles and magnetically ordered bicelles. The challenge was that introducing an isotopically enriched atom in linear hydrocarbons is synthetically difficult. As such, *trans*-decalin was targeted as a slowly tumbling guest that can have ^{2}H atoms synthetically installed in a single position. The most accessible enriched atom is deuterium caused by the reduction of the corresponding tosylhydrazone.[32] ^{2}H EXSY is expected to show an exchange peak between CD_2 up and CD_2 down; therefore, we can measure tumbling rate in micelles and bicelles.
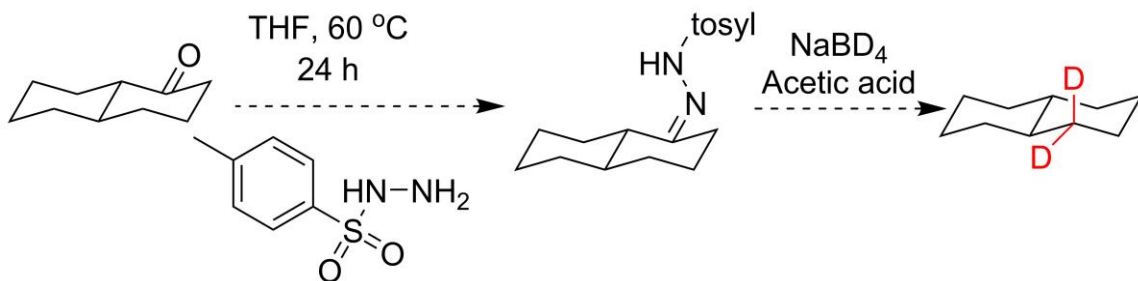
Figure 5.26. Proposed synthesis of enriched trans-decalin for kinetic tumbling studies.

5.12. Conclusion

In solution, the cavitand is able to freely "breathe" as it breaks its hydrogen bond seam. In more confined spaces, such as micelles and bicelles, the cavitand is much more biased to bind to less sterically hindered guests despite the favorable trimethylammonium binding handle and guest size. The more aligned systems such as bicelles show a much lower exchange than micelles, yet the presence of lipids encourages encapsulation. Steric interactions between the rims and the charged guests result in a fast in/out exchange rate. Finally, parallel lipid stacking within magnetically ordered bicelles results in confinement of the walls of the cavitands, which causes faster exchange rates compared to the more curved micellar environment. Continued work in this field will address the tumbling motion in magnetically ordered bicelles.

5.13. References

(1)   Rudkevich, D. M.; Hilmersson, G.; Rebek, J. Intramolecular hydrogen bonding controls the exchange rates of guests in a cavitand. *J. Am. Chem. Soc.* **1997**, *119*, 9911-9912.

(2)   Hooley, R. J.; Van Anda, H. J.; Rebek, J. Cavitands with revolving doors regulate binding selectivities and rates in water. *J. Am. Chem. Soc.* **2006**, *128*, 3894-3895.

(3)   Hooley, R. J.; Biros, S. M.; Rebek, J., Jr. Normal hydrocarbons tumble rapidly in a deep, water-soluble cavitand. *Chem. Commun.* **2006**, 509-510.

(4)   Menozzi, E.; Onagi, H.; Rheingold, A. L.; Rebek, J. Extended cavitands of nanoscale dimensions. *Eur. J. Org. Chem.* **2005**, 3633-3636.

(5)   Hooley, R. J.; Biros, S. M.; Rebek, J., Jr. A deep, water-soluble cavitand acts as a phase-transfer catalyst for hydrophobic species. *Angew. Chem. Int. Ed.* **2006**, *45*, 3517-3519.

(6)   Hooley, R. J.; Rebek, J., Jr. Deep cavitands provide organized solvation of reactions. *J. Am. Chem. Soc.* **2005**, *127*, 11904-11905.

(7)   Hooley, R. J.; Van Anda, H. J.; Rebek, J., Jr. Extraction of hydrophobic species into a water-soluble synthetic receptor. *J. Am. Chem. Soc.* **2007**, *129*, 13464-13473.

(8)   Hooley, R. J.; Gavette, J. V.; Mettry, M.; Ajami, D.; Rebek, J. Unusual orientation and reactivity of alkyl halides in water-soluble cavitands. *Chem. Sci.* **2014**, *5*, 4382-4387.

(9)   Zhang, K. D.; Ajami, D.; Gavette, J. V.; Rebek, J., Jr. Alkyl groups fold to fit within a water-soluble cavitand. *J. Am. Chem. Soc.* **2014**, *136*, 5264-5266.

(10)   Schramm, M. P.; Hooley, R. J.; Rebek, J., Jr. Guest recognition with micelle-bound cavitands. *J. Am. Chem. Soc.* **2007**, *129*, 9773-9779.

(11)   Gan, H. Y.; Benjamin, C. J.; Gibb, B. C. Nonmonotonic Assembly of a Deep-Cavity Cavitand. *J. Am. Chem. Soc.* **2011**, *133*, 4770-4773.

(12)   Gan, H. Y.; Gibb, B. C. ITC analysis of guest binding to a deep-cavity cavitand. *Supramol. Chem.* **2010**, *22*, 808-814.

(13)   Rebek, J. Assembly and encapsulation with self-complementary molecules. *Chem. Soc. Rev.* **1996**, *25*, 255-&.

(14)   Schramm, M. P.; Rebek, J. Moving targets: Recognition of alkyl groups. *Chem. Eur. J.* **2006**, *12*, 5924-5933.

(15)   Trembleau, L.; Rebek, J., Jr. Interactions between a surfactant and cavitand in water blur distinctions between host and guest. *Chem. Commun.* **2004**, 58-59.

(16)   Liu, Y.; Liao, P.; Cheng, Q.; Hooley, R. J. Protein and small molecule recognition properties of deep cavitands in a supported lipid membrane determined by calcination-enhanced SPR spectroscopy. *J. Am. Chem. Soc.* **2010**, *132*, 10383-10390.

(17)   Liu, Y.; Taira, T.; Young, M. C.; Ajami, D.; Rebek, J., Jr.; Cheng, Q.; Hooley, R. J. Protein recognition by a self-assembled deep cavitand monolayer on a gold substrate. *Langmuir* **2012**, *28*, 1391-1398.

(18)   Liu, Y.; Young, M. C.; Moshe, O.; Cheng, Q.; Hooley, R. J. A Membrane-Bound Synthetic Receptor that Promotes Growth of a Polymeric Coating at the Bilayer-Water Interface. *Angew. Chem. Int. Ed.* **2012**, *51*, 7748-7751.

(19)   Liu, S.; Gan, H.; Hermann, A. T.; Rick, S. W.; Gibb, B. C. Kinetic resolution of constitutional isomers controlled by selective protection inside a supramolecular nanocapsule. *Nature* **2010**, *2*, 847-852.

(20)   Liu, S.; Russell, D. H.; Zinnel, N. F.; Gibb, B. C. Guest packing motifs within a supramolecular nanocapsule and a covalent analogue. *J. Am. Chem. Soc.* **2013**, *135*, 4314-4324.

(21)   Heinz, T.; Rudkevich, D. M.; Rebek, J., Jr. Molecular Recognition within a Self-Assembled Cylindrical Host. *Angew. Chem. Int. Ed.* **1999**, *38*, 1136-1139.

(22)   Kulasekharan, R.; Jayaraj, N.; Porel, M.; Choudhury, R.; Sundaresan, A. K.; Parthasarathy, A.; Ottaviani, M. F.; Jockusch, S.; Turro, N. J.; Ramamurthy, V. Guest Rotations within a Capsuleplex Probed by NMR and EPR Techniques. *Langmuir* **2010**, *26*, 6943-6953.

(23)   Rechavi, D.; Scarso, A.; Rebek, J., Jr. Isotopomer encapsulation in a cylindrical molecular capsule: a probe for understanding noncovalent isotope effects on a molecular level. *J. Am. Chem. Soc.* **2004**, *126*, 7738-7739.

(24)   Shivanyuk, A.; Rebek, J., Jr. Social isomers in encapsulation complexes. *J. Am. Chem. Soc.* **2002**, *124*, 12074-12075.

(25)   Ryan, D. A.; Rebek, J., Jr. A carbohydrate-conjugated deep cavitand permits observation of caviplexes in human serum. *J. Am. Chem. Soc.* **2011**, *133*, 19653-19655.

(26)   Durr, U. H.; Gildenberg, M.; Ramamoorthy, A. The magic of bicelles lights up membrane protein structure. *Chem. Rev.* **2012**, *112*, 6054-6074.

(27)   Durr, U. H.; Soong, R.; Ramamoorthy, A. When detergent meets bilayer: birth and coming of age of lipid bicelles. *Prog. Nucl. Magn. Reson. Spectrosc.* **2013**, *69*, 1-22.

(28)   Opella, S. J. Structure determination of membrane proteins in their native phospholipid bilayer environment by rotationally aligned solid-state NMR spectroscopy. *Acc. Chem. Res.* **2013**, *46*, 2145-2153.

(29)   Murray, D. T.; Das, N.; Cross, T. A. Solid state NMR strategy for characterizing native membrane protein structures. *Acc. Chem. Res.* **2013**, *46*, 2172-2181.

(30)   De Angelis, A. A.; Opella, S. J. Bicelle samples for solid-state NMR of membrane proteins. *Nat. Protoc.* **2007**, *2*, 2332-2338.

(31)   Diller, A.; Loudet, C.; Aussenac, F.; Raffard, G.; Fournier, S.; Laguerre, M.; Grelard, A.; Opella, S. J.; Marassi, F. M.; Dufourc, E. J. Bicelles: A natural 'molecular goniometer' for structural, dynamical and topological studies of molecules in membranes. *Biochimie* **2009**, *91*, 744-751.

(32)   Srivastava, S.; Lenoble, W. J. Set Mechanism in the Lithium Aluminum Deuteride Reduction of Chloroadamantanes, and Its Induction by Remote Substituents. *Tetrahedron Lett.* **1984**, *25*, 4871-4874.

Chapter 6: Experimental Section

6.1 General Information

^{1}H, ^{13}C, ^{2}H, ^{31}P and 2D EXSY NMR spectra were recorded on a either Varian Inova 300 MHz, 400 MHz or 500 MHz NMR spectrometer, or a Bruker 600 MHz or 700 MHz spectrometer and processed using MestReNova by Mestrelab Research S.L. Proton (^{1}H) and deuterium (^{2}H) chemical shifts are reported in parts per million (δ) with respect to tetramethylsilane (Si(CH$_3$)$_4$, δ=0), and referenced internally with respect to the protio solvent impurity. Carbon (^{13}C) chemical shifts are reported in parts per million (δ) with respect to tetramethylsilane (Si(CH$_3$)$_4$, δ=0), and referenced internally with respect to the solvent ^{13}C signal (enriched trimethylammonium, CDCl$_3$ or DMSO-d_6). Deuterated NMR solvents were obtained from Cambridge Isotope Laboratories, Inc., Andover, MA, and used without further purification. Mass spectra were obtained with either LC-TOF, ESI-MS, or MALDI. LC-TOF was recorded on either an Agilent 6210 LC TOF mass spectrometer using electrospray ionization with fragmentation voltage set at 115 V and processed with an Agilent MassHunter Operating System. Electrospray mass spectra were recorded on an Agilent 6210 LC TOF mass spectrometer using electrospray ionization and processed with an Agilent MassHunter Operating System. MALDI mass spectra were obtained using a PE Biosystems DE-STR MALDI TOF spectrometer operating in refractive mode at 2100 eV. Room temperature UV/Vis spectroscopy was performed on a Cary 50 Photospectrometer using the Varian Scans program to collect data. Cyclic voltammetry was performed using a CH Instruments Electrochemical Analyzer with a glassy carbon working electrode, a Pt wire auxiliary, and Ag/AgCl for the reference

electrode. All other materials were obtained from Aldrich Chemical Company, St. Louis, MO., Oakwood Chemical, Inc, Estill, SC, Fisher Scientific Co., Pittsburgh, PA, and Combi-Blocks Inc. San Diego, CA. Materials were used as received. Solvents were dried through a commercial solvent purification system (Pure Process Technologies, Inc.). Molecular modeling (semi-empirical calculations) was performed using the Hartree-Fock force field using SPARTAN.

6.2. Chapter 2 Experimental.

1.24 Resorcinarene
1.24a: $R_1 = (CH_2)_3OH$
$R_2 = CH_3$
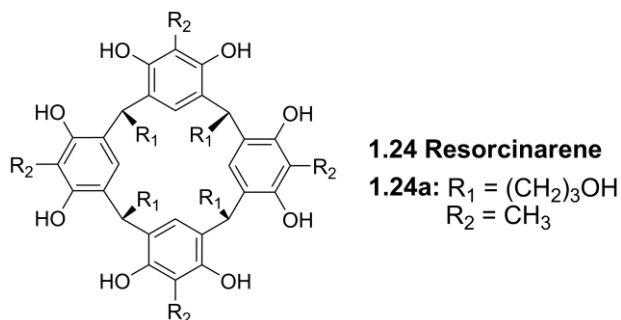
Preparation of Methylresorcinarene 1.24c: In a 250 mL flask equipped with stir bar, concentrated HCl (30 mL) was added to 2-methylresorcinol (20.0 g, 0.161 mol) in methanol (120 mL) then 2,3-dihydrofuran (12.2 mL, 0.161 mol) was added slowly to the mixture. The reaction mixture was heated to 70 ⁰C for 96 h. The product precipitated from solution as an off-white powder and was collected by vacuum filtration. The crude product was recrystallized in acetone to dissolve impurities, allowing the pure product to by isolated by vacuum filtration as a white powder (27.85 g, 89 %). ^{1}H NMR (DMSO-d_6) δ 8.62 (s, 8H), 7.27 (s, 4H), 4.19 (t, J = 7.8 Hz, 4H), 4.10 (br s, 4H), 3.44 (t, J = 6.7 Hz, 8H), 2.24 (q, J = 6.7 Hz, 8H), 1.94 (s, 12H), 1.35 (qn, J = 6.7 Hz, 8H). Observed spectra consistent with literature values.[1]

2.1a: R₁ = (CH₂)₃OH 41%
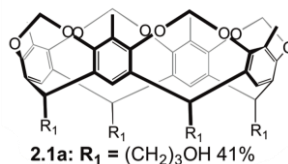
Preparation of Methylene Bridged Cavitand 2.1a: In a 500 mL flask equipped with stir bar, the mixture of **1.14c** (5.00 g, 6.44 mmol), K_2CO_3 (10.7 g, 77.2 mmol), and DMA (120 mL) were mixed in room temperature. Bromochloromethane (6.5 mL, 96.6 mmol) was added slowly to the solution then stirred at 65 ^{0}C for 74 h. The reaction was cooled to ambient temperature, poured into 300 mL DI water, and neutralized with 10 % aq. HCl. The product precipitated from solution as an orange/brown powder and was collected by vacuum filtration. Crude product was purified by column chromatography using 10 % methanol in methylene chloride. When concentrating the product was recrystallized in acetonitrile to remove yield off white powder solid (2.03 g, 41 %). ^{1}H NMR (DMSO-d_6) δ 7.43 (s, 4H), 5.86 (d, J = 7.4 Hz, 4H), 4.59 (t, J = 6.1 Hz, 4H), 4.43 (t, J = 5.1 Hz, 4H), 4.19 (d, J = 7.4 Hz, 4H), 3.48 (q, J =5.9 Hz, 8H), 2.35 (q, J = 5.9 Hz, 8H), 1.88 (s, 12H), 1.42 (qn, J = 5.9 Hz, 8H). Observed spectra consistent with literature values.[1]

Ac₂O, Pyridine
Rt, 24 hr

2.1a: R₁ = (CH₂)₃OH 41%
2.1b: R₁ = (CH₂)₃OAc 71%
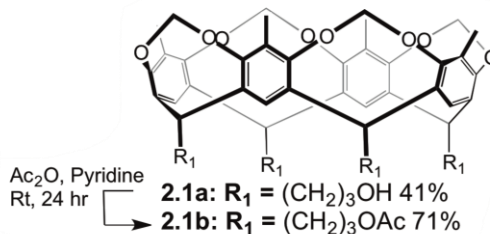
Preparation of Protected OAc Footed Cavitand 2.1b: In a 500 mL flask equipped

with stir bar, **2.1a** (4.05 g, 4.91 mmol), pyridine (60 mL), and acetic anhydride (60 mL)

was stirred for 16 h at ambient temperature. The reaction mixture was then poured into

150 mL of water. The product precipitated from solution as collected as sticky solid. The

crude sticky solid was sonicated in methanol to remove the pyridine, allowing the

collection of pure product as a white powder (3.70 g, 71 %). ^{1}H NMR (CDCl₃) δ 6.93 (s,

4H), 5.86 (d, J = 6.9 Hz, 4H), 4.82 (t, J = 9.1 Hz, 4H), 4.23 (d, J = 6.9 Hz, 4H), 4.15 (t, J

= 6.5 Hz, 8H), 2.26 (q, J = 7.0 Hz, 8H), 2.03 (s, 12H), 1.95 (s, 12H), 1.69 (qn, J = 7.0 Hz,

8H). Observed spectra consistent with literature values.[1]

2.2: R₁ = (CH₂)₃OAc
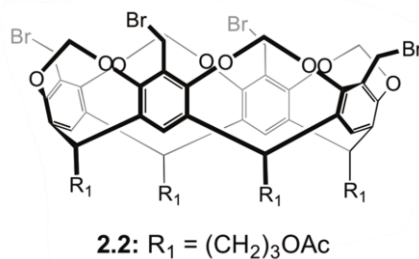
Preparation of Tetra-bromo Cavitand 2.2: In a 500 mL flask equipped with stir bar,

2.1b (1.00 g, 1.01 mmol), n-bromosuccinimide (0.791 g, 4.44 mmol), and benzoyl

peroxide (0.049 g, 0.201 mmol), was heated in 100 mL carbon tetrachloride (CCl₄) at 76

ºC for 72 h. The precipitate byproduct was then isolated off and discarded, as the solution

was concentrated under vacuum. The pure product was collected as a white powder

(0.942 g, 71 %). ^{1}H NMR (CDCl$_3$) δ 7.09 (s, 4H), 6.01 (d, J = 6.7 Hz, 4H), 4.82 (t, J = 8.1 Hz, 4H), 4.55 (d, J = 6.7, 4H), 4.39 (s, 8H), 4.15 (t, J = 6.5 Hz, 8H), 2.28 (q, J = 6.7 Hz, 8H), 2.05 (s, 12H), 1.67 (qn, J = 6.7 Hz, 8H). Observed spectra consistent with literature values.[1]

2.3: R$_1$ = (CH$_2$)$_3$OAc
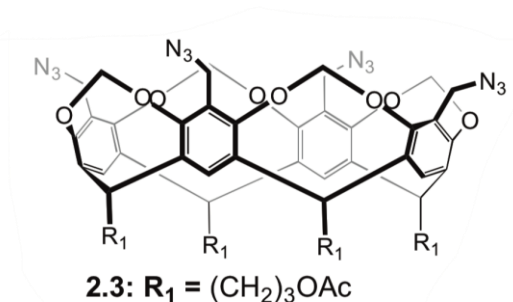
Preparation of Tetra-azide Cavitand 2.3: In a 100 mL flask equipped with stir bar, **2.2** (1.50 g, 1.12 mmol) was mixed with sodium azide (0.5 M in DMSO, 10 mL) in 10 mL tetrahydrofuran (THF) at ambient temperature for 24 h. After that time, the mixture was poured into 50 mL of water and solid was collected by vacuum filtration. The sticky product was sonicated in 50 mL of methanol, causing the solid to become a pure, white powder (1.30 g, 90 %). ^{1}H NMR (300 MHz, CDCl$_3$) δ 7.13 (s, 4H), 5.95 (d, J = 7.2 Hz, 4H), 4.85 (t, J = 7.0 Hz, 4H), 4.39 (d, J = 7.2 Hz, 4 H), 4.33 (s, 8H), 4.18 (t, J = 7.0 Hz, 8H), 2.31 (q, J = 7.0 Hz, 8H), 2.07 (s, 12H), 1.70 (qn, J = 7.0 Hz, 8H). ^{13}C NMR (100 MHz, CDCl3) δ 171.1, 153.9, 137.8, 122.8, 120.3, 99.8, 64.1, 45.1, 41.1, 36.5, 27.1, 21.0. Observed spectra consistent with literature values.[2]
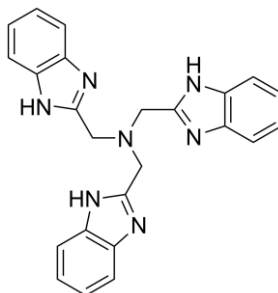
Blm benzimidazole co-catalyst: To a 100 mL round bottom flask equipped with a stir bar was added *o*-phenylenediamine (5.00 g, 42.3 mmol), nitrilotriacetic acid (2.95 g, 15.4 mmol), and ethylene glycol (33 mL). The solution was refluxed for 48 h at 200 ºC and then cooled to ambient temperature. Upon cooling, the crude product precipitated from solution as a lavender-colored solid. The crude product was collected by vacuum filtration, rinsed with cold ethanol, and recrystallized from ethanol (30 mL). Pure product was collected as pale pink crystals (4.1 g, 80 %). ^{1}H NMR (300 MHz, DMSO-d_6) δ 7.60-7.58 (6H, m), 7.20-7.17 (6H, m) and 4.16 (6H, s). Observed spectra consistent with literature values.[3]

2.4a: R_1 = $(CH_2)_3OAc$
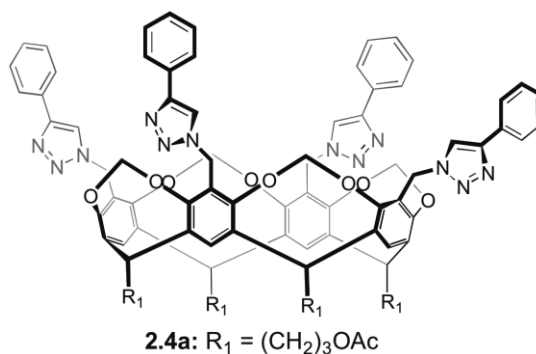
Preparation of Phenyl OAc-Footed Cavitand 2.4a$_1$: In a 100 mL flask equipped with stir bar, **2.3** (0.400 g, 0.360 mmol), copper (II) sulfate pentahydrate (0.015 g, 0.1 mmol), and L-sodium ascorbate (0.039 g, 0.210 mmol) were mixed in 3 mL DMSO:H$_2$O

(4:1). Then slowly phenyl acetylene (0.228 mL, 2.08 mmol) was added. The reaction mixture was heated for 24 h at 100 ºC and then cooled to ambient temperature. The mixture was pour into 20 mL water, the product was precipitated as a pale brown solid (0.445 g, 92 **%).** ^{1}H NMR (300 MHz, CDCl$_3$) δ 7.82 (d, J = 5.2 Hz, 8H), 7.77 (s, 4H), 7.37 (t, J = 5.2 Hz, 8H), 7.29 (t, J = 5.2 Hz, 4H), 7.23 (s, 4H), 5.81 (d, J = 5.7 Hz, 4H), 5.30 (s, 8H), 4.87 (t, J = 6.3 Hz, 4H), 4.40 (d, J = 5.7 Hz, 4H), 4.18 (t, J = 5.1 Hz, 8H), 2.33 (q, J = 5.1 Hz, 8H), 1.70 (qn, J = 5.4 Hz, 8H). ^{13}C NMR (100 MHz, CDCl$_3$) δ 171.3, 154.2, 147.8, 137.9, 130.6, 129.0, 128.4, 126.0, 121.4, 121.1, 120.2, 99.6, 64.2, 44.3, 36.8, 27.2, 26.9, 21.2. MS (ESI) observed m/z 1588.6103 (M + Na)$^+$, expected m/z 1588.6052 (M + Na)$^+$.

2.4a: R$_1$ = (CH$_2$)$_3$OH
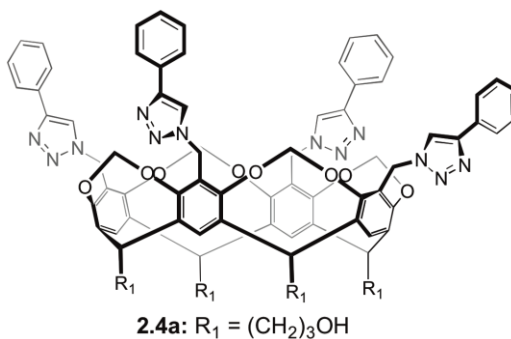
Preparation of Phenyl OH-Footed Cavitand 2.4a$_2$: In a 25 mL round bottom flask, OAc footed **2.4a** (0.252 g, 0.160 mmol) and cesium carbonate (0.315 g, 0.97 mmol) were mixed in 6 mL methanol:dichloromethane (1:1). The reaction mixture was stirred for 16 h at ambient temperature, and then the solvent was removed *in vacuo*. The remaining solid was sonicated in water (20 mL) to remove the salt, and the insoluble product was collected by vacuum filtration to yield yellow solid (0.187 g, 83 %). ^{1}H NMR (300 MHz, DMSO-d_6) δ 8.51 (s, 4H), 7.85 (d, J = 7.5 Hz, 8H), 7.77 (s, 4H), 7.44 (t, J = 7.5 Hz, 8H),

7.33 (t, J = 7.5 Hz, 4H), 6.11 (d, J = 7.5 Hz, 4H), 5.36 (s, 8H), 4.67 (t, J = 6.5 Hz, 4H), 4.48 (br, 4H), 4.37 (d, J = 7.5 Hz, 4H), 3.49 (t, J = 6.5 Hz, 8H), 2.43 (q, J = 6.5 Hz, 8H), 1.41 (qn, J = 6.5 Hz, 8H). ^{13}C NMR (100 MHz, DMSO-d_6) δ 153.8, 150.4, 150.2, 147.53, 138.8, 137.9, 124.3, 124.0, 123.7, 122.1, 120.2, 100.1, 61.0, 44.2, 37.4, 31.5, 26.3. MS (MALDI) observed m/z 1397.1 (M + H)$^+$, expected m/z 1397.6 M (M + H)$^+$.

2.4b: R$_1$ = (CH$_2$)$_3$OAc
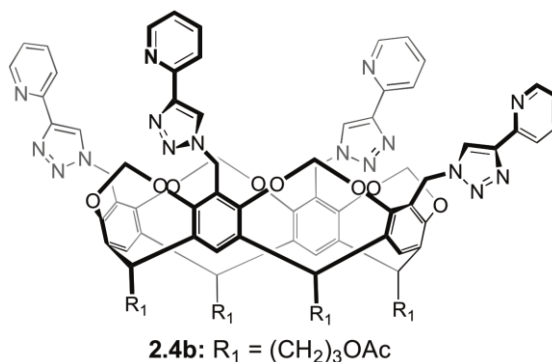
Preparation of pyridyl OAc-Footed Cavitand 2.4b$_1$: In a 100 mL flask equipped with stir bar, **2.3** (0.300 g, 0.260 mmol), copper (II) sulfate pentahydrate (0.012 g, 0.078 mmol), and L-sodium ascorbate (0.030 g, 0.160 mmol) were mixed in 3 mL DMSO:H$_2$O (4:1). Then 2- ethynylpyridine (0.129 mL, 1.14 mmol) was added slowly. The reaction was stirred for 24 h at 100 °C and then cooled to ambient temperature. The reaction mixture was poured into 10 mL of water in order to precipitate the product as a pale brown powder (0.316 g, 78 %). ^{1}H NMR (300 MHz, CDCl$_3$) δ 8.51 (br d, J = 3.5 Hz, 4H), 8.14 (br d, J = 5.5 Hz, 4H), 8.10 (s, 4H), 7.70 (td, J = 5.5, 0.9 Hz, 4H), 7.22 (s, 4H), 7.17 (br dd, J = 5.5, 0.9, 4H), 5.80 (d, J = 5.4 Hz, 4H), 5.29 (s, 8H), 4.82 (t, J = 5.3 Hz, 4H), 4.32 (d, J = 5.4 Hz, 4H), 4.17 (t, J = 5.3 Hz, 8H), 2.30 (q, J = 5.3 Hz, 8H), 2.03 (s, 12H), 1.67 (qn, J = 5.3 Hz, 8H). ^{13}C NMR (100 MHz, CDCl$_3$) δ 171.3, 154.2, 150.3, 149.5, 148.3, 138.0, 137.0, 123.1, 122.5, 121.1, 120.6, 99.6, 64.2, 44.4, 41.1, 36.7, 27.18,

26.9, 21.1. MS (MALDI) observed m/z 1591.8 (M+ Na)$^+$, expected m/z 1591.6 (M + Na)$^+$.

2.4b: R_1 = $(CH_2)_3OH$
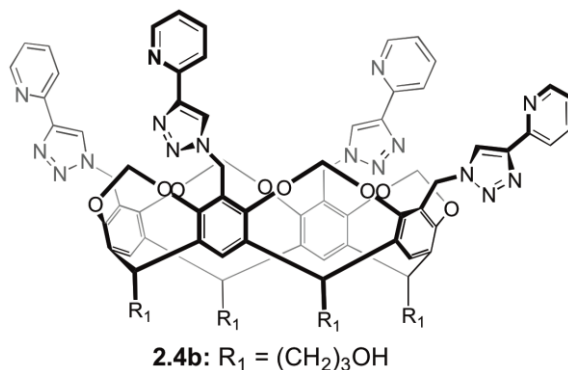
Preparation of pyridyl OAc-Footed Cavitand 2.4b$_2$: In a 100 mL flask equipped with stir bar, OAc footed **2.4b$_1$** (0.300 g, 0.190 mmol) and cesium carbonate (0.372 g, 1.14 mmol) were mixed in 6 mL methanol:dichloromethane (1:1) and stirred at ambient temperature for 12 h. The solvent was removed *in vacuo*, and the remaining solid was sonicated in 10 mL water to remove the salt. The precipitate product was collected by vacuum filtration as off white solid (0.267 g, 99 %). ^{1}H NMR (300 MHz, DMSO-d_6) δ 8.58 (br d, J = 5.1 Hz, 4H), 8.51 (s, 4H), 7.97 (br d, J = 7.8 Hz, 4H), 7.87 (td, J = 7.8, 1.5 Hz, 4H), 7.77 (s, 4H), 7.33 (br ddd, J = 5.1, 1.5, 4H), 6.08 (d, J = 7.8 Hz, 4H), 5.40 (s, 8H), 4.64 (t, J = 6.8 Hz, 4H), 4.39 (d, J = 7.8 Hz, 4H), 3.47 (t, J = 6.8 Hz, 8H), 2.42 (q, J = 6.8 Hz, 8H), 1.42 (qn, J = 6.8 Hz, 8H). ^{13}C NMR (100 MHz, CDCl$_3$) δ 153.8, 150.6, 150.2, 147.6, 138.8, 137.8, 124.4, 123.6, 122.0, 120.1, 100.1, 61.0, 44.2, 37.4, 31.5, 26.4. MS (MALDI) observed m/z 1423.3 (M + Na)$^+$, expected m/z 1423.5 (M + Na)$^+$.
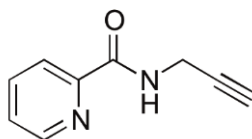
Preparation of 4-pyridyl amide Alkyne ligand 6.2.1: In a 25 mL flask equipped with stir bar, isonicotinic acid (0.384 g, 3.12 mmol), carbonyldiimidazole (0.506 g, 3.12 mmol) were mixed in 5 mL of THF for 10 min. then the propargylamine (0.200 mL, 3.12 mmol) was added slowly to the reaction mixture and stirred at ambient temperature for 24 h. The solvent was removed *in vacuo*, leaving yellow oily crude product. The crude product was purified by column chromatography (7 % methanol in methylene chloride) and then by recrystallization using ethyl acetate and hexanes. Pure product was obtained as colorless prisms (0.200g, 40 %). ^{1}H NMR (300 MHz, CDCl$_3$) δ 8.71 (dd, J = 4.5, 1.2 Hz, 2H), 7.61 (dd, J = 4.5, 1.2 Hz, 2H), 6.76 (b, 1H), 4.24 (dd, J = 3.9, 1.8 Hz, 2H), 2.28 (t, J = 1.8 Hz, 1H). ^{13}C NMR (100 MHz, CDCl$_3$) δ165.5, 150.8, 141.1, 121.1, 79.0, 72.5, 30.11. MS (ESI) observed *m/z* 160.0731 (M + H)$^+$, expected *m/z* 160.0715 (M + H)$^+$.
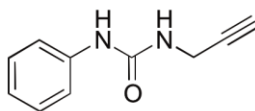
Preparation of phenyl urea alkyne ligand 6.2.2: A two-neck 25 mL round bottom flask equipped with a stir bar was evacuated and filled with nitrogen. DMF (1 mL, anhydrous), propargylamine (0.100 mL, 0.015 mmol), and phenylisocyanate (0.117 mL, 0.015 mmol) were added through a septum via syringe, and the reaction mixture was heated to 90 ºC for 16 h. After this time, the reaction mixture was cooled to ambient temperature and poured into 3 mL of water, causing the product to precipitate as a white

powder. The product was collected by vacuum filtration and dried (0.131 g, 52 %).

1HNMR (300 MHz, DMSO-$d6$) 8.65 (s, 1H), 7.38 (d, $J = 7.7$ Hz, 2H), 7.23 (t, $J = 7.7$ Hz, 2H), 6.90 (t, $J = 7.3$ Hz, 1H), 6.43 (t, $J = 5.6$ Hz, 1H), 3.88 (dd, $J = 5.6, 2.4$, Hz, 2H), 3.09 (t, $J = 2.4$ Hz, 1H). Observed spectra consistent with literature values.[4]

2.4c: $R_1 = (CH_2)_3OAc$
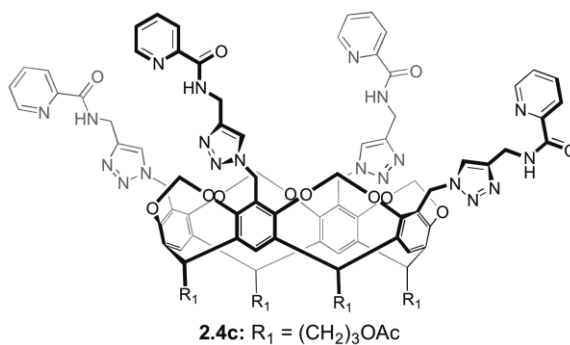
Preparation of 4-pyridyl amide OAc-Footed Cavitand 2.4c₁: To a 10 mL round bottom flask equipped with a stir bar, cavitand **2.3** (0.308 g, 0.270 mmol), alkyne ligand **6.2.1** (0.187 g, 1.17 mmol), Blm₃ co-ligand (0.033 g, 0.080 mmol), copper (II) sulfate pentahydrate (0.013 g, 0.080 mmol), and L-sodium ascorbate (0.032 g, 0.160 mmol) were mixed in 4 mL DMSO: H_2O (4:1). The reaction mixture was stirred at 100 ºC for 24 h. The reaction mixture was poured into 20 mL water, causing the product to precipitate as an off-white solid. (0.452 g, 95 %). ^{1}H NMR (300 MHz, CD₃CN) δ 8.65 (t, $J = 4.4$ Hz, 4 H), 8.46 (br d, $J = 3.0$ Hz, 4H), 8.03 (br d, $J = 5.7$ Hz, 4H), 7.83 (td, $J = 5.7, 1.2$ Hz, 4H), 7.64 (s, 4H), 7.45 (s, 4H), 7.42 (ddd, $J = 5.7, 3.6, 0.9$, 4H), 5.71 (d, $J = 5.7$ Hz, 4H), 5.20 (s, 8H), 4.73 (t, $J = 6.0$ Hz, 4H), 4.67 (d, $J = 4.4$ Hz, 8H), 4.10 (t, $J = 6.0$ Hz, 8H) 3.97 (d, $J = 5.7$ Hz, 4H), 2.41 (q, $J = 6.0$ Hz, 8H), 1.98 (s, 12H), 1.59 (qn, $J = 6.0$ Hz, 8H). ^{13}C NMR (100 MHz, CDCl₃) δ 171.2, 164.6, 153.9, 149.6, 148.3, 144.8, 137.5, 126.5, 123.1,

122.3, 121.3, 120.9, 99.6, 64.1, 43.9, 41.0, 36.6, 35.0, 27.0, 21.1. MS (MALDI) observed *m/z* 1819.4 (M + Na)[+], expected *m/z* 1819.7 (M + Na)[+].

2.4c: $R_1 = (CH_2)_3OH$
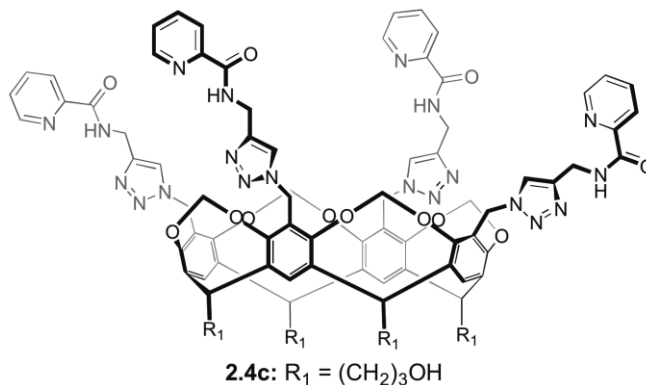
Preparation of 4-pyridyl amide OH-Footed Cavitand 2.4c$_2$: To a 25 mL round bottom flask equipped with a stir bar containing **2.4c$_1$** (0.900 g, 0.500 mmol) and cesium carbonate (0.980 g, 3.01 mmol) was mixed in 10 mL methanol:dichloromethane (1:1). The reaction mixture was stirred at ambient temperature for 16 h. The solvent was then removed by rotary evaporation, and the remaining solid was sonicated in 30 mL water to dissolve the salt impurity. The insoluble product was collected as a brown solid (0.711 g, 87 %). ^{1}H NMR (300 MHz, DMSO-*d*$_6$) δ 9.19 (t, *J* = 5.4 Hz, 4H), 8.60 (ddd, *J* = 5.7,2.4,1.5 Hz, 4H), 8.00 (dt, *J* = 7.8, 0.9), 7.92 (td, *J* = 7.8,1.8 Hz, 4H) 7.89 (s, 4H), 7.70 (s, 4H), 7.55 (ddd, *J* = 7.5, 4.8, 1.5, 4H), 5.89 (d, *J* = 7.6 Hz, 4H), 5.21 (s, 8H), 4.56 (t, *J* = 7.8 Hz, 4H), 4.52 (d, *J* = 6.0, 8H), 4.44 (br t), 4.17 (d, *J* = 7.6 Hz, 4H), 3.45 (br q, *J* = 6.5 Hz, 8H), 2.38 (q, *J* = 6.5 Hz, 8H), 1.38 (qn, *J* = 6.5, 8H). ^{13}C NMR (100 MHz, DMSO-*d*$_6$) δ 164.0, 153.1, 150.4, 149.1, 145.2, 138.7, 138.4, 127.2, 124.1, 122.5, 122.1, 99.4, 60.4, 43.2, 36.8, 34.7, 30.9, 25.7. MS (MALDI) observed *m/z* 1651.3 (M + Na)[+], expected *m/z* 1651.6 (M + Na)[+].

2.4d: R$_1$ = (CH$_2$)$_3$OAc
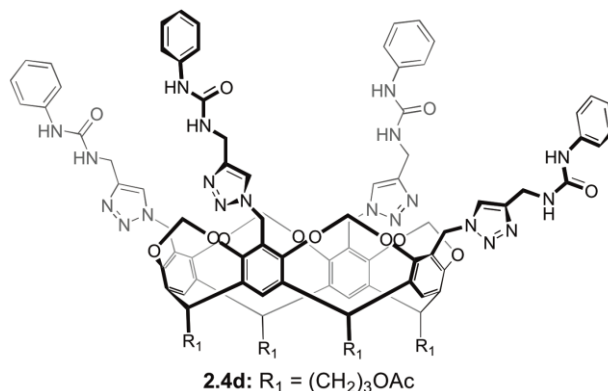
Preparation of Phenyl Urea OAc-Footed Cavitand 2.4d$_1$: To a 10 mL round bottom flask equipped with a stir bar was added **2.3** (0.100 g, 0.086 mmol), **6.2.2** (0.066 g, 0.380 mmol), copper (II) sulfate pentahydrate (0.004 g, 0.026 mmol), Blm$_3$ (0.011 g, 0.026 mmol), L-sodium ascorbate (0.010 g, 0.052 mmol), and mixed in DMSO:H$_2$O (4:1, 2 mL). The reaction mixture was heated for 16 h at 100 °C and then cooled to ambient temperature. The mixture was poured into 8 mL water, the product precipitated as a pale brown solid (0.116 g, 72 %). ^{1}H NMR (300 MHz, CDCl$_3$) δ 7.87 (br, 4H), 7.63 (br, 4H), 7.35 (m, 8H), 7.16 (m, 12H), 6.85 (t, J = 7.5 Hz, 4H), 6.53 (br, 4H), 5.95 (d, J = 7.6 Hz, 4H), 5.23 (s, 8H), 4.60 (t, J = 6.0 Hz, 4H), 4.29 (s, 8H), 4.22 (d, J = 7.6 Hz, 4H), 4.05 (t, J = 6.0 Hz, 8H), 2.39 (m, 8H), 1.94 (s, 12H), 1.55 (m, 8H). ^{13}C NMR (100 MHz, CDCl$_3$): δ 154.1, 137.9, 137.6, 129.1, 123.7, 122.9, 120.4, 119.3, 99.9, 64.2, 45.2, 41.1, 36.6, 27.1, 26.8, 21.2.
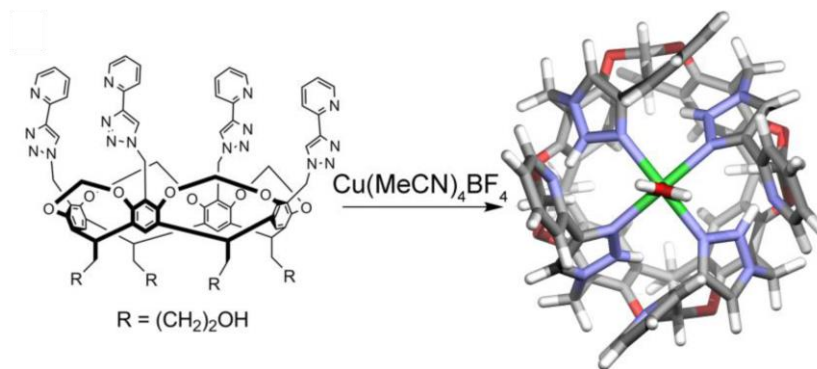
Preparation of 2-pridyl cavitand 2.4b₂•Cu: In a 10 mL round bottom flask equipped with a stir bar was **2.4b₂** (0.142 g, 0.100 mmol) and tetrakis(acetonitrile)copper(I) tetrafluoroborate (0.191 g, 0.610 mmol) were sonicated in 2 mL methanol until a homogenous suspension was formed. The precipitate was filtered off and rinsed with methanol (0.114 g, 77 %). The NMR peaks were broad and poorly defined so no integral values or coupling constants were obtained. MS (MALDI) observed *m/z* 1463.6 M⁺, expected *m/z* 1463.5 M⁺.
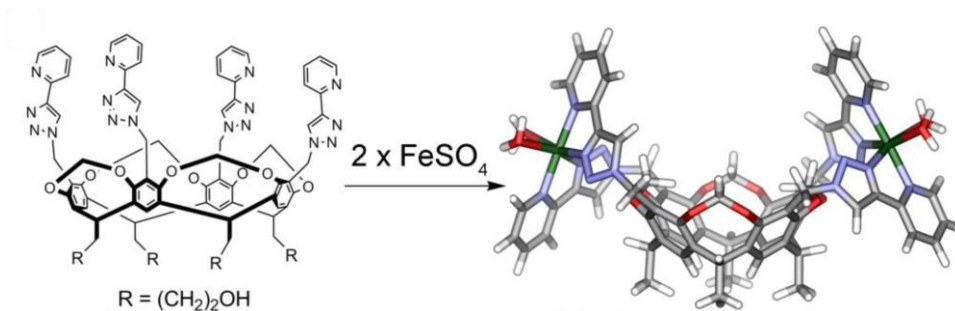
Preparation of 2-pridyl cavitand 2.4b₂•Fe2: In a 10 mL round bottom flask flask equipped with a stir bar was **2.4b₂** (0.089 g, 0.064 mmol) and iron (II) sulfate heptahydrate (0.106 g, 0.380 mmol) were sonicated in 2 mL methanol until a homogeneous suspension was formed. The precipitate was filtered off and rinsed with methanol (0.096 g, 99 %). The NMR peaks were broad and poorly defined so no integral

values or coupling constants were obtained. MS (MALDI) observed m/z 1644.7 $(M+2H_2O+SO_4)_+$, expected m/z 1644.4 $(M+2H_2O+SO_4)^+$.
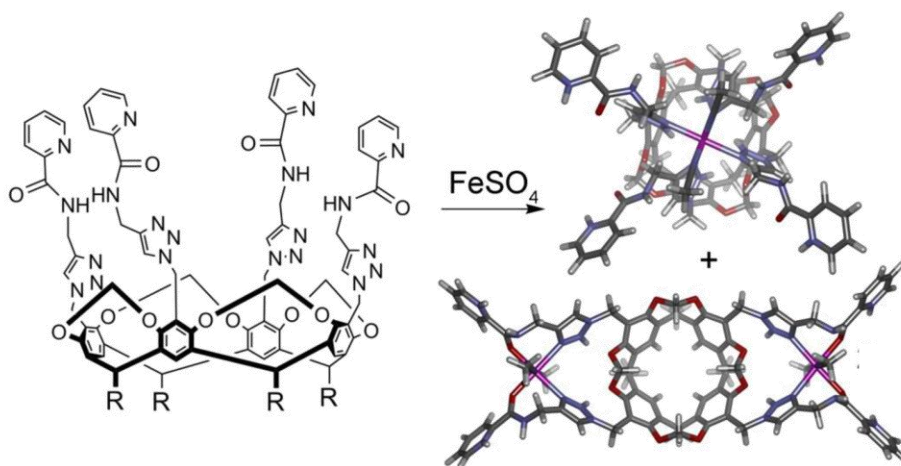
Preparation of 2-pyridyl amide OH-footed cavitand 2.4c$_2$•Fe$_x$: In a 25 mL round bottom flask equipped with a stir bar **2.4c$_2$** (0.300 g, 0.180 mmol) and iron (II) sulfate heptahydrate (0.310 g, 1.10 mmol) were sonicated in 2 mL methanol until a homogenous suspension was formed. The red- brown precipitate was collected as a brown solid (0.309 g, 99 %). The ^{1}H NMR peaks were broad and poorly defined so no integral values or coupling constants were obtained. MS (MALDI) observed m/z 1684.0 M$^+$, expected m/z 1684.6 M$^+$.

General Oxidation Procedures Catalyzed by 2.4b$_2$•Fe$_2$, 2.4c•Fe$_2$, and **2.4c$_2$•Cu$_2$, 2.6•Fe$_3$ 2.6•Ni$_3$** In a 2 mL scintillation vial equipped with a stir bar was added catalyst (3.77 x 10^{-3} mmol, 10 mol %), oxidant (^{t}BuOOH or H$_2$O$_2$ 0.377 mmol) and substrate (3.77 x 10^{-2} mmol) in 0.150 mL solvent (water:acetonitrile or water:propionitrile). The reaction was stirred for 24 h at 60 °C. Aliquots were taken and passed through a silica/magnesium sulfate plug with 1.5 mL ether before being analyzed by GCMS. The

reactions were performed in triplicate, and the average yield is reported. All yields are based on recovered starting material.

2.6 R = (CH₂)₃OAc
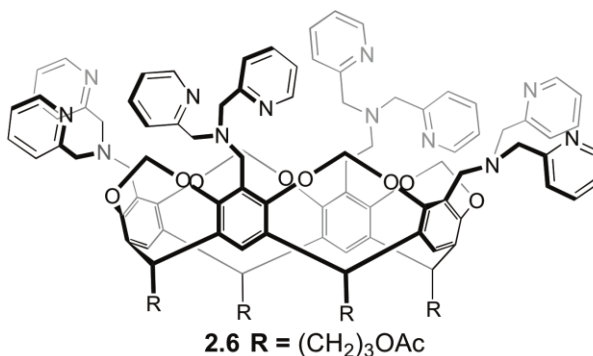
Preparation of dipicolyamine OAc footed Cavitand 2.6: In a 100 mL flask equipped with stir bar, **2.2** (200 mg, 0.15 mmol) was mixed with 2-picolylamine (134 mg, 0.67 mmol), and K_2CO_3 (340 mg, 2.45 mmol) in 10 mL acetonitrile at ambient temperature for 24 h under N_2 atmosphere. After that time, the reaction mixture was filtered to remove K_2CO_3, then extracted with dichloromethane and ammonium chloride solution. The organic layers were removed *in vacuo*. The sticky product was sonicated in 50 mL of ether, causing the solid to become a pure, white powder (164 mg, 61 %). ^{1}H NMR (400 MHz, CDCl₃) δ8.70 (d, J = 5.0 Hz, 4H), 7.89 (t, J = 7.9 Hz, 4H), 7.80 (d, J = 8.1 Hz, 4H), 7.36 (t, J = 5.8 Hz, 4H), 7.13 (s, 4H), 5.95 (d, *J* = 7.2 Hz, 4H), 4.85 (t, *J* = 7.0 Hz, 4H), 4.39 (d, *J* = 7.2 Hz, 4 H), 4.33 (s, 8H), 4.18 (t, *J* = 7.0 Hz, 8H), 3.95 (s, 16H), 2.31 (q, *J* = 7.0 Hz, 8H), 2.07 (s, 12H), 1.70 (qn, *J* = 7.0 Hz, 8H).
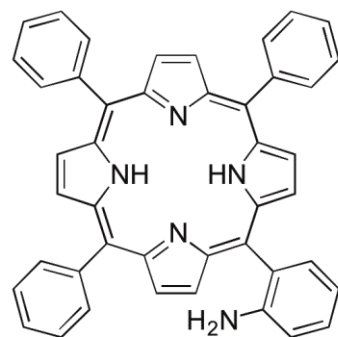
2.8
5-(*O*-Aminophenyl)
10, 15, 20-triphenyl porphyrin

Synthesis of 5-(*O*-Aminophenyl) 10, 15, 20-triphenyl porphyrin 2.8: Modified from

a literature procedure:[5-7] In a 500 ml round bottom flask equipped with a stir bar was

combined benzaldehyde (1.1 mL, 1.0 mmol) and 2-nitrobenzaldehyde (3.3 g, 2.1 mmol)

in glacial acetic acid. The reaction mixture was stirred under N_2 pressure at 110 ℃ for 3

hours. In a fractional distillation apparatus 1*H*-pyrrole (3 mL, 0.97 mmol) was heated at

200 ℃. The collected fractions was transported under N_2 pressure to a mixture of glacial

acidic acid and added drop wise for 20 mins. The mixture immediately changed color

from yellow to dark purple. After the addition was complete, reaction was stirred for 20

min under 110 ℃ under N_2 pressure. Mixture was cool to room temperatures before the

addition of conc. HCl (30 mL) and $SnCl_2.7H_2O$ (4 g). Reaction was refluxed for 3 h.

Mixture was carefully neutralized with $^+NH_4OH$ at 0 ℃. Mixture was filtered and

extracted 3 times with mixture of DCM:Brian. The organic layer was dried with Na_2SO_4,

filtered, and the solvent removed under reduced pressure. 5-(*O*-Aminophenyl) 10, 15, 20-

triphenyl porphyrin was isolated as dark purple solid (10 mg, 15%) from an silica column

eluted by toluene followed by 1:1 EtOAc:Toluene. ^1H NMR (300 MHz, $CDCl_3$): δ 8.86

(br s, 8H, β-pyrrole protons), 8.67(br d, 1H, protons of nitro-substituted phenyl), 8.45 (br

d, 1H, protons of nitro- substituted phenyl), 8.29-8.29 (br m, 5H, phenyl protons), 7.97 (br t, 2H, protons of nitro- substituted phenyl), 7.79 (br s, 10H, phenyl protons), -2.70 (s, 2H, NH protons). Observed spectra consistent with literature values.
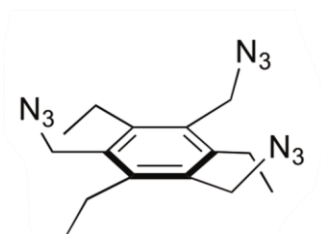
Synthesis of 1,3,5-Tris(azidomethyl)-2,4,6-triethylbenzene 2.13. Following similar literature procedures.[8] In a 25 ml round bottom flask equipped with a stir bar was combined 1,3,5-tris(bromomethyl)-2,4,6-trimethyl-benzene **5** (1.0 g, 2.3 mmol) and sodium azide (18 mL, 0.5 M in DMSO, 9.0 mmol). The reaction mixture was stirred for 24h at room temperature. The solution was then diluted in 100 ml H_2O and extracted with dichloromethane. The organic layer was dried with Na_2SO_4, filtered, and the solvent removed under reduced pressure to yield **6** as a white solid (621 mg, 84%). ^{1}H NMR (300 MHz, CDCl$_3$): δ 4.50 (6H, s), 3.86 (q, J = 7.7 Hz, 6H), 1.25 (t, J = 7.7 Hz, 9H); ^{13}C NMR (100 MHz, CDCl$_3$): δ 144.9, 130.0, 47.9, 23.2, 15.7.
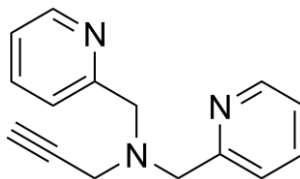
Synthesis of N,N-bis(2-pyridylmethyl)-N-propargylamine 2.10. N,N-bis(2-pyridylmethyl)-N-propargylamine was synthesized according to literature procedures.[9] Di-(2-picolyl)amine (10.0 mmol, 1.08 mL) was dissolved in MeCN (20 mL). K_2CO_3 (40

mmol, 5.4 g) was added to the solution followed by dropwise addition of propargyl bromide (80% in toluene, 10 mmol, 1.09 mL). The reaction mixture was stirred for 24 h before being diluted with dichloromethane. The diluted reaction mixture was filtered to remove K_2CO_3, then washed with dichloromethane before being concentrated under vacuum. N,N-bis(2-pyridylmethyl)-N-propargylamine was isolated as yellow oily solid (2.28 g, 96%) from an alumina column eluted by EtOAc in dichloromethane (0% - 40%). After purification, the solvent was rapidly removed by rotary evaporation and the product was stored under nitrogen. ^1H NMR (300 MHz, CDCl$_3$): δ 8.57 (d, J = 4.2 Hz, 2H), 7.66 (td, J = 1.2, 7.8 Hz, 2H), 7.52 (d, J = 7.8 Hz, 2H), 7.17 (td, J = 5.4, 7.2 Hz, 2H), 3.93 (4H, s), 3.43 (d, J = 2.4 Hz, 2H), 2.30 (t, J = 2.4 Hz, 1H); ^{13}C NMR (75 MHz, CDCl$_3$): δ 159.0, 149.5, 136.7, 123.4, 122.3, 73.9, 59.7, 42.79; HRMS (ESI): calcd. (M+Na$^+$) 260.1164, found 260.1159.
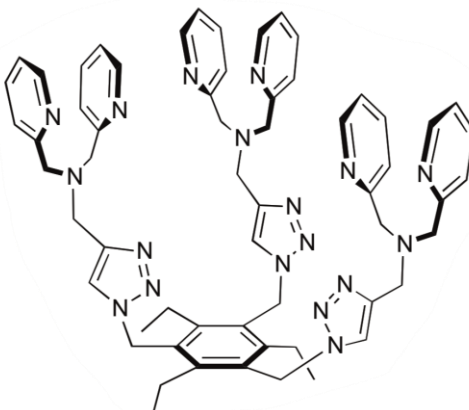
Synthesis of Hexapicolyl ligand 2.14. In a sealed tube flushed with nitrogen was combined 1,3,5-tris(azidomethyl)-2,4,6-triethylbenzene **2.13** (50 mg, 0.15 mmol), *N,N*-bis(2-pyridylmethyl)-*N*-propargylamine **2.10** (180 mg, 0.76 mmol), CuSO$_4$·5H$_2$O (12 mg, 0.05 mmol), sodium ascorbate (18 mg, 0.09 mmol), BIm$_3$ co-catalyst (19 mg, 0.05

mmol), and 2 mL of 1:1 ^{t}BuOH:H$_2$O. The reaction mixture was stirred for 24 h at 80 ºC. The solvent was removed under vacuum, redissolved in dichloromethane (20 mL) and added to an aqueous solution of Na$_2$EDTA (15 mL). This mixture was stirred for 1 h to remove any bound copper from the ligand. The organic layer was separated, dried with Na$_2$SO$_4$, filtered and the solvent removed under reduced pressure to yield a brown, tar-like substance (130 mg, 82 % yield). The ligand was purified via rapid flash chromatography with an alumina column eluted by EtOAc in dichloromethane (0% - 40%). The product was then recrystallized from CH$_2$Cl$_2$ under a nitrogen atmosphere. After purification, the product was stored under nitrogen. CAUTION: organic azides are explosive, and should be handled carefully. ^{1}H NMR (300 MHz, CDCl$_3$): δ 8.46 (dt, $J =$ 4.7, 1.4 Hz, 6H), 7.61(td, $J =$ 7.6, 1.8 Hz, 6H), 7.51 (td, $J =$ 7.8, 1.2 Hz, 6H), 7.45 (s, 3H), 7.11 (ddd, $J =$ 7.4, 4.9, 1.4 Hz, 6H), 5.62 (s, 6H), 3.76 (s, 6H), 3.75 (s, 12H), 2.80 (q, $J =$ 7.4 Hz, 6H), 0.92 (t, $J =$ 7.3 Hz, 9H). ^{13}C NMR (75 MHz, CDCl$_3$): δ 158.9, 148.8, 146.2, 144.2, 136.4, 129.6, 123.2, 122.7, 121.9, 59.3, 48.4, 47.8, 23.5, 15.2. ESI-TOF [MNa$^+$] calcd 1061.5616, found 1061.5734.
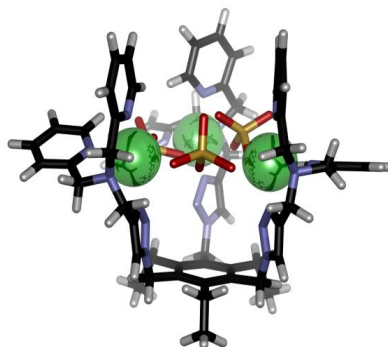
Synthesis of 2.14•Fe₃(SO₄)₃. In a dry two-dram vial flushed with nitrogen, **2.14** (100 mg, 0.16 mmol) was dissolved in dichloromethane (1 mL). In a separate two-dram vial FeSO$_4$·7H$_2$O (48 mg, 0.17 mmol) was dissolved in MeOH (1 mL). The two solutions were combined and sonicated for 5 min before collecting a brown precipitate (221 mg, 92%). mp: >250 °C (decomp). ESI-TOF [**2.14**•Fe$_3$(SO$_4$)$_2$•H$_2$O•OH]$^+$ calcd 1061.5616, found 1061.5734. Elemental Analysis: Theoretical (C$_{60}$H$_{66}$Fe$_4$N$_{18}$O$_{16}$S$_4$): C: 43.76, H: 4.04, N: 14.31. Theoretical (C$_{60}$H$_{66}$Fe$_3$N$_{18}$O$_{12}$S$_3$): C: 48.20, H: 4.45, N: 16.86. Found: C: 45.07, H: 4.39, N: 15.22. ICP analysis (Fe): 3.76%. NMR analysis: The broadness of the ^{1}H NMR spectrum limited accurate spectral assignments due to the paramagnetic nature of the complex, and so the peaks are not transcribed here.

General procedure for oxidation reactions: In a 0.3 mL conical vial, catalyst (4 µmol, 10 mol%) was dissolved in 0.25 mL solvent (1:1 MeCN:H$_2$O). ^{t}BuOOH (0.40 mmol, 10 equiv.), and substrate (0.04 mmol, 1 equiv.) were added. The reaction mixture was stirred for 24 h at 60 ℃. Aliquots were taken and passed through a silica gel pipet plug with ether before being analyzed by GCMS. All yields are based on GCMS analysis via integrative comparison to an internal standard. Product identification was determined by comparison to authentic samples via fragmentation pattern matching in MS.

2.16
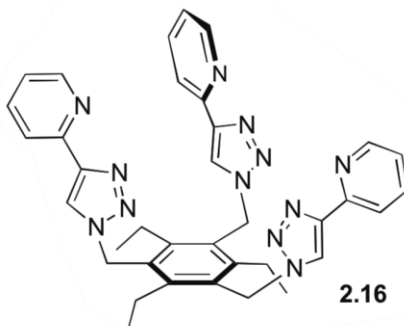
Synthesis of Trispyridyl ligand 2.16. In a 10 ml round bottom flask equipped with a stir bar was combined CuSO$_4$·5H$_2$O (23 mg, 0.09 mmol), sodium ascorbate (36 mg, 0.18 mmol), and 1,3,5-tris(azidomethyl)-2,4,6-triethylbenzene **2.13** (100mg, 0.31 mmol) in 4 mL of 4:1 DMSO:H$_2$O. To this mixture was added 2-ethynyl pyridine **2.15** (97 μL, 0.92 mmol) and the reaction mixture was stirred for 24 h at 100 ºC. After being cooled to room temperature, 15 mL of water was added and the resulting gray precipitate was collected by vacuum filtration. The crude precipitate was dissolved in dichloromethane and washed with an aqueous solution of Na$_2$EDTA. The organic layer was dried with Na$_2$SO$_4$, filtered, and the solvent removed under reduced pressure to yield **2.16** as a gray solid (175 mg, 90%). ^{1}H NMR (400 MHz, CDCl$_3$): δ 8.46 (d, J = 4.5 Hz, 3H), 8.18 (d, J = 7.9 Hz, 3H), 8.08 (s, 3H), 7.76 (td, J = 7.8, 1.5 Hz, 3H), 7.21 (dd, J = 6.8, 5.2 Hz, 3H), 5.73 (s, 6H), 2.84 (q, J = 7.4 Hz, 6H), 1.00 (t, J = 7.5 Hz, 9H). ^{13}C NMR (100 MHz, CDCl$_3$): δ 150.1, 149.0, 148.2, 146.9, 137.3, 129.8, 123.1, 121.8, 120.6, 48.2, 23.8, 15.5. ESI-TOF [MH$^+$] calcd 637.3259, found 637.3227.
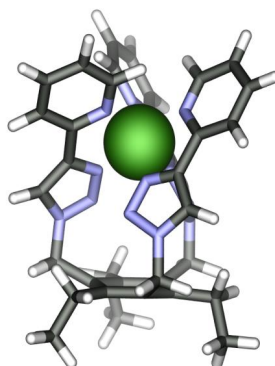
Synthesis of 2.16•FeSO₄. In a dry two-dram vial flushed with nitrogen, **2.16** (25 mg, 0.04 mmol) was dissolved in MeOH (1.5 mL). In a separate 2-dram vial $FeSO_4 \cdot 7H_2O$ (65 mg, 0.24 mmol) was dissolved in MeOH (1 mL). The two solutions were combined and sonicated for 5 min before collecting a brown precipitate (30 mg, 97%). ESI-TOF [**2.16**•Fe(HSO₄)]$^+$ calcd 881.2, found 881.4. NMR analysis: The broadness of the ^{1}H NMR spectrum limited accurate spectral assignments due to the paramagnetic nature of the complex, and so the peaks are not transcribed here.
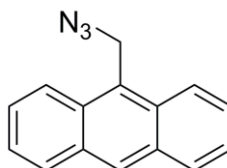
Synthesis of 9-Anthracenylmethyl azide 2.17: Adapted from a literature procedure.[10] 9-Anthracenemethanol (1.50 g, 7.40 mmol) was dissolved in dichloromethane (30 mL). SOCl₂ (810 µL, 11.1 mmol) was then added at 0 ℃. After mixing for 2 h, the solvent was removed under vacuum. The resultant residue was redissolved in DMF (10 mL), and sodium azide (0.77 g, 12.0 mmol) was added. The reaction mixture was heated for 4 h at 60 ℃, cooled to room temperature and diluted with 50 mL water. The mixture was then extracted with ethyl acetate. The organic layer was separated, dried with Na₂SO₄, filtered

and the solvent removed under reduced pressure to yield 9-anthracenylmethyl azide **2.17** as a yellow solid (1.70 g, 97% yield). CAUTION: organic azides are explosive, and should be handled carefully. ^{1}H NMR (400 MHz, CDCl$_3$) δ 8.50 (1H, s), 8.28 (d, J = 8.4 Hz, 2H), 8.06 (d, J = 8.4 Hz, 2H), 7.59 (t, J = 8.0 Hz, 2H), 7.50 (t, J = 8.0 Hz, 2H), 5.33 (2H, s); ^{13}C NMR (100 MHz, CDCl$_3$) δ 131.4, 130.7, 129.3, 129.0, 126.9, 125.2, 123.5, 46.4; EIMS: found 233.1 [M$^+$] calculated for C$_{15}$H$_{11}$N$_3$: 233.1.

2.18
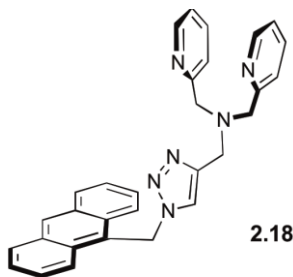
Synthesis of Dipicolyl ligand 2.18. In a sealed tube was combined 9-anthracenylmethyl azide **2.17** (100 mg, 0.43 mmol), *N,N*-bis(2-pyridylmethyl)-*N*-propargylamine **2.10** (160 mg, 0.64 mmol), CuSO$_4$·5H$_2$O (32 mg, 0.13 mmol), sodium ascorbate (42 mg, 0.25 mmol), BIm$_3$ co-catalyst (52 mg, 0.13 mmol), and 10 mL of 4:1 DMSO:H$_2$O. The reaction mixture was stirred for 24 h at 110 ºC before removing the solvent and redissolving in dichloromethane (20 mL) and adding an aqueous solution of Na$_2$EDTA (15 mL). This mixture was stirred for 1 h to remove any bound copper from the ligand. The organic layer was separated, dried with Na$_2$SO$_4$, filtered and the solvent removed under reduced pressure to yield **2.18** as a brown solid (90 mg, 53 %). ^{1}H NMR (400 MHz, CDCl$_3$): δ 8.56 (s, 1H), 8.34 (d, J = 4.5 Hz, 2H), 8.28 (d, J = 8.7 Hz, 2H), 8.05 (d, J = 8.0 Hz, 2H), 7.61 (m, 2H), 7.40 (m, 2H), 7.45 (td, J = 7.6, 1.6 Hz, 2H), 7.30 (d, J = 7.6 Hz, 2H), 7.07 (d, J = 5.9 Hz, 1H), 6.97 (dd, J = 6.4, 5.2 Hz, 2H), 6.47 (s, 2H),

5.30 (s, 1H), 3.69 (d, 4H), 2.58 (s, 2H). ^{13}C NMR (125 MHz, CDCl$_3$): δ 158.19, 148.7, 136.6, 131.4, 131.2, 130.8, 129.7, 129.4, 129.3, 127.6, 125.7, 125.4, 124.0, 123.5, 123.1, 122.9, 122.1, 59.4, 48.8, 46.4, 41.0. ESI/APCI [MH$^+$] calcd 470.22, found 471.0.
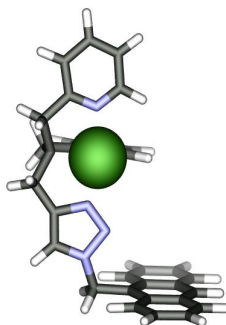
Synthesis of 2.18•FeSO$_4$. In a dry two-dram vial flushed with nitrogen, **2.18** (40.0 mg, 0.038 mmol) was dissolved in MeOH (1.5 mL). In a separate 2-dram vial FeSO$_4$·7H$_2$O (30 mg, 0.192 mmol) was dissolved in MeOH (1 mL). The two solutions were combined and sonicated for 5 min before collecting a brown precipitate (21 mg, 90% yield). ESI-TOF [**2.18**•Fe(SO$_4$)•H$_2$O•H]$^+$ calcd 643.13, found 643.48. ICP analysis (Fe): 1.64%. The broadness of the ^{1}H NMR spectrum limited accurate spectral assignments due to the paramagnetic nature of the complex, and so the peaks are not transcribed here.

2.19
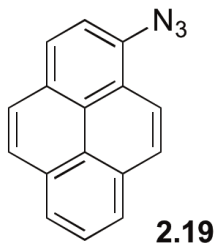
Synthesis of 1-Azidopyrene 2.19: In a sealed tube equipped with a stir bar 1-aminopyrene (5.0 g, 20 mmol) was dissolved in 500 μL H$_2$SO$_4$ and 10 mL hexane. Then

slowly added at 0 ℃ NaNO$_2$ (400 mg, 22 mmol) followed by sodium azide (300 mg, 20 mmol). After mixing for 2 h 0 ℃, the reaction mixture was mixed at ambient temperature for 16 h. The mixture was acidified with 1 mL 1M HCl and extracted with dichloromethane. The organic layer was separated, dried with Na$_2$SO$_4$, filtered and the solvent removed under reduced pressure to yield 1-Azidopyrene **2.19** as dark orange/black oil (2.5g, 50% yield). CAUTION: organic azides are explosive, and should be handled carefully. ^{1}H NMR (400 MHz, CDCl$_3$): δ 8.06 8.20 (6H, m), 8.24 8.29 (3H, m). ^{13}C NMR (125 MHz, CDCl$_3$): 112.0, 118.9, 121.0, 123.5, 124.3, 124.9, 125.3, 126.5, 126.9, 127.1, 129.4, 130.8, 131.3. Observed spectra consistent with literature values.[11]

2.20
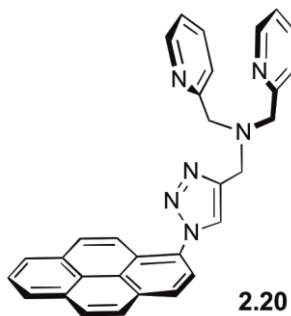
Synthesis of Dipicolyl ligand 2.20. In a sealed tube was combined 1-pyrene azide **2.19** (100 mg, 0.44 mmol), *N,N*-bis(2-pyridylmethyl)-*N*-propargylamine **2.10** (160 mg, 0.64 mmol), CuSO$_4$·5H$_2$O (32 mg, 0.13 mmol), sodium ascorbate (42 mg, 0.25 mmol), BIm$_3$ co-catalyst (52 mg, 0.13 mmol), and 10 mL of 4:1 DMSO:H$_2$O. The reaction mixture was stirred for 24 h at 110 ℃ before removing the solvent and redissolving in dichloromethane (20 mL) and adding an aqueous solution of Na$_2$EDTA (15 mL). This mixture was stirred for 1 h to remove any bound copper from the ligand. The organic layer was separated, dried with Na$_2$SO$_4$, filtered and the solvent removed under reduced

pressure to yield **2.18** as a brown solid (90 mg, 53 %). ^{1}H NMR (400 MHz, CDCl$_3$): δ 8.54 (d, *J* = 4.9 Hz, 2H), 8.33 − 7.73 (m, 12H), 7.73 − 7.58 (m, 2H), 7.36 (d, *J* = 8.1 Hz, 1H), 7.15 (t, *J* = 6.2 Hz, 2H), 3.99 (s, 4H), 2.59 (s, 2H), 1.24 (s, 2H).

Synthesis of 2.20•FeSO₄. In a dry two-dram vial flushed with nitrogen, **2.20** (40.0 mg, 0.038 mmol) was dissolved in MeOH (1.5 mL). In a separate 2-dram vial FeSO$_4$·7H$_2$O (30 mg, 0.192 mmol) was dissolved in MeOH (1 mL). The two solutions were combined and sonicated for 5 min before collecting a brown precipitate 82% yield. The broadness of the ^{1}H NMR spectrum limited accurate spectral assignments due to the paramagnetic nature of the complex, and so the peaks are not transcribed here.

2.21
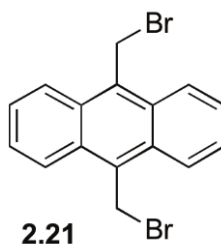
Synthesis of 9.10-bis(chloromethyl)anthracene 2.21: In a 10 ml round bottom flask equipped with a stir bar was combined anthracene (0.95 g, 5.31 mmol, 1 equiv) and paraformaldehyde (55.0 mmol, 10 equiv) in 10 mL hydrogen bromide solution in acetic acid (30% CAUTION: hydrogen bromide gas is toxic) and stir for 20 min. Next, ZnBr (1.97 g, 8.75 mmol) was slowly added drop wise to the reaction mixture over a period of 1 h yielding a dark yellow solution. The reaction mixture was stirred and heated to 90 °C for 72 h as turned dark green. The mixture was cooled, filtered, washed with water, and then dried. Recrystallization from dioxane furnished pure 9,10-bis(bromomethyl)-

anthracene **2.21.** Yield 653 mg (34%). [^1]H NMR (400 MHz, CDCl$_3$): δ 8.56-8.54 (m, 4H), 7.78-7.75 (m, 4H), 5.78 (s, 4H). Observed spectra consistent with literature values.[12]

2.22
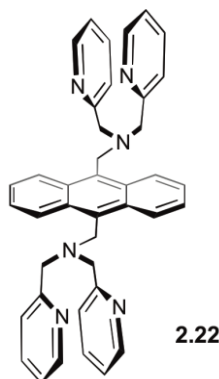
Synthesis of Dipicolyl ligand 2.22. In a sealed tube was combined 1-pyrene azide **2.19** (100 mg, 0.44 mmol), *N,N*-bis(2-pyridylmethyl)-*N*-propargylamine **2.10** (160 mg, 0.64 mmol), CuSO$_4$·5H$_2$O (32 mg, 0.13 mmol), sodium ascorbate (42 mg, 0.25 mmol), BIm$_3$ co-catalyst (52 mg, 0.13 mmol), and 10 mL of 4:1 DMSO:H$_2$O. The reaction mixture was stirred for 24 h at 110 ºC before removing the solvent and redissolving in dichloromethane (20 mL) and adding an aqueous solution of Na$_2$EDTA (15 mL). This mixture was stirred for 1 h to remove any bound copper from the ligand. The organic layer was separated, dried with Na$_2$SO$_4$, filtered and the solvent removed under reduced pressure to yield **2.18** as a brown solid (90 mg, 53 %). [^1]H NMR (400 MHz, CDCl$_3$): δ 8.54 (d, *J* = 4.9 Hz, 2H), 8.33 – 7.73 (m, 12H), 7.73 – 7.58 (m, 2H), 7.36 (d, *J* = 8.1 Hz, 1H), 7.15 (t, *J* = 6.2 Hz, 2H), 3.99 (s, 4H), 2.59 (s, 2H), 1.24 (s, 2H).

Synthesis of 2.22•FeSO₄. In a dry two-dram vial flushed with nitrogen, **2.22** (80.0 mg, 0.133 mmol) was dissolved in MeOH (1.5 mL). In a separate 2-dram vial FeSO₄·7H₂O (70 mg, 0.448 mmol) was dissolved in MeOH (1 mL). The two solutions were combined and sonicated for 5 min before collecting a brown precipitate (107 mg, 95% yield). The broadness of the ^{1}H NMR spectrum limited accurate spectral assignments due to the paramagnetic nature of the complex, and so the peaks are not transcribed here.

6.3. Chapter 3 Experimental
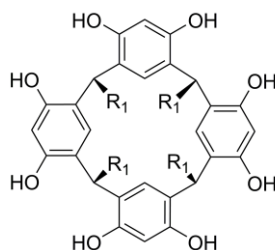
1.24 Resorcinarene
1.24a: R₁ = C₁₁H₂₃

Synthesis of Resorcinarene C₁₁-cavitand 1.24a: To a 500 mL round bottom flask equipped with a stir bar was added resorcinol (20 g, 180 mmol) and dodecanal (12.2 mL, 792 mmol) in ethanol (120 mL) with concentrated hydrochloride acid (30 mL). Mixture was stir at 80 °C for 96 h. Reaction was quickly poured into 200 mL of H₂O then filter with vacuum filtration. Product was then suspended in H₂O and refiltered. For purification, the product was recrystallized in hot acetone to yield 18.5 g, 73% yield. [1]H

NMR: (400 MHz, CDCl$_3$): δ 9.62–9.29 (m, 8 H), 7.19 (s, 4 H), 6.09 (s, 4 H), 4.29 (t, 4 H, J=15.2Hz), 2.21, 1.38 and 1.26 (m, 80 H), and 0.87 (t, 12 H, J=13.2); ^{13}C NMR (400 MHz, CDCl$_3$): δ 150.1, 149.8, 124.5, 123.5, 102.6, 102.4, 33.6, 33.4, 32.2, 30.2, 30.1, 30.0, 29.7, 28.4, 23.1, 14.6. Observed spectra consistent with literature values.[13]
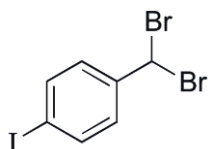
Synthesis of 4-iodo-α,α-dibromotoluene 6.3.1: an oven dried 250 mL round bottom flask equipped with a stir bar was mixed 4-iodobenzaldehyde (3.35 g, 14.4 mmol), boron tribromide (1.51 mL, 15.9 mmol) in anhydrous methylene chloride (70 mL). The reaction mixture was stirred at room temperature for 24 h. the reaction was then quenched by water (70 mL) slowly. The precipitate was filtered off and discarded. The filtrate solution was collected and extracted with 50 mL of methylene chloride three times. The organic layers were dried and concentrated *in vacuo*, leaving 4.75 g (88 %) pure product as a white powder. ^{1}H NMR (300 MHz, D$_2$O) δ 7.72 (d, J = 8.4 Hz, 2H), 7.32 (d, J = 8.4 Hz, 2H), 6.58 (s, 1H). Observed spectra consistent with literature values.[14]

$R_1 = C_{11}H_{23}$
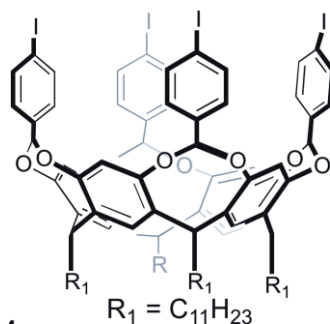
Synthesis of Iodo cavitand 3.1: To a 100 mL round bottom flask equipped with a stir bar was added **1.14** (1.00 g, 0.900 mmol) in DMA (50 mL, degassed), slowly the 4-iodobenzalbromide **6.3.1** (1.49 g, 3.98 mmol), and DBU (1.08 mL, 7.24 mmol) were added. The reaction mixture was stirred under nitrogen at 60 °C for 48 h. The reaction was then cooled to room temperature and poured in 100 mL of water, causing the product was precipitate as a brown clay like on the sides of the beaker. The water was filtered off, and the remaining solid was purified by column chromatography using DCM as elution solvent. The product-containing fractions were concentrated *in vacuo*, leaving product (0.453 g, 30 %) as a white solid. ^{1}H NMR (300 MHz, CDCl$_3$): δ 7.78 (d, *J* = 8.3 Hz, 8 H), 7.41 (d, *J* = 8.3 Hz, 8H), 7.25 (s, 4H), 6.62 (s, 4H), 5.38 (s, 4H), 4.91 (t, *J* = 7.8 Hz, 4H), 2.31 (q, *J* = 6.3 Hz, 8H), 1.45 (m, 8H), 1.28 (br s, 64 H), 0.90 (t, *J* = 6.0 Hz, 12H). ^{13}C NMR (100 MHz, CDCl$_3$): δ 154.4, 139.2, 138.3, 137.8, 128.4, 121.2, 116.7, 107.1, 95.4, 36.7, 32.2, 29.9, 28.2, 22.9, 14.4.

3.2
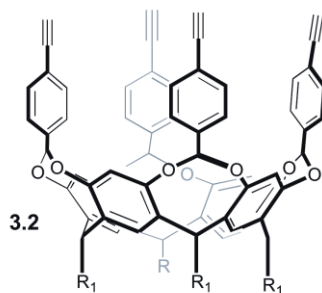
Synthesis of Tetraacetylene cavitand 3.2: To a sealed tube equipped with a stir bar was added **3.1** (119 mg, 0.061 mmol), Pd(PPh₃)₂Cl₂ (9 mg, 0.012 mmol), CuI (5 mg, 0.024 mmol), diethylamine (2 mL), and trimethylsilylacetylene (0.190 mL, 1.33 mmol). The reaction mixture was refluxed at 60 °C for 24 h and then cooled to room temperature. Mixture of water and hexanes (1:1) were added to the reaction mixture, and the product was extracted into hexanes 3X. The combined organic layers were rinsed with 10 % aq. HCl (20 mL) and water (20 mL). The organic layers were dried and concentrated *in vacuo*, leaving the crude product. The crude product was triturated in methanol, and the TMS-protected product was collected by vacuum filtration as a white solid (0.062 g). The TMS-protected product was dissolved THF (2 mL) with tetrabutylammonium fluoride (10 eq) and stirred at ambient temperature for 16 h. After this time, water and hexanes were added (10 mL each) and the product was extracted into hexanes. The aqueous layer was rinsed with hexanes (5 mL) an additional two times, and the combined organic layers were dried and concentrated *in vacuo*, leaving product as a white solid (52 mg, 55%). ^{1}H NMR (300 MHz, CDCl₃): δ 7.64 (d, *J* = 8.4 Hz, 8H), 7.57 (d, *J* = 8.4 Hz, 8H), 7.26 (s, 4H), 6.66 (s, 4H), 5.45 (s, 4H), 4.93 (t, *J* = 7.8 Hz, 4H), 2.33 (m, 8H), 1.46 (m, 8H), 1.28 (br, 64 H), 0.89 (t, 12H). ^{13}C NMR (100 MHz, CDCl₃): δ 154.5, 139.2, 132.4, 126.5,

123.1, 121.1, 116.8, 107.3, 83.3, 78.2, 59.0, 36.7, 32.1, 29.9, 28.2, 22.9, 14.3.

6.3.1 Example of Failed Donor Cavitand Synthesis
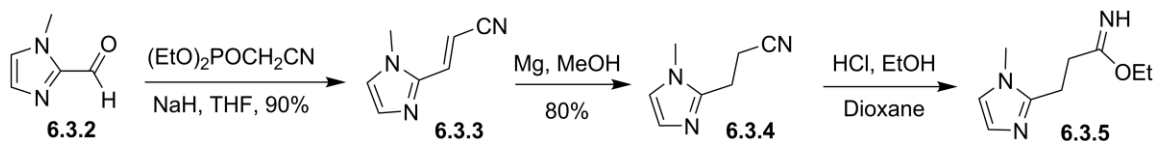
Synthesis of 3-(1-methyl-1H-imidazol-2-yl)acrylonitrile 6.3.2: NaH (25 mmol, 60 %, 1.0 g) was added to a dry 100 mL round-bottomed flask equipped with septum and magnetic stirrer, and the flask placed under an argon atmosphere. Dry THF (50 mL) was added via syringe and the solution cooled to 0 °C. Diethyl cyanomethyl phosphonate (12.33 mmol, 2.22 g, 1.97 mL) was added via syringe over a period of 10 min and the slurry stirred for 1h. 1-Methyl-2-imidazolecarboxaldehyde **6.3.2** (1.37g, 12.33 mmol) in dry THF (5 mL) was added dropwise via syringe and the mixture allowed to warm slowly to ambient temperature. After 5 h, the excess NaH was quenched by cooling to 0 °C and dropwise addition of MeOH (5 mL) and water (10 mL). The mixture was diluted with ether (200 mL) and poured into a separatory funnel. The organic layer was removed and the aqueous layer extracted with ether (3 x 30 mL). The combined organic extracts were washed with water (10 mL) and saturated brine (10 mL). The solution was dried (MgSO$_4$), filtered, and the solvent removed by rotary evaporation to yield a brown solid, which was purified by column chromatography (SiO$_2$; CH$_2$Cl$_2$/MeOH 99:1) to yield nitrile **6.3.3** (1.28g, 78 %) as a white solid, R$_f$ 0.5 (CH$_2$Cl$_2$/MeOH 20:1). ^{1}H NMR (600 MHz, CDCl$_3$) δ 3.72 (s, 3H); 6.31 (d, J = 12 Hz, 1H); 6.99 (br s, 1H); 7.13 (br s, 1H); 7.17 (d, J = 12 Hz, 1H), ESIMS m/z: calcd for C$_7$H$_7$N$_3$, 133; found M+H$^+$ 134.
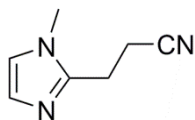
Synthesis of 3-(1-methyl-1H-imidazol-2-yl)propanenitrile 6.3.4: Magnesium turnings (1.5 g) were added to a 100 mL round-bottomed flask containing a cooled (0 ºC) solution of nitrile **6.3.3** (170 mg, 1.28 mmol) in dry MeOH (15 mL) and the reaction allowed to warm slowly to ambient temperature. After 16 h stirring, the reaction was cooled to 0 ºC and the excess Mg quenched by slow, dropwise addition of 6 N HCl (40 mL) with rapid stirring over a period of 1 h. The solution was neutralized with NaOH and NaHCO$_3$ to pH ~8. CH$_2$Cl$_2$ (100 mL) was added and the mixture poured into a separatory funnel. The organic layer was removed and the aqueous layer extracted with CH$_2$Cl$_2$ (3 x 20 mL). The combined organic extracts were washed with water (20 mL) and saturated brine (20 mL). The solution was dried (MgSO$_4$), filtered, and the solvent removed by rotary evaporation to yield a brown oil, which was purified by column chromatography (SiO$_2$; CH$_2$Cl$_2$/MeOH 99:1) to yield nitrile **6.3.4** (135 mg, 80 %) as a white solid, R$_f$ 0.5 (CH$_2$Cl$_2$/MeOH 20:1). ^{1}H NMR (600 MHz, CDCl$_3$) δ 2.87 (d, J = 7.2 Hz, 2H); 3.00 (d, J = 7.2 Hz, 2H); 3.61 (s, 3H); 6.83 (br s, 1H); 6.95 (br s, 1H), ESIMS m/z: calcd for C$_7$H$_9$N$_3$, 135; found M+H$^+$ 136.
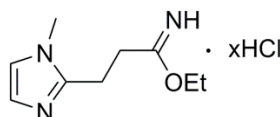
Synthesis of ethyl-3-(1-methyl-imidazol-2-yl)propanimidate hydrochloride 6.3.5: To a flame-dried 2-necked flask equipped with stirrer and septum under argon atmosphere

was added nitrile **6.3.4** (100 µL), anhydrous ethanol (200 µL, Aldrich, dried with 4Å molecular sieves) and 4 N HCl in dioxane (3 mL, Aldrich, anhydrous) at 0 ℃. The flask was sealed and stirred at ambient temperature for 12 h. The solvent was removed in vacuo and the product *immediately* used in the next step. ^{1}H NMR (600 MHz, DMSO-d_6) δ 1.17 (t, $J = 7.2$ Hz, 3H); 2.93 (t, $J = 7.2$ Hz, 2H); 3.15 (t, $J = 7.2$ Hz, 2H); 3.80 (s, 3H); 4.06 (q, $J = 7.2$ Hz, 2H); 7.56 (d, $J = 4$ Hz, 1H); 7.60 (d, $J = 4$ Hz, 1H).
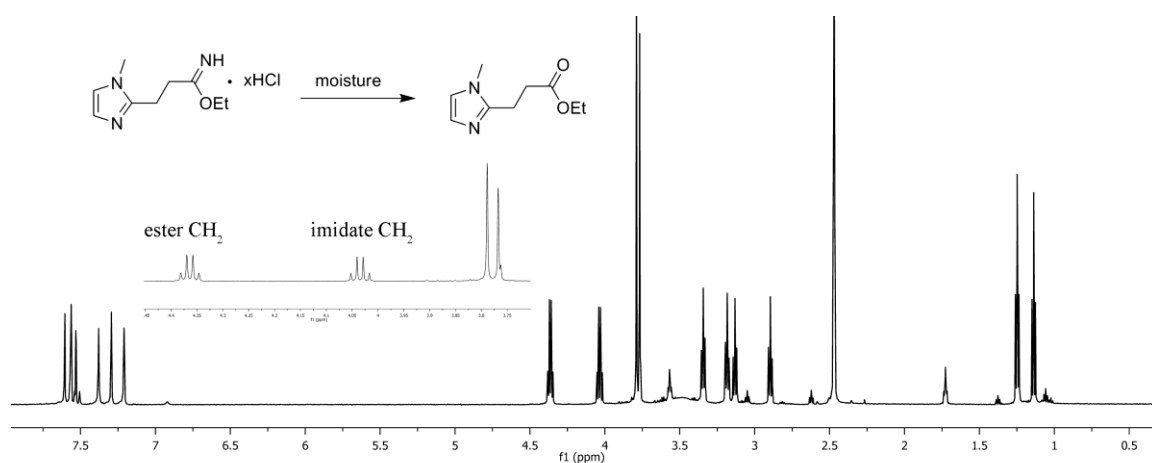
Figure 6.1. Decomposition of imidate (^{1}H NMR spectrum, 600 MHz, DMSO-d_6).
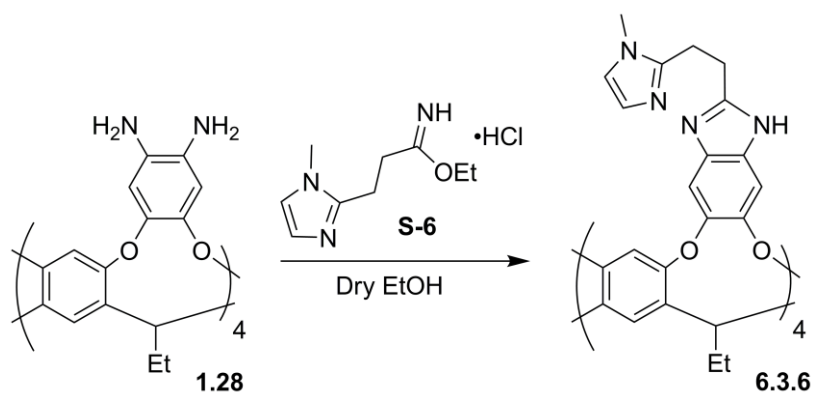
217
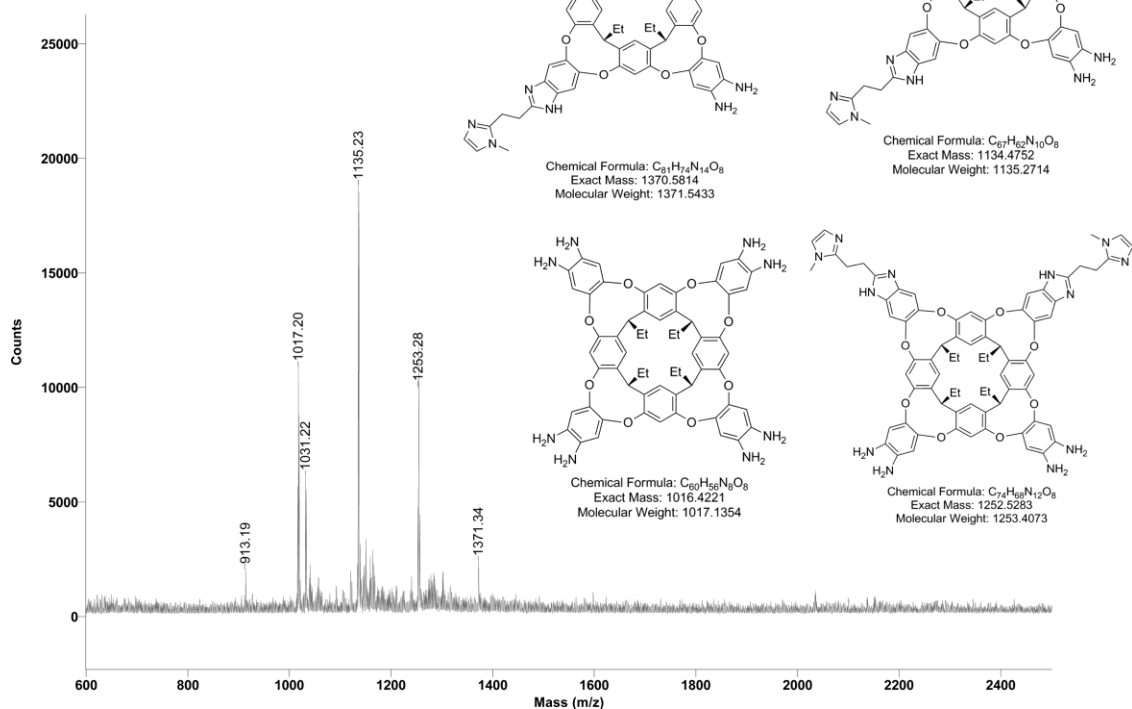
Figure 6.2. Mass spectrum (MALDI-TOF) of the products obtained upon attempted synthesis of symmetrical 4-walled cavitand **6.3.6.**
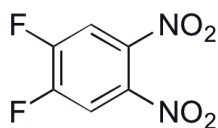
Synthesis of 1,2-Difluoro-4,5-dinitrobenzene: (CAUTION: reaction conditions can cause explosion if heated too rapidly). A 2 L three-necked round bottom flask equipped with a reflux condenser, a large magnetic stir bar, containing 70 mL of fuming HNO_3 was placed in an ice bath (0 °C). Using an additional funnel, careful addition of 50 mL of

H$_2$SO$_4$ (95%) slowly over 1 h followed by the slow addition of 3,4-difluoro-nitrobenzene (25 g) over 20 min. The resulting mixture was stirred at room temperature for another 1 h. The flask was then placed in a sand bath and slowly heated to 65 °C over a period of 4 h (increments of 3 °C/15min). The reaction mixture was then stirred at 65 °C for 72 h. The flask was subsequently cooled to room temperature, and the content was poured SLOWLY with constant stirring over 500 mL of crushed ice resulting in the evolution of nitric oxides gas (toxic). The light blue needle-like solid product was then collected by vacuum filtration and washed with 500 mL of distilled water. The crude powder was recrystallized in hot EtOH, pure product then thoroughly dried under vacuum (12 h at room temperature) to yield 13.5 g of 1,2-difluoro-4,5-dinitrobenzene. ^{1}H NMR (400 MHz, CDCl$_3$): δ = 9.18 (2H, t, J = 7.5 Hz).

1.27 Octanitro Cavitands
R$_1$ = C$_{11}$H$_{23}$
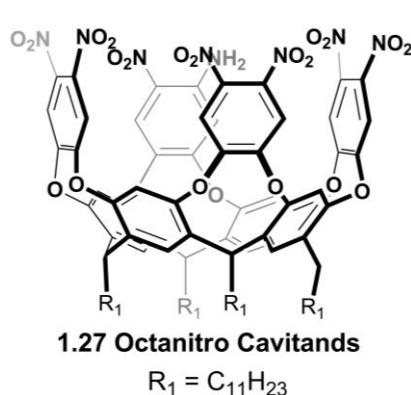
Synthesis of C$_{11}$-Octanitro Octanitro Cavitand 1.27: Following a previously reported procedure.[15] Undecyl-footed resorcinarene[16] (1.29 g, 1.16 mmol) was dissolved in 25 mL dimethylformamide before being treated with triethylamine (1.62 mL, 11.6 mmol). To this reaction mixture was added 4,5-difluoro-1,2-dinitrobenzene (1.0 g, 4.90

mmol). The reaction mixture was stirred at 65 ºC for 18 h before being cooled to room temperature and poured into 200 mL water. The yellow precipitate was collected by vacuum filtration and purified by flash chromatography using 3:1 CH_2Cl_2/hexanes as the eluent. A light yellow solid was isolated (1.0 g, 49 % yield). ^{1}H NMR (300 MHz, DMSO-d_6): δ 8.81 (s, 8H), 8.22 (s, 4H), 7.79 (s, 4H), 5.52 (t, $J = 7.9$ Hz, 4H), 2.36 (q, $J = 6.6$ Hz, 8H), 1.40-1.22 (m, 72H), 0.84 (t, $J = 6.3$ Hz, 12H).
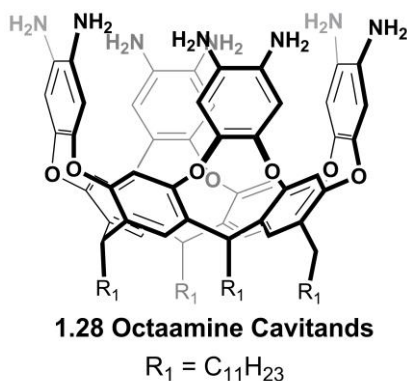
1.28 Octaamine Cavitands
$R_1 = C_{11}H_{23}$

Synthesis of C_{11} Octaamine Cavitand 1.28: Following a previously reported procedure:[17] To a suspension of octanitro cavitand (400 mg, 0.227 mmol) in ethanol (11.4 mL) and concentrated HCl (2.9 mL) was added SnCl$_2$•2H$_2$O (3.28 g, 14.54 mmol). The reaction mixture was stirred at 65 ºC for 18 h before cooling to room temperature and adding ca. 10 mL H$_2$O. An off-white precipitate was collected upon vacuum filtration. The precipitate was dried under vacuum and used without further purification. ^{1}H NMR (300 MHz, DMSO-d_6): δ 7.66 (s, 4H), 7.17 (s, 4H), 7.11 (s, 8H), 5.49 (t, $J = 8.0$ Hz, 4H), 2.36-2.17 (m, 8H), 1.46-1.13 (m, 72H), 0.85 (t, $J = 6.3$ Hz, 12H)

3.4 Thiobenzamidazole Cavitands
3.4: $R_1 = C_{11}H_{23}$
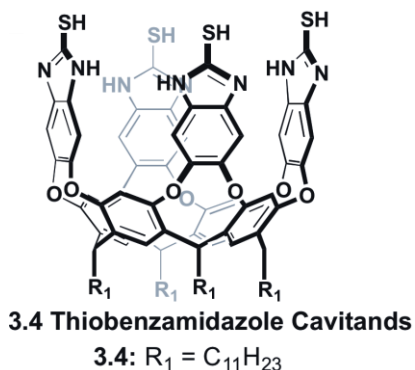
Synthesis of Thiobenzamidazole Cavitands 3.4: Following a previously reported procedure.[18] To a 50 mL round bottom flask equipped with a stir bar was added octaamine cavitand (500 mg, 0.50 mmol) and degassed carbon disulfite (0.15 mL, 2.16 mmol) with potassium hydroxide (120 mg, 2.16 mmol) in a mixture of 1:2 Ethanol:Water (30 mL). Reaction was heated over 18 h at 80 °C before cooling to room temperature. After cooling 5 mL of water and 10 mL acetic acid was added slowly and sonicated. Light orange precipitate was collected upon vacuum filtration (290 mg, 34 % yield) and used without further purification. ^{1}H NMR (400 MHz, DMSO-d_6 at 350 K) δ 11.8 (br s, 8 H, NH), 7.51 (s, 4 H, arom), 7.5 (s, 4 H, arom), 7.35 (s, 8 H, arom) 5.38 (t, 4 H, J= 7.5 Hz, CH-methine), 2.25 (m, 8 H, alkyl), 1.20 (m, 72H, alkyl), 0.83 (t, 12 H, J= 7.5 Hz, CH3), ^{13}C NMR (125 MHz, DMSO-d_6 at 350 K) δ 169.8, 154.5, 146.9, 133.8, 129.1, 124.4, 115.4, 104, 30.8, 28.7, 28.6, 28.5, 28.3, 21.6, 13.3.
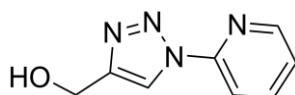
Synthesis of Methanol-triazolpyridine 6.3.7: 2-azidopyridine (500 mg, 4.16 mmol), propargyl alcohol (0.72 mL, 12.48 mmol), CuSO₄•5H₂O (103 mg, 0.412 mmol), L-

sodium ascorbate (225 mg, 1.13 mmol), and BIm$_3$ (171 mg, 0.412 mmol) were combined in a 1:1 mixture of ^{t}BuOH and water. The reaction mixture was stirred for 18 h at 80 ºC before removing the solvent and dissolving in CH$_2$Cl$_2$ and washing with an aqueous solution of Na$_2$EDTA to remove any copper present. The organic layer was dried with Na$_2$SO$_4$, filtered and the solvent was removed to yield a tan solid (76 %). ^{1}H NMR (300 MHz, DMSO-d_6): δ 8.64 (s, 1H), 8.57 (dt, J = 4.9, 1.3 Hz, 1H), 8.13 − 8.03 (m, 2H), 7.66 − 7.43 (m, 1H), 5.34 (t, J = 5.7 Hz, 1H), 4.63 (d, J = 5.8 Hz, 2H). ^{13}C NMR (75 MHz, DMSO-d_6): δ 149.1, 148.9, 148.6, 140.0, 124.1, 119.6, 113.6, 54.9. ESI MH$^+$ m/z expected 177.0771, found 177.0779.
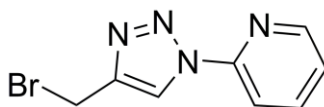
Synthesis of Bromomethyl-triazolylpyridine 3.6: Methanol-triazolylpyridine **6.3.7** (176 mg, 1.0 mmol) was suspended in 7 mL CH$_2$Cl$_2$ before adding PBr$_3$ (103 μL, 1.1 mmol). The reaction mixture was stirred for 2 h before removing solvent and adding water and sonicating to crash out the product. Beige solid was collected by vacuum filtration (85 %). ^{1}H NMR (300 MHz, CDCl$_3$) δ 8.62 (s, J = 33.8 Hz, 37H), 8.51 (s, 1H), 8.19 (d, J = 7.9 Hz, 36H), 7.99 − 7.86 (m, 40H), 7.37 (dd, J = 7.1, 5.1 Hz, 38H), 4.66 (s, 85H). ^{13}C NMR (100 MHz, CDCl$_3$): δ 149.0, 148.7, 145.1, 139.3, 123.9, 120.4, 113.9, 21.5. ESI MH$^+$ m/z expected 238.9927, found 239.0032.

3.5a: R₁ = C₁₁H₂₃, R₂ =
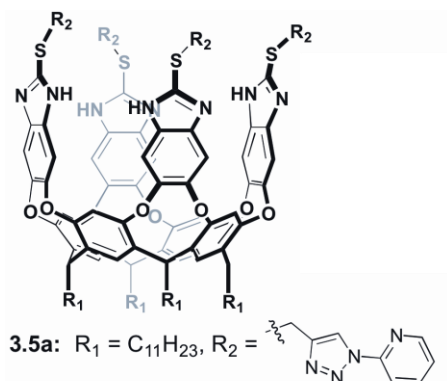
Synthesis of the Functionalized Thiobenzimidazole 3.5a: In 50 mL round bottom flask equipped with a stir bar was added thiobenzamidazole cavitands **3.4** (936 mg, 0.55 mmol) and 2 mL of DBU in 100 mL of THF. Reaction was stir at room temperature for 5 min followed by the addition of bromide substrates bromomethyl-triazolpyridine **3.6** (1.05 g, 4.43 mmol) slowly to the mixture. After complete addition, the reaction was heated to 80 C over 24 h. THF was removed by rotary evaporation and precipitate was suspended in ethyl acetate for purification. A tan colored precipitated was collected upon vacuum filtration (93% yield). ^{1}H NMR (400 MHz, CDCl$_3$ and 5% DMSO-d_6 at 350 K) δ 8.61 (s, 8H), 8.39 (d, J = 5.0 Hz, 4H), 7.98 (d, J = 8.5 Hz, 4H), 7.91 − 7.76 (t, J = 8.1 Hz, 4H), 7.73 (s, 8H), 7.56 (s, 4H), 7.19 (s, 4H), 5.73 (t, J = 8.1 Hz, 4H) 2.25 (m, 8 H), 1.20 (m, 72H), 0.83 (t, 12 H, J= 7.5 Hz). ^{13}C NMR (125 MHz, CDCl$_3$ and 5% DMSO-d_6 at 350 K) δ 190.5, 166.3, 156.2, 148.9, 139.3, 135.8, 120.7, 113.8, 77.7, 77.4, 77.0, 54.7, 48.9, 38.2, 32.6, 32.1, 29.9, 29.6, 29.1, 28.3, 26.9, 24.1, 22.9, 19.6, 14.3.
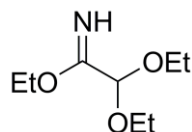
Synthesis of Ethyl-2,2-diethoxyethanimidate: Sodium metal (92 mg, 4.0 mmol) was dissolved in 4 mL anhydrous ethanol before adding diethoxyacetonitrile (556 μL, 4.0 mmol). The reaction mixture was stirred at room temperature overnight before removing the solvent, diluting in CH_2Cl_2, and washing with water. The aqueous layer was extracted 3 times with CH_2Cl_2 and the combined organic layers were dried with Na_2SO_4, filtered and the solvent was removed under reduced pressure to yield 252 mg of a clear oil (36 %). ^{1}H NMR (400 MHz, CDCl$_3$): δ 7.84 (s, 1H), 4.77 (s, 1H), 4.22 (q, J = 7.1 Hz, 2H), 3.84-3.33 (m, 4H), 1.32 (t, J = 7.1 Hz, 3H), 1.23 (t, J = 7.0 Hz, 6H). ^{13}C NMR (100 MHz, CDCl$_3$): δ 168.2, 96.4, 62.0, 61.8, 15.2, 14.3. ESI MH$^+$ m/z expected 176.2329, found 176.1298.

3.7 Octaethylacetal Cavitands
$R_1 = C_{11}H_{23}$
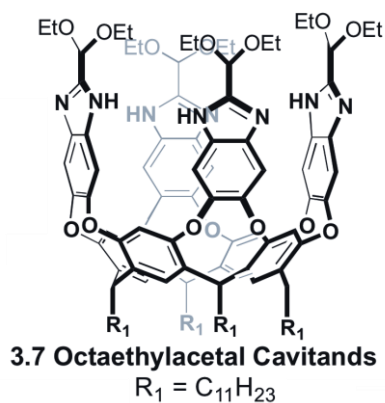
Synthesis of C$_{11}$-Octaethylacetal Cavitands 3.7: Following a previously reported procedure:[5] Octamine cavitand **1.8a** (175 mg, 0.104 mmol) and ethyl-2,2-diethoxyethanimidate (148 mg, 8.4 mmol) were combined in 3 mL anhydrous ethanol before adding trifluoroacetic acid (151 μL, 1.96 mmol). The reaction mixture was stirred

at 70 ºC for 18 h before cooling to 0 ºC and collecting precipitate by vacuum filtration and washed with hexanes to remove excess imidate. A peach precipitate was obtained (158 mg, 77 % yield). ^{1}H NMR (400 MHz, CDCl$_3$): δ 7.94 (s, 8H), 7.47 (s, 4H), 7.20 (s, 4H), 5.71 (t, J = 8.0 Hz, 4H), 5.67 (s, 4H), 3.78-3.46 (m, 16H), 2.22 (q, J = 5.7 Hz, 8H), 1.56-1.07 (m, 96H), 0.89 (t, J = 6.6 Hz, 12H). ^{13}C NMR (100 MHz, CDCl$_3$): δ 155.6, 151.9, 150.3, 135.7, 130.3, 123.8, 116.4, 110.1, 94.8, 63.1, 33.5, 32.4, 32.1, 29.9, 29.6, 28.2, 22.9, 15.1, 14.3.
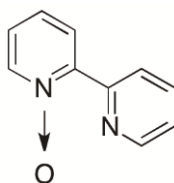
Synthesis of 2,2'-Bipyridine-*N*-oxide: Following a previously reported procedure.[19] 2,2'-bipyridine (1g, 6.4 mmol) was dissolved in trifluoroacetic acid (4.9 mL, 64.0 mmol) before adding H$_2$O$_2$ (30 % in H$_2$O, 1.1 mL, 9.6 mmol). The reaction mixture was stirred for 2 h before neutralizing with 6 M NaOH and extracting with CHCl$_3$ (4 x 10 mL). The combined organic layers were washed with brine, dried with Na$_2$SO$_4$, filtered and the solvent was removed under reduced pressure. The crude product was placed under vacuum to obtain 716 mg of a white solid (65 %). ^{1}H NMR (400 MHz, CDCl$_3$) δ 8.90 (dt, J = 8.1, 1.0 Hz, 1H), 8.73 (ddd, J = 4.8, 1.7, 0.9 Hz, 1H), 8.32 (dd, J = 6.5, 1.1 Hz, 1H), 8.19 (dd, J = 8.0, 2.1 Hz, 1H), 7.84 (td, J = 7.8, 1.8 Hz, 1H), 7.42 − 7.33 (m, 2H), 7.28 (dt, J = 4.9, 2.9 Hz, 1H).
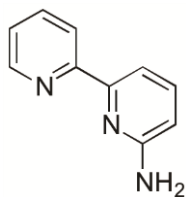
Synthesis of 6-Amino-2,2′-bipyridine: Following a previously reported procedure.[20] 2,2′-bipyridine-*N*-oxide (710 mg, 4.12 mmol) was dissolved in toluene (40 mL). The reaction mixture was cooled to 0 ℃ before adding ^{t}BuNH$_2$ (2.28 mL, 21.9 mmol) followed by *p*-toluenesulfonyl chloride (1.81 g, 9.48 mmol). The reaction mixture was stirred for 24 h before adding 40 mL trifluoroacetic acid and heating to 70 ℃. Stirring was continued at 70 ℃ for 24 h before removing the solvent and diluting with CH$_2$Cl$_2$ and quenching with saturated aqueous NaHCO$_3$ until pH of 8-9 was reached. The aqueous layer was extracted with CH$_2$Cl$_2$ (5 x 15 mL). The combined organic layers were washed with brine, dried with Na$_2$SO$_4$, filtered and the solvent was removed to yield a red precipitate. The crude product was dissolved in methyl-*tert*-butylether and decanting off solution leaving behind the solid. HCl solution (2 M in Et$_2$O, 4 mL, 8 mmol) was added to the solution and the precipitate was collected and washed with methyl-*tert*-butylether. The precipitate was dissolved in CH$_2$Cl$_2$ and washed with saturated aqueous NaHCO$_3$ solution. The aqueous layer was extracted with CH$_2$Cl$_2$ (4 x 15 mL) and the combined organic layers were dried with Na$_2$SO$_4$, filtered and the solvent was removed yielding a red precipitate. The product was purified by silica gel flash chromatography eluting with CH$_2$Cl$_2$ followed by 1 % MeOH in CH$_2$Cl$_2$. A light brown solid was obtained (173 mg, 25 %). ^{1}H NMR (400 MHz, CDCl$_3$): δ 8.66 (ddd, *J* = 4.8, 1.7, 0.9 Hz, 1H), 8.27 (dt, *J* = 8.1, 1.0 Hz, 1H), 7.78 (td, *J* = 7.8, 1.8 Hz, 1H), 7.71 (dd, *J* = 7.4, 0.5

Hz, 1H), 7.58 (dd, J = 9.7, 5.9 Hz, 1H), 7.27 (ddd, J = 7.5, 4.8, 1.1 Hz, 1H), 6.56 (dd, J = 8.2, 0.5 Hz, 1H), 4.66 (s, 2H).

General Procedure 6.3.8: Synthesis of aryl-imine cavitands

3.7 (1 eq.), aryl amine (6 eq.), and La(OTf)$_3$ (40 mol %) were combined in toluene. The reaction mixture was stirred for 18 h at 110 ℃ before removing the solvent under reduced pressure and sonicating in ether to remove excess arylamine. Pure product was collected upon vacuum filtration.

General Procedure 6.3.9: Synthesis of alkyl-imine cavitands *via* transimination:

Aryl-imine cavitand (1 eq.) and alkylamine (5 eq.) were combined in CH$_2$Cl$_2$ (1 mL) and stirred for 2 min before removing the solvent under reduced pressure. The crude precipitate was sonicated in diethyl ether to remove excess alkylamine and the byproduct, 2-aminopyridine or 6-amino-2,2'-bipyridine. Pure product was collected upon vacuum filtration.

3.9: R$_1$= C$_{11}$H$_{23}$,
R' = 6-(2,2'-bipyridine) (86%)
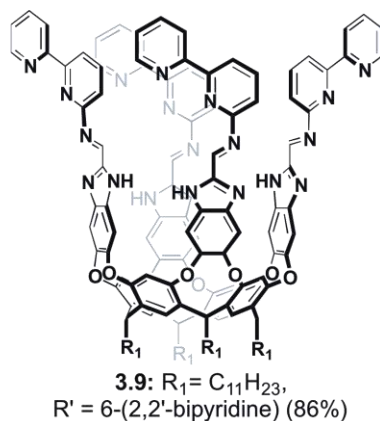
Synthesis of 6-(2,2'-bipyridine) Cavitand 3.9: Following general procedure **6.3.8**: Tetradiethoxy acetal cavitand **3.7** (122 mg, 0.062 mmol), 6-amino-2,2'-bipyridine (64 mg, 0.371 mmol) and La(OTf)$_3$ (11 mg, 0.025 mmol) were combined in a 20 mL high pressure vessel and stirred for 18 h. A red orange precipitate was obtained (122 mg, 86 % yield). ^{1}H NMR (400 MHz, CDCl$_3$ and 5% DMSO-d_6): δ 8.63 (d, J = 4.4 Hz, 4H), 8.09 (d, J = 8.0 Hz, 4H), 7.98 (s, 4H), 7.79 (t, J = 7.7 Hz, 4H), 7.72 – 7.63 (m, 4H), 7.46 (s, 4H), 7.38-7.32 (m, 8H), 7.16 (s, 4H), 6.98 (d, J = 8.7 Hz, 4H), 5.60 (t, J = 7.4 Hz, 4H), 2.19 (q, J =5.4 Hz, 8H), 1.36-1.16 (m, 72H), 0.80 (t, J = 7.0 Hz, 12H). ^{13}C NMR (125 MHz, CDCl$_3$ and 5% DMSO-d_6): δ 156.4, 155.9, 150.9, 150.2, 149.5, 147.2, 141.8, 137.5, 136.5, 135.5, 124.9, 123.6, 122.1, 120.9, 117.1, 112.6, 110.0, 33.6, 32.6, 32.2, 30.0, 29.6, 28.4, 22.9, 14.3. MS (MALDI) m/z 2286.1 (MH)$^+$, expected m/z 2286.18 (MH)$^+$. ATR FT-IR: 2923.1, 2853.0, 1661.7, 1605.3, 1485.9, 1429.5, 1455.9, 1402.5, 1330.0, 1270.4, 1028.7, 993.8, 887.5, 810.3, 774.8, 661.4.
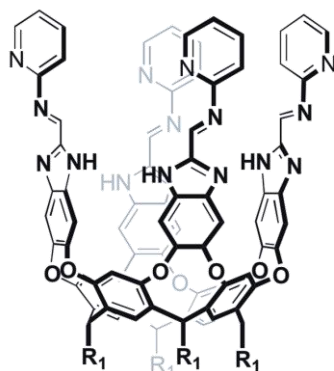
3.8: R' = 2-pyridine
3.8a: R$_1$= C$_{11}$H$_{23}$ (77%)

Synthesis of Pyridine Cavitand 3.8: Following general procedure **6.3.8**: Diethoxy acetal cavitand **3.7** (150 mg, 0.076 mmol), 2-aminopyridine (43 mg, 0.457 mmol) and La(OTf)$_3$ (13 mg, 0.030 mmol). A red orange precipitate was obtained (116 mg, 77 % yield). ^{1}H NMR (400 MHz, CDCl$_3$ and 5 % DMSO-d_6): δ 7.66 (d, 4H), 7.60 (br t, 8H), 6.87 (d, J = 8.9 Hz, 4H), 6.61 (t, J = 5.6 Hz, 4H), 5.56 (br s, 4H), 2.16 (br s, 8H), 1.43-1.13 (m, 72H), 0.81 (br 12H). ^{13}C NMR (125 MHz, CDCl$_3$ and 5 % DMSO-d_6): δ 207.2, 156.1, 152.3, 149.7, 148.9, 137.1, 135.6, 123.5, 117.1, 53.6, 43.2, 32.2, 31.1, 30.0, 29.7, 28.41, 22.93, 14.3. MS (ESI) m/z 1971 (MH)$^+$, expected m/z 1979.0 (MH)$^+$ ATR FT-IR: 2924.6, 1662.7, 1457.2, 1158.8, 1927.5, 885.1, 722.5, 661.1.
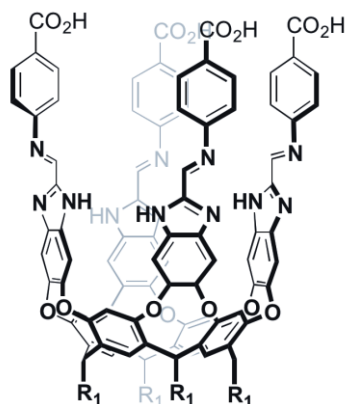
3.10: R₁= C₁₁H₂₃,
R' = p-C₆H₄CO₂H (70%)

Synthesis of Carboxyphenyl Cavitand 3.10: Following general procedure **6.3.8**: Tetradiethoxy acetal cavitand **3.7** (50 mg, 0.025 mmol), *p*-aminobenzoic acid (26 mg, 0.20 mmol) and La(OTf)$_3$ (6 mg, 0.010 mmol) were combined in a 1 mL toluene in a 10 mL high pressure vessel and stirred for 18 h. A red orange precipitate was obtained (38 mg, 70 % yield). ^{1}H NMR (300 MHz, CDCl$_3$ and 5 % DMSO-d_6): δ 8.10 (t, *J* = 7.7 Hz, 4H), 7.84 (d, *J* = 7.7 Hz, 8H), 7.46 (s, 4H), 7.24 (s, 4H), 6.61 (d, *J* = 6.9 Hz, 8H), 5.73 (t, *J* = 8.3 Hz, 4H), 2.26 (q, *J* = 6.9 Hz, 8H), 1.44-1.10 (m, 72H), 0.87 (t, *J* = 6.9 Hz, 12H). ^{13}C NMR (125 MHz, CDCl$_3$ and 5 % DMSO-d_6) δ 168.9, 155.4, 151.3, 135.5, 131.6, 123.8, 121.6, 119.4, 113.4, 96.3, 67.8, 66.9, 33.3, 31.8, 29.6, 29.6, 29.2, 28.0, 25.5, 22.5, 14.9, 14.0. MS (ESI) *m/z* 2148 (MH)$^+$, expected *m/z* 2150 (MH)$^+$.

3.11: R$_2$ = -CH$_2$-(2-pyridyl)
(73%)
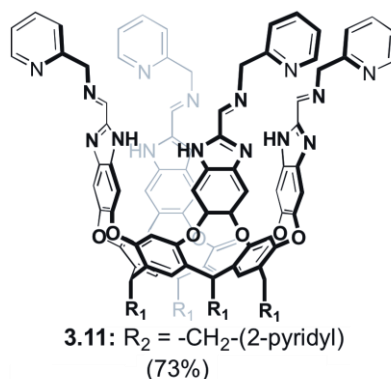
Synthesis of Alkyl Pyridine Cavitand 3.11: Following general procedure **6.3.9**: Tetra-bipyridyl Cavitand **3.9**, (135 mg, 0.059 mmol), 2-picolylamine (30 µL, 0.35 mmol) and 3 mL CH$_2$Cl$_2$. Obtained 86 mg precipitate (73 % yield). ^{1}H NMR (600 MHz, CDCl$_3$ and 5 % DMSO-d_6): δ 8.44 (br s, 4H), 7.99-7.58 (br, 12H), 7.26-7.12 (m, 20H), 5.70 (br, 4H), 4.02 (s, 8H), 2.24 (br, 8H), 1.46-1.20 (m, 72H), 0.82 (t, J = 6.3 Hz, 12H). ^{13}C NMR (150 MHz, CDCl$_3$ and 5 % DMSO-d_6) δ 152.3, 151.0, 144.2, 132.1, 130.7, 117.9, 117.2, 111.9, 108.2, 103.9, 35.7, 35.6, 35.4, 35.3, 35.1, 35.0, 28.8, 27.1, 25.0, 24.6, 23.5, 17.9, 10.5, 9.5. MS (ESI) m/z 2033 (MH)$^+$, expected m/z 2034 (MH)$^+$.

3.12: R' = -(CH₂)₂NMe₂
(81%)
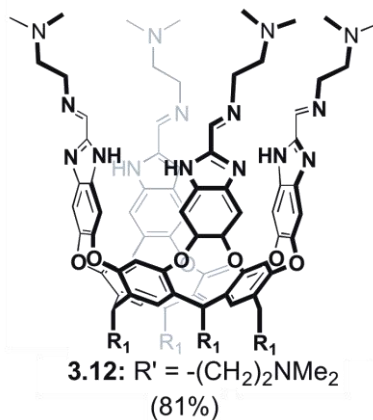
Synthesis of *N,N*-dimethylethyleneimine Cavitand 3.12: Following general procedure **6.3.9**: Tetra-bipyridyl cavitand **3.9** (20 mg, 0.0087 mmol), *N,N*-dimethylethylenediamine (5 µL, 0.044 mmol) and 1 mL CH₂Cl₂. Obtained 12 mg precipitate (81 % yield). ¹H NMR (500 MHz, CDCl₃ and 5 % DMSO-d_6): δ 7.82 (s, 4H), 7.68 (s, 8H), 7.49 (s, 4H), 7.21 (s, 4H), 5.57 (t, *J* = 8.0 Hz, 4H), 2.90 (br s, 8H), 2.68 (br s, 8H), 2.47 (br s, 8H), 2.17 (s, 24H), 1.44-1.18 (m, 72H), 0.77 (t, *J* = 5.9 Hz, 12H). ¹³C NMR (125 MHz, CDCl₃) δ 155.8, 149.6, 137.7, 135.0, 123.4, 116.7, 113.4, 108.8, 67.8, 56.1, 53.5, 44.9, 37.0, 33.3, 31.8, 29.6, 29.3, 28.0, 25.5, 22.5, 14.0. MS (MALDI) *m/z* 2010.3 (MH)⁺, expected *m/z* 2011.33 (MH)⁺. ATR FT-IR: 3410.9, 2254.2, 2128.1, 1658.1, 1266.5, 1159.0, 1014.8, 1023.23, 760.9.
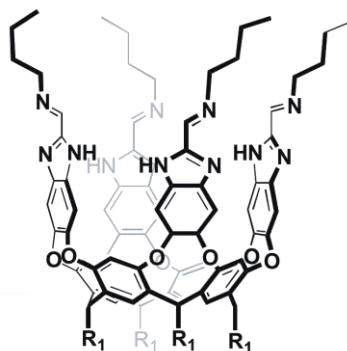
3.13: $R_2 = n\text{-}C_4H_9$ (89%)

Synthesis of *n*-butylimine Cavitand 3.13: Following general procedure **6.3.9**: **3.9** (50 mg, 0.022 mmol), *n*-butylamine (11 μL, 0.11 mmol) and 1 mL CH_2Cl_2. Obtained 20 mg precipitate (89 % yield). ^1H NMR (500 MHz, $CDCl_3$ and 2 % DMSO-d_6): δ 7.82 (s, 8H), 7.54 (s, 4H), 7.15 (s. 8H), 5.71 (br s, 4H), 3.02 (br s, 8H), 2.22 (br s, 8H), 1.72 (br s, 8H), 1.43-1.20 (m, 80H), 0.88 (m, 24H). ^{13}C NMR (125 MHz, $CDCl_3$ 2 % DMSO-d_6) δ 159.5, 155.6, 147.8, 137.3, 135.1, 124.4, 116.6, 112.7, 108.5, 40.6, 40.4, 40.3, 40.1, 33.5, 31.8, 30.2, 29.8, 29.6, 29.3, 28.2, 22.6, 19.7, 14.2, 14.0, 13.7. MS (ESI) *m/z* 1893 (MH)$^+$, expected *m/z* 1895 (MH)$^+$.

6.4. Chapter 4 Experimental.
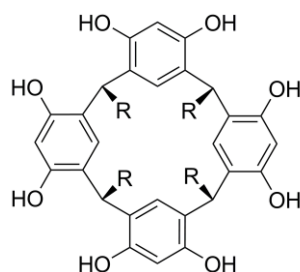
1.24 Resorcinarene
b: $R = CH_2CH_3$

Synthesis of Resorcinarene C$_2$-cavitand 1.24b: To a 500 mL round bottom flask equipped with a stir bar was added resorcinol (25 g, 237 mmol) and DMF (18 mL, 1 mol) in ethanol (200 mL) with concentrated hydrochloride acid (50 mL). Mixture was stir at

70 ℃ for 96 hours under nitrogen atmospheres. Reaction was quickly poured into 200 mL of H_2O then filter with vacuum filtration. Product was then suspended in H_2O and refiltered. For purification, the product was recrystallized in hot ethanol to yield 18.5 g, 73% yield.[21]
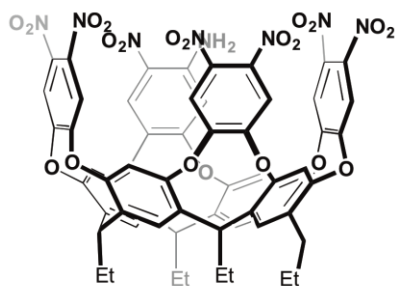
1.27 Octanitro Cavitands

Synthesis of C₂-Octanitro Octanitro Cavitand 1.27: Following a previously reported procedure.[15] Resorcinarene **1.24b** (3 g, 5 mmol) was dissolved in 250 mL dimethylformamide before added 4,5-difluoro-1,2-dinitrobenzene (4.0 g, 2.0 mmol). The reaction mixture was then treated with triethylamine drop wise (11.2 mL, 80.4 mmol). The reaction mixture was stirred at 65 ℃ for 18 h before being cooled to room temperature and poured into 200 mL 1M HCl. The yellow precipitate was collected by vacuum filtration and purified by sonication in dichloromethane four times. A light yellow solid was isolated (1.8 g, 50 % yield). ¹H NMR (300 MHz, DMSO-d_6): δ 8.80 (s, 8H), 8.30 (s, 4H), 7.81 (s, 4H), 5.52 (t, J = 7.9 Hz, 4H), 2.36 (q, J = 6.6 Hz, 8H), 0.84 (t, J = 6.3 Hz, 12H).
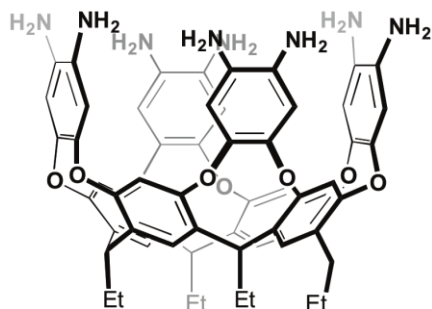
1.28 Octaamine Cavitands

Synthesis of C$_2$ Octaamine Cavitand 1.28: Following a previously reported procedure:[17] To a suspension of octanitro cavitand **1.27** (300 mg, 0.237 mmol) in ethanol (21.5 mL) and concentrated HCl (6 mL) was added SnCl$_2$•2H$_2$O (2.56 g, 11.34 mmol). The reaction mixture was stirred at 65 °C for 18 h before cooling to room temperature and adding only 6 mL H$_2$O. An off-white precipitate was collected upon vacuum filtration. The precipitate was dried under vacuum and used without further purification. ^{1}H NMR (300 MHz, DMSO-d_6): δ 7.66 (s, 4H), 7.17 (s, 4H), 7.11 (s, 8H), 5.49 (t, J = 8.0 Hz, 4H), 2.36-2.17 (m, 8H), 0.85 (t, J = 6.3 Hz, 12H).
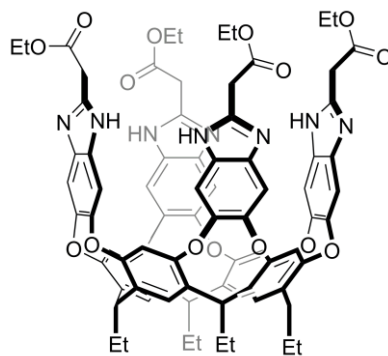
4.1 Tetraester Cavitand

Synthesis of Tetraester Cavitand 4.1: Following a previously reported procedure:[17] The cavitand C$_2$-octaamine **1.28** (280 mg, 0.24 mmol) and the imidate (380 mg, 1.95

mmol) were combined in anhydrous 6 mL EtOH and heated at reflux overnight under N_2 atmosphere. The mixture was cooled to room temperature, concentrated with rotary evaporator, and suspended in 10 mL dichloromethane. The suspension was filtered and washed with 3 times with DCM. The solid was dried under high vacuum for 48 h to yield the product as a off white colored solid (147 mg, 43%). ^{1}H NMR (THF-d_8:D_2O = 2:1, 600 MHz): δ 1.36 (t, 12H, J = 7.2 Hz), 1.60 (t, 12H, J = 7.2 Hz), 2.71 (dqr, 8H, J = 8.2, 7.2 Hz), 4.57 (qr, 8H, J = 7.2 Hz), 6.00 (t, 4H, J = 8.2 Hz), 7.80 (s, 4H), 8.15 (s, 4H), 8.40 (s, 8H). ^{13}C NMR (THF-d_8:D_2O = 2:1, 150 MHz): δ 12.8, 14.1, 25.8, 36.2, 62.7, 67.9, 110.0, 117.4, 124.4, 132.0, 136.1, 149.3, 151.4, 156.8, 168.4.
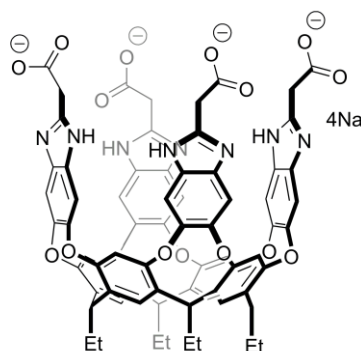
4.2 tetracarboxylate Cavitand

Synthesis of Tetraester Cavitand 4.2: Following a previously reported procedure:[17] (102 mg, 0.073 mmol) was dissolved in a mixture of THF (9 mL) and water (6 mL), and NaOH (96 mg, 2.4 mmol) was added as a solid. After the mixture was stirred for 1 h, a precipitate had formed. Additional water (1 mL) gave a clear solution, and stirring was continued at room temperature for 73 h. The THF was slowly removed from the solution by rotary evaporation (100rph, -25BAR) over the course of 1 h, allowing a cohesive

precipitate to form (faster evaporation gives material that is too fine to allow filtration). The solid was collected by filtration and dried under high vacuum to give the product as off white solid (79 mg, 79%). ^{1}H NMR (D$_2$O, 400 MHz): δ 1.17 (t, 12H, J = 7.0 Hz), 2.47 (dqr, 8H, J = 8.2, 7.0 Hz), 3.84 (s, 8H), 5.82 (t, 4H, J = 8.2 Hz), 7.51 (s, 4H), 7.83 (s, 4H), 7.92 (s, 8H). ^{13}C NMR (D$_2$O, 125 MHz): δ 12.5, 25.6, 35.8, 38.3, 117.3, 123.4, 135.4, 148.7, 154.0, 156.6, 175.4.
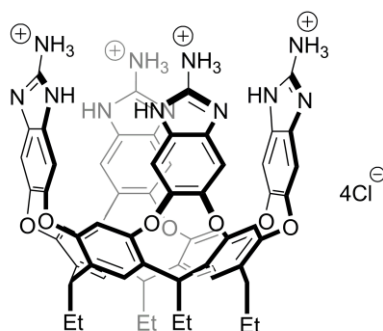
4.9 2-aminobenzimidazole Cavitands

Synthesis of Aminobenzimidazole Cavitand 4.9: Following a procedure slightly modified from published methods:[22] Octaamine cavitand **1.28** (454 mg, 0.44 mmol) in EtOH was stirred for 15 min at room temperature under N$_2$ atmosphere. A solution of cyanogen bromide (300 mg, 2.83 mmol) in EtOH was added drop wise over 15 min. The reaction mixture was stirred for 24 h at room temperature. The mixture was then cooled to 0 °C and basified to pH ~9. Solvent was removed by rotatory evaporation. The solid was redissolved in MeOH and 2 drop of 1M HCl was added, a white precipitate was formed. The cavitand was obtained as light red solid (232 mg, 45% yield). ^{1}H NMR (500 MHz, DMSO-d_6), δ: 12.1 (s, 8H), 8.7 (s, 8H), 7.79 (s, 4H), 7.74 (s, 8H), 7.65 (s, 4H), 5.33 (t, J = 7.8 Hz, 4H), 2.24 (m, 8 H), 0.85 (t, J = 7.2 Hz, 12H); ^{13}C NMR (125 MHz,

DMSO-d_6) δ: 155.9, 152.0, 148.7, 135.6, 127.1, 125.3, 117.1, 107.4, 35.7, 25.2, 19.8, 12.4; m.p. > 300 ºC (decomp). MALDI-MS: $C_{64}H_{53}N_{12}O_8^+$ [M - 4Cl - 3H]$^+$: expected: 1117.4104; found: 1117.3110. Data is consistent with previous publication.
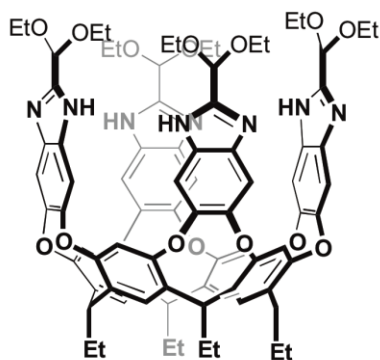
4.10 Octaethylacetal Cavitands

Synthesis of C2-Octaethylacetal Cavitands 4.10: Octamine cavitand **1.28** (400 mg, 0.34 mmol) and ethyl-2,2-diethoxyethanimidate (0.44 g, 25.0 mmol) were combined in 10 mL anhydrous ethanol before adding trifluoroacetic acid (34 μL, 1.96 mmol, 20 eq.) under N$_2$ atmosphere. The reaction mixture was stirred at 70 ºC for 18 h before cooling to -5 ºC for 24 h. The precipitate was collected by vacuum filtration and washed with ethanol to remove excess imidate. A peach precipitate was obtained (292 mg, 57 % yield). ^{1}H NMR (400 MHz, CDCl$_3$: 5% DMSO-d_6): δ 7.94 (s, 8H), 7.47 (s, 4H), 7.20 (s, 4H), 5.71 (t, J = 8.0 Hz, 4H), 5.67 (s, 4H), 3.78-3.46 (m, 16H), 2.22 (q, J = 5.7 Hz, 8H), 0.89 (t, J = 6.6 Hz, 12H). ^{13}C NMR (100 MHz, CDCl$_3$: 5% DMSO-d_6): δ 155.6, 151.9, 150.3, 135.7, 130.3, 123.8, 116.4, 110.1, 94.8, 63.1, 33.5, 32.4, 32.1, 14.3.

4.11
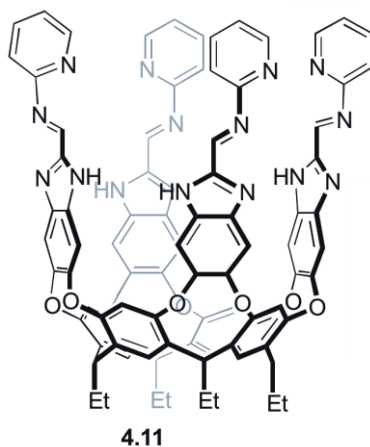
Synthesis of C₂-Pyridine Cavitand 4.11: Following modified general procedure **S3.1**: Diethoxy acetal cavitand **4.10** (150 mg, 1 eq. 0.102 mmol), 2-aminopyridine (60 mg, 8.2 eq. 0.82 mmol) and La(OTf)$_3$ (13 mg, 40 mol %, 0.041 mmol) were combined in toluene under N$_2$ atmosphere. The reaction mixture was stirred for 16 h at 110 ºC before collecting the crude product as yellow/orange solid by vacuum filtration. The precipitate was sonicating in ether to remove excess arylamine. A red orange precipitate was obtained (85 mg, 80 % yield). ^{1}H NMR (400 MHz, DMSO-d_6): δ 7.87 (d, 4H), 7.62 (br t, 8H), 7.10 (s, 2H), 6.77 (s, 2H), 6.72 (d, $J = 8.9$ Hz, 2H), 6.64 (t, $J = 5.6$ Hz, 2H), 5.30 (br t, 2H), 5.34 (br t, 2H), 2.38 (br s, 4H), 2.28 (br s, 4H), 0.92 (br s, 6H), 0.81 (br s, 6H). ^{13}C NMR (125 MHz, DMSO-d_6): δ 207.2, 156.1, 152.3, 149.7, 148.9, 137.1, 135.6, 123.5, 117.1, 53.6, 43.2, 32.2, 31.1, 30.0, 14.4.

4.14
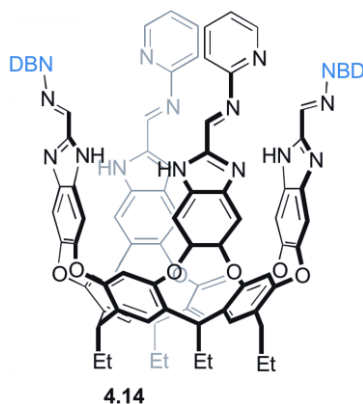
Synthesis of NBD-Pyridine Cavitand 4.14: Following general procedure **S3.2**: C$_2$-pyridine cavitand **4.11** (120 mg, 1 eq. 0.081 mmol), **4.12** (31 mg, 2 eq. 0.16 mmol) and 3 mL CH$_2$Cl$_2$. Obtained red precipitate (90 % yield). ^{1}H NMR (600 MHz, CDCl$_3$ and 5 % DMSO-d_6): δ 8.42 (d, $J = 8$ Hz, 2H), 7.88 (s, 2H), 7.62 (br t, 2H), 7.0 (d, $J = 8$ Hz, 2H), 6.88 (d, $J = 29$ Hz, 2H), 6.64 (t, $J = 5.6$ Hz, 2H), 5.62 (br t, 4H), 2.22 (q, $J = 5.7$ Hz, 8H), 0.89 (t, $J = 6.6$ Hz, 12H).

4.16 Thiobenzamidazole Cavitands

Synthesis of C$_2$-Thiobenzamidazole Cavitand 4.16: To a 50 mL round bottom flask equipped with a stir bar was added octaamine cavitand **1.28b** (500 mg, 0.50 mmol) and degassed carbon disulfite (0.15 mL, 2.16 mmol) with potassium hydroxide (120 mg, 2.16 mmol) in a mixture of 1:1 methanol:THF (10 mL). Reaction was heated over 18 h at 60 ºC. solvent was removed and precipitate was sonicate in 5 mL of water. A light red

240

precipitate was collected upon vacuum filtration 420 mg, 82 % yield. ^{1}H NMR DMSO-d_6

at 350 K; δ 11.8 (br s, 4 H), 7.51 (s, 4 H, arom), 7.5 (s, 4 H, arom), 7.35 (s, 8 H, arom)

5.38 (t, 4 H, J = 7.5 Hz). 2.25 (m, 8 H), 0.83 (t, 12 H, J = 7.5 Hz), ^{13}C NMR (150 MHz,

DMSO-d_6 at 350 K): δ. 172.2, 167.1, 155.3, 148.1, 135.5, 131.8, 129.6, 128.8, 125.4,

116.7, 116.1, 109.4, 67.6, 35.6, 35.4, 34.3, 29.9, 29.2, 28.5, 25.0, 23.4, 22.6, 21.3, 12.6.

6.5. Chapter 5 Experimental.

5.3
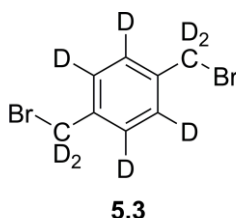
Preparation of Di-bromo Xylene-d_8: In a 50 mL flask equipped with stir bar, xylene-

d_8 (300 μl, 2.4 mmol), N-bromosuccinimide (960 mg, 5.4 mmol), and benzoyl peroxide

(60 mg, 0.2 mmol), was heated in 25 mL THF at 50 °C for 72 h. The precipitate

byproduct was then isolated off and discarded, as the solution was concentrated under

vacuum. The pure product was collected as a white powder (94 %). ^{2}H NMR (600 MHz,

CDCl$_3$) δ 7.50 (s, 4D), 4.61 (s, 4D).

5.4
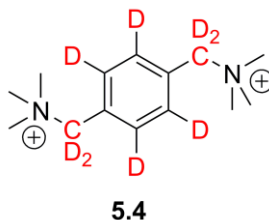
Synthesis of α, α'-dimethylammonium-p-xylene-d_8 5.4: 1,2,4,5-d_4, benzene 3,6-

bis(bromomethyl-d_2) **5.3** (100 mg, 0.37 mmol) was dissolved in dichloromethane (5 mL)

before adding trimethylamine (50 mg, 0.9 mmol) dropwise. The mixture was stir at 60 °C for 2 h. the white precipitate was collected by vacuum filtration. The crude product was placed under vacuum to obtain 80 mg of white solid (94% yield). ^{1}H NMR (400 MHz, D$_2$O) δ 3.14 (s, 18H). ^{2}H NMR (400 MHz, D$_2$O) δ 7.55 (s, 4H), 3.33 (s, 4H). ^{13}C NMR (100 MHz, D$_2$O) δ 133.1, 129.8, 52.7, 29.7.
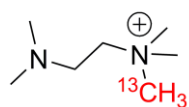
5.5

Synthesis of N, N, N, N', N' Pentamethyl-1,2-Ethanediaminium iodide-^{13}C 5.5: tetramethylethylenediamine (0.5 mL, 3.3 mmol) was dissolved in 1 mL of acetonitrile at 0 °C before addition of iodomethane-^{13}C (0.2 mL, 3.3 mmol) dropwise. Precipitate was collected by vacuum filtration to obtain 650 mg of white solid (76% yield). ^{1}H NMR (400 MHz, D$_2$O) δ 3.53 (t, 2H), 3.21 (t, J = 145 Hz, 9H, ^{13}C-^{1}H coupling), 2.90 (m, 2H), 2.33 (d, J = 1.6 Hz, 6H), ^{13}C NMR (100 MHz, D$_2$O) δ 54.3, 54.1, 53.5, 51.2, 44.3.
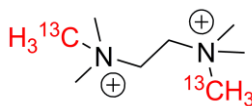
5.6

Synthesis of N, N, N, N', N', N' Hexamethyl-1,2-Ethanediaminium Diiodide-^{13}C 5.6: N, N, N, N', N' Pentamethyl-1,2-Ethanediaminium iodide-^{13}C (300 mg, 1.15 mmol) was dissolved in 1 mL of acetonitrile at 0 °C before addition of Iodomethane-^{13}C (0.1 mL, 1.2 mmol) dropwise. Precipitate was collected by vacuum filtration to obtain 256 mg of white solid (56% yield). ^{1}H NMR (400 MHz, D$_2$O) δ 4.04 (t, 4H), 3.32 (t, J = 145 Hz, 18H, ^{13}C-^{1}H coupling), ^{13}C NMR (100 MHz, D$_2$O) δ 54.3, 47.1.

5.7
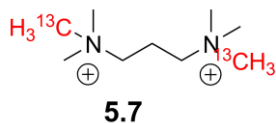
Synthesis of N, N, N, N', N', N' Hexamethyl-1,3-propyldiaminium Diiodide-^{13}C
5.7: tetramethyl-1,3-diaminopropane (0.1 mL, 0.6 mmol) was dissolved in 2 mL of
acetonitrile at 0 °C before addition of Iodomethane-^{13}C (0.09 ml, 1.32 mmol) dropwise.
Precipitate was collected by vacuum filtration to obtain 220 mg of white solid (88%
yield). ^{1}H NMR (400 MHz, D$_2$O) δ 3.47 (m, 4H), 3.23 (t, J = 145 Hz, 18H, ^{13}C-^{1}H
coupling) 2.41 (m, 2H), ^{13}C NMR (100 MHz, D$_2$O) δ 62.6, 53.5, 17.6.

5.8
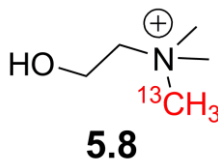
Synthesis of ^{13}C-enriched Choline 5.8: N,N,N,N',N'-Pentamethyl-1,2-
ethanediaminium iodide-^{13}C (300 mg, 1.15 mmol) was dissolved in 1 mL of acetonitrile
at 0 °C before addition of iodomethane-^{13}C (0.1 mL, 1.2 mmol) dropwise. Precipitate
was collected by vacuum filtration to obtain 256 mg of white solid (56% yield). ^{1}H NMR
(400 MHz, D$_2$O) δ 4.08 (b t, 2H), 3.50 (b t, 2H), 3.22 (t, J = 145 Hz, 18H, ^{13}C-^{1}H
coupling), ^{13}C NMR (100 MHz, D$_2$O) δ 54.3, 47.1.

Micelle Preparation

We made micelles with $q = 3.2$ (q = long chain lipid/short chain lipid) by mixing together DHPC and DMPC dissolved in chloroform. The chloroform was evaporated off under a stream of nitrogen, the lipids were lyophilized for 4 hours before the bicelles were prepared to get rid of TFA and chloroform, and the solid lipids were dissolved in HEPES buffer, pH = 6.5. NMR samples were prepared by dissolving 250 μL of the lipid mixture in 200 μL HEPES buffer, pH = 6.5, and 50 μL D_2O for a lock.

Ordered Bicelle Preparation

Based on literature recommendations,[23] we used DHPC as the short chain lipid and DMPC as the long chain lipid. The procedure for synthesis of the bicelles was taken from the literature.[24] We made bicelles with $q = 3.2$ (q = long chain lipid/short chain lipid) by mixing together DHPC and DMPC dissolved in chloroform. The chloroform was evaporated off under a stream of nitrogen, the lipids were lyophilized for 4 hours before the bicelles were prepared to get rid of TFA and chloroform, and the solid lipids were dissolved in HEPES buffer, pH = 6.5. This solution was subjected to 5 min of vortexing, followed by 30 min in a water bath at 45 °C, followed by 15 min in an ice bath. This process was repeated five times until the lipids were clear and non-viscous at 4 °C and milky-white and solid at room temperature, indicative of bicelle formation. NMR samples were prepared by dissolving 250 μL of the bicelles in 200 μL HEPES buffer, pH = 6.5, and 50 μL D_2O for a lock. This solution was added to a glass 5 mm NMR tube.

6.6 Selected NMR Spectra of New Scaffolds
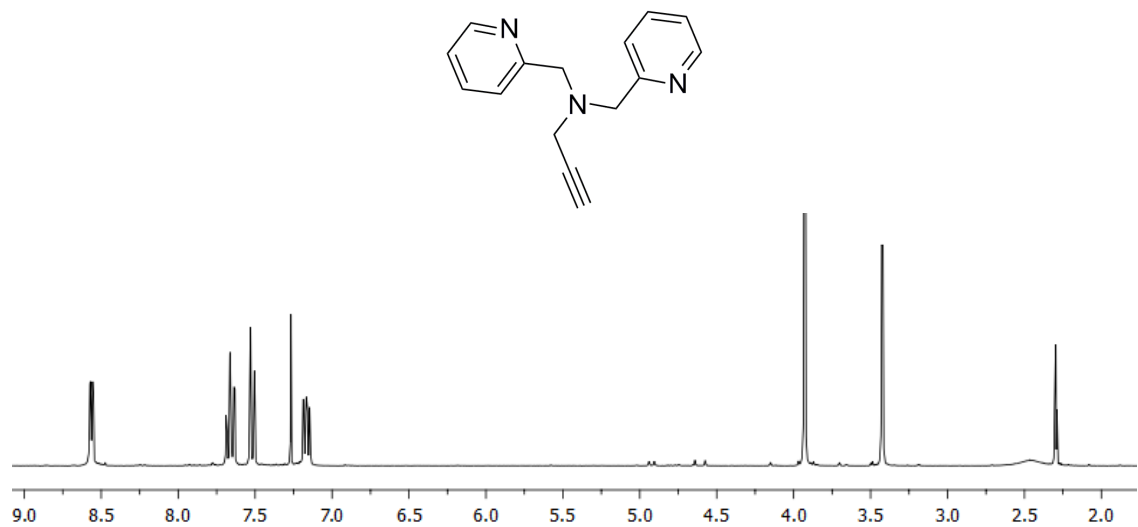
Figure 6.3. ^{1}H NMR spectrum of dipicolylpropargylamine **2.10** (400 MHz, CDCl$_3$, 298K).
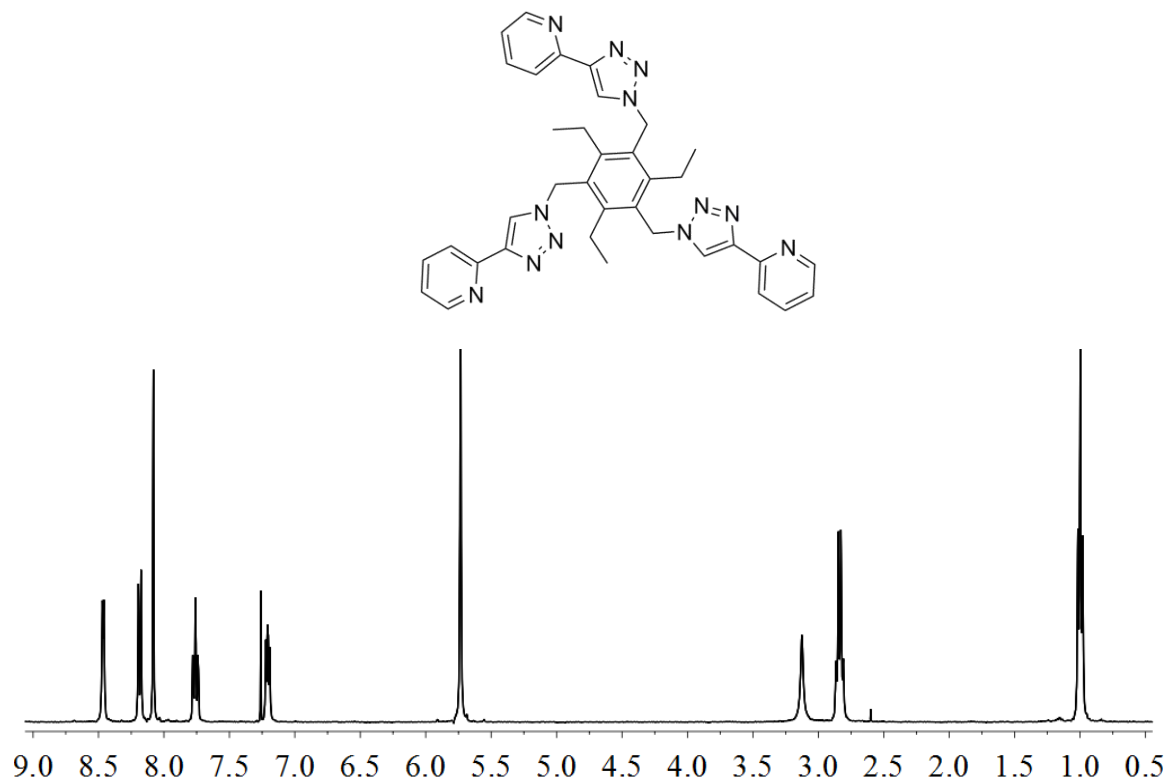
Figure 6.4. ^{1}H NMR spectrum of tris-pyridyl ligand **2.16** (400 MHz, CDCl$_3$, 298K).
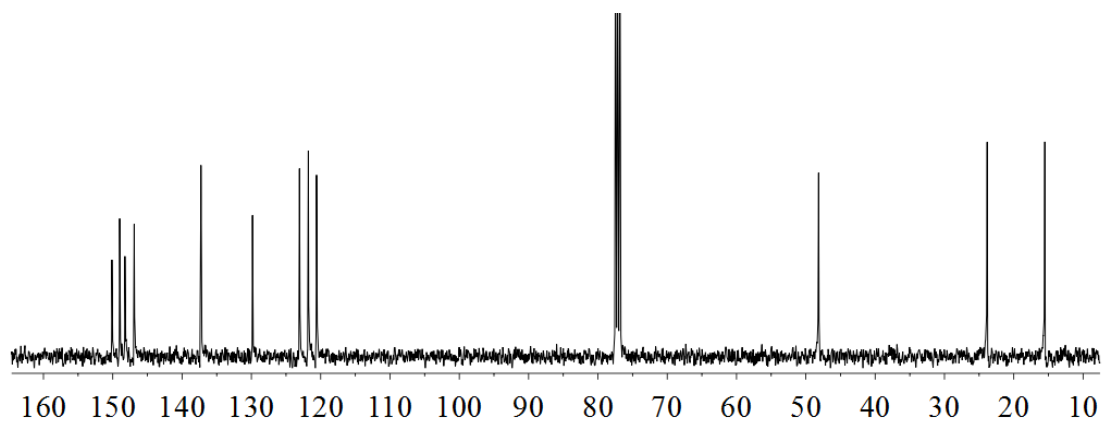
Figure 6.5. ^{13}C NMR spectrum of tris-pyridyl ligand **2.16** (100 MHz, CDCl$_3$, 298K).
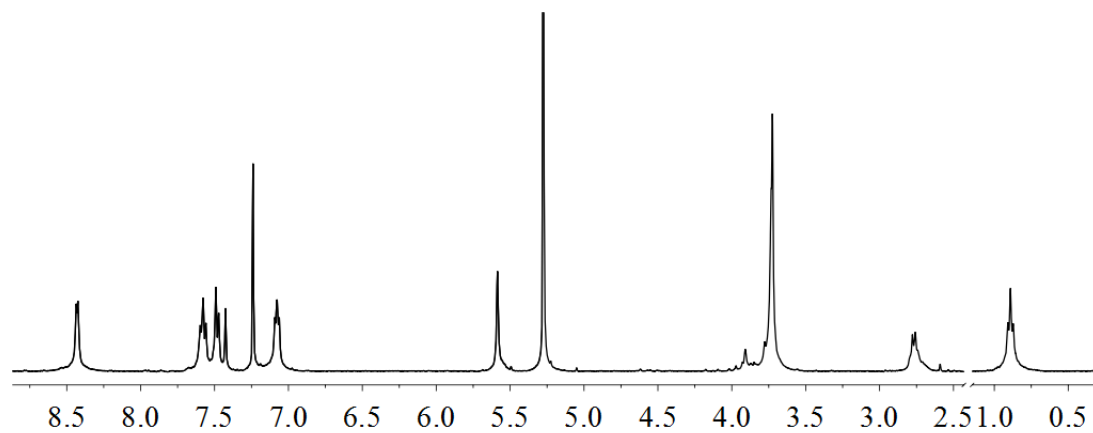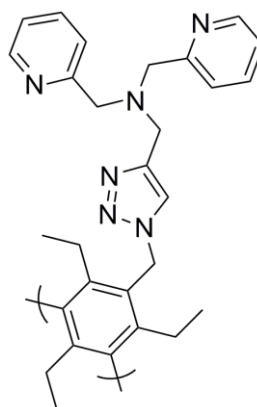
Figure 6.6. ^1H NMR spectrum of hexapicolyl ligand **2.14** (400 MHz, CDCl$_3$, 298K).
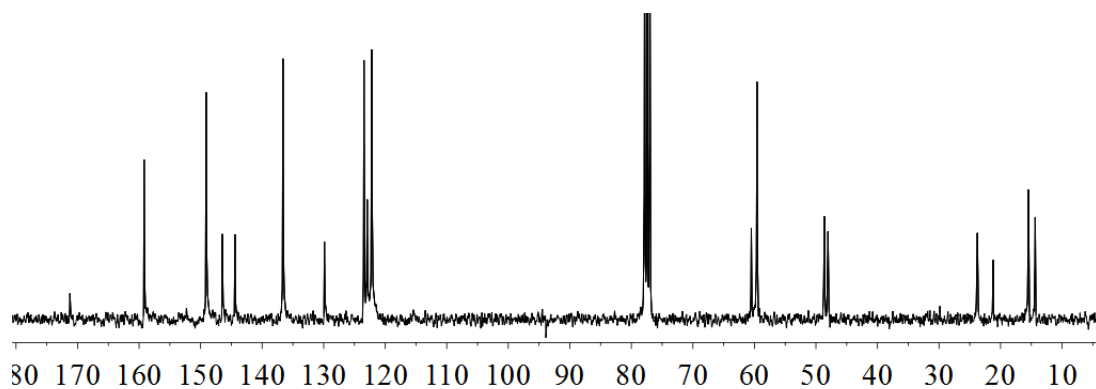
Figure 6.7. ^{13}C NMR spectrum of hexapicolyl ligand **2.14** (100 MHz, CDCl$_3$, 298K).
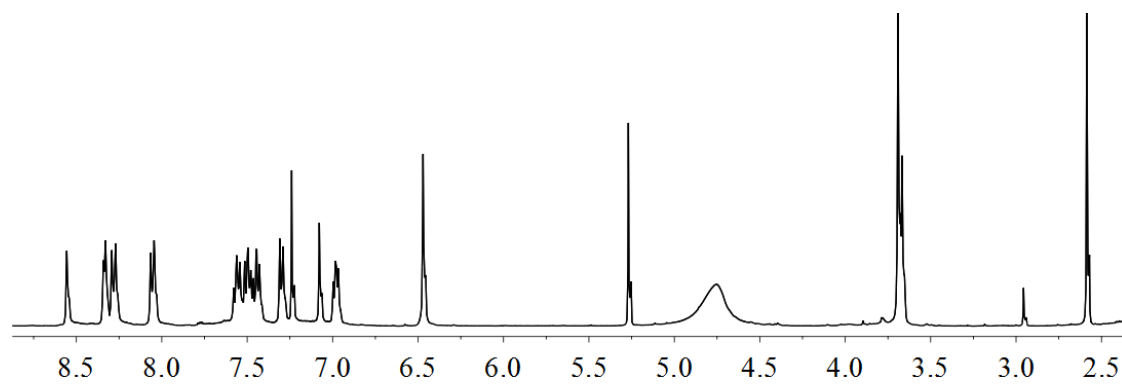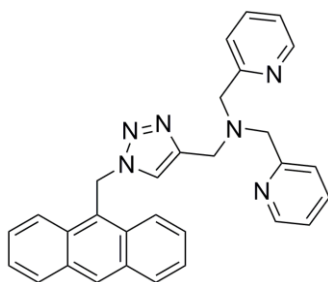
Figure 6.8. ^1H NMR spectrum of dipicolyl ligand **2.18** (400 MHz, CDCl$_3$, 298K).

247
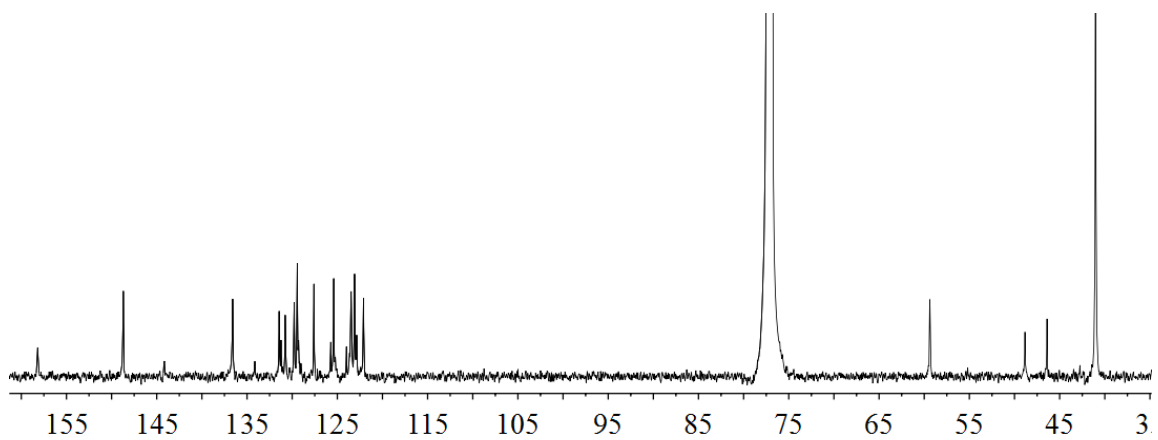
Figure 6.9. ^{13}C NMR spectrum of Dipicolyl ligand **2.18** (100 MHz, CDCl$_3$, 298K).
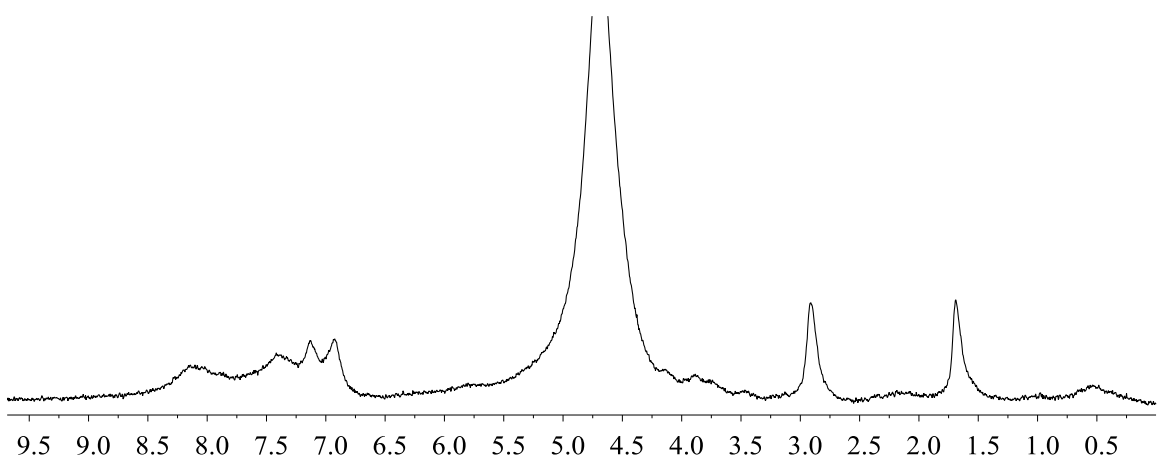
Figure 6.10. ^{1}H NMR spectrum of hexapicolyl complex **2.14**•Fe$_3$(SO$_4$)$_3$ (600 MHz, CD$_3$CN and D$_2$O, 298K).
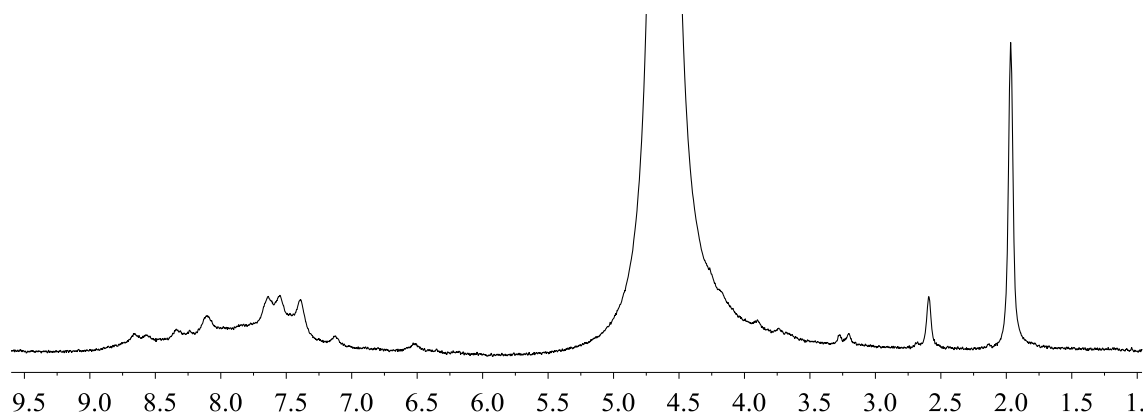
Figure 6.11. ^{1}H NMR spectrum of dipicolyl complex **2.18•FeSO$_4$** (600 MHz, D$_2$O and 10% CD$_3$CN, 298K).

Bipyridyl Imine Cavitand 3.9
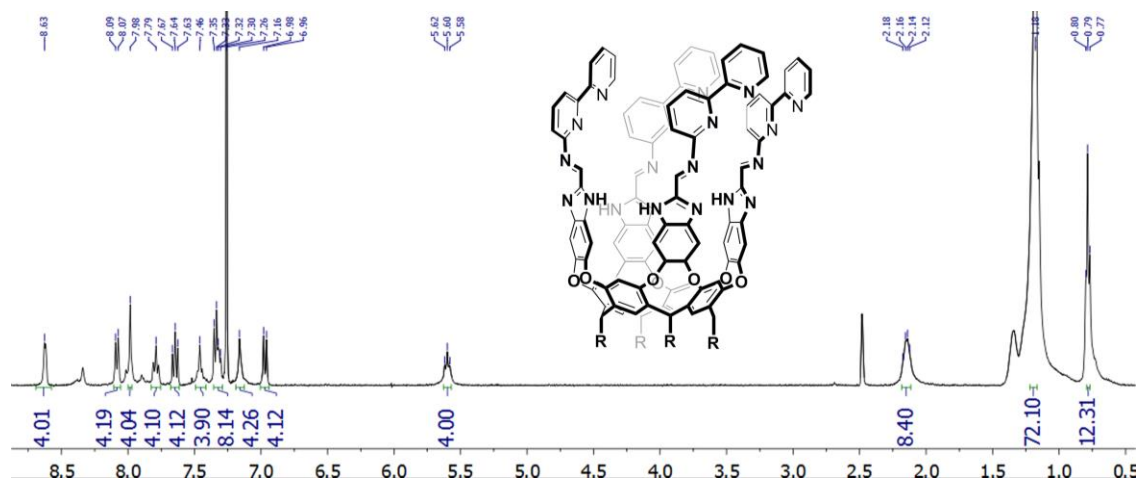
Figure 6.12. ^{1}H NMR spectrum of cavitand **3.9** (400 MHz, CDCl$_3$ and 5 % DMSO-d_6, 298 K).
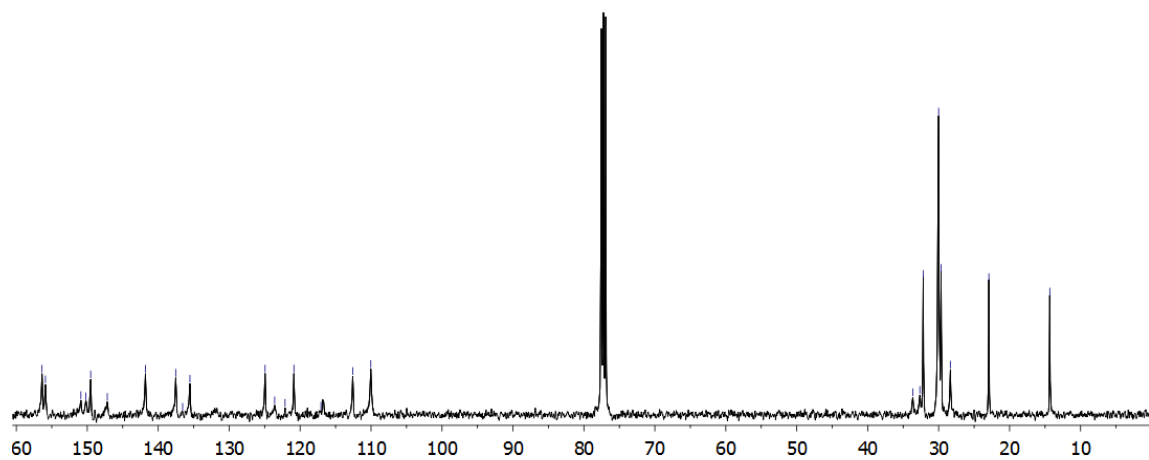
Figure 6.13. ^{13}C NMR spectrum of cavitand **3.9** (125 MHz, CDCl$_3$ and 5 % DMSO-d_6, 298 K).

Pyridyl Imine Cavitand 3.8
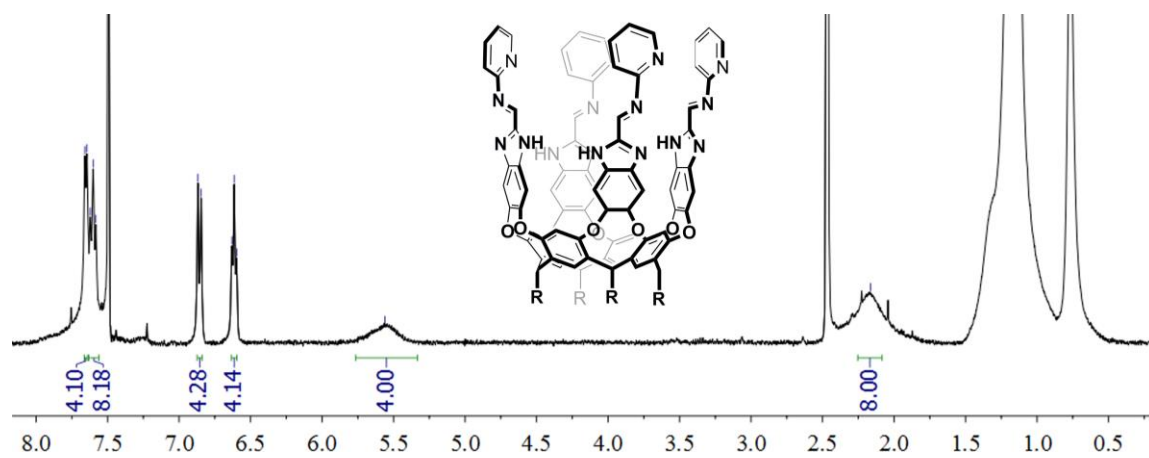
Figure 6.14. ^1H NMR spectrum of cavitand **3.8** (400 MHz, CDCl$_3$ and 5 % DMSO-d_6, 298 K).
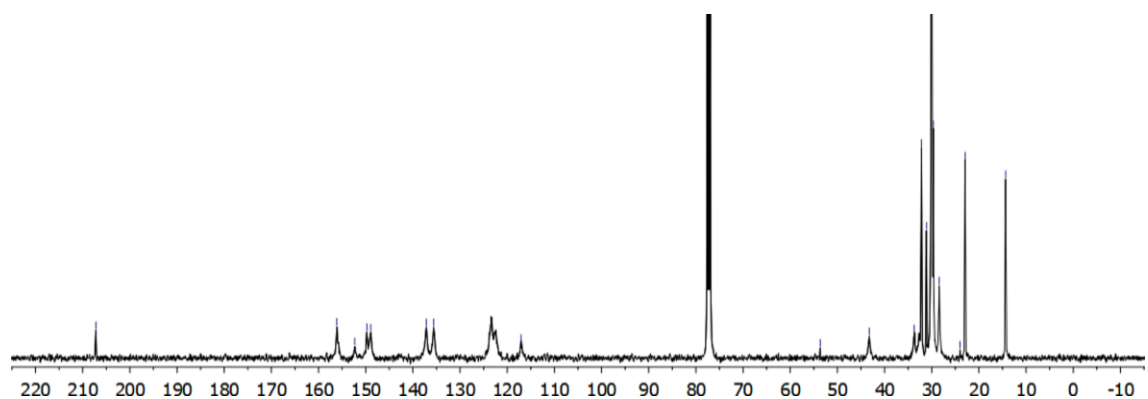
Figure 6.15. ^{13}C NMR spectrum of **3.8** (125 MHz, CDCl$_3$ and 5 % DMSO-d_6, 298 K).

Benzoic Acid Imine Cavitand 3.10
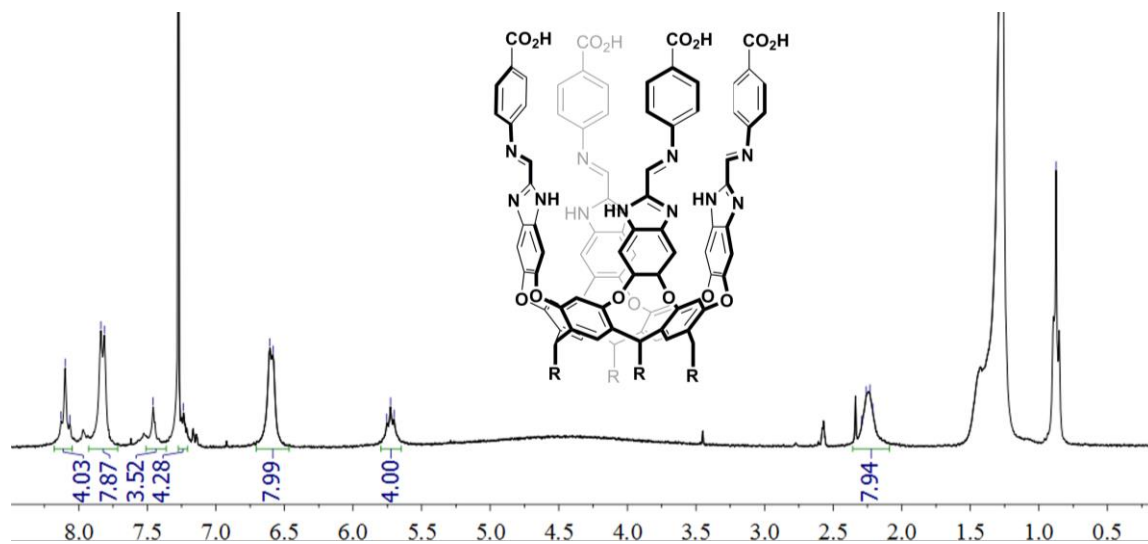
Figure 6.16. ^{1}H NMR spectrum of **3.10** (300 MHz, CDCl$_3$ and 5 % DMSO-d_6, 298 K).
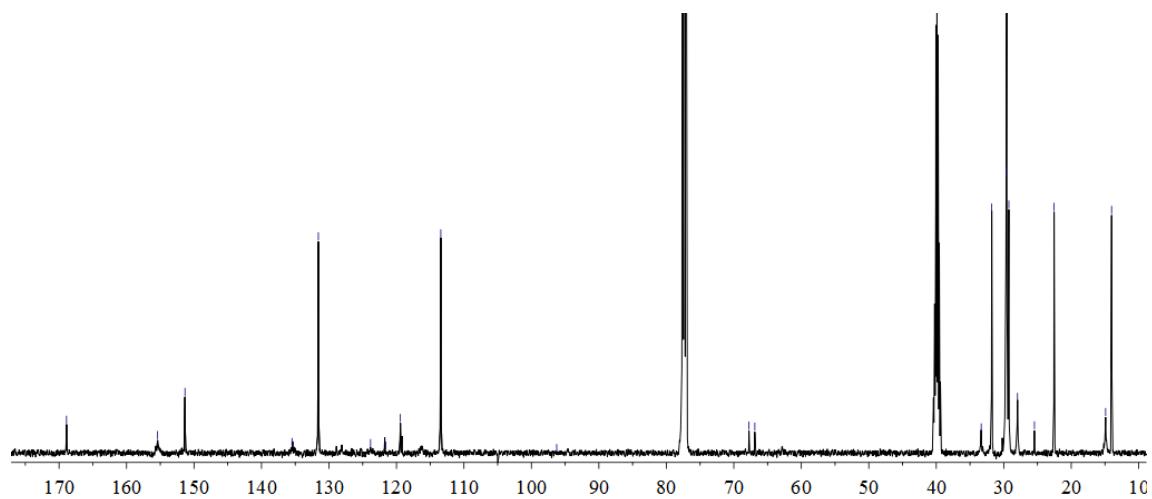
Figure 6.17. ^{13}C NMR spectrum of **3.10** (125 MHz, CDCl$_3$ and 5 % DMSO-d_6, 298 K).

Picolyl Imine Cavitand 3.11
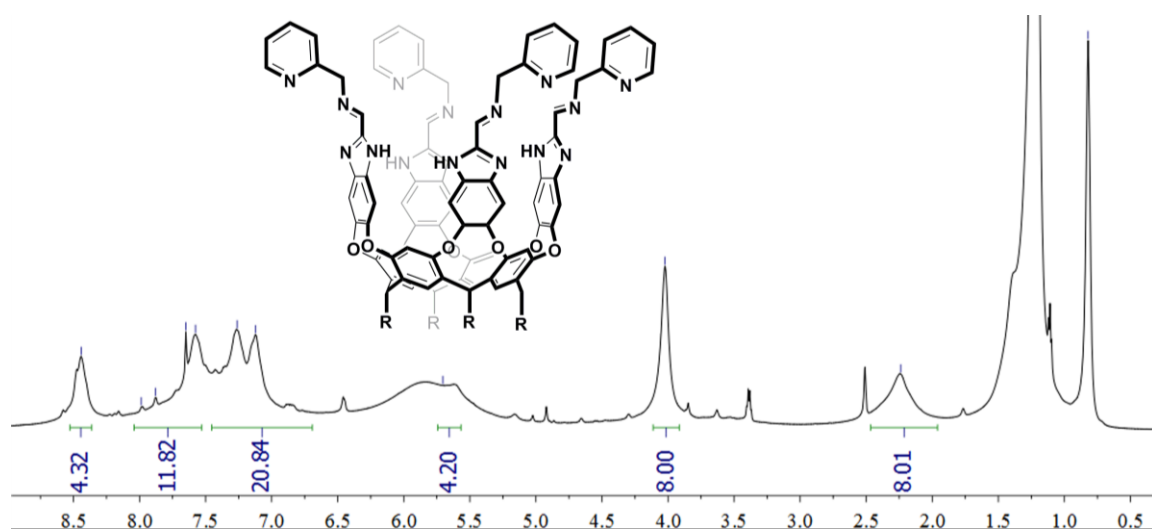
Figure 6.18. ^{1}H NMR spectrum of **3.11** (600 MHz, CDCl$_3$ and 5 % DMSO-d_6, 298 K).
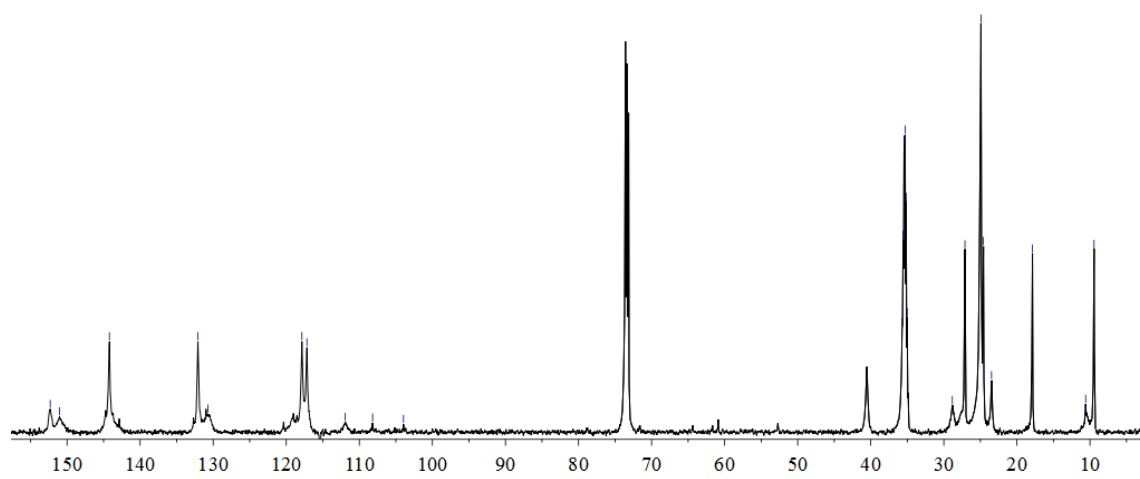
Figure 6.19. ^{13}C NMR spectrum of **3.11** (150 MHz, CDCl$_3$ and 5 % DMSO-d_6, 298 K).

Dimethylethylenediamine Imine Cavitand 3.12
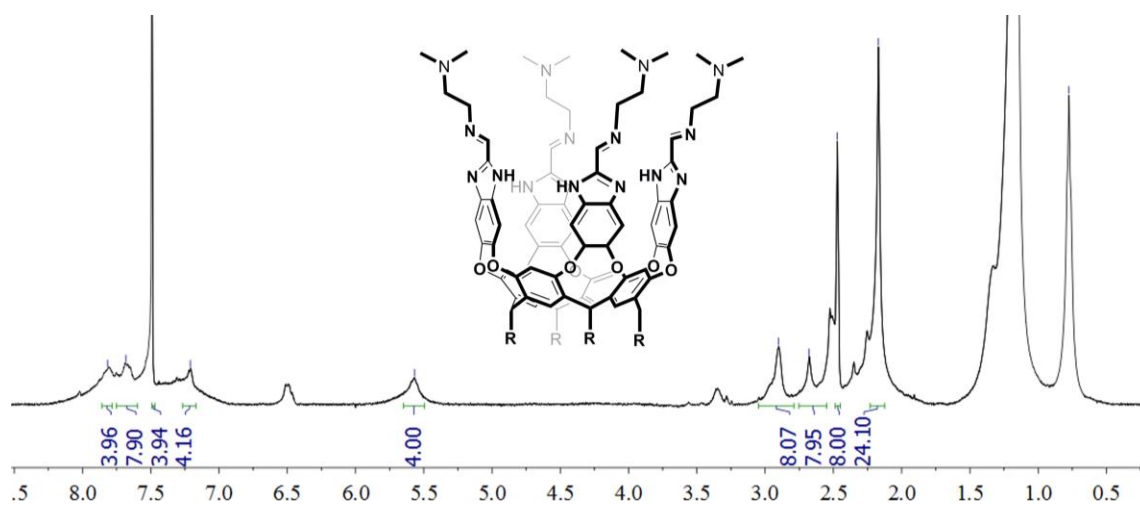
Figure 6.20. ^{1}H NMR spectrum of **3.12** (500 MHz, CDCl$_3$ and 5 % DMSO-d_6, 298 K).
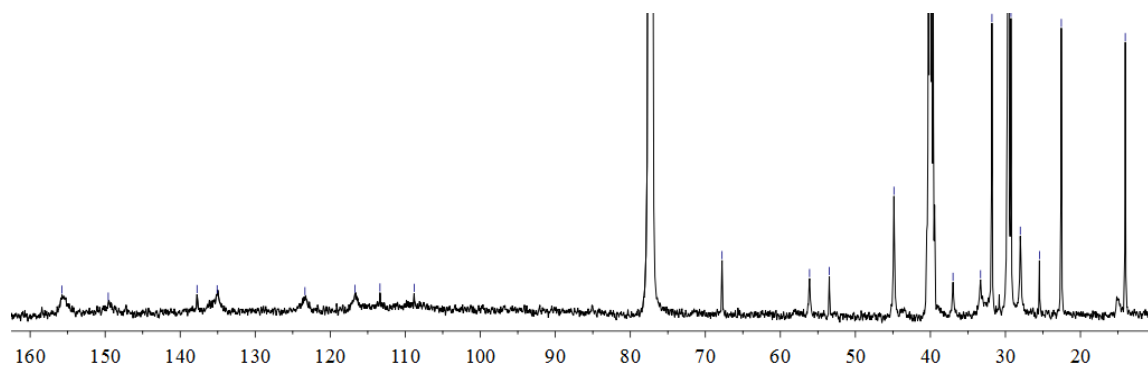
Figure 6.21. ^{13}C NMR spectrum of **3.12** (150 MHz, CDCl$_3$ and 5 % DMSO-d_6, 298 K).

Butyl Imine Cavitand
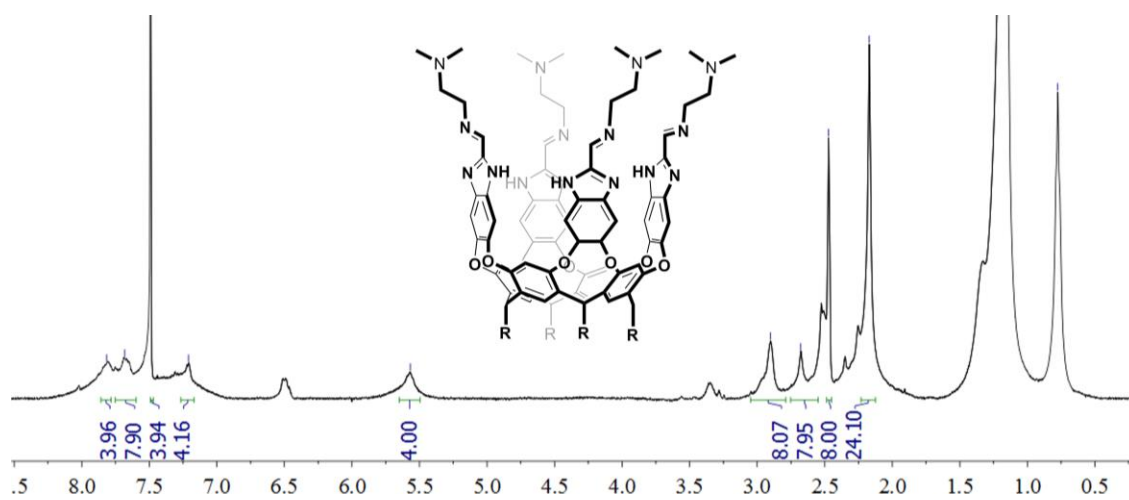
Figure 6.22. ^{1}H NMR spectrum of **3.13** (500 MHz, CDCl$_3$ and 5 % DMSO-d_6, 298 K).
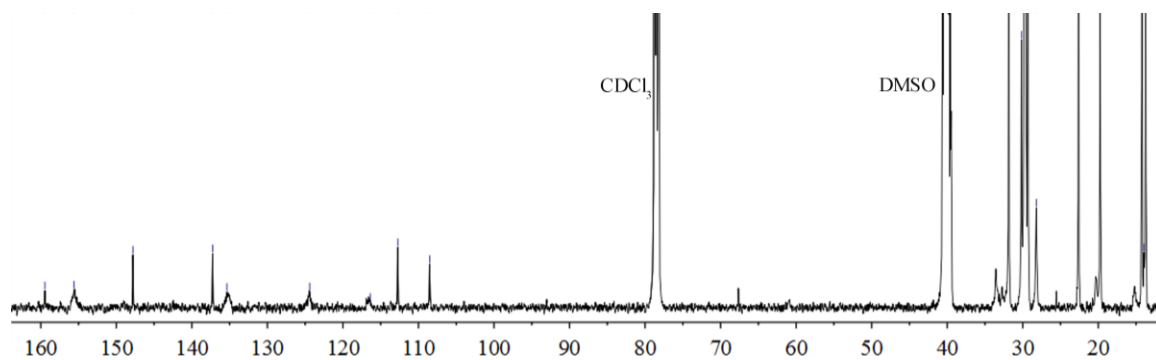
Figure 6.23. ^{13}C NMR spectrum of **3.13** (125 MHz, CDCl$_3$ and 2 % DMSO-d_6, 298 K).
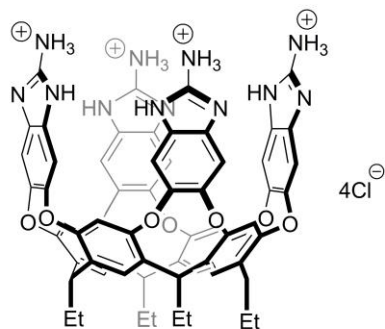
4.9 2-aminobenzimidazole Cavitand
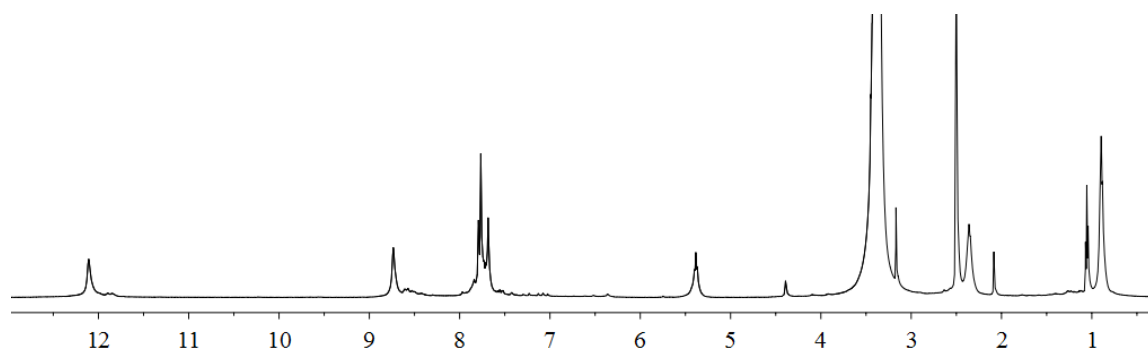
Figure 6.24. ^{1}H NMR spectrum of positive cavitand 4.9 (500 MHz, DMSO-d_6, 298 K).

4.10 Octaethylacetal Cavitand
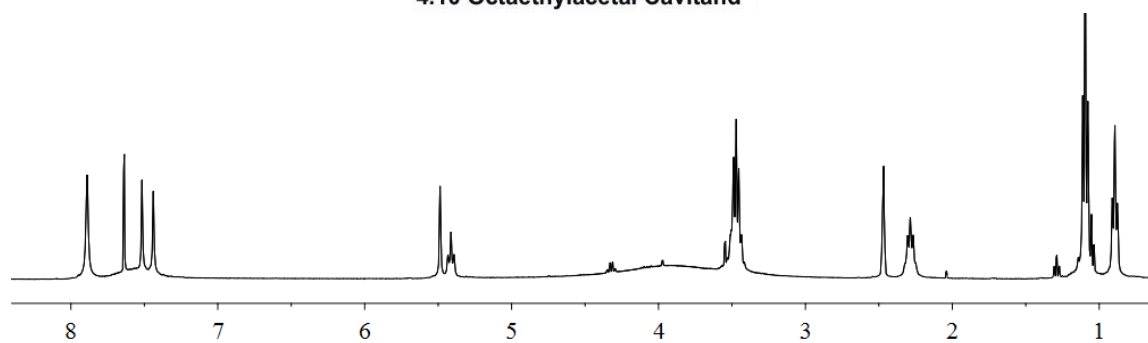
Figure 6.25. ^{1}H NMR spectrum of C$_2$-cavitand 4.10 (400 MHz, DMSO-d_6, 298 K).
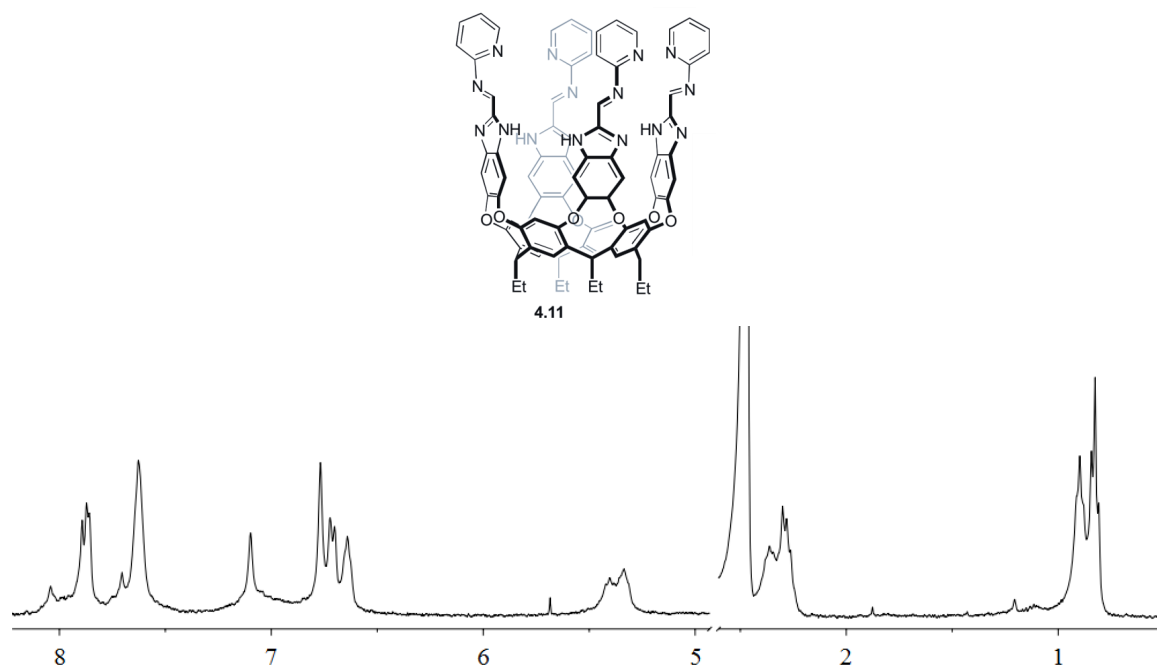
Figure 6.26. ^{1}H NMR spectrum of C$_2$-cavitand **4.11** (600 MHz, DMSO-d_6, 298 K).
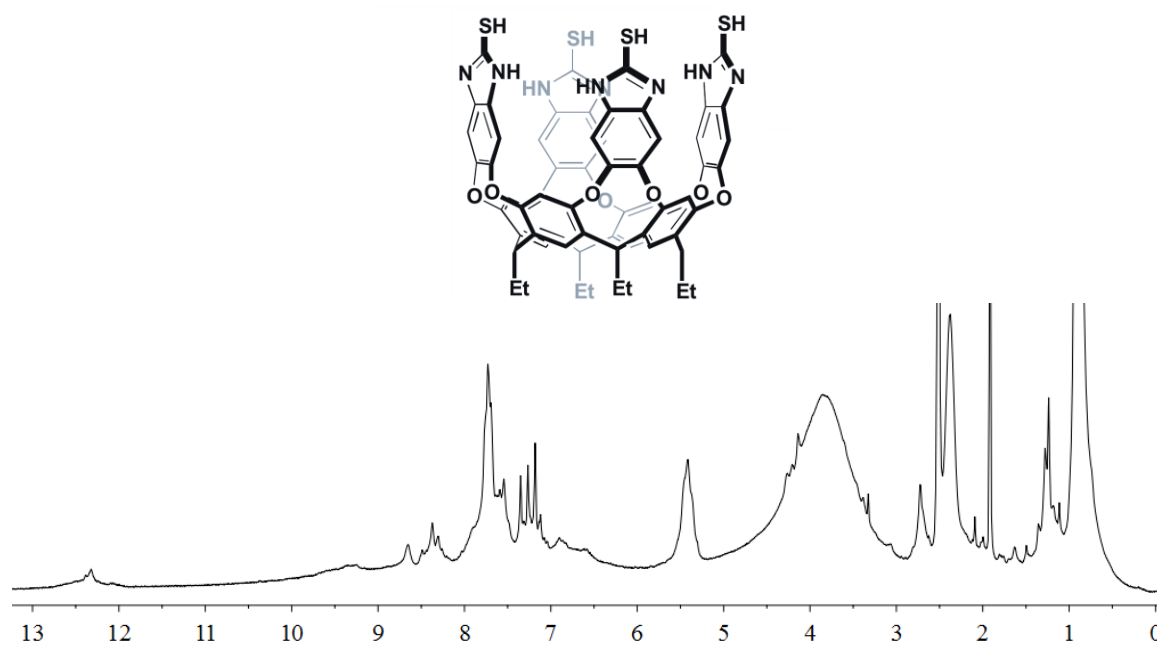
Figure 6.27. ^{1}H NMR spectrum of thiobenzamidazole **4.16** (600 MHz, DMSO-d_6, 298 K).

256
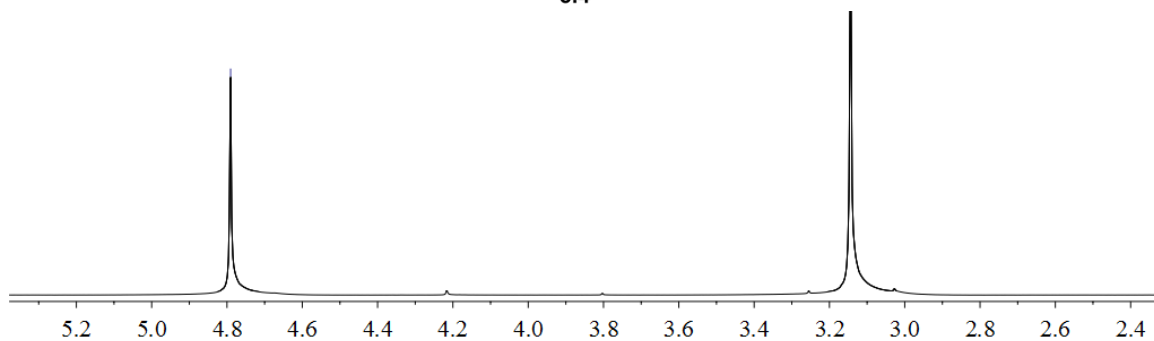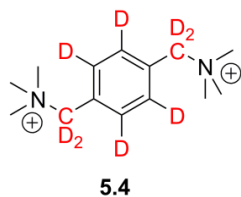
Figure 6.28. ^{1}H NMR spectrum of α, α'-trimethylammonium-*p*-xylene-d_8 **5.4** (400 MHz, D$_2$O, 298 K).
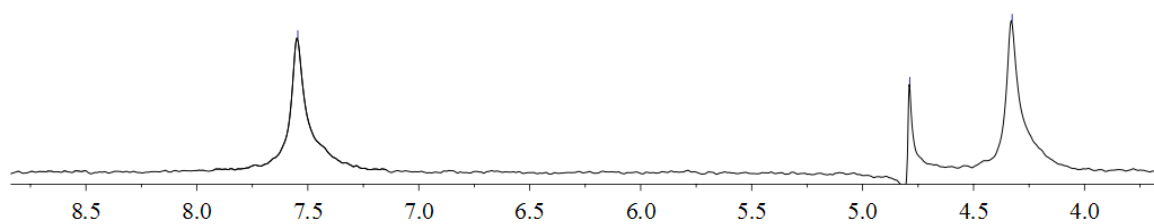
Figure 6.29. ^{2}H NMR spectrum of α, α'-trimethylammonium-*p*-xylene-d_8 (400 MHz, D$_2$O, 298 K).
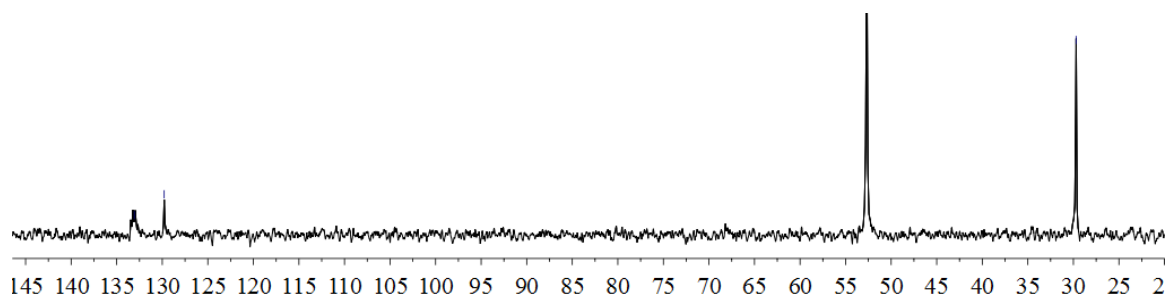
Figure 6.30. ^{13}C NMR spectrum of α, α'-trimethylammonium-*p*-xylene-d_8 (100 MHz, D$_2$O, 298 K).
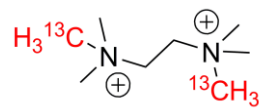
5.6
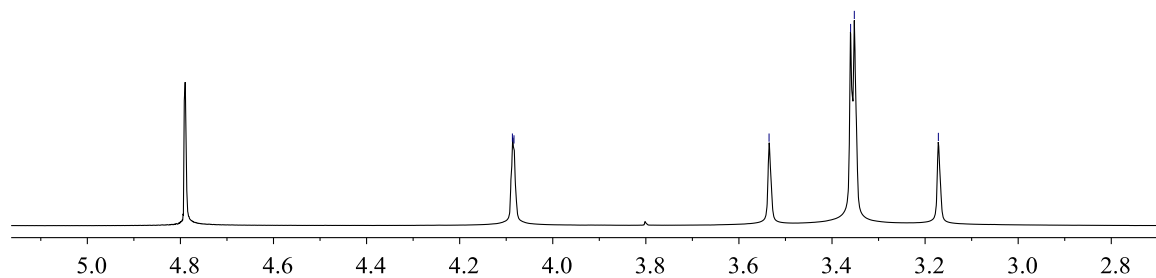
Figure 6.31. ^{1}H NMR spectrum of N,N,N,N',N',N' hexamethyl-1,2-ethanediaminium diiodide-^{13}C (400 MHz, D$_2$O, 298 K).
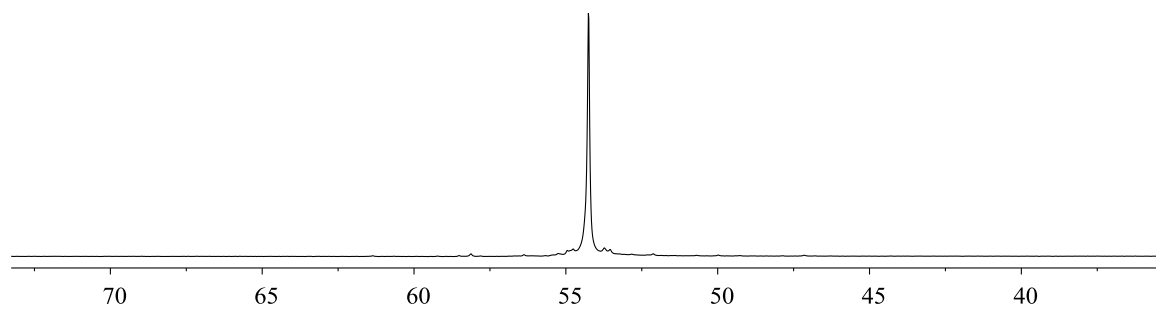
Figure 6.32. ^{13}C NMR spectrum of N,N,N,N',N',N' hexamethyl-1,2-ethanediaminium diiodide-^{13}C (100 MHz, D$_2$O, 298 K).
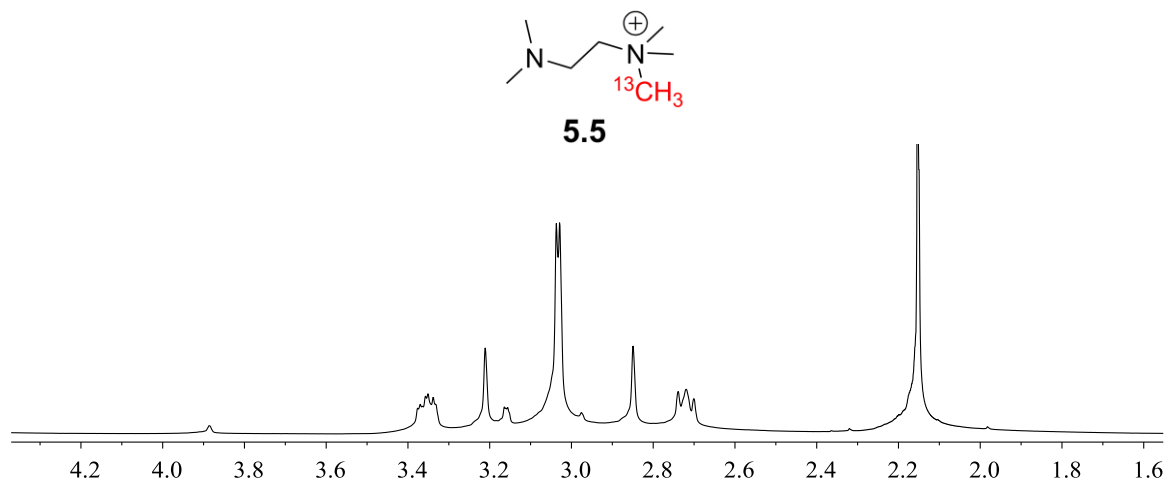
Figure 6.33. ^{1}H NMR spectrum of N,N,N,N',N' pentamethyl-1,2-ethanediaminium iodide-^{13}C (400 MHz, D$_2$O, 298 K).
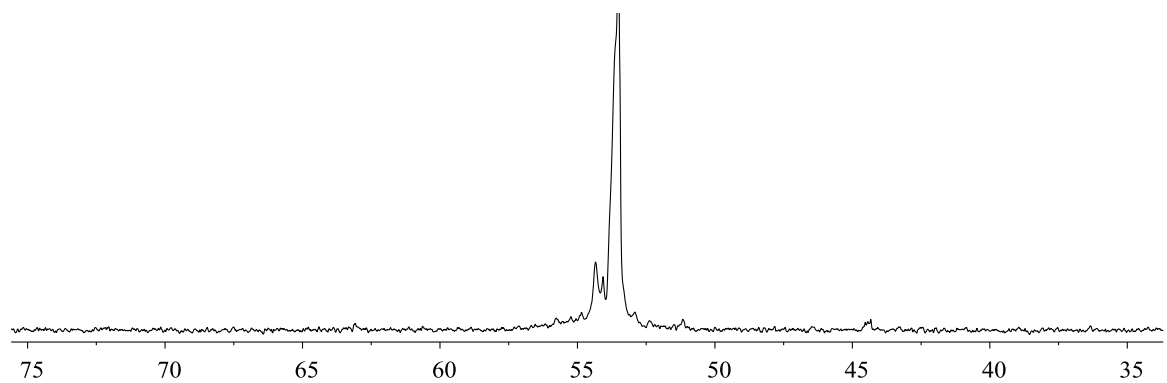
Figure 6.34. ^{13}C NMR spectrum of N,N,N,N',N' pentamethyl-1,2-ethanediaminium iodide-^{13}C (100 MHz, D$_2$O, 298 K).
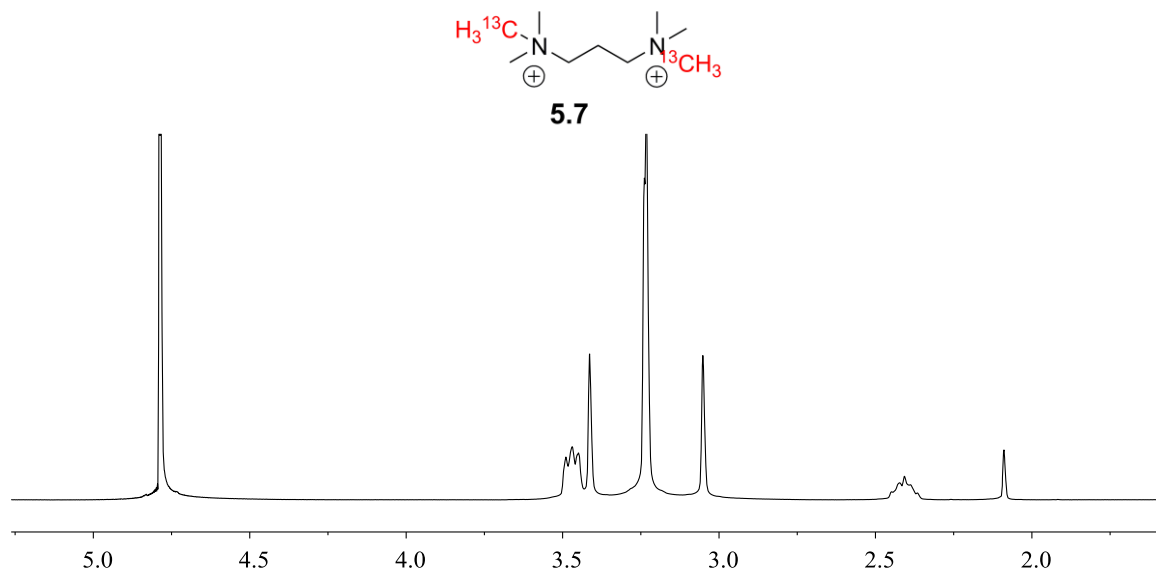
Figure 6.35. ^{1}H NMR spectrum of N,N,N,N',N',N' hexamethyl-1,3-propyldiaminium diiodide-^{13}C **5.7** (400 MHz, D$_2$O, 298 K).
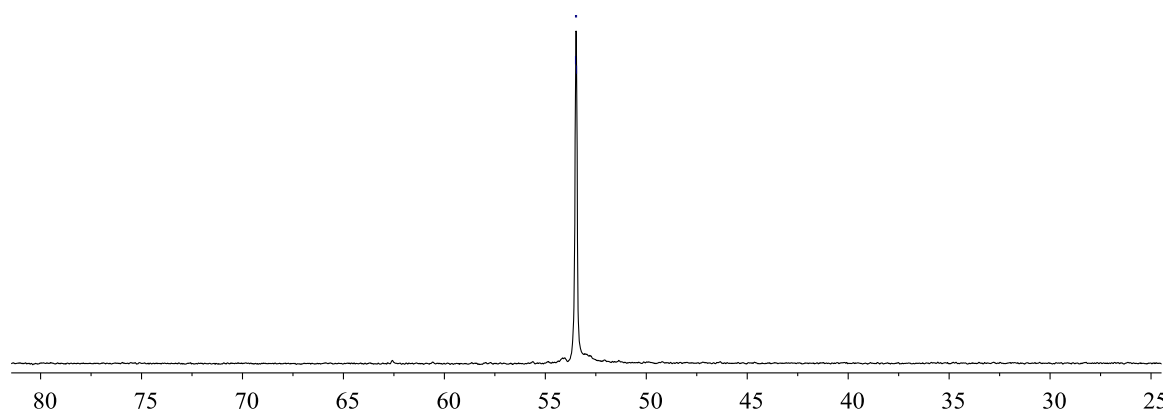
Figure 6.36. ^{13}C NMR spectrum of N,N,N,N',N',N' hexamethyl-1,3-propyldiaminium diiodide-^{13}C (400 MHz, D$_2$O, 298 K).

5.8
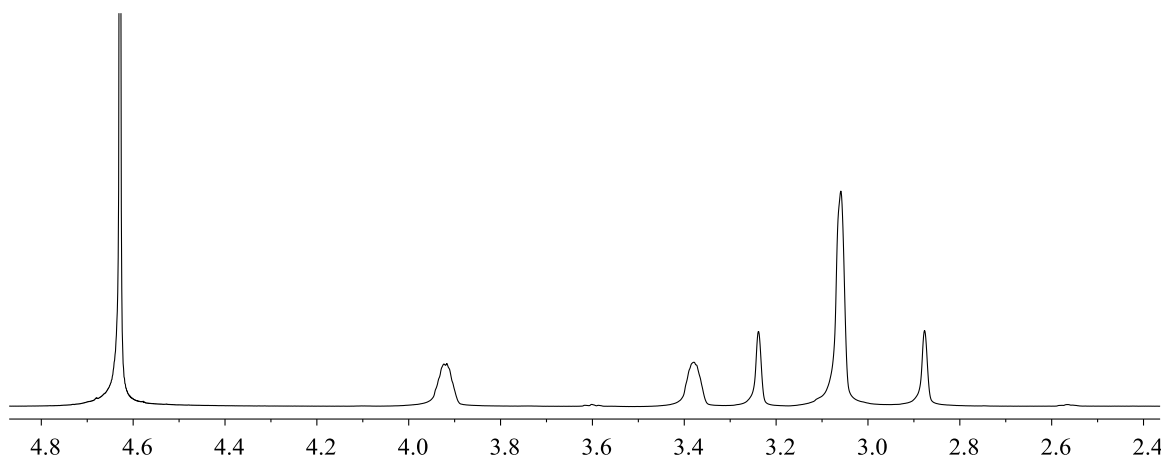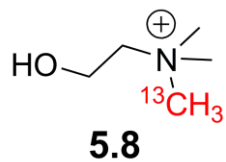
Figure 6.37. ¹H NMR spectrum of choline iodide-¹³C (400 MHz, D₂O, 298 K).
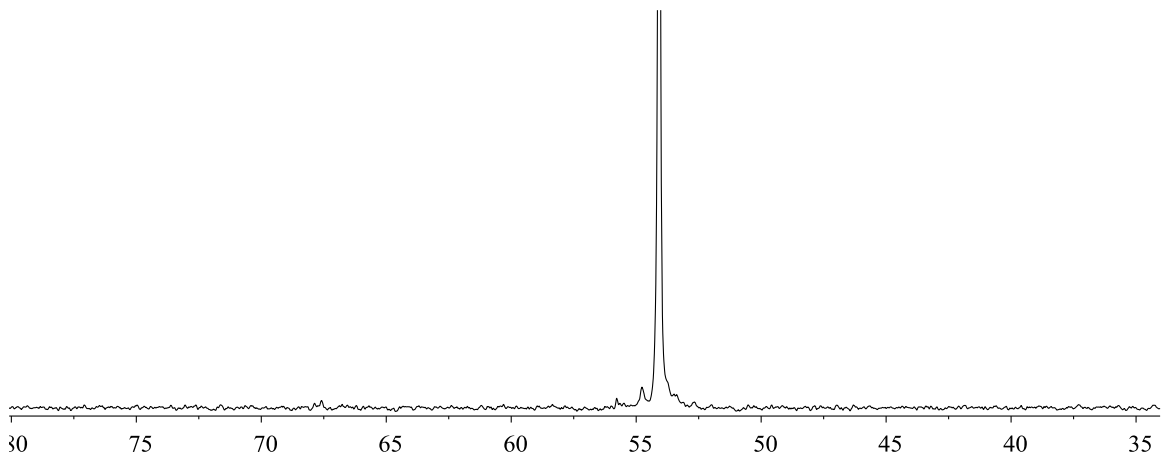
Figure 6.38. ¹³C NMR spectrum of choline iodide-¹³C (100 MHz, D₂O, 298 K).

6.7. NMR Spectra of Metal Titrations
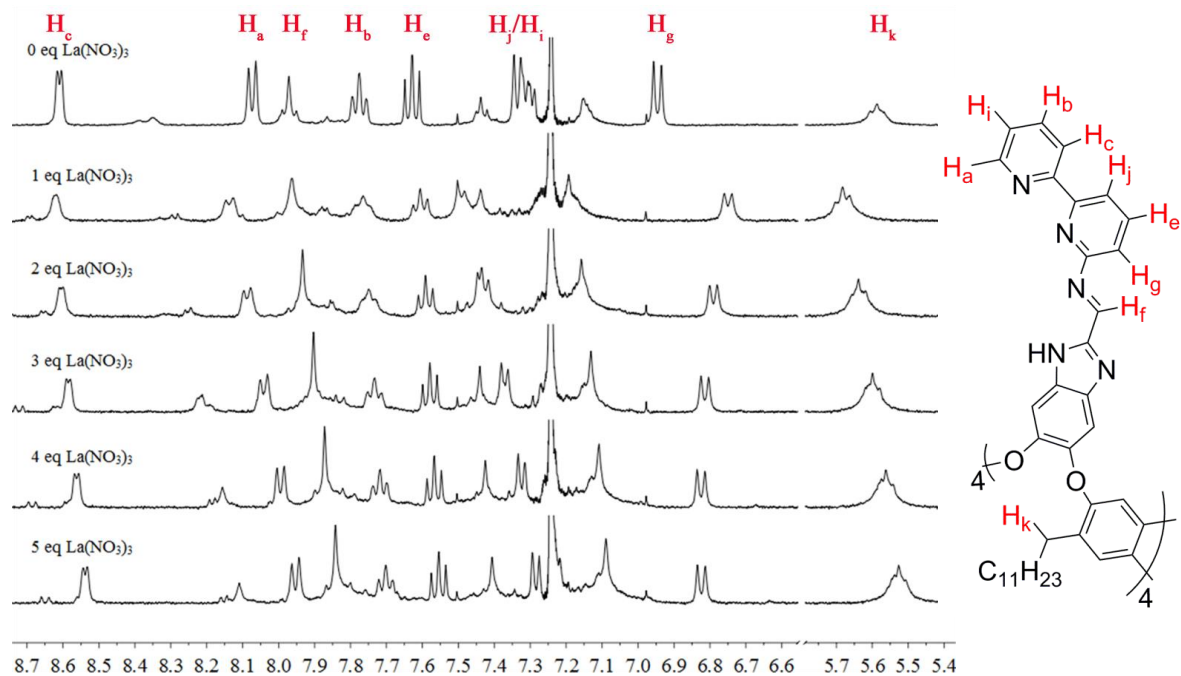
Figure 6.39. Downfield regions of the ^{1}H NMR spectra (400 MHz, 298 K, 5 % DMSO-d_6 in CDCl$_3$, 2.5 mM **3.9**) of the addition of La(NO$_3$)$_3$ to Bipyridyl Imine Cavitand **3.9**.
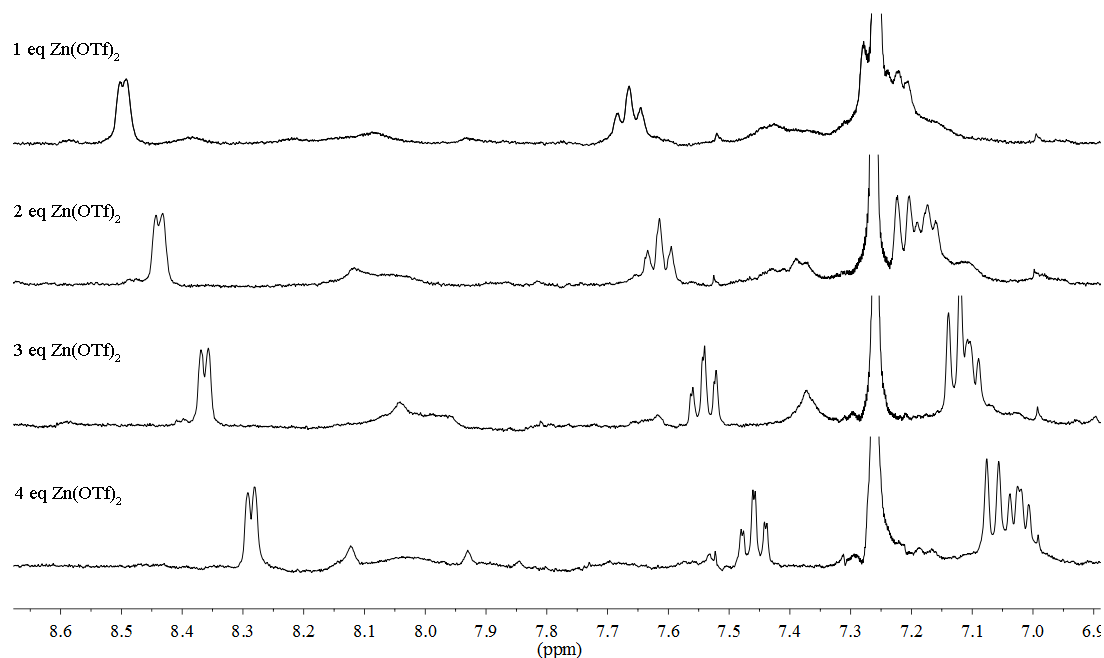
Figure 6.40. Downfield regions of the ^{1}H NMR spectra (400 MHz, 298 K, 5 % DMSO-d_6

in CDCl$_3$, 2.3 mM **3.11**) of the addition of Zn(OTf)$_2$ to Picolyl Imine Cavitand **3.11**.
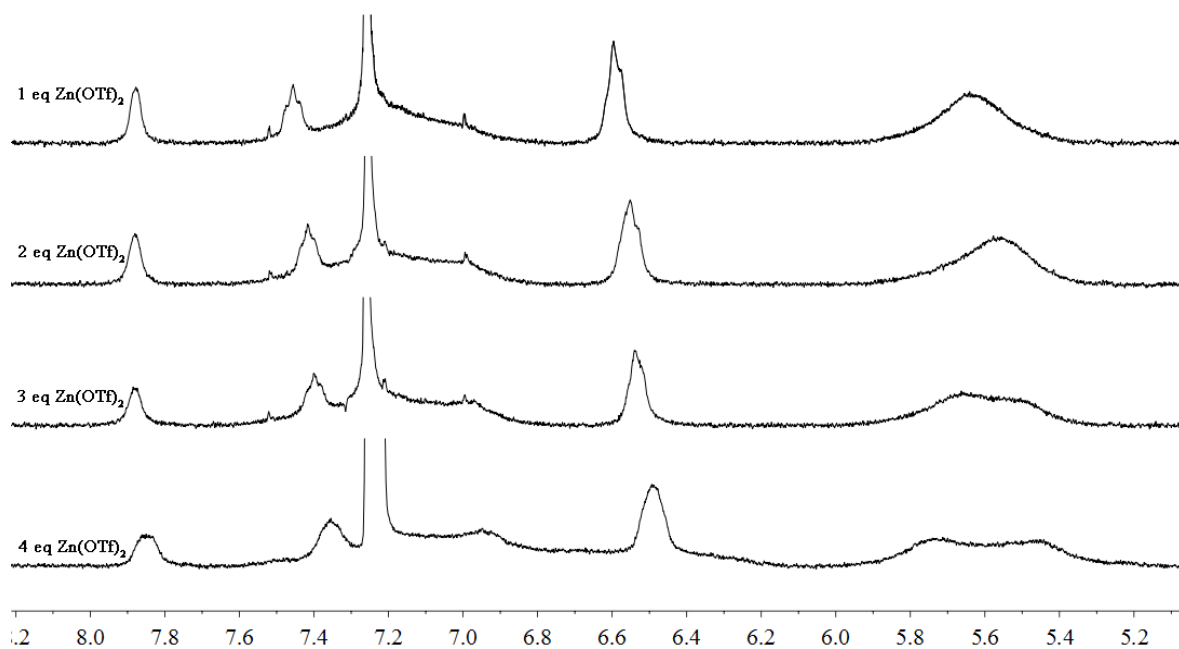
Figure 6.41. Downfield regions of the ^{1}H NMR spectra (400 MHz, 298 K, 1 % DMSO-d_6

in CDCl$_3$, 2.3 mM **3.8**) of the addition of Zn(OTf)$_2$ to pyridyl imine cavitand **3.8**.

263
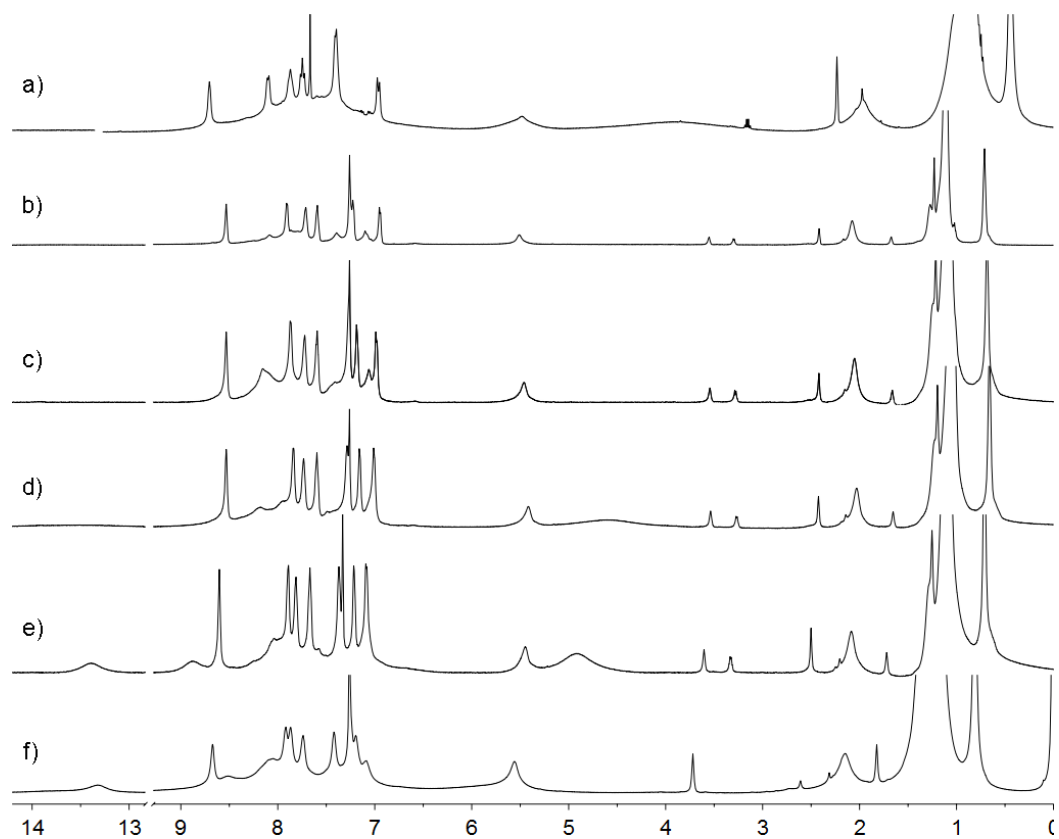
Figure 6.42. Variable temperature ^{1}H NMR spectra of Bipyridyl Imine Cavitand **3.9** (600 MHz, CDCl$_3$ and 2 % DMSO-d_6) at a) 25 °C, b) 20 °C, c) 0 °C, d) -20 °C, e) -40 °C f) -50 °C.
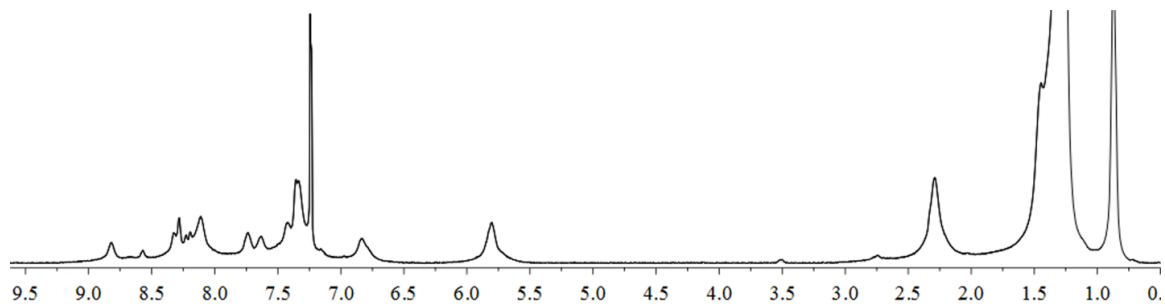
Figure 6.43. ^{1}H NMR spectrum of the Zn(OTf)$_2$ complex of Bipyridyl Imine Cavitand **3.9** in the absence of DMSO additive (600 MHz, CDCl$_3$, 298 K).

6.8. NMR Spectra of Solvent Titrations
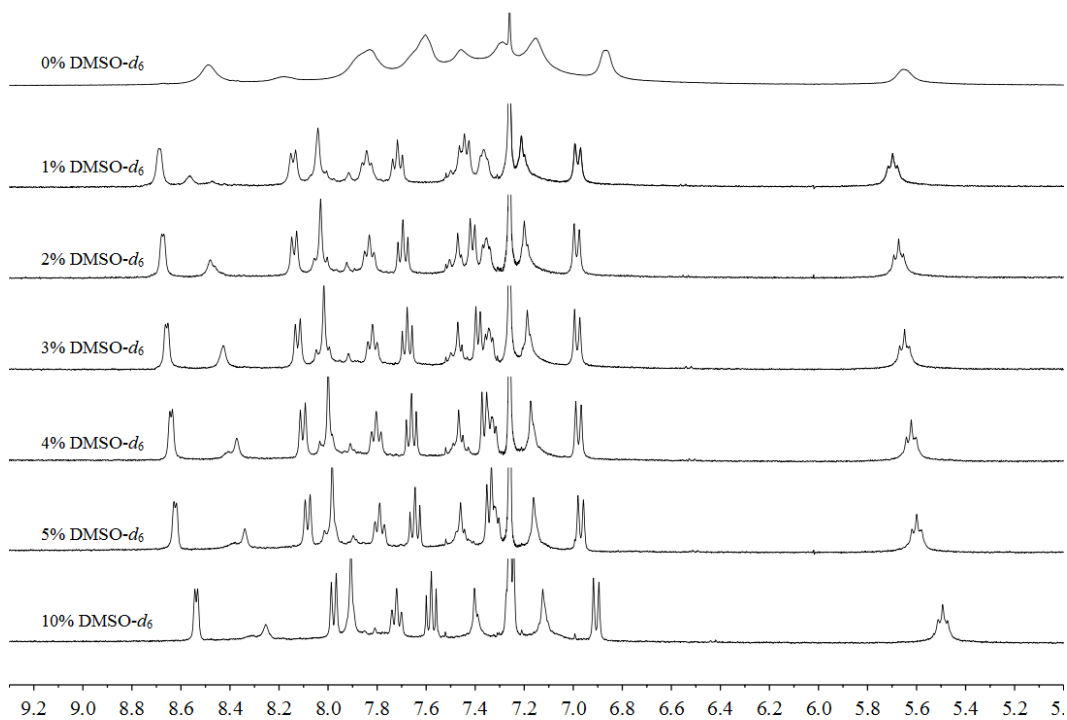
Figure 6.44. Downfield regions of the ^{1}H NMR spectra (400 MHz, 298 K, CDCl$_3$, 4 mM

3.9) upon the addition of DMSO-d_6 to a CDCl$_3$ solution of dipyridyl imine cavitand **3.9**.
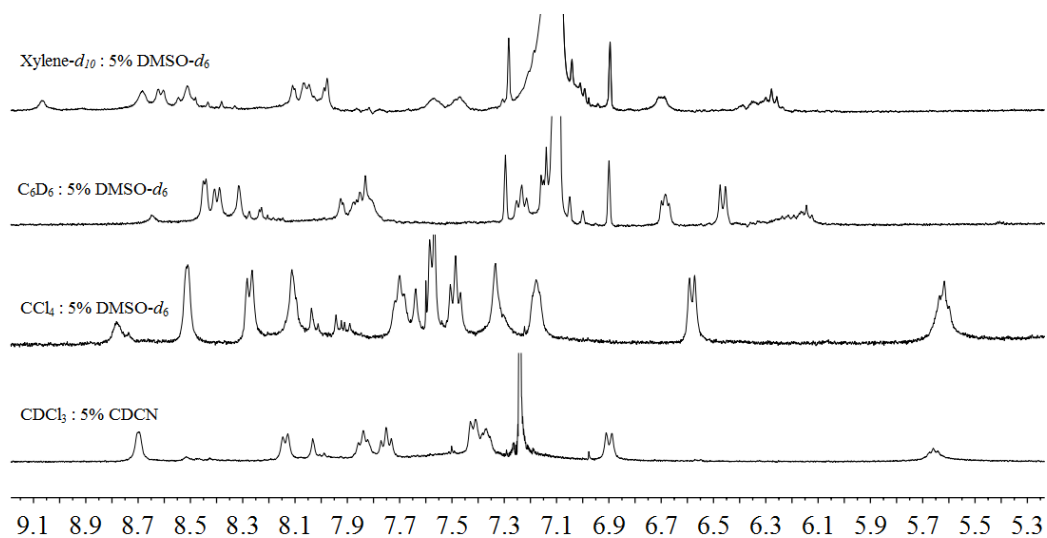
Figure 6.45. Downfield regions of the ^{1}H NMR spectra of 4 mM picolyl imine cavitand

3.11 in various solvent media (400 MHz, 298 K, 4 mM **3.11**).

6.9.1 NMR Spectra of Guest Binding Experiments: in Solution
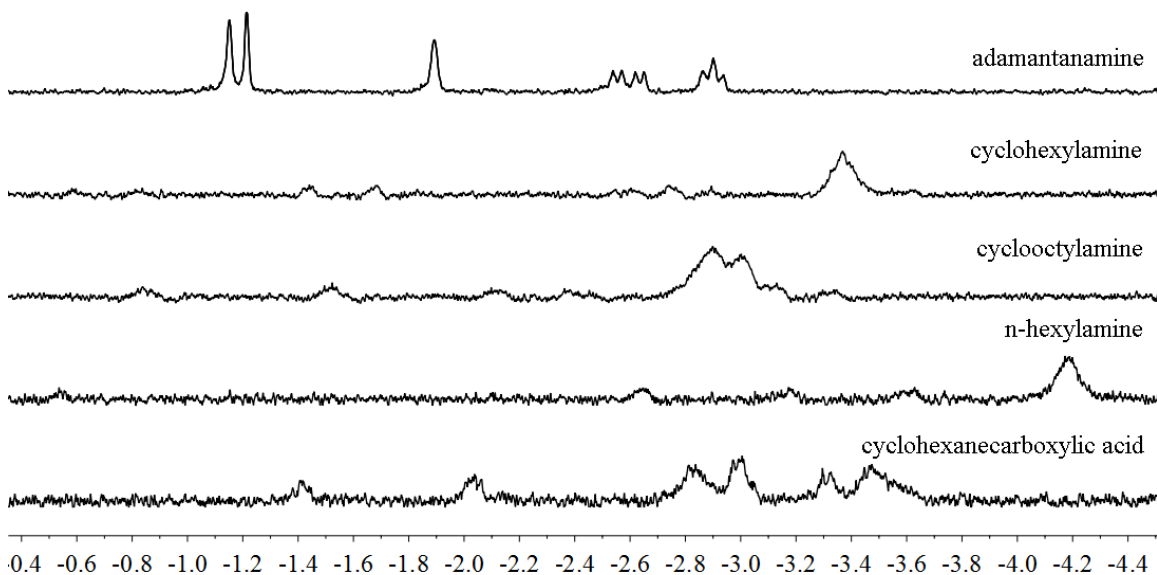
Figure 6.31. Upfield regions of the ^{1}H NMR spectra (400 MHz, 5 % DMSO-d_6 in CDCl$_3$, 298 K, 4 mM **3.11**) obtained upon addition of excess protic guests to picolyl imine cavitand **3.11**.
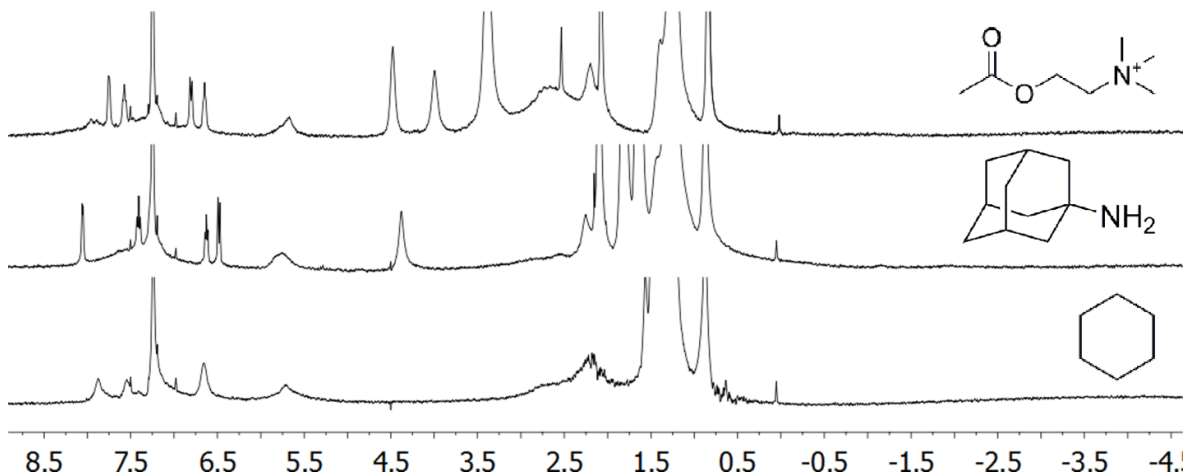
Figure 6.32. ^{1}H NMR spectra (400 MHz, 5 % DMSO-d_6 in CDCl$_3$, 298 K, 4 mM **3.8**) obtained upon addition of excess guests to pyridyl imine cavitand **3.8**.
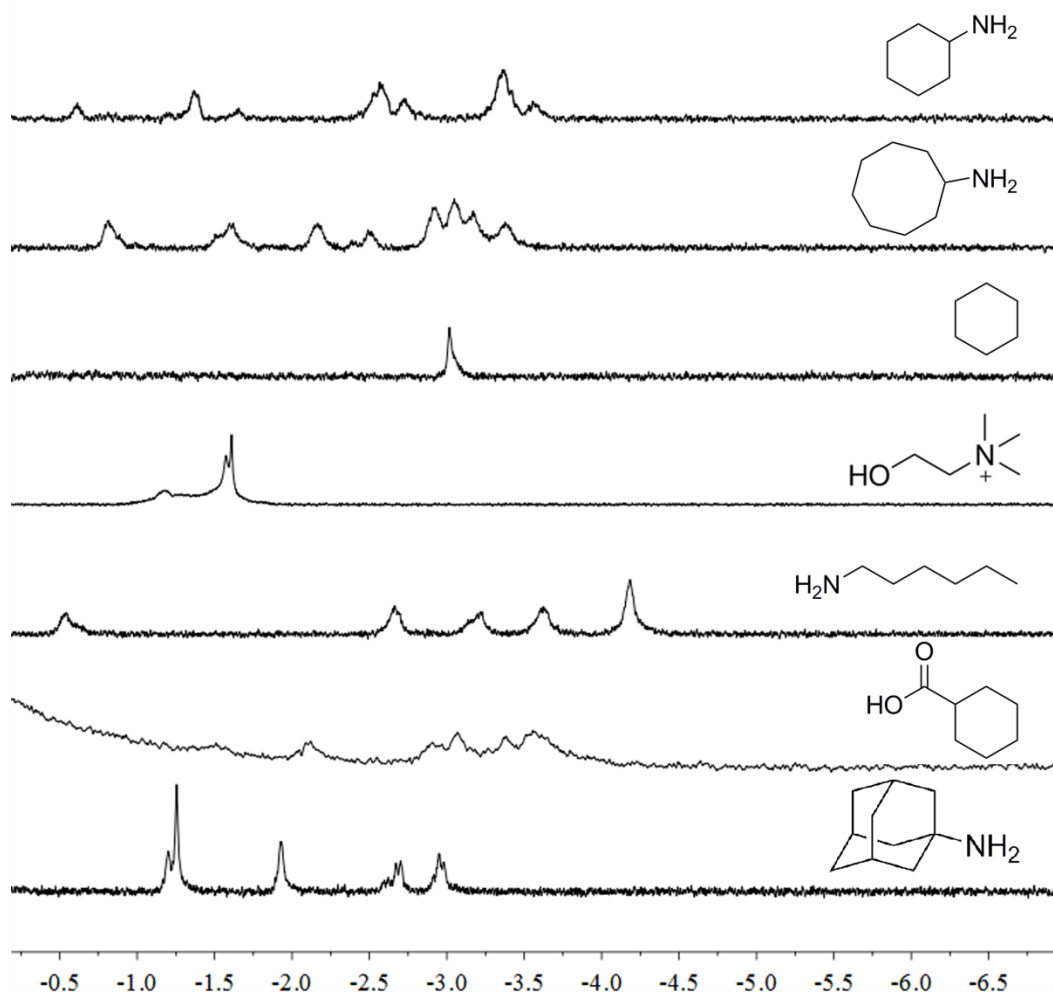
Figure 6.33. Upfield regions of the ^{1}H NMR spectra (400 MHz, 5 % DMSO-d_6 in CDCl$_3$, 298 K, 4 mM **3.13**) obtained upon addition of excess guests to butyl imine cavitand **3.13**.
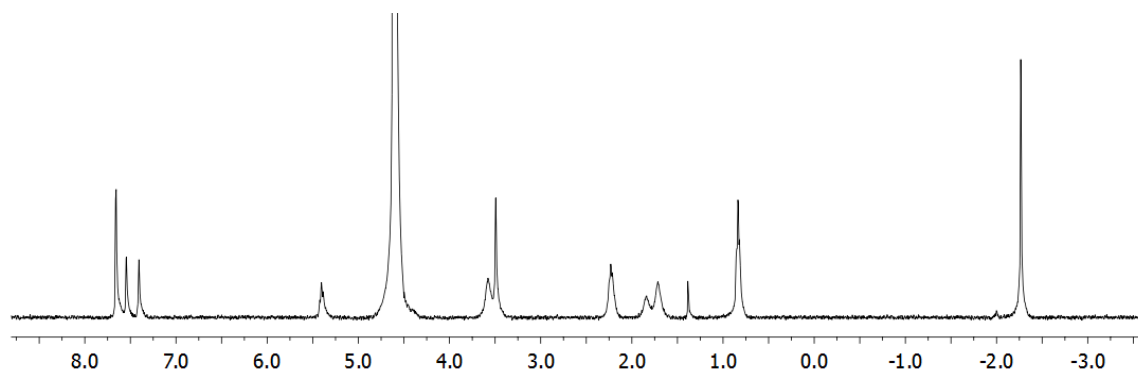
Figure 6.34. ¹H NMR spectrum (400 MHz, D₂O, 298 K) obtained upon addition of 1eq

cyclooctane to 1.8 mM cavitand **4.2**.
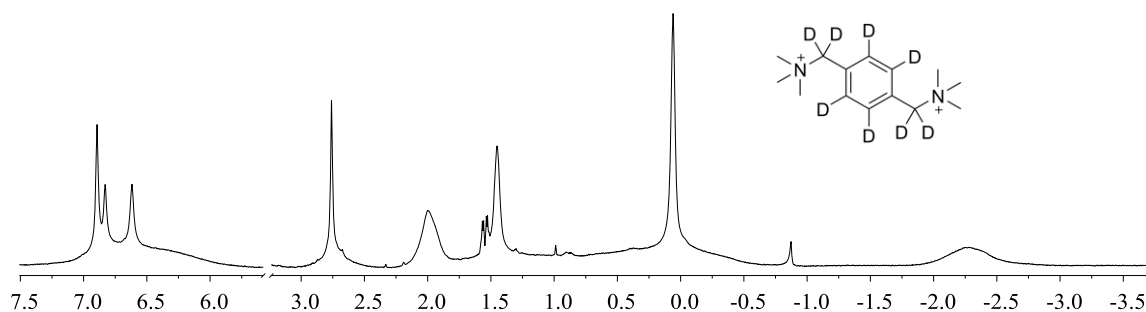
Figure 6.35. ¹H NMR spectrum (400 MHz, D₂O, 298 K) obtained upon addition of 5eq of

α, α'-dimethylammonium-*p*-xylene-*d*₈ to 1.8 mM cavitand **4.2**.
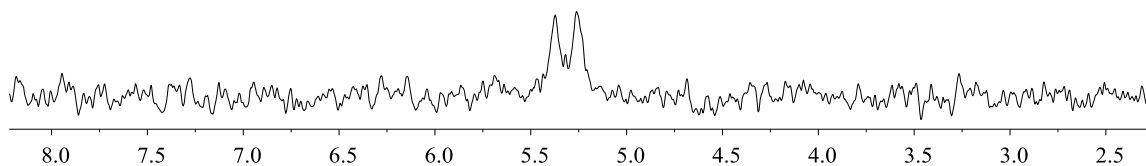
Figure 6.36. ²H NMR spectrum (400 MHz, D₂O, 298 K) obtained upon addition of 5eq of

α, α'-dimethylammonium-*p*-xylene-*d*₈ to 1.8 mM cavitand **4.2**.
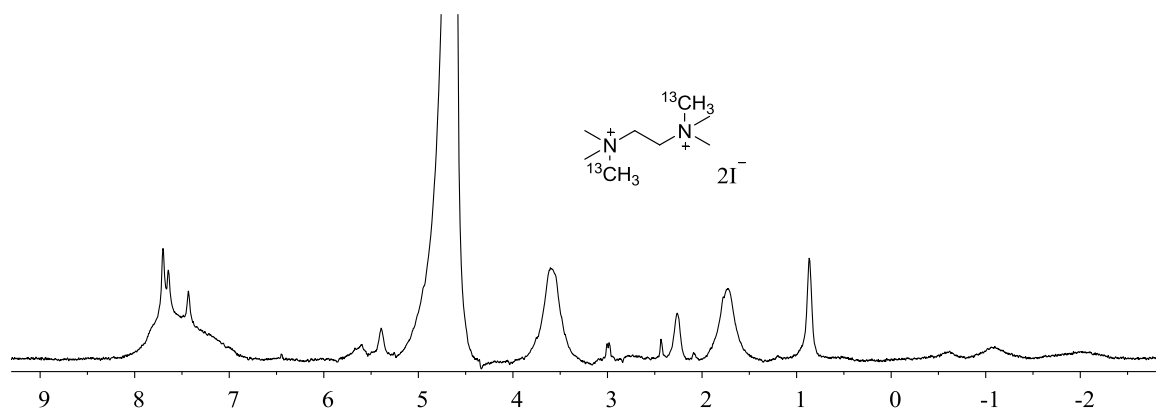
Figure 6.37. ^{1}H NMR spectrum (400 MHz, D$_2$O, 298 K) obtained upon addition of 1.2 eq

of N,N,N,N',N',N' examethyl-1,2-ethanediaminium Diiodide-^{13}C to 1.8 mM cavitand **4.2**.
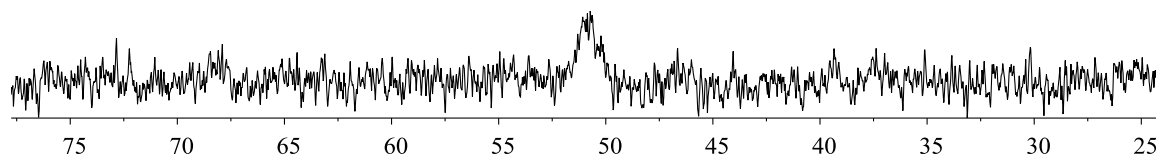
Figure 6.38. ^{13}C NMR spectrum (400 MHz, D$_2$O, 298 K) obtained upon addition of 1.2eq

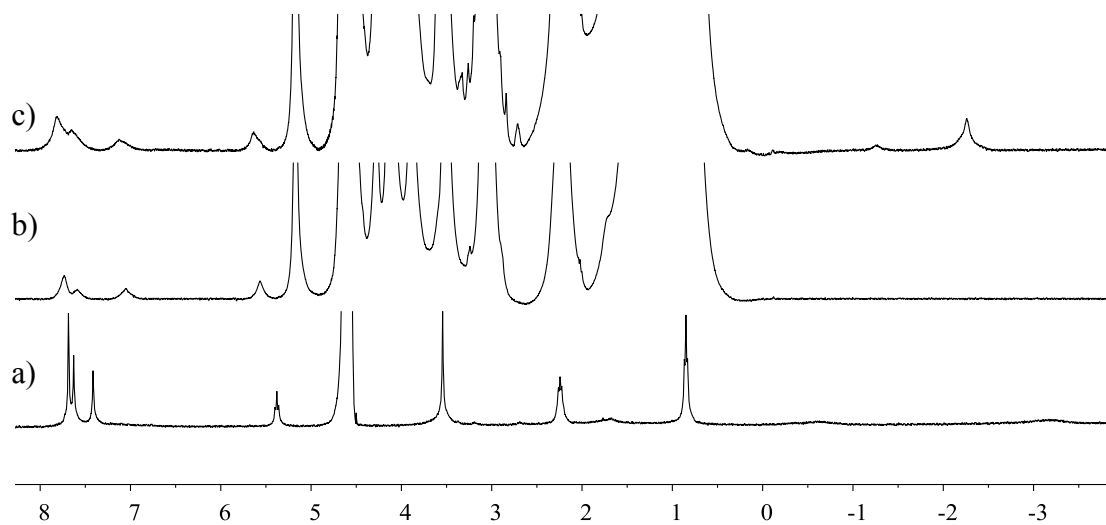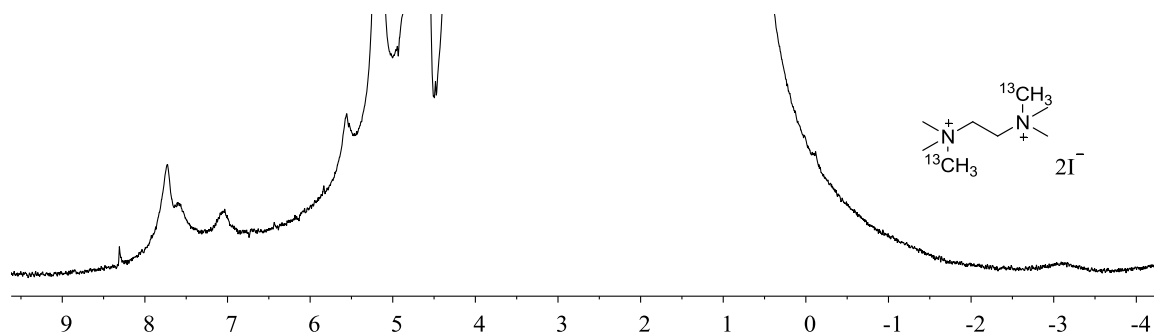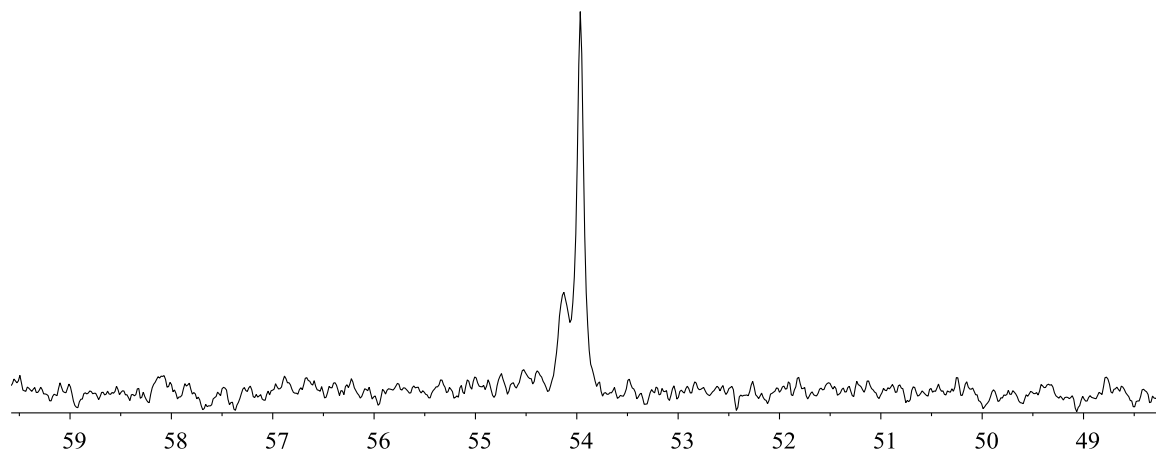of N,N,N,N',N',N' hexamethyl-1,2-ethanediaminium Diiodide-^{13}C to 1.8 mM cavitand **4.2**.
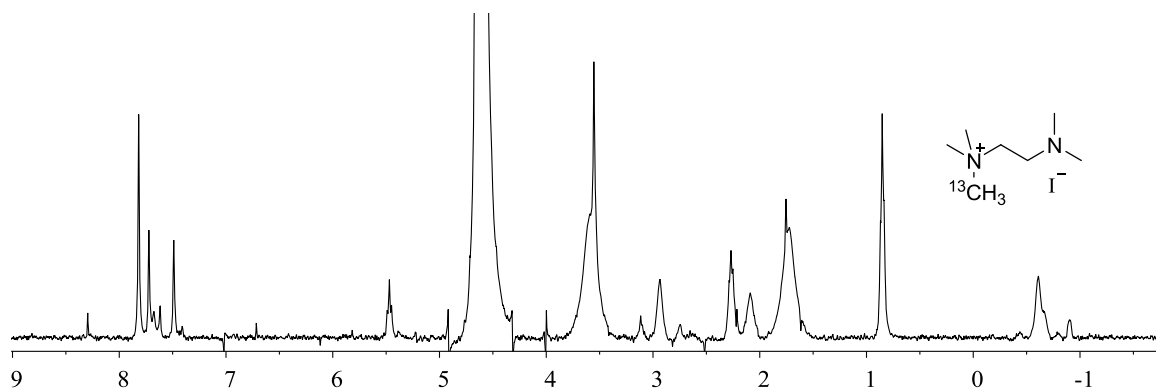
Figure 6.39. ^{1}H NMR spectrum (400 MHz, D$_2$O, 298 K) obtained upon addition of 1.2 eq

of N,N,N,N',N' pentamethyl-1,2-ethanediaminium iodide-^{13}C to 1.8 mM cavitand **4.2**.
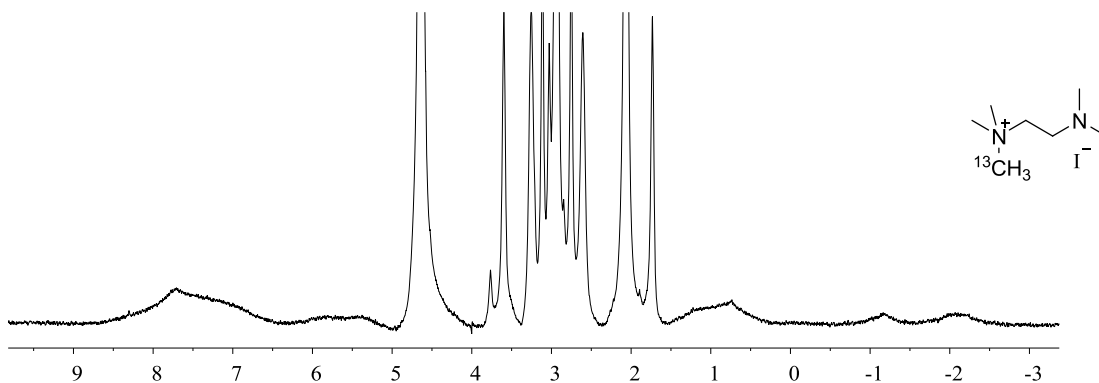
Figure 6.40. ^{1}H NMR spectrum (400 MHz, D$_2$O, 298 K) obtained upon addition of excess of N,N,N,N',N' pentamethyl-1,2-ethanediaminium iodide-^{13}C to 1.8 mM cavitand **4.2**.
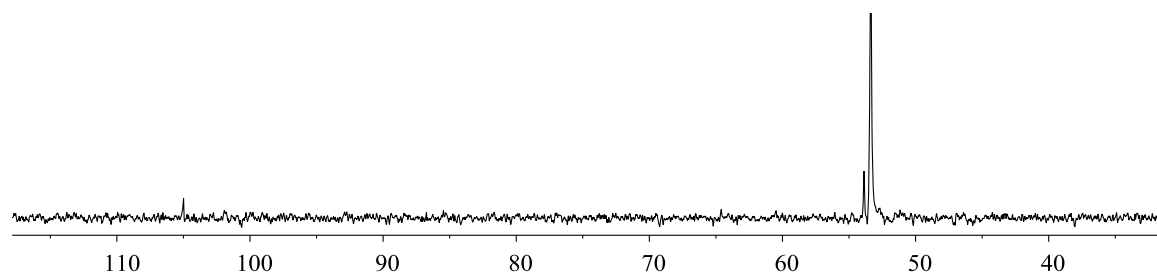
Figure 6.41. ^{13}CNMR spectrum (100 MHz, D$_2$O, 298 K) obtained upon addition of 1.2eq of N,N,N,N',N' pentamethyl-1,2-ethanediaminium iodide-^{13}C to 1.8 mM cavitand **4.2**.
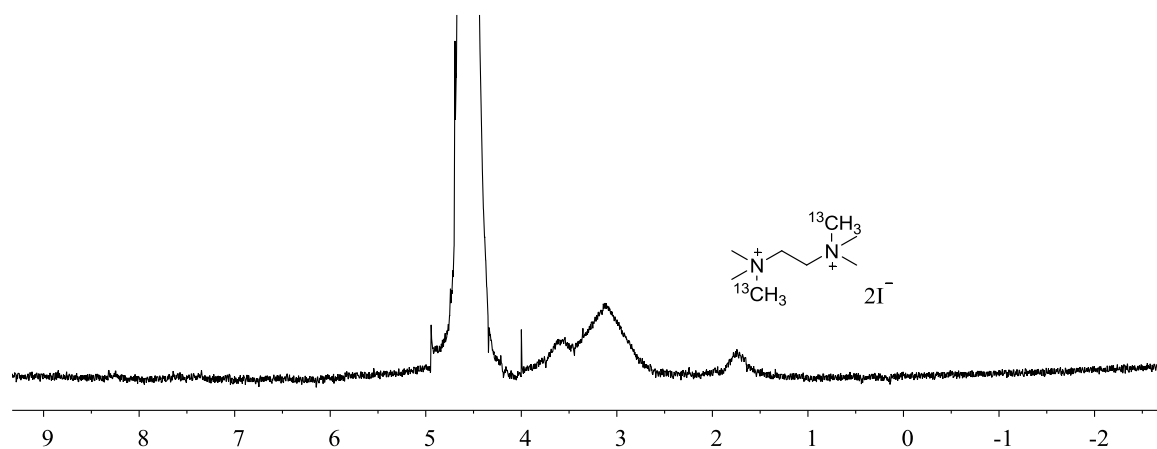
Figure 6.42. ^{1}H NMR spectrum (400 MHz, D$_2$O, 298 K) obtained upon addition of 3eq of N,N,N,N',N',N' hexamethyl-1,2-ethanediaminium Diiodide-^{13}C to 1.8 mM cavitand **4.2**.
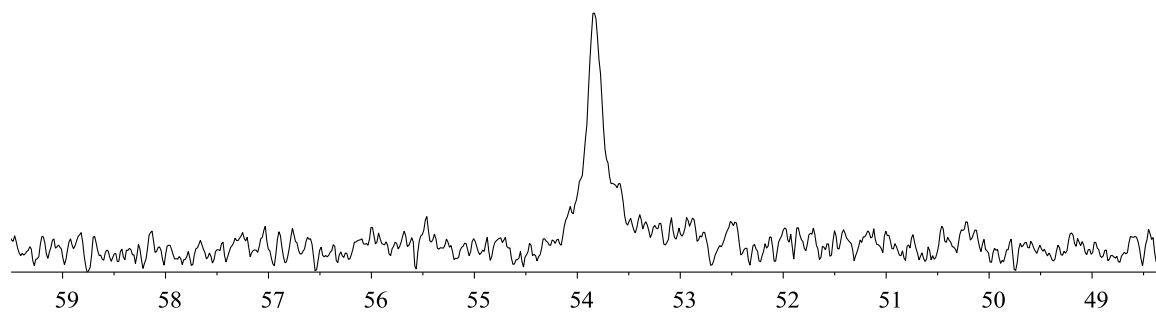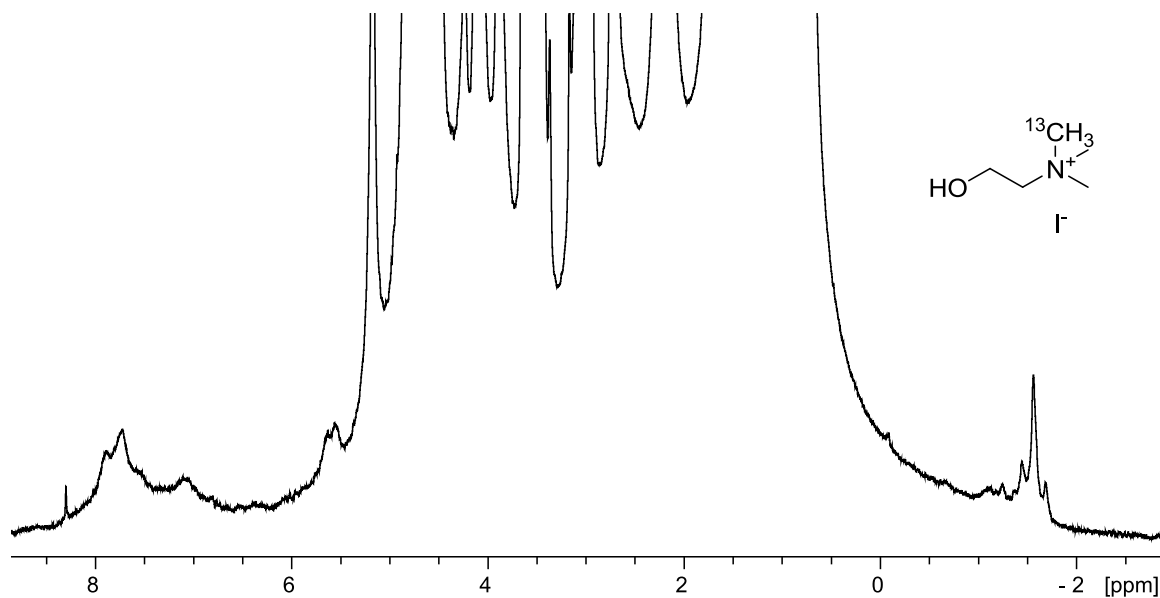
Figure 6.43. ^{13}C NMR spectrum (400 MHz, D$_2$O, 298 K) obtained upon addition of 3eq of N,N,N,N',N',N' hexamethyl-1,2-ethanediaminium diiodide-^{13}C to 1.8 mM cavitand **4.2**.

6.9.2 NMR Spectra of Guest Binding Experiments: in Lipids
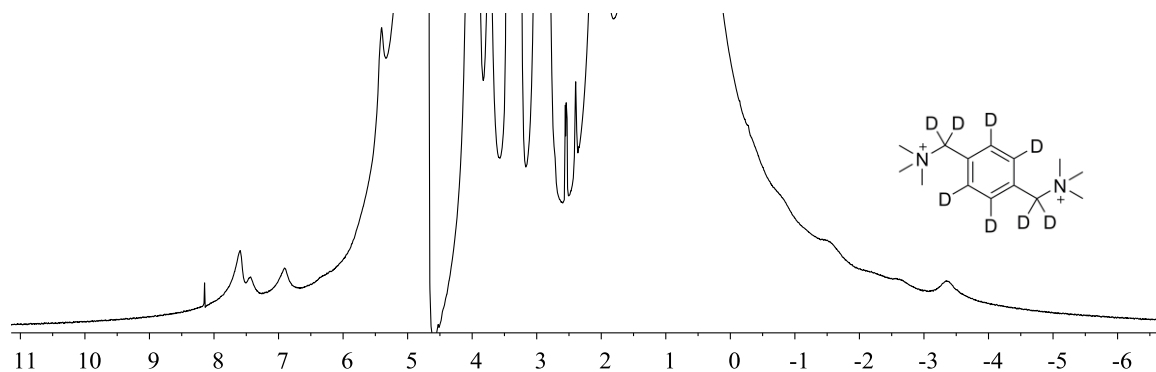
Figure 6.44. ^{1}H NMR spectrum (600 MHz, D$_2$O, 283.15 K) obtained upon addition of 5eq of α, α'-dimethylammonium-*p*-xylene-*d*$_8$ to 1.8 mM cavitand **4.2** in micelles.
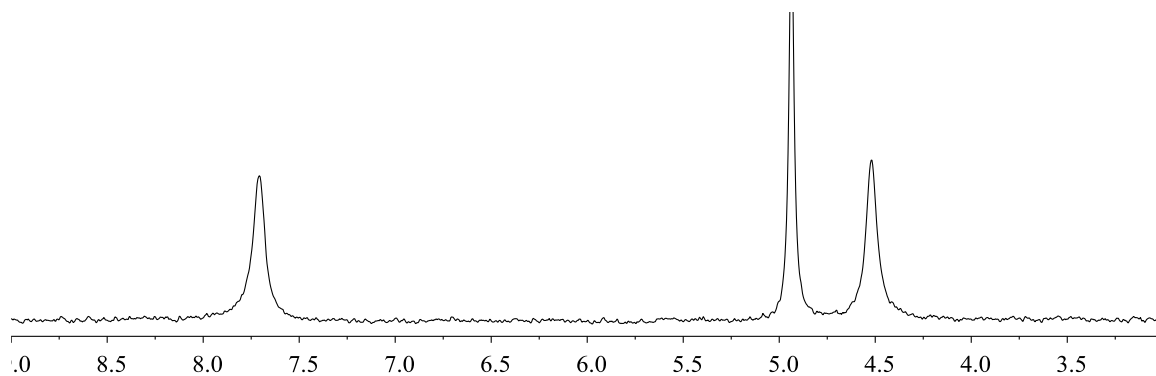
Figure 6.45. ^{2}H NMR spectrum (700 MHz, D$_2$O, 283.15 K) obtained upon addition of 5eq

of α, α'-dimethylammonium-*p*-xylene-*d*$_8$ to 1.8 mM cavitand **4.2** in micelles.
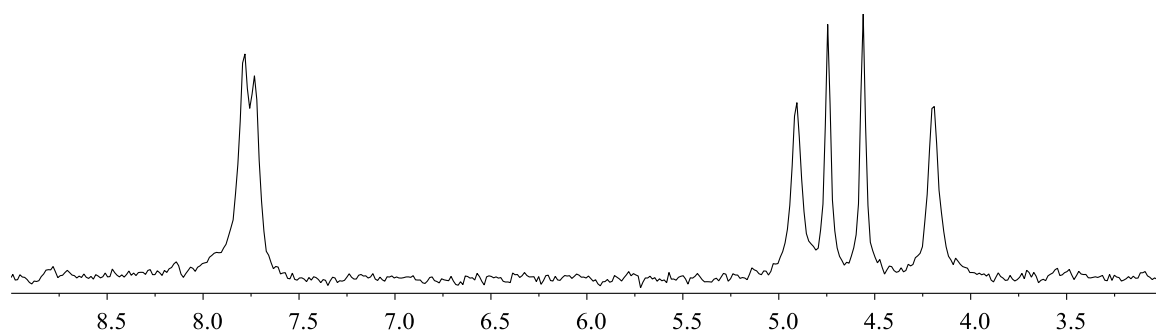
Figure 6.46. ^{2}H NMR spectrum (700 MHz, D$_2$O, 308.15 K) obtained upon addition of 5eq

of α, α'-dimethylammonium-*p*-xylene-*d*$_8$ to 1.8 mM cavitand **4.2** in bicelle.
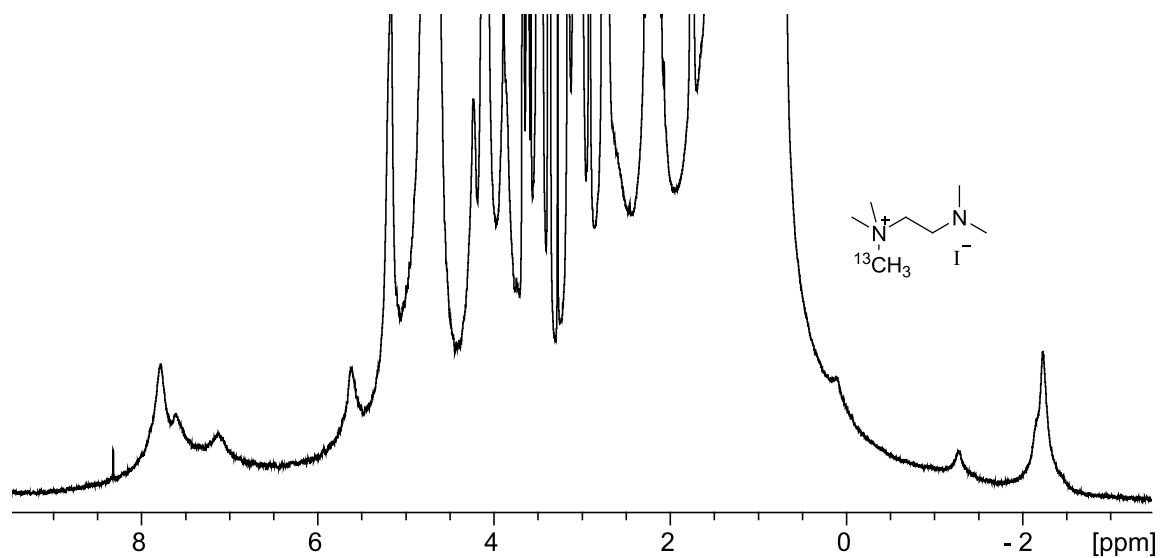
Figure 6.47. ^1H NMR spectrum (600 MHz, D_2O, 298 K) obtained upon addition of 1.2 eq

of N,N,N,N',N' pentamethyl-1,2-ethanediaminium iodide-^{13}C to 1.8 mM cavitand **4.2** in
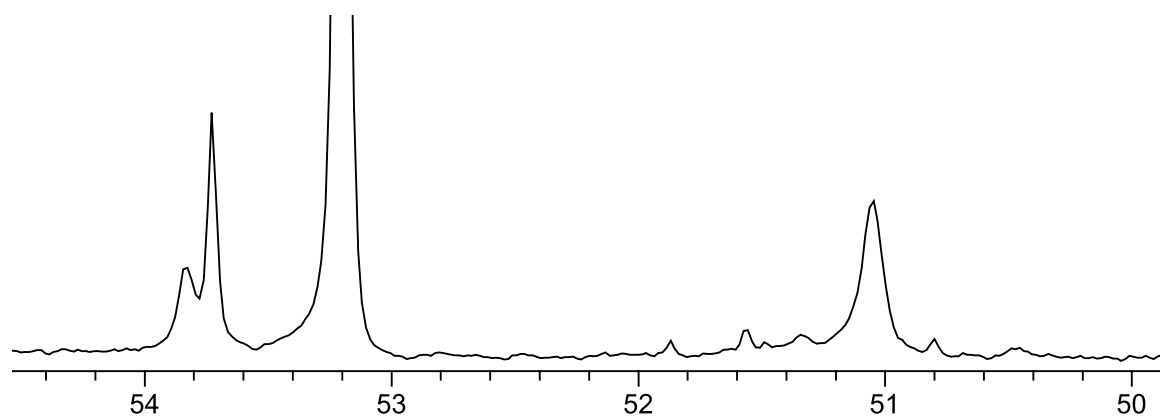
micelles.

Figure 6.48. ^{13}C NMR spectrum (150 MHz, D_2O, 298 K) obtained upon addition of 1.2eq

of N,N,N,N',N' pentamethyl-1,2-ethanediaminium iodide-^{13}C to 1.8 mM cavitand **4.2** in

micelles.

Figure 6.49. ^{1}H NMR spectrum (400 MHz, D$_2$O, 298 K) of a) 1.8 mM of cavitand **4.2** b) 1.8 mM of cavitand **4.2** followed by the addition of micelles. c) 1.8 mM of cavitand **4.2** in micelles solution followed by addition of 1.2eq of N,N,N,N',N' pentamethyl-1,2-ethanediaminium iodide-^{13}C.

Figure 6.50. ^{1}H NMR spectrum (400 MHz, D$_2$O, 298 K) obtained upon addition of 3eq of N,N,N,N',N',N' hexamethyl-1,2-ethanediaminium diiodide-^{13}C to 1.8 mM cavitand **4.2** in micelles.

Figure 6.51. ^{13}C NMR spectrum (100 MHz, D$_2$O, 298 K) obtained upon addition of 3 eq of N,N,N,N',N',N' hexamethyl-1,2-ethanediaminium diiodide-^{13}C to 1.8 mM cavitand **4.2** in micelles.

Figure 6.52. ^{1}H NMR spectrum (600 MHz, D$_2$O, 283.15 K) obtained upon addition of 5eq of choline iodide-^{13}C to 3 mM cavitand **4.2** in micelles.
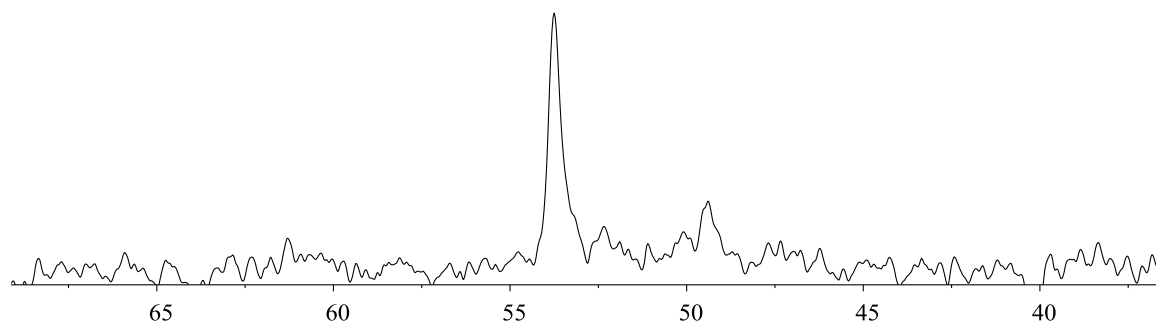
Figure 6.53. ^{13}C NMR spectrum (125 MHz, D$_2$O, 283.15 K) obtained upon addition of 5eq of choline iodide-^{13}C to 3 mM cavitand **4.2** in micelles.

6.10. 2D NMR Spectra of Guest Binding Experiments in Lipids
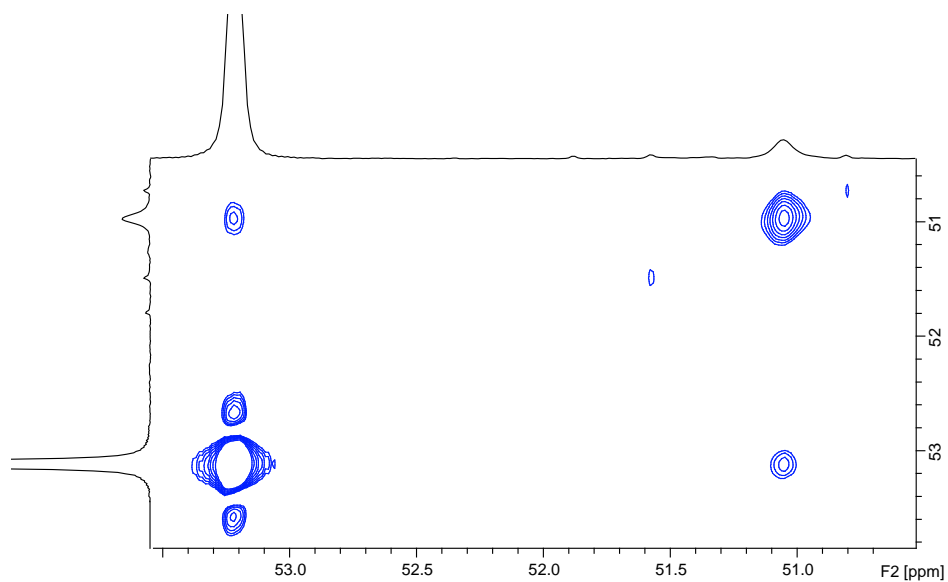
Figure 6.54. ^{13}C 2D EXSY spectrum of 1.2eq of N,N,N,N',N' pentamethyl-1,2-ethanediaminium iodide-^{13}C and 3 mM cavitand **4.2** in micelles (150 MHz, D$_2$O, 298 K, 50 ms mixing time).
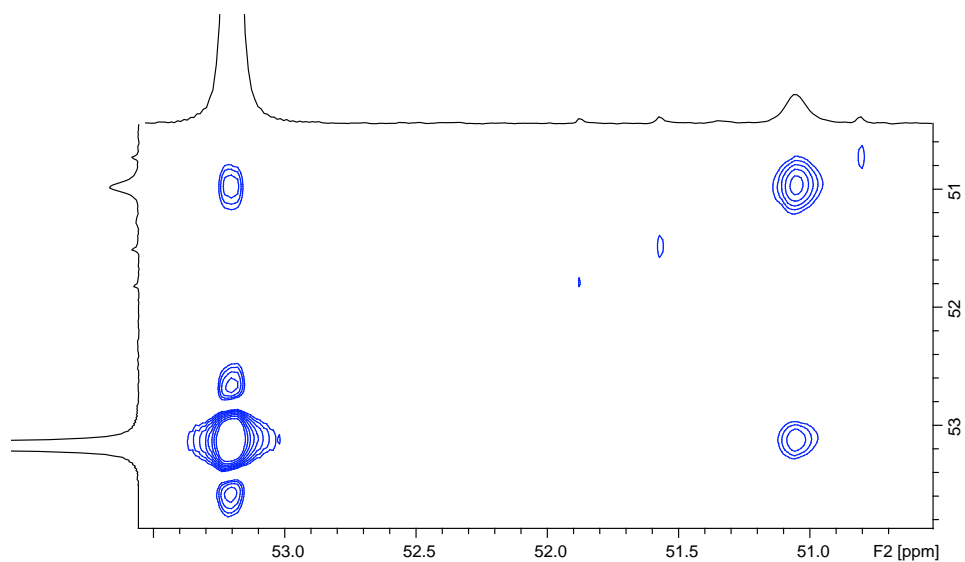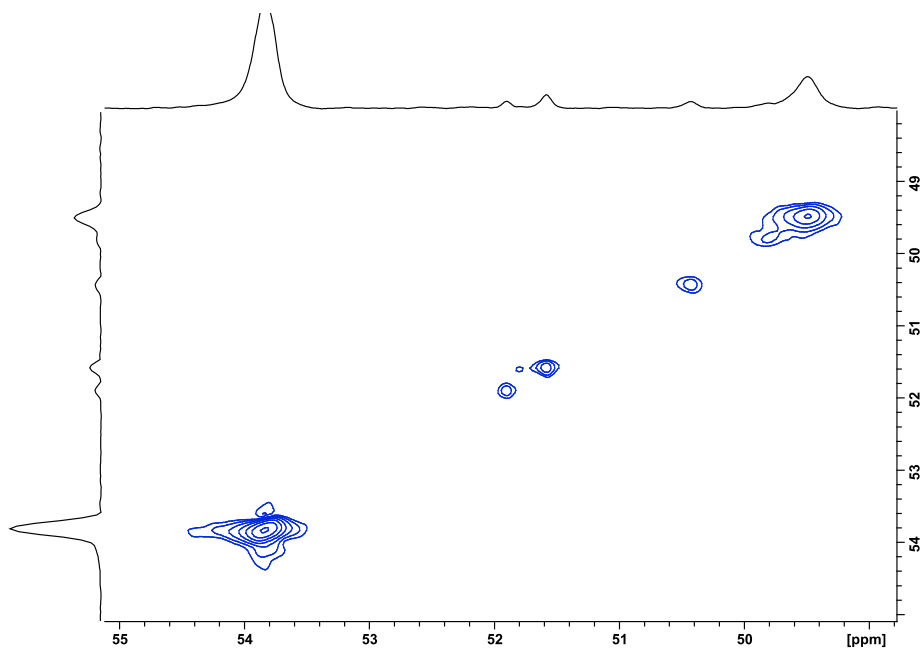
Figure 6.55. ^{13}C 2D EXSY spectrum of 1.2eq of N,N,N,N',N' pentamethyl-1,2-ethanediaminium iodide-^{13}C and 3 mM cavitand **4.2** in micelles (150 MHz, D$_2$O, 298 K, 75 ms mixing time).
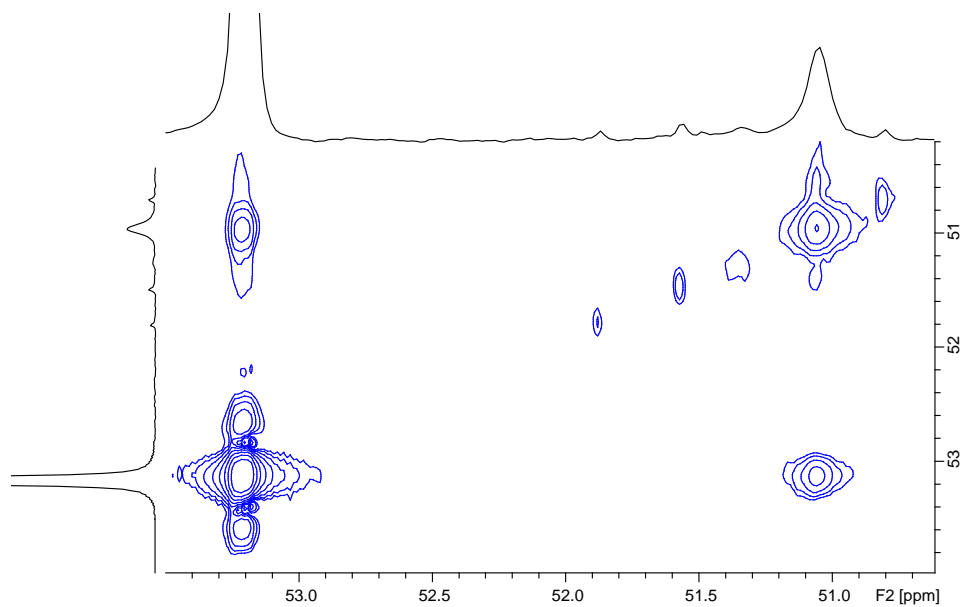
Figure 6.56. ^{13}C 2D EXSY spectrum of 1.2eq of N,N,N,N',N' pentamethyl-1,2-ethanediaminium iodide-^{13}C and 3 mM cavitand **4.2** in micelles (150 MHz, D$_2$O, 298 K, 100 ms mixing time).
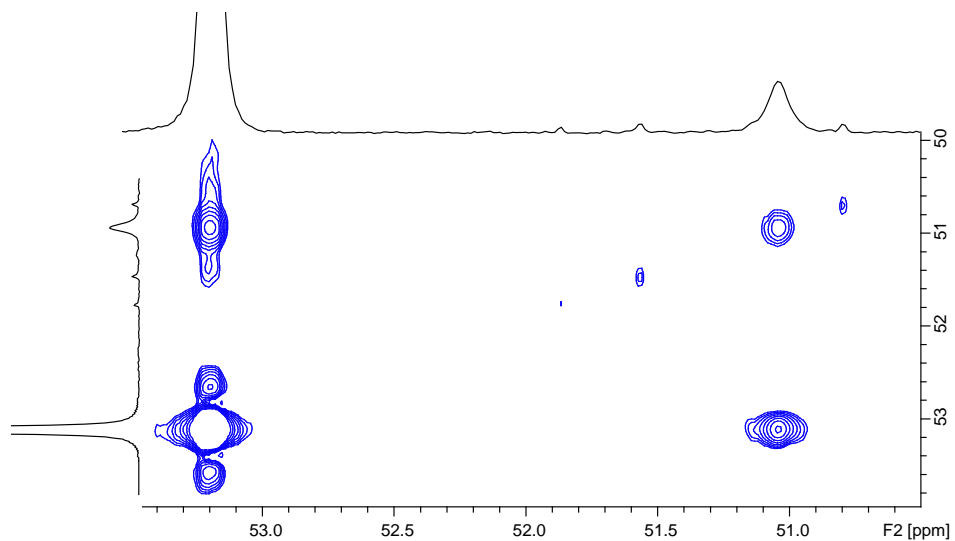
Figure 6.57. ^{13}C 2D EXSY spectrum of 1.2eq of N,N,N,N',N' pentamethyl-1,2-ethanediaminium iodide-^{13}C and 3 mM cavitand **4.2** in micelles (150 MHz, D$_2$O, 298 K, 250 ms mixing time).
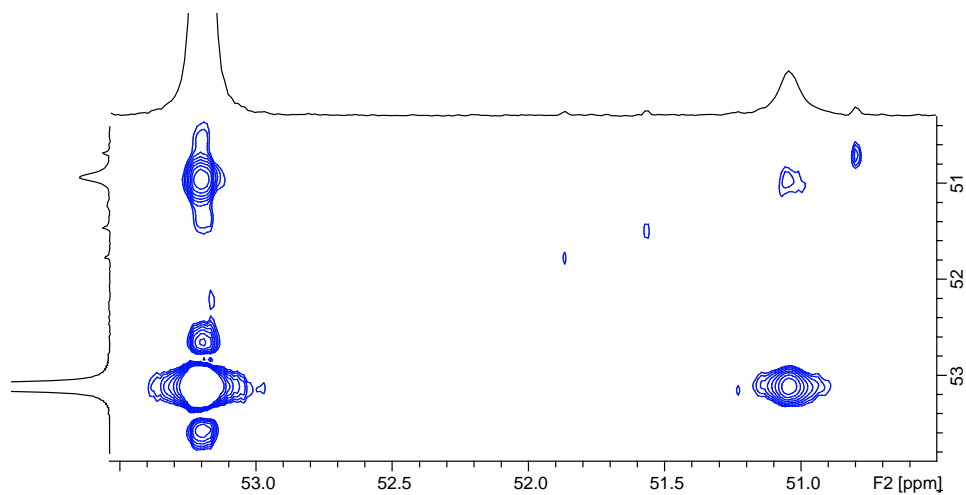
Figure 6.58. ^{13}C 2D EXSY spectrum of 1.2eq of N,N,N,N',N' pentamethyl-1,2-ethanediaminium iodide-^{13}C and 3 mM cavitand **4.2** in micelles (150 MHz, D$_2$O, 298 K, 400 ms mixing time).
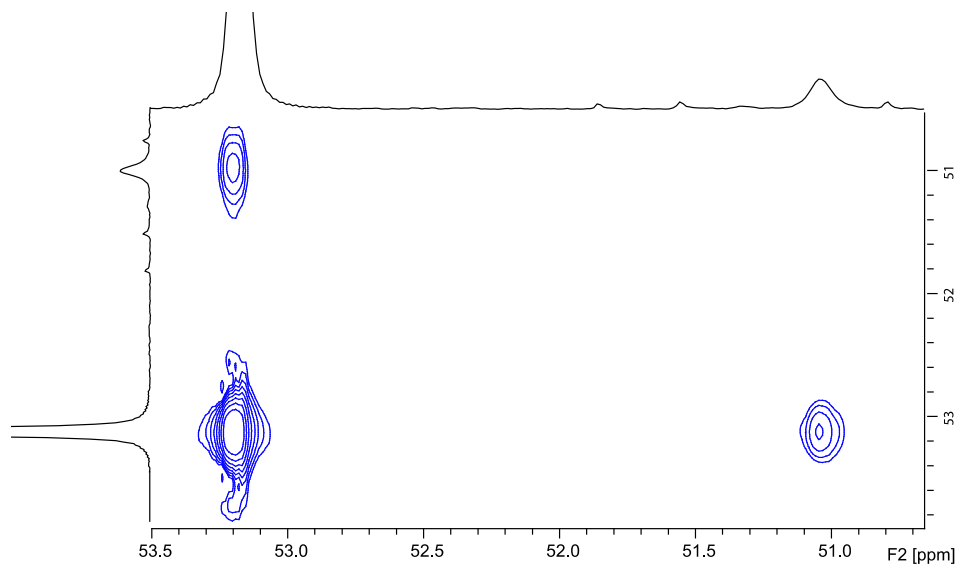
Figure 6.59. [13]C 2D EXSY spectrum of 1.2 eq of N,N,N,N',N' pentamethyl-1,2-ethanediaminium iodide-^{13}C and 3 mM cavitand **4.2** in micelles (150 MHz, D_2O, 298 K, 500 ms mixing time).
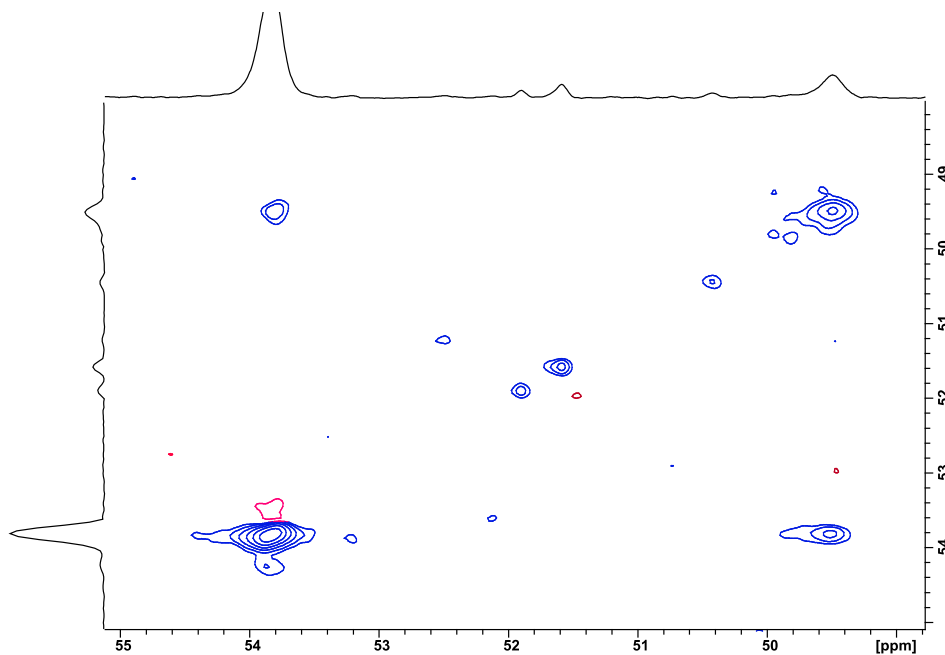

Figure 6.60. [13]C 2D EXSY spectrum of 5 eq of Choline Iodide-^{13}C and 3 mM cavitand **4.2** in micelles (150 MHz, D_2O, 298 K, 3 ms mixing time).
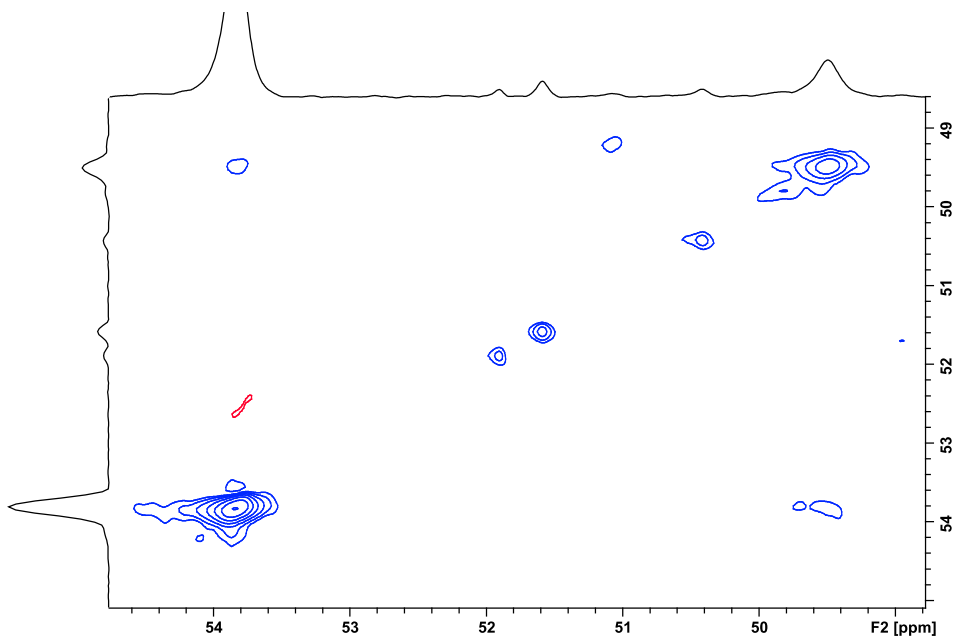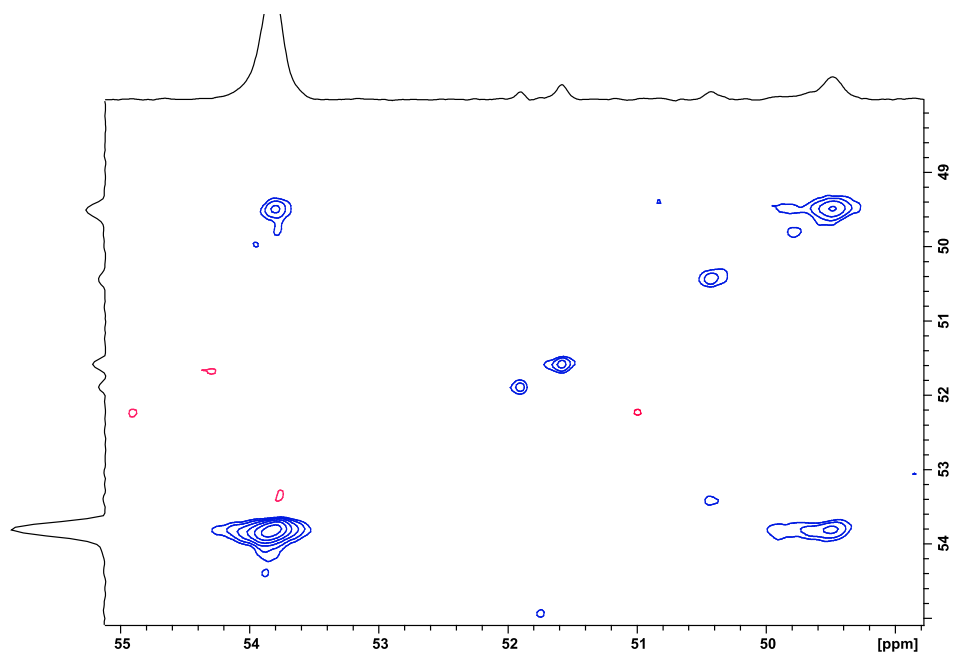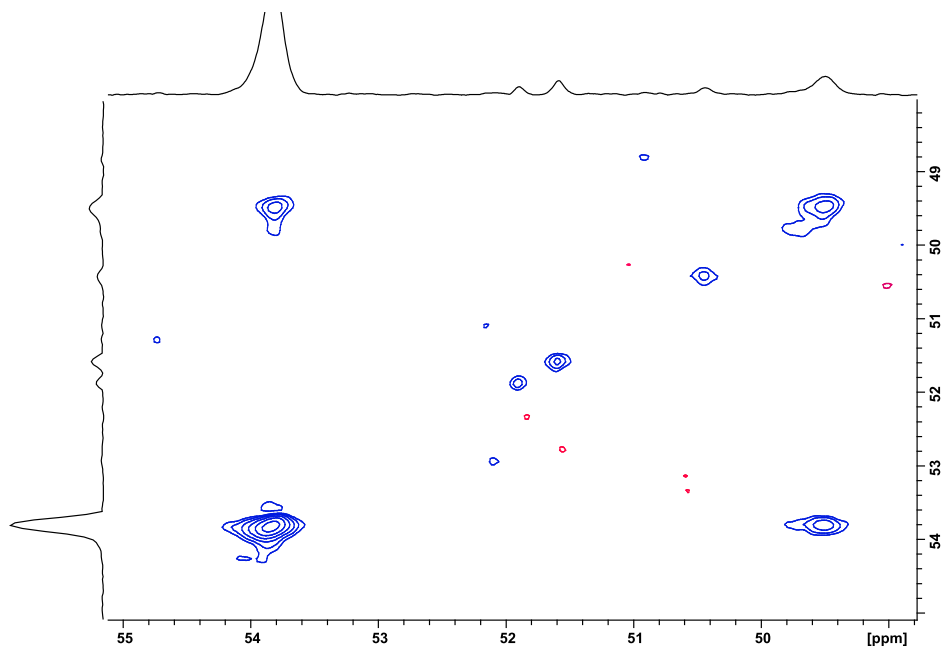
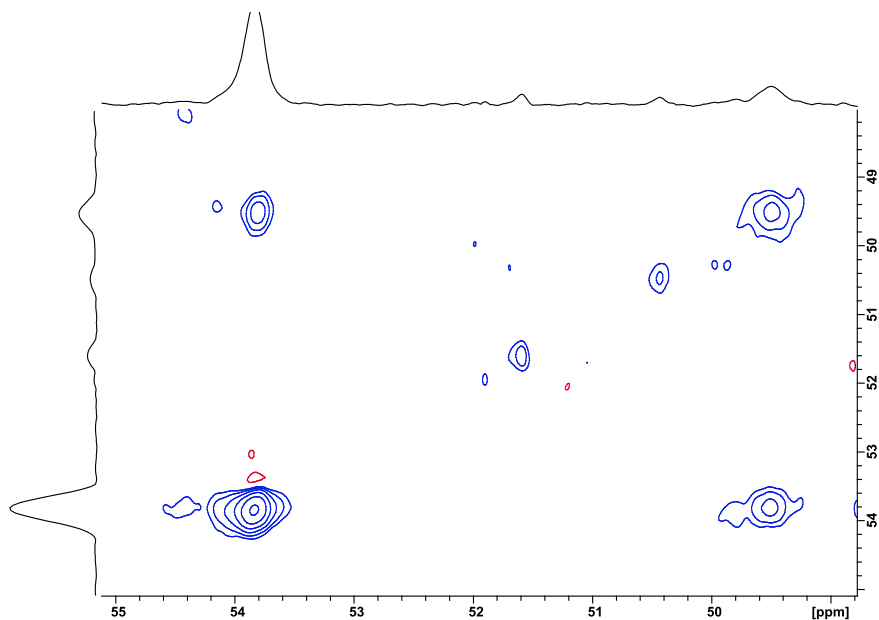**Figure 6.61.** ^{13}C 2D EXSY spectrum of 5 eq of Choline Iodide-^{13}C and 3 mM cavitand **4.2** in micelles (150 MHz, D$_2$O, 298 K, 50 ms mixing time).
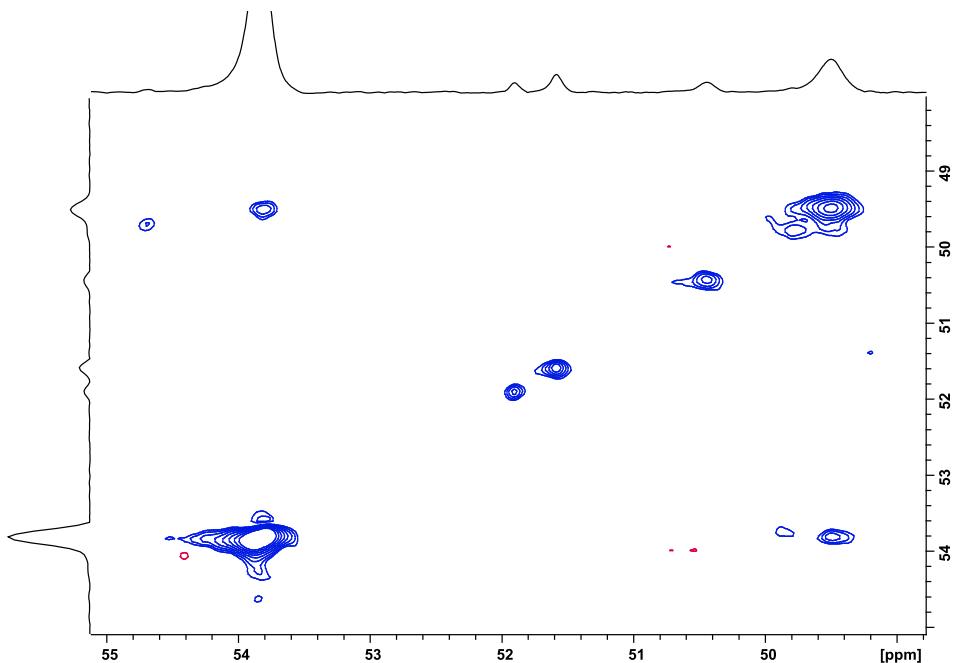
Figure 6.62. ^{13}C 2D EXSY spectrum of 5 eq of Choline Iodide-^{13}C and 3 mM cavitand **4.2** in micelles (150 MHz, D$_2$O, 298 K, 75 ms mixing time).
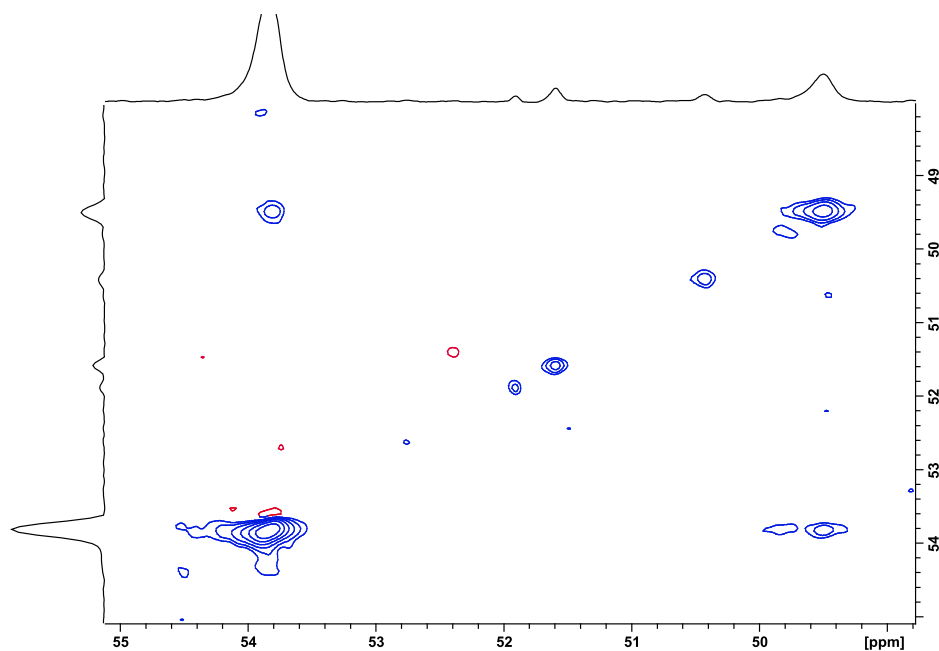
Figure 6.63.^{13}C 2D EXSY spectrum of 5eq of Choline Iodide-^{13}C and 3 mM cavitand **4.2** in micelles (150 MHz, D$_2$O, 298 K, 100 ms mixing time).

**Figure 6.64.**^{13}C 2D EXSY spectrum of 5 eq of Choline Iodide-^{13}C and 3 mM cavitand **4.2** in micelles (150 MHz, D$_2$O, 298 K, 150 ms mixing time).

Figure 6.65. ^{13}C 2D EXSY spectrum of 5 eq of Choline Iodide-^{13}C and 3 mM cavitand **4.2** in micelles (150 MHz, D$_2$O, 298 K, 200 ms mixing time).

Figure 6.666. ^{13}C 2D EXSY spectrum of 5eq of Choline Iodide-^{13}C and 3 mM cavitand **4.2** in micelles (150 MHz, D$_2$O, 298 K, 250 ms mixing time).

Figure 6.67. ^{13}C 2D EXSY spectrum of 5eq of Choline Iodide-^{13}C and 3 mM cavitand **4.2** in micelles (150 MHz, D$_2$O, 298 K, 300 ms mixing time).
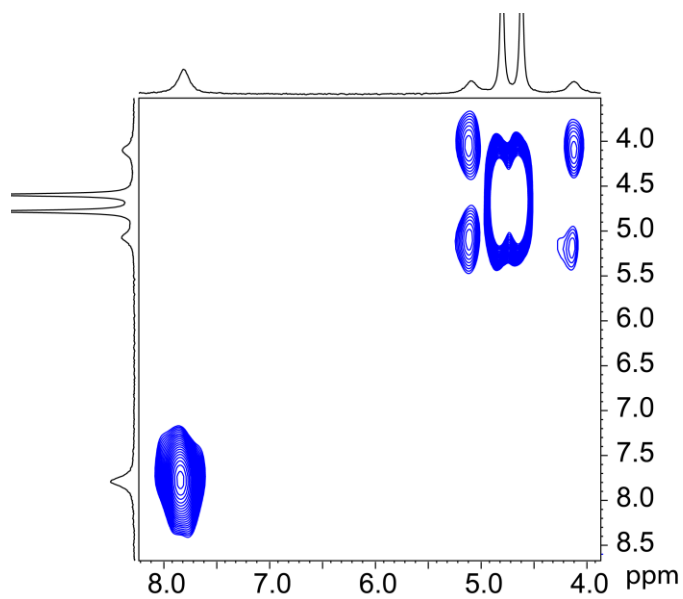
Figure 6.68. ^{2}H EXSY spectrum of micellar system with 5 mM cavitand **4.2** and 1.2 eq. Deuterated labeled xylene-d_8 **5.4** (H$_2$O, 700 MHz, mixing time = 10 ms, 298 K).
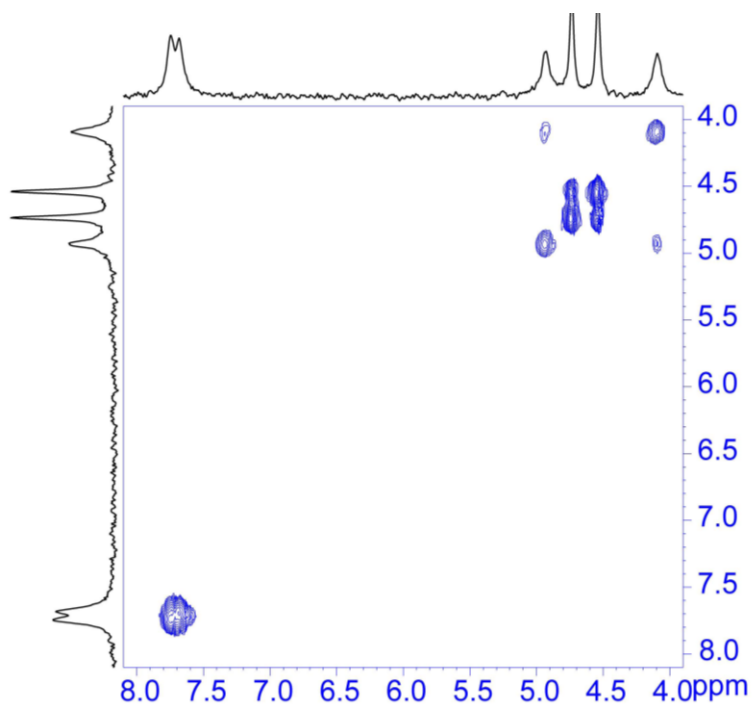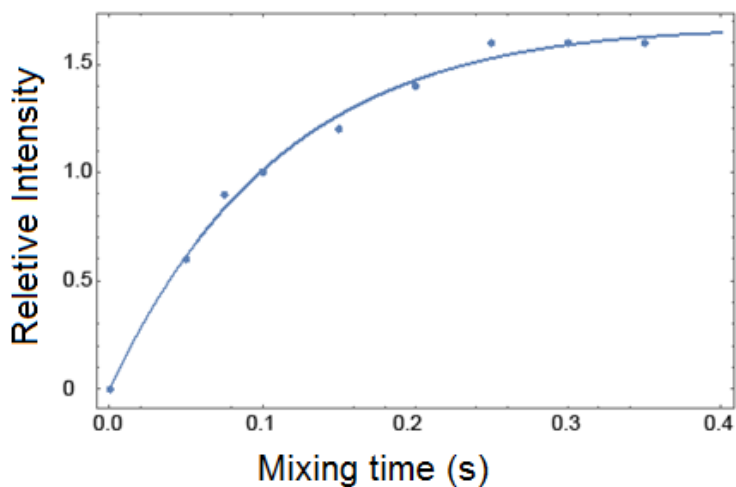
Figure 6.69. ^{2}H EXSY spectrum of micellar system with 5 mM cavitand **4.2** and 1.2 eq. Deuterated labeled xylene-d_8 **5.4** (H$_2$O, 700 MHz, mixing time = 5 ms, 298 K).

Figure 6.70. ^{13}C EXSY calculated exchange rate of micellar system with 5 mM cavitand **4.2** and 3 eq. ^{13}C- 2-(dimethylamino)-N,N,N-trimethylethanaminium **5.8** (D$_2$O, 150 MHz, 298 K, mixing time = 3 ms, 75 ms, 100 ms, 250 ms, 275, 300 ms, 350 ms).
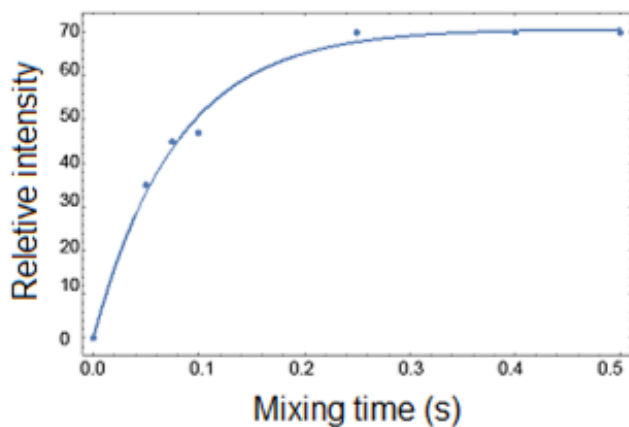
Figure 6.71. ^{13}C EXSY calculated exchange rate of micellar system with 5 mM cavitand **4.2** and 3 eq. ^{13}C- 2-(dimethylamino)-N,N,N-trimethylethanaminium **5.5** with in/out cross peaks (D_2O, 150 MHz, 298 K, mixing time = 3 ms, 75 ms, 100 ms,125 ms, 250 ms, 400 ms, 500 ms).
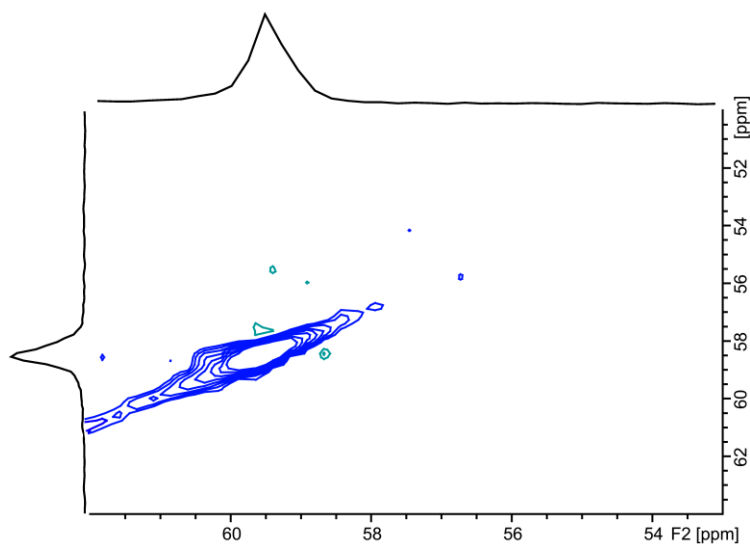

Figure 6.72. ^{13}C 2D EXSY spectrum of 5eq of Choline Iodide-^{13}C and 5 mM cavitand **4.2** in bicelles (150 MHz, D_2O, 308.15 K, 3 ms mixing time).
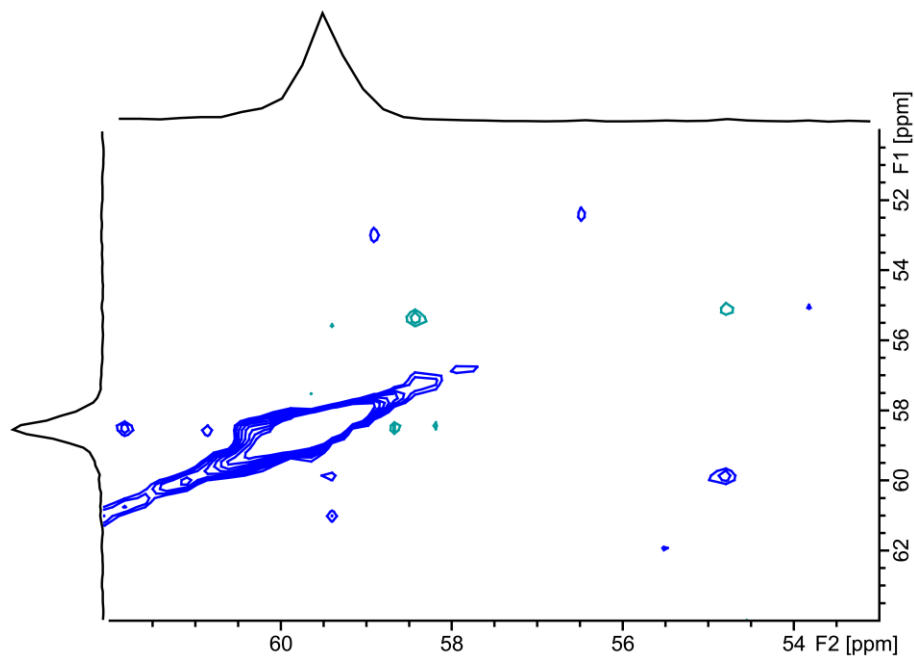
Figure 6.73. ^{13}C 2D EXSY spectrum of 5eq of Choline Iodide-^{13}C and 5 mM cavitand **4.2** in bicelles (150 MHz, D$_2$O, 308.15 K, 100 ms mixing time).
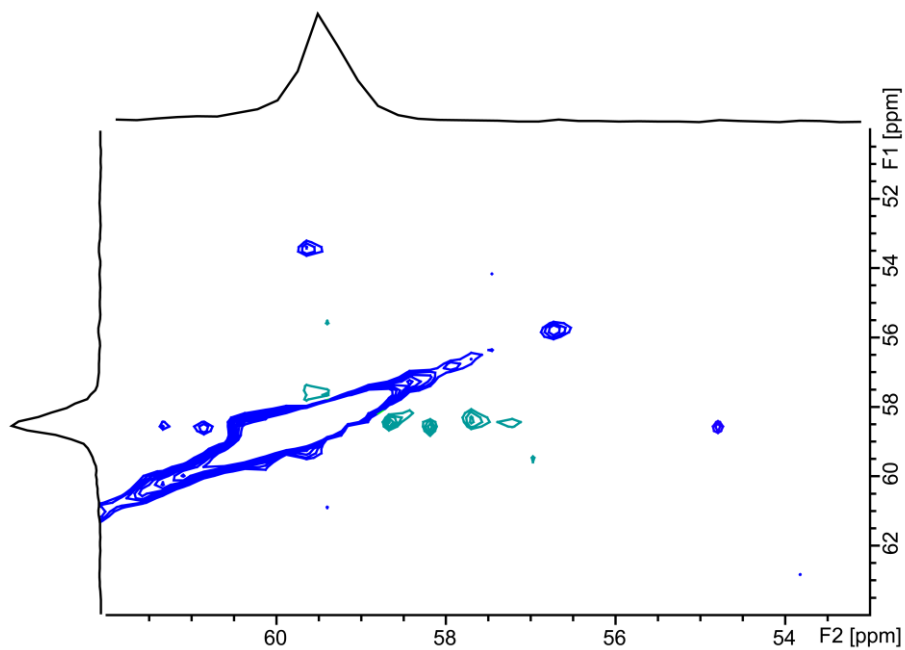

Figure 6.74. ^{13}C 2D EXSY spectrum of 5eq of Choline Iodide-^{13}C and 5 mM cavitand **4.2** in bicelles (150 MHz, D$_2$O, 308.15 K, 150 ms mixing time).
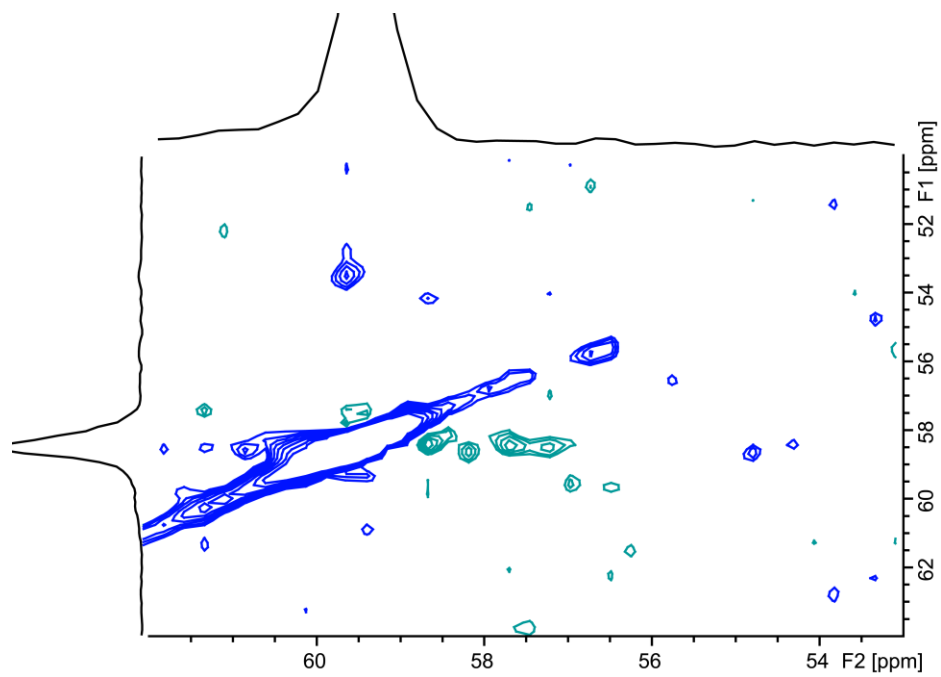
Figure 6.75. [13]C 2D EXSY spectrum of 5eq of Choline Iodide-^{13}C and 5 mM cavitand **4.2** in bicelles (150 MHz, D_2O, 308.15 K, 250 ms mixing time).
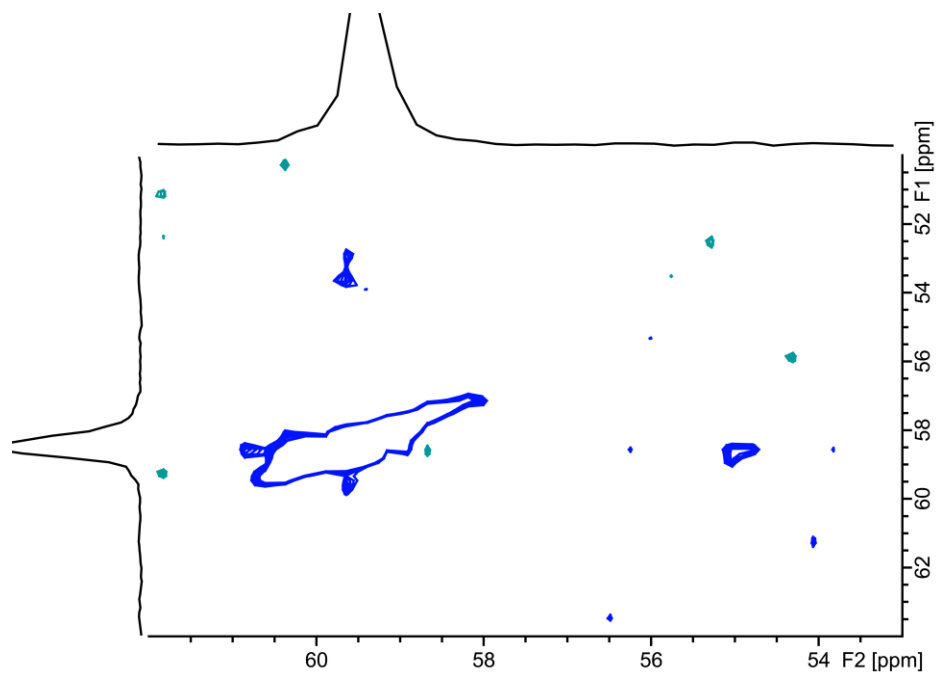
Figure 6.76. ^{13}C 2D EXSY spectrum of 5eq of Choline Iodide-^{13}C and 5 mM cavitand **4.2** in bicelles (150 MHz, D$_2$O, 308.15 K, 500 ms mixing time).
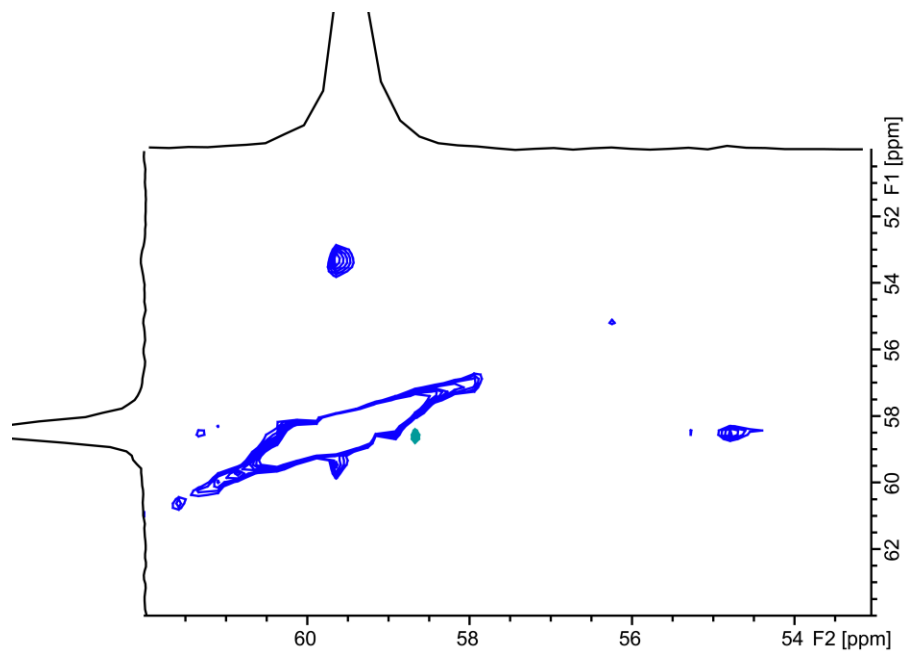

Figure 6.77. ^{13}C 2D EXSY spectrum of 5eq of Choline Iodide-^{13}C and 5 mM cavitand **4.2** in bicelles (150 MHz, D$_2$O, 308.15 K, 750 ms mixing time).

Figure 6.78. ^{13}C 2D EXSY spectrum of 5eq of Choline Iodide-^{13}C and 5 mM cavitand **4.2** in bicelles (150 MHz, D_2O, 308.15 K, 1000 ms mixing time).

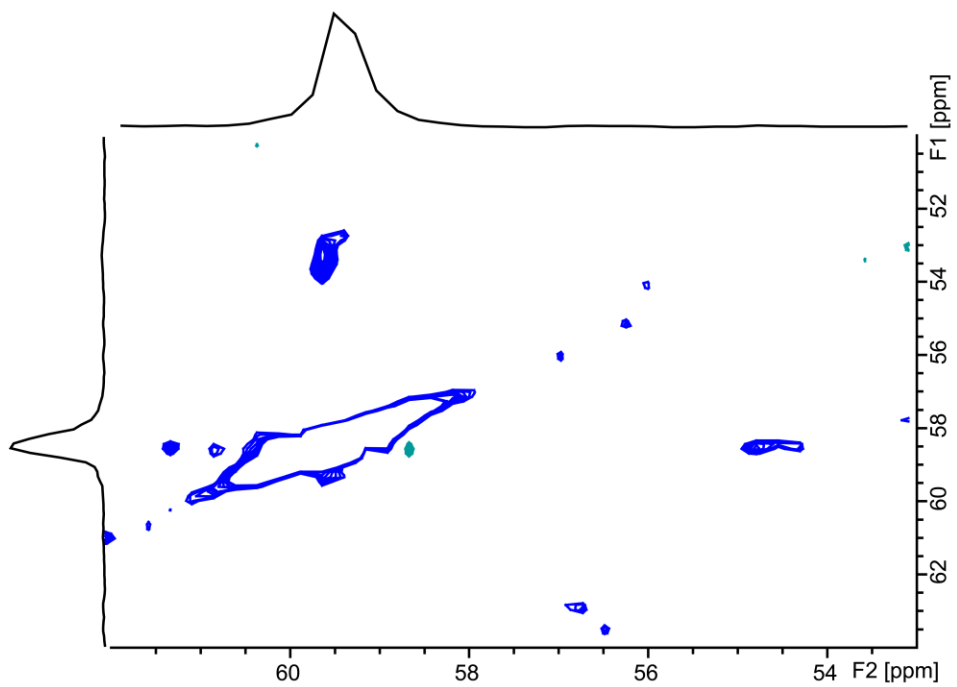**Figure 6.79.** Full ^{13}C 2D EXSY spectrum of 5eq of N,N,N,N',N' pentamethyl-1,2-ethanediaminium iodide-^{13}C and 5 mM cavitand **4.2** in bicelles (150 MHz, D$_2$O, 308.15 K, 250 ms mixing time).

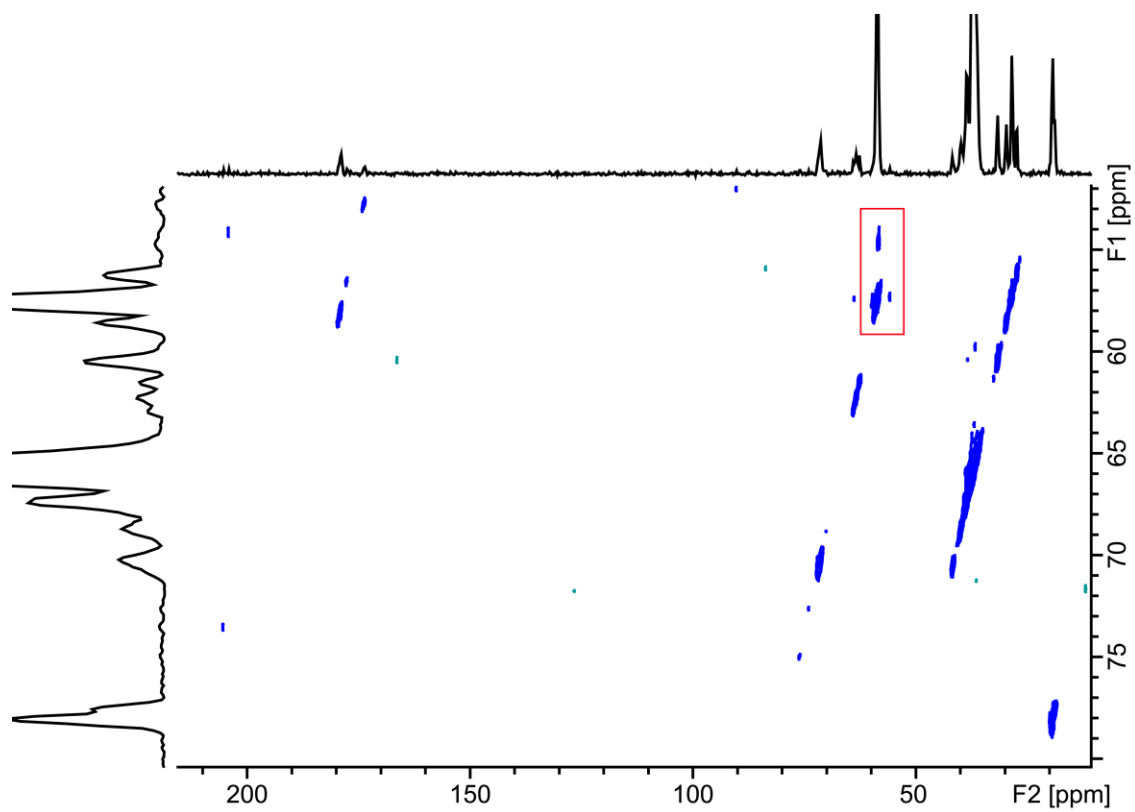**Figure 6.80.** ^{13}C 2D EXSY spectrum of 5eq of N,N,N,N',N' pentamethyl-1,2-ethanediaminium iodide-^{13}C and 5 mM cavitand **4.2** in bicelles (150 MHz, D$_2$O, 308.15 K, 3 ms mixing time).

Figure 6.81. ^{13}C 2D EXSY spectrum of 5eq of N,N,N,N',N' pentamethyl-1,2-ethanediaminium iodide-^{13}C and 5 mM cavitand **4.2** in bicelles (150 MHz, D$_2$O, 308.15 K, 10 ms mixing time).
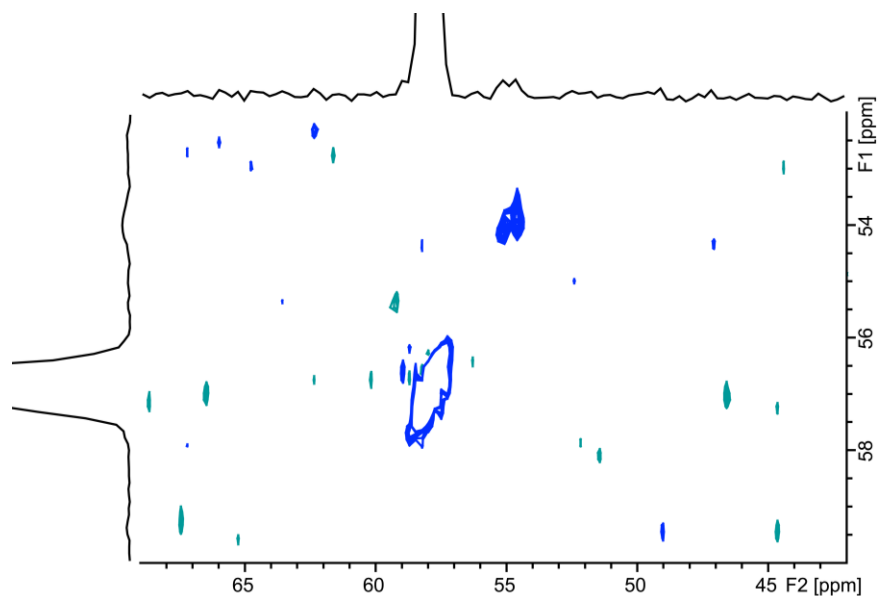
Figure 6.82. ^{13}C 2D EXSY spectrum of 5eq of N,N,N,N',N' pentamethyl-1,2-ethanediaminium iodide-^{13}C and 5 mM cavitand **4.2** in bicelles (150 MHz, D$_2$O, 308.15 K, 30 ms mixing time).

Figure 6.83. ^{13}C 2D EXSY spectrum of 5eq of N,N,N,N',N' pentamethyl-1,2-ethanediaminium iodide-^{13}C and 5 mM cavitand **4.2** in bicelles (150 MHz, D$_2$O, 308.15 K, 40 ms mixing time).
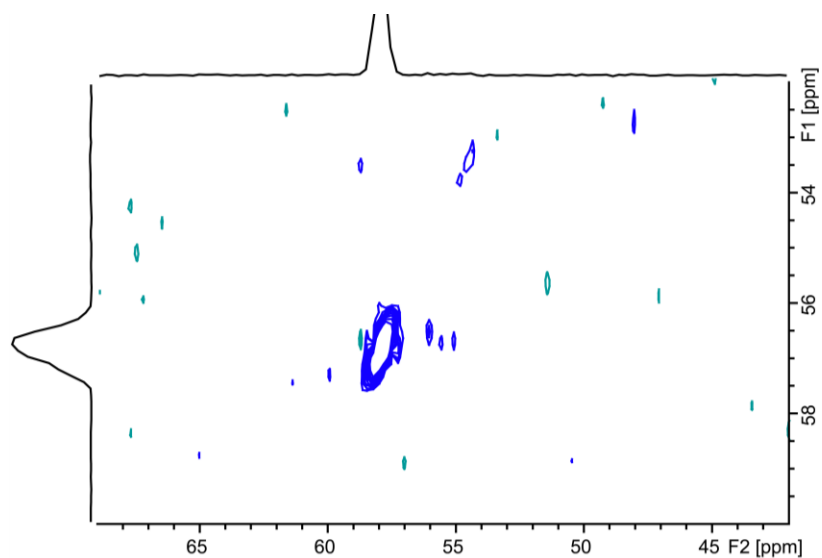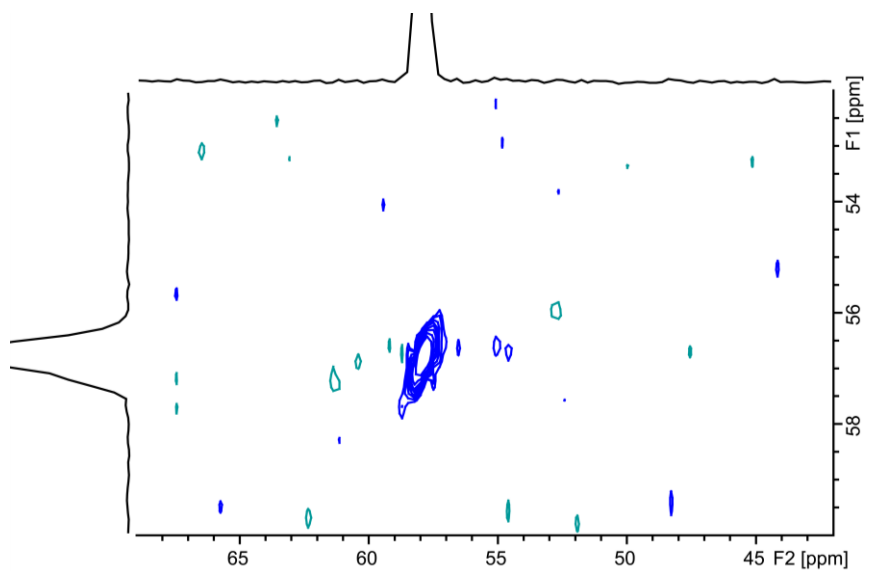
Figure 6.84. ¹³C 2D EXSY spectrum of 5eq of N,N,N,N',N' pentamethyl-1,2-ethanediaminium iodide-¹³C and 5 mM cavitand **4.2** in bicelles (150 MHz, D₂O, 308.15 K, 50 ms mixing time).
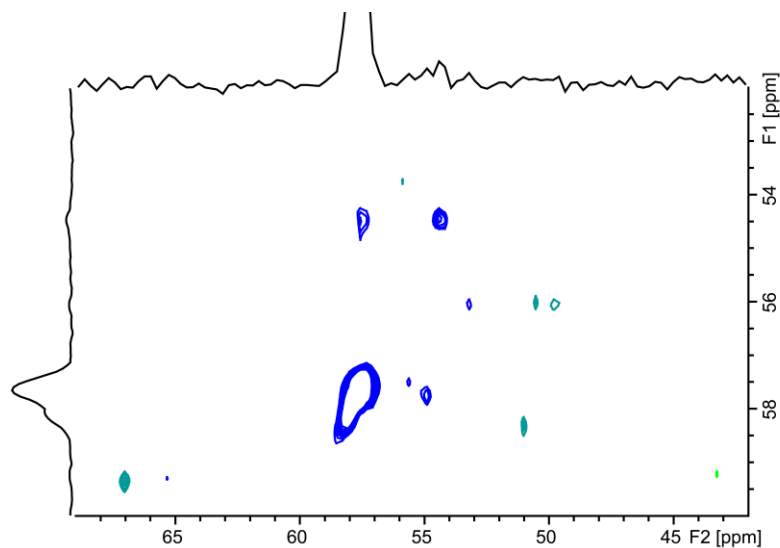
Figure 6.85. ¹³C 2D EXSY spectrum of 5eq of N,N,N,N',N' pentamethyl-1,2-ethanediaminium iodide-¹³C and 5 mM cavitand **4.2** in bicelles (150 MHz, D₂O, 308.15 K, 100 ms mixing time).
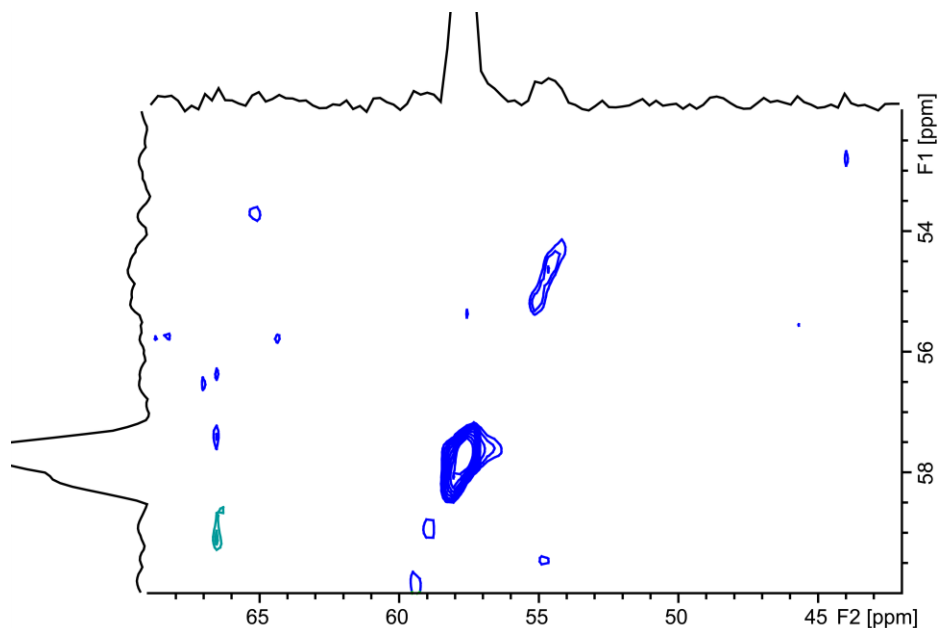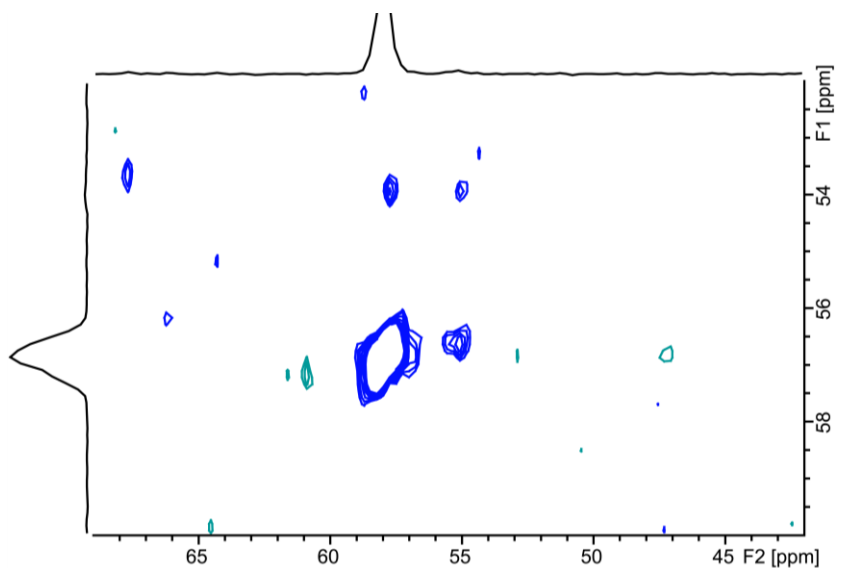
Figure 6.86. ^{13}C 2D EXSY spectrum of 5eq of N,N,N,N',N' pentamethyl-1,2-ethanediaminium iodide-^{13}C and 5 mM cavitand **4.2** in bicelles (150 MHz, D$_2$O, 308.15 K, 250 ms mixing time).

Figure 6.87. ^{13}C 2D EXSY spectrum of 5eq of N,N,N,N',N' pentamethyl-1,2-ethanediaminium iodide-^{13}C and 5 mM cavitand **4.2** in bicelles (150 MHz, D$_2$O, 308.15 K, 250 ms mixing time).
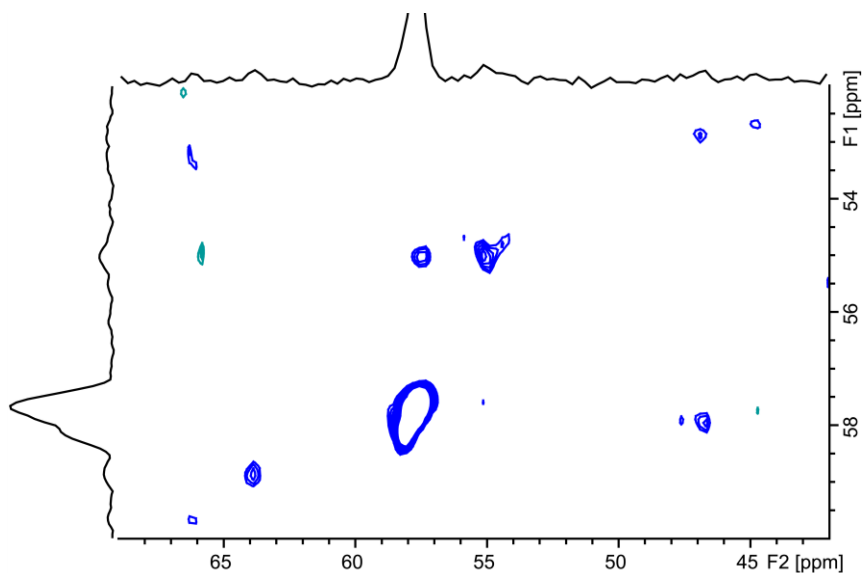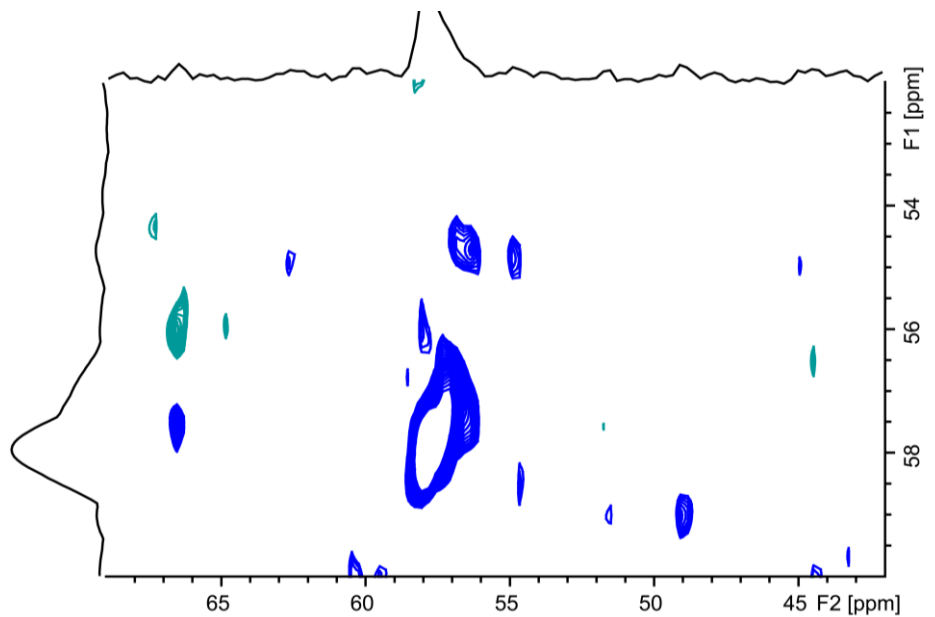
6.11. References:

(1)   Mezo, A. R.; Sherman, J. C. Water-Soluble Cavitands: Synthesis of Methylene-Bridged Resorcin[4]arenes Containing Hydroxyls and Phosphates at Their Feet and Bromomethyls and Thiomethyls at Their Rims. *J. Org. Chem.* **1998**, *63*, 6824-6829.

(2)   Djernes, K. E.; Moshe, O.; Mettry, M.; Richards, D. D.; Hooley, R. J. Metal-coordinated water-soluble cavitands act as C-H oxidation catalysts. *Org. Lett.* **2012**, *14*, 788-791.

(3)   Woollard-Shore, J. G.; Holland, J. P.; Jones, M. W.; Dilworth, J. R. Nitrite reduction by copper complexes. *Dalton Trans* **2010**, *39*, 1576-1585.

(4)   Sanphanya, K.; Wattanapitayakul, S. K.; Prangsaengtong, O.; Jo, M.; Koizumi, K.; Shibahara, N.; Priprem, A.; Fokin, V. V.; Vajragupta, O. Synthesis and evaluation of 1-(substituted)-3-prop-2-ynylureas as antiangiogenic agents. *Bioorg. Med. Chem. Lett.* **2012**, *22*, 3001-3005.

(5)   Gardner, M.; Guerin, A. J.; Hunter, C. A.; Michelsen, U.; Rotger, C. Self-assembly of zinc aminoporphyrins. *New J. Chem.* **1999**, *23*, 309-316.

(6)   Lembo, A.; Tagliatesta, P.; Cicero, D.; Leoni, A.; Salvatori, A. A glycyl-substituted porphyrin as a starting compound for the synthesis of a pi-pi-stacked porphyrin-fullerene dyad with a frozen geometry. *Org. Biomol. Chem.* **2009**, *7*, 1093-1096.

(7)   Cho, W. S.; Kim, H. J.; Littler, B. J.; Miller, M. A.; Lee, C. H.; Lindsey, J. S. Rational synthesis of trans-substituted porphyrin building blocks containing one sulfur

or oxygen atom in place of nitrogen at a designated site. *J. Org. Chem.* **1999**, *64*, 7890-7901.

(8)   Wallace, K. J.; Hanes, R.; Anslyn, E.; Morey, J.; Kilway, K. V.; Siegel, J. Preparation of 1,3,5-tris(aminomethyl)-2,4,6-triethylbenzene from two versatile 1,3,5-tri(halosubstituted) 2,4,6-triethylbenzene derivatives. *Synthesis* **2005**, 2080-2083.

(9)   Rosenthal, J.; Lippard, S. J. Direct detection of nitroxyl in aqueous solution using a tripodal copper(II) BODIPY complex. *J. Am. Chem. Soc.* **2010**, *132*, 5536-5537.

(10)   Lu, D. L.; Lei, J. Y.; Tian, Z. D.; Wang, L. Z.; Zhang, J. L. Cu2+ fluorescent sensor based on mesoporous silica nanosphere. *Dyes Pigments* **2012**, *94*, 239-246.

(11)   Bag, S. S.; Kundu, R. Installation/Modulation of the Emission Response via Click Reaction. *J. Org. Chem.* **2011**, *76*, 3348-3356.

(12)   Yin, L. N.; Liu, Q. X.; Wu, X. M.; Cheng, F. J.; Guo, J. H. 9,10-Bis(dichlorethylaminomethyl)anthracene. *Acta Cryst. E.* **2006**, *62*, O2510-O2511.

(13)   Misra, T. K.; Chen, T. S.; Liu, C. Y. Phase transfer of gold nanoparticles from aqueous to organic solution containing resorcinarene. *J. Colloid Interface Sci.* **2006**, *297*, 584-588.

(14)   Xi, H. P.; Gibb, C. L. D.; Gibb, B. C. Functionalized deep-cavity cavitands. *J. Org. Chem.* **1999**, *64*, 9286-9288.

(15)   Rudkevich, D. M.; Hilmersson, G.; Rebek, J. Self-folding cavitands. *J. Am. Chem. Soc.* **1998**, *120*, 12216-12225.

(16)   Hoegberg, A. G. S. Cyclooligomeric phenol-aldehyde condensation products. 2. Stereoselective synthesis and DNMR study of two 1,8,15,22-tetraphenyl[14]metacyclophan-3,5,10,12,17,19,24,26-octols. *J. Am. Chem. Soc.* **1980**, *102*, 6046-6050.

(17)   Biros, S. M.; Ullrich, E. C.; Hof, F.; Trembleau, L.; Rebek, J. Kinetically stable complexes in water: The role of hydration and hydrophobicity. *J. Am. Chem. Soc.* **2004**, *126*, 2870-2876.

(18)   Asadi, A.; Ajami, D.; Rebek, J. Bent Alkanes in a New Thiourea-Containing Capsule. *J. Am. Chem. Soc.* **2011**, *133*, 10682-10684.

(19)   Yin, J.; Xiang, B.; Huffman, M. A.; Raab, C. E.; Davies, I. W. A General and Efficient 2-Amination of Pyridines and Quinolines. *J. Org. Chem.* **2007**, *72*, 4554-4557.

(20)   Yin, J.; Xiang, B.; Huffman, M. A.; Raab, C. E.; Davies, I. W. A general and efficient 2-amination of pyridines and quinolines. *J. Org. Chem.* **2007**, *72*, 4554-4557.

(21)   Niederl, J. B.; Vogel, H. J. Aldehyde-resorcinol condensations. *J. Am. Chem. Soc.* **1940**, *62*, 2512-2514.

(22)   Soberats, B.; Sanna, E.; Martorell, G.; Rotger, C.; Costa, A. Programmed enzyme-mimic hydrolysis of a choline carbonate by a metal-free 2-aminobenzimidazole-based cavitand. *Org. Lett.* **2014**, *16*, 840-843.

(23)   Howard, K. P.; Opella, S. J. High-resolution solid-state NMR spectra of integral membrane proteins reconstituted into magnetically oriented phospholipid bilayers. *J. Magn Reson. B.* **1996**, *112*, 91-94.

(24)   De Angelis, A. A.; Opella, S. J. Bicelle samples for solid-state NMR of membrane proteins. *Nat. Protoc.* **2007**, *2*, 2332-2338.